Supporting Information for

Ligand exchange at tetra-coordinated beryllium centres

Magnus R. Buchner[a]*, Dušan Ćoćić[b,c], Sergei I. Ivlev[a], Nils Spang[a], Matthias Müller[a] and Ralph Puchta[b]*

a Philipps-Universität Marburg

b Friedrich-Alexander-Universität Erlangen-Nürnberg

c Faculty of Science, University of Kragujevac

Table of Contents

Experimental procedures

Caution! Beryllium and its compounds are regarded as toxic and carcinogenic. As the biochemical mechanisms that cause beryllium associated diseases are still unknown,[1, 2] special (safety) precautions are strongly advised.[3]

General experimental techniques

All manipulations were performed under an inert gas atmosphere of argon either by working in a glove box or by using *Schlenk* techniques. Benzene was dried by refluxing over sodium and subsequent distillation under argon, while dichloromethane and chloroform were dried over CaH_2. C_6D_6 and toluene-d_7 were dried over Na/K-alloy and CD_2Cl_2 and $CDCl_3$ over CaH_2. All NMR solvents were freshly distilled before use and all NMR spectra were recorded in *J. Young* NMR tubes. $BeCl_2$, $BeBr_2$ and BeI_2 were prepared according to the literature.[4, 5] PCy_3 was purchased from ABCR and used as received, while PMe_3 was synthesized following literature procedure.[6]

X-ray structure determination

Single crystals were selected under a pre-dried argon stream in perfluorinated polyether (Fomblin YR 1800, Solvay Solexis) and mounted using the MiTeGen MicroLoop system at ambient temperature. X-ray diffraction data was collected using the monochromated Cu-K_α (λ = 1.54178 Å) radiation of a *Stoe* StadiVari diffractometer equipped with a Xenocs Microfocus Source and a Dectris Pilatus 300 K detector or monochromated Mo-K_α (λ = 0.71073 Å) radiation of a *Stoe* IPDS 2 diffractometer equipped with an Image Plate detector. Evaluation, integration and reduction of the diffraction data was carried out using the X-AREA software suite.[7] Multi-scan absorption correction was applied with the LANA module of the X-AREA software suite. The structures were solved with dual-space methods (SHELXT-2018/2) and refined against F^2 (SHELXL-2018/3) using the SHELXLE software package.[8-10] All atoms were located by Difference Fourier synthesis and non-hydrogen atoms refined anisotropically. Hydrogen atoms were refined using the "riding model" approach with isotropic displacement parameters 1.2 times of that of the preceding carbon atom. For the crystal data and details of the structure determination see tables S1 – S3. CCDC 2239416 – 2239422 contain the supplementary crystallographic data for this paper. This data can be obtained free of charge from The Cambridge Crystallographic Data Centre.

NMR spectroscopy

^1H, ^9Be, ^{13}C and ^{31}P NMR spectra were recorded on *Bruker* Avance III HD300 and Avance III AV500 spectrometers. The latter was equipped with a *Prodigy* Cryo-Probe. ^1H (300 / 500 MHz) and ^{13}C (76 / 126 MHz) NMR chemical shifts are given relative to the solvent signal for C_6D_6 (7.16 and 128.1 ppm), toluene-d_7 (2.09/6.98/7.00/7.09 and 20.4/125.5/128.3/129.2/137.9 ppm), $CDCl_3$ (7.26 and 77.2 ppm) and CD_2Cl_2 (5.32 and 53.8 ppm). ^9Be (42 MHz) and ^{31}P (122 and 202 MHz) NMR spectroscopy used 0.43 [M] $BeSO_4$ in D_2O and 85 % H_3PO_4 as an external standard, respectively. NMR spectra were processed with the MESTRENOVA software package.[11]

IR spectroscopy

IR spectra were recorded on a *Bruker* alpha FTIR spectrometer equipped with a diamond ATR unit in an argon-filled glovebox. Processing of the spectra was performed with the OPUS [12] software package and MESTRENOVA.[11]

Synthesis and characterization

*General procedure for the synthesis of [(PMe$_3$)$_2$BeX$_2$] (**1a-c**):* A *Schlenk* flask was charged with 100 mg beryllium halide and suspended in 20 ml of benzene. To this mixture approximately three equivalents PMe$_3$ were added with an air-displacement pipette inside a glove box. The reaction vessel was closed immediately and stirred at ambient temperature overnight. Subsequent removal of all volatiles *in vacuo* gave the title compounds in quantitative yields as colourless solids. Crystals of **1b** and **1c** were grown from an oversaturated benzene solution at ambient temperature over the course of several weeks.

*[(PMe$_3$)$_2$BeCl$_2$] (**1a**):* ^{1}H NMR (500 MHz, C_6D_6) δ = 0.76 (s, 1H); ^{1}H NMR (500 MHz, Tol-d$_8$) δ = 0.68 (vt, $|^{2}J_{PH} + {}^{4}J_{PH}|$ = 3.5 Hz); ^{1}H NMR (300 MHz, $CDCl_3$) δ = 1.25 (d, $^{2}J_{PH}$ = 8.6, 1H); ^{9}Be NMR (70 MHz, C_6D_6) δ = 4.6 (bs, $\omega_{1/2}$ = 31.9 Hz); ^{9}Be NMR (42 MHz, $CDCl_3$) δ = 4.1 (t, $^{1}J_{BeP}$ = 41.0, $\omega_{1/2}$ = 10.3 Hz); ^{31}P NMR (202 MHz, C_6D_6) δ = −46.2 (bs, $\omega_{1/2}$ = 184.0 Hz); ^{31}P NMR (202 MHz, Tol-d$_8$) δ = −45.2 (q, $^{1}J_{BeP}$ = 39.7 Hz); ^{31}P NMR (122 MHz, $CDCl_3$) δ = −44.1 (q, $^{1}J_{BeP}$ = 41.0 Hz).

*[(PMe$_3$)$_2$BeBr$_2$] (**1b**):* ^{1}H NMR (500 MHz, C_6D_6) δ = 0.76 (vt, $|^{2}J_{PH} + {}^{4}J_{PH}|$ = 3.6 Hz); ^{1}H NMR (500 MHz, Tol-d$_8$) δ = 0.79 (dd, $^{2}J_{PH}$ = 2.6 Hz, $^{4}J_{PH}$ = 1.6 Hz); ^{1}H NMR (500 MHz, $CDCl_3$) δ = 1.32 (dd, $^{2}J_{PH}$ = 3.9 Hz, $^{4}J_{PH}$ = 3.9 Hz); ^{9}Be NMR (42 MHz, C_6D_6) δ = 2.8 (t, $^{1}J_{BeP}$ = 42.7 Hz, $\omega_{1/2}$ = 3.1 Hz); ^{9}Be NMR (42 MHz, Tol-d$_8$) δ = 2.7 (d, $^{1}J_{BeP}$ = 41.7 Hz, $\omega_{1/2}$ = 5.2 Hz); ^{9}Be NMR (42 MHz, $CDCl_3$) δ = 2.6 (t, $^{1}J_{BeP}$ = 43.6, $\omega_{1/2}$ = 3.3 Hz); ^{31}P NMR (202 MHz, C_6D_6) δ = −46.5 (q, $^{1}J_{BeP}$ = 42.7 Hz); ^{31}P NMR (122 MHz, Tol-d$_8$) δ = −46.8 (q, $^{1}J_{BeP}$ = 42.4 Hz); ^{31}P NMR (122 MHz, $CDCl_3$) δ = -45.2 (q, $^{1}J_{BeP}$ = 43.6 Hz); ^{13}C NMR (126 MHz, C_6D_6) δ = 9.3 (vt, $|^{1}J_{PC} + {}^{3}J_{PC}|$ = 12.0 Hz); ^{13}C NMR (126 MHz, Tol-d$_8$) δ = 9.2 (vt, $|^{1}J_{PC} + {}^{3}J_{PC}|$ = 11.8 Hz); ^{13}C NMR (126 MHz, $CDCl_3$) δ = 10.0 (vt, $|^{1}J_{PC} + {}^{3}J_{PC}|$ = 12.5 Hz). IR (cm^{-1}): 2978 (w), 2910 (w), 1473 (w), 1422 (m), 1305 (w), 1289 (m), 967 (m), 948 (s), 910 (w), 869 (w), 851 (w), 744 (s), 689 (m), 585 (s), 543 (vs), 522 (vs).

*[(PMe$_3$)$_2$BeI$_2$] (**1c**):* ^{1}H NMR (500 MHz, C_6D_6) δ = 0.79 (dd, $^{2}J_{PH}$ = 4.2 Hz, $^{4}J_{PH}$ = 4.0 Hz); ^{1}H NMR (500 MHz, Tol-d$_8$) δ = 0.81 – 0.89 (m); ^{1}H NMR (500 MHz, CD_2Cl_2) δ = 1.38 (dd, $^{2}J_{PH}$ = 4.1 Hz, $^{4}J_{PH}$ = 4.1 Hz, 1H); ^{1}H NMR (300 MHz, $CDCl_3$) δ = 1.40 (dd, $^{2}J_{PH}$ = 4.0, $^{4}J_{PH}$ = 4.0, 1H); ^{9}Be NMR (42 MHz, C_6D_6) δ = −2.2 (t, $^{1}J_{BeP}$ = 44.6 Hz, $\omega_{1/2}$ = 3.8 Hz); ^{9}Be NMR (42 MHz, CD_2Cl_2) δ = −2.2 (t, $^{1}J_{BeP}$ = 45.6 Hz); ^{9}Be NMR (42 MHz, $CDCl_3$) δ = −2.2 (t, $^{1}J_{BeP}$ = 45.4 Hz, $\omega_{1/2}$ = 4.6 Hz); ^{31}P NMR (202 MHz, C_6D_6) δ = −49.6 (q, $^{1}J_{BeP}$ = 44.6 Hz); ^{31}P NMR (202 MHz, Tol-d$_8$) δ = −50.4 (q, $^{1}J_{BeP}$ = 43.8 Hz); ^{31}P NMR (202 MHz, CD_2Cl_2) δ = −48.3 (q, $^{1}J_{BeP}$ = 45.6 Hz); ^{31}P NMR (202 MHz, $CDCl_3$) δ = −47.9 (q, $^{1}J_{BeP}$ = 45.3 Hz); ^{13}C NMR (126 MHz, C_6D_6) δ = 9.5 (dd, $^{1}J_{PC}$ = 14.3 Hz, $^{3}J_{PC}$ = 13.2 Hz); ^{13}C NMR (126 MHz, CD_2Cl_2) δ = 10.2 (vt, $|^{1}J_{PC} + {}^{3}J_{PC}|$ = 14.3 Hz); ^{13}C NMR (126 MHz, $CDCl_3$) δ = 10.3 (dd, $^{1}J_{PC}$ = 15.0 Hz, $^{3}J_{PC}$ = 13.2 Hz). IR (cm^{-1}): 2972 (w), 2957 (w), 2908 (w), 2809 (w), 1420 (m), 1307 (w), 1287 (m), 1034 (w), 948 (s), 851 (w), 783 (w), 744 (m), 696 (w), 594 (m), 512 (m), 483 (vs), 416 (w).

*General procedure for the synthesis of [(PMe$_3$)BeX$_2$]$_2$ (**2a-c**):* 50 mg of compound **1a-c** and an equimolar amount of the corresponding beryllium halide were weighed into a *Schlenk* flask and 20 ml benzene was added. Stirring of the obtained suspension at ambient temperature overnight resulted in a colourless solution. Removal of all volatiles *in vacuo* gave the title compounds as colourless solids in quantitative yield. Crystals of **2a**, **2b** and **2c** were grown from an oversaturated benzene solution at ambient temperature over the course of several weeks.

*[(PMe$_3$)BeCl$_2$]$_2$ (**2a**):* ^{1}H NMR (300 MHz, C_6D_6) δ = 0.69 (d, $^{2}J_{PH}$ = 8.5 Hz); ^{1}H NMR (500 MHz, CD_2Cl_2) δ = 1.32 (d, $^{2}J_{PH}$ = 8.5 Hz); ^{1}H NMR (500 MHz, $CDCl_3$) δ = 1.35 (d, $^{2}J_{PH}$ = 8.6 Hz); ^{9}Be NMR (42 MHz, C_6D_6) δ = 5.7 (d, $^{1}J_{BeP}$ = 56.4, $\omega_{1/2}$ = 6.4 Hz); ^{9}Be NMR (42 MHz, CD_2Cl_2) δ = 5.2 (d, $^{1}J_{BeP}$ = 56.3 Hz, $\omega_{1/2}$ = 9.7 Hz); ^{31}P NMR (122 MHz, C_6D_6) δ = −47.3 (q, $^{1}J_{BeP}$ = 56.4 Hz); ^{31}P NMR (202 MHz, CD_2Cl_2) δ = −45.4 (q, $^{1}J_{BeP}$ = 56.3 Hz); ^{31}P NMR (122 MHz, $CDCl_3$) δ = −45.9 (q, $^{1}J_{BeP}$ = 56.0 Hz); ^{13}C NMR (76 MHz, C_6D_6) δ = 8.2

(d, $^{1}J_{PC}$ = 25.6 Hz); ^{13}C NMR (126 MHz, CD_2Cl_2) δ = 9.0 (d, $^{1}J_{PC}$ = 26.0 Hz. IR (cm^{-1}): 2994 (w), 2910 (w), 1587 (w), 1483 (w), 1422 (m), 1313 (w), 1291 (m), 1110 (w), 997 (m), 950 (s), 885 (m), 751 (s), 693 (s), 651 (vs), 520 (vs), 506 (vs), 449 (w), 418 (w).

*[(PMe$_3$)BeBr$_2$]$_2$ (**2b**):* ^{1}H NMR (500 MHz, C_6D_6) δ = 0.73 (d, $^{2}J_{PH}$ = 8.7 Hz); ^{1}H NMR (500 MHz, $CDCl_3$) δ = 1.38 (d, $^{2}J_{PH}$ = 8.7 Hz); ^{9}Be NMR (42 MHz, C_6D_6) δ = 3.1 (d, $^{1}J_{BeP}$ = 58.2 Hz, $\omega_{1/2}$ = 7.8 Hz); ^{31}P NMR (202 MHz, C_6D_6) δ = −47.7 (q, $^{1}J_{BeP}$ = 58.2 Hz); ^{31}P NMR (202 MHz, $CDCl_3$) δ = −46.7 (q, $^{1}J_{BeP}$ = 57.1 Hz); ^{13}C NMR (126 MHz, C_6D_6) δ = 7.9 (d, $^{1}J_{PC}$ = 27.2 Hz). IR (cm^{-1}): 2982 (w), 2910 (w), 1420 (m), 1307 (w), 1289 (m), 973 (s), 952 (s), 851 (w), 787 (w), 751 (m), 602 (vs), 502 (vs), 463 (vs).

*[(PMe$_3$)BeI$_2$]$_2$ (**2c**):* ^{1}H NMR (300 MHz, C_6D_6) δ = 0.77 (d, $^{2}J_{PH}$ = 8.8 Hz); ^{1}H NMR (500 MHz, Tol-d_8) δ = 0.78 (dd, $^{2}J_{PH}$ = 8.9 Hz, $^{4}J_{PH}$ = 1.3 Hz); ^{1}H NMR (500 MHz, $CDCl_3$) δ = 1.42 (d, $^{2}J_{PH}$ = 8.9 Hz); ^{9}Be NMR (42 MHz, C_6D_6) δ = −6.3 (d, $^{1}J_{BeP}$ = 58.5 Hz, $\omega_{1/2}$ = 12.8 Hz); ^{31}P NMR (202 MHz, C_6D_6) δ = −53.8 (q, $^{1}J_{BeP}$ = 58.5 Hz); ^{31}P NMR (202 MHz, Tol-d_8) δ = −54.0 (q, $^{1}J_{BeP}$ = 54.3 Hz); ^{31}P NMR (202 MHz, $CDCl_3$) δ = −52.0 (q, $^{1}J_{BeP}$ = 62.6 Hz); ^{13}C NMR (76 MHz, C_6D_6) δ = 7.6 (d, $^{1}J_{PC}$ = 29.6 Hz). IR (cm^{-1}): 2976 (w), 2904 (w), 1593 (w), 1534 (w), 1483 (w), 1458 (w), 1415 (m), 1340 (w), 1305 (w), 1287 (m), 1230 (w), 1081 (w), 1040 (w), 1003 (w), 967 (s), 950 (s), 879 (w), 863 (w), 848 (w), 834 (w), 785 (w), 749 (s), 730 (w), 683 (m), 622 (w), 575 (s), 551 (m), 457 (vs), 410 (vs).

*General procedure for the synthesis of [(PCy$_3$)BeX$_2$]$_2$ (**3a-c**):* A *Schlenk* flask was loaded with 50 mg of beryllium halide and an equimolar amount of PCy_3 and 20 ml benzene were added. The obtained colourless suspension was stirred overnight at ambient temperature. Removal of all volatiles *in vacuo* gave the title compounds as colourless solids in quantitative yield. Crystals of **3a** and **3b** were grown from an oversaturated benzene solution at ambient temperature over the course of several days.

*[(PCy$_3$)BeCl$_2$]$_2$ (**3a**):* ^{1}H NMR (500 MHz, C_6D_6) δ = 1.00 – 1.34 (m, 3H), 1.47 – 1.61 (m, 1H), 1.64 – 1.80 (m, 4H), 1.99 – 2.25 (m, 3H); ^{1}H NMR (500 MHz, CD_2Cl_2) δ = 1.18 – 1.37 (m, 3H), 1.52 – 1.66 (m, 2H), 1.68 – 1.74 (m, 1H), 1.76 – 1.88 (m, 2H), 1.91 – 2.15 (m, 3H). ^{9}Be NMR (42 MHz, C_6D_6) δ = 6.5 (bs, $\omega_{1/2}$ = 53.4 Hz); ^{9}Be NMR (42 MHz, CD_2Cl_2) δ = 6.5 (bs, $\omega_{1/2}$ = 74.0 Hz); ^{9}Be NMR (42 MHz, $CDCl_3$) δ = 7.9 (bs, $\omega_{1/2}$ = 53.6 Hz); ^{31}P NMR (202 MHz, C_6D_6) δ = −12.8 (bs); ^{31}P NMR (202 MHz, C_7D_8) δ = −15.0 (q, $^{1}J_{BeP}$ = 41.5 Hz); ^{31}P NMR (202 MHz, CD_2Cl_2) δ = -12.2 (bq, $^{1}J_{BeP}$ = 62.8 Hz); ^{31}P NMR (202 MHz, $CDCl_3$) δ = −12.7 (bs); ^{13}C NMR (126 MHz, C_6D_6) δ = 26.3 (s), 27.8 (d, $^{2}J_{PC}$ = 10.0 Hz), 29.4 (s), 31.3 (d, $^{1}J_{PC}$ = 17.4 Hz); ^{13}C NMR (126 MHz, CD_2Cl_2) δ = 26.4 (s), 27.9 (d, $^{2}J_{PC}$ = 10.4 Hz), 29.3 (s), 31.1 (d, $^{1}J_{PC}$ = 18.7 Hz). IR (cm^{-1}): 2923 (s), 2851 (s), 1479 (m), 1446 (s), 1348 (w), 1328 (w), 1301 (w), 1271 (w), 1216 (w), 1177 (m), 1122 (w), 1081 (w), 1034 (w), 1006 (m), 918 (w), 889 (m), 853 (m), 822 (w), 677 (vs), 651 (vs), 551 (vs), 512 (s), 492 (s), 463 (s), 445 (vs), 428 (s).

*[(PCy$_3$)BeBr$_2$]$_2$ (**3b**):* ^{1}H NMR (300 MHz, C_6D_6) δ = 1.09 – 1.33 (m, 3H), 1.45 – 1.62 (m, 1H), 1.63 – 1.84 (m, 4H), 2.02 – 2.39 (m, 3H); ^{9}Be NMR (42 MHz, C_6D_6) δ = 4.1 (bs, $\omega_{1/2}$ = 65.7 Hz); ^{31}P NMR (122 MHz, C_6D_6) δ = −17.2 (bs); ^{13}C NMR (76 MHz, C_6D_6) δ = 26.3 (s), 27.8 (d, $^{2}J_{PC}$ = 10.1 Hz), 29.4 (s), 31.8 (d, $^{1}J_{PC}$ = 18.1 Hz). IR (cm^{-1}): 2927 (s), 2849 (m), 1595 (w), 1532 (w), 1483 (w), 1444 (m), 1413 (w), 1389 (w), 1344 (w), 1328 (w), 1301 (w), 1269 (w), 1260 (w), 1230 (w), 1207 (w), 1179 (w), 1169 (w), 1124 (w), 1114 (w), 1081 (w), 1044 (w), 1028 (w), 1006 (m), 963 (w), 918 (w), 885 (m), 851 (m), 824 (w), 598 (s), 522 (vs), 492 (s), 463 (s), 430 (vs).

*[(PCy$_3$)BeI$_2$]$_2$ (**3c**):* ^{1}H NMR (500 MHz, C_6D_6) δ = 1.04 – 1.24 (m, 3H), 1.46 – 1.58 (m, 1H), 1.62 – 1.76 (m, 4H), 2.00 – 2.19 (m, 2H), 2.26 – 2.39 (m, 1H); ^{9}Be NMR (42 MHz, C_6D_6) δ = −1.1 (bm, $\omega_{1/2}$ = 134.0 Hz); ^{31}P NMR (202 MHz, C_6D_6) δ = −24.0 (bm); ^{13}C NMR (126 MHz, C_6D_6) δ = 26.2 (s), 27.6 (d, $^{2}J_{PC}$ = 9.8 Hz), 29.3 (s), 32.4 (d, $^{1}J_{PC}$ = 19.3 Hz). IR (cm^{-1}): 2929 (vs), 2851 (s), 1442 (s), 1346 (w), 1324 (w), 1299 (w), 1269 (w), 1212 (w), 1201 (w), 1173 (w), 1116 (w), 1073 (w), 1046 (w), 1030 (w), 1003 (m), 914 (w), 887 (m), 851 (m), 820 (w), 783 (w), 753 (w), 702 (w), 573 (m), 496 (s), 473 (vs), 461 (s), 441 (s), 424 (vs).

X-ray crystallographic details

Table S1: Crystal data and details of the structure determination for $[(PMe_3)_2BeBr_2]$ (**1b**) and $[(PMe_3)_2BeI_2]$ (**1c**).

	$[(PMe_3)_2BeBr_2]$ (**1b**)	$[(PMe_3)_2BeI_2]$ (**1c**)
Empirical formula	$C_6H_{18}BeBr_2P_2$	$C_6H_{18}BeI_2P_2$
Relative molecular mass	320.97	414.95
Crystal system	monoclinic	monoclinic
Space group (No.)	$P2_1/m$ (11)	$P2_1$ (4)
Radiation / Å	1.54186	0.71073
a / Å	6.4872(13)	12.590(3)
b / Å	14.511(3)	16.310(3)
c / Å	21.904(4)	14.450(3)
α / deg	90	90
β / deg	93.41(3)	92.60(3)
γ / deg	90	90
V / Å^3	2058.3(7)	2964.2(10)
Z	6	8
$F(000)$ / e	948.0	1552.0
$\rho_{calc.}$ / g·cm^{-3}	1.554	1.860
μ / mm^{-1}	9.307	4.417
ϑ range / °	3.66 – 75.40	1.41 – 25.75
Range of Miller indices	−8 ≤ h ≤ 6	−15 ≤ h ≤ 15
	−10 ≤ k ≤ 18	−19 ≤ k ≤ 19
	−26 ≤ l ≤ 26	−17 ≤ l ≤ 17
Reflections collected, unique	15324, 4285	63958, 18009
Restraints, parameters	0, 182	41, 422
R_{int}	0.026	0.0295
R_1 ($I \geq 2\sigma(I)$)	0.034	0.032
R_1 *(all data)*	0.048	0.035
wR_2 ($I \geq 2\sigma(I)$)	0.089	0.079
wR_2 *(all data)*	0.095	0.080
S	0.986	1.031
$\Delta\rho_{min}$, $\Delta\rho_{max}$ / e·Å^{-3}	−0.70, 0.68	−0.91, 1.50
Flack parameter x	--	0.01(3)
Volume fraction of the 2nd twin component	--	0.3930(13)

Table S2: Crystal data and details of the structure determination for $[(PMe_3)BeCl_2]_2$ (**2a**), $[(PMe_3)BeBr_2]_2$ (**2b**) and $[(PMe_3)BeI_2]_2$ (**2c**).

	$[(PMe_3)BeCl_2]_2$ (**2a**)	$[(PMe_3)BeBr_2]_2$ (**2b**)	$[(PMe_3)BeI_2]_2$ (**2c**)
Empirical formula	$C_6H_{18}Be_2Cl_4P_2$	$C_6H_{18}Be_2Br_4P_2$	$C_6H_{18}Be_2I_4P_2$
Relative molecular mass	311.96	489.80	677.76
Crystal system	monoclinic	monoclinic	monoclinic
Space group (No.)	$P2_1/c$ (14)	$P2_1/c$ (14)	$P2_1/c$ (14)
Radiation / Å	0.71073	0.71073	1.54178
a / Å	6.2043(13)	6.4585(4)	6.9935(2)
b / Å	9.517(3)	13.3248(11)	13.2512(2)
c / Å	13.879(3)	9.9155(9)	10.5272(2)
α / deg	90	90	90
β / deg	100.175(17)	91.180(6)	96.498(2)
γ / deg	90	90	90
V / Å^3	806.6(3)	853.13(12)	969.31(4)
Z	2	2	2
F(000) / e	320.0	464.0	608.0
$\rho_{calc.}$ / g·cm^{-3}	1.284	1.907	2.322
μ / mm^{-1}	0.898	9.590	51.819
ϑ range / °	2.608 – 26.756	2.561 – 29.368	5.388 – 78.522
Range of Miller indices	−7 ≤ h ≤ 7	−8 ≤ h ≤ 8	−8 ≤ h ≤ 8
	−12 ≤ k ≤ 12	−16 ≤ k ≤ 18	−16 ≤ k ≤ 16
	−17 ≤ l ≤ 17	−13 ≤ l ≤ 13	−13 ≤ l ≤ 7
Reflections collected, unique	10259, 1703	11112, 2298	17624, 2067
Restraints, parameters	0, 67	0, 67	0, 67
R_{int}	0.179	0.048	0.069
R_1 ($I \geq 2\sigma(I)$)	0.092	0.044	0.057
R_1 (all data)	0.106	0.049	0.058
wR_2 ($I \geq 2\sigma(I)$)	0.247	0.115	0.154
wR_2 (all data)	0.260	0.117	0.155
S	1.112	0.987	1.092
$\Delta\rho_{min}$, $\Delta\rho_{max}$ / *e*·Å^{-3}	−0.99, 1.08	−0.89, 1.18	−1.73, 2.71
Volume fraction of the 2nd twin component	--	0.273(2)	--

Table S3: Crystal data and details of the structure determination for $[(PCy_3)BeCl_2]_2$ (**3a**) and $[(PCy_3)BeBr_2]_2$ (**3b**).

	$[(PCy_3)BeCl_2]_2$ (**3a**)	$[(PCy_3)BeBr_2]_2$ (**3b**)
Empirical formula	$C_{36}H_{66}Be_2Cl_4P_2$ $2(C_6D_6)$	$C_{36}H_{66}Be_2Br_4P_2$
Relative molecular mass	889.00	898.48
Crystal system	triclinic	triclinic
Space group (No.)	$P\bar{1}$ (2)	$P\bar{1}$ (2)
Radiation / Å	0.71073	0.71073
a / Å	8.3749(4)	9.5773(19)
b / Å	10.6551(5)	10.134(2)
c / Å	15.0815(7)	10.971(2)
α / deg	69.384(3)	95.17(3)
β / deg	82.093(4)	110.54(3)
γ / deg	71.718(4)	90.53(3)
V / Å^3	1195.48(10)	992.1(4)
Z	1	1
F(000) / e	472.0	460.0
$\rho_{calc.}$ / g·cm^{-3}	1.218	1.504
μ / mm^{-1}	0.346	4.161
ϑ range / °	1.443 – 26.745	1.992 – 29.277
Range of Miller indices	−10 ≤ h ≤ 10	−13 ≤ h ≤ 13
	−13 ≤ k ≤ 13	−13 ≤ k ≤ 13
	−17 ≤ l ≤ 19	−14 ≤ l ≤ 15
Reflections collected, unique	15532, 5046	16237, 5339
Restraints, parameters	0, 253	0, 199
R_{int}	0.038	0.067
R_1 ($I \geq 2\sigma(I)$)	0.027	0.035
R_1 *(all data)*	0.031	0.057
wR_2 ($I \geq 2\sigma(I)$)	0.074	0.081
wR_2 *(all data)*	0.076	0.086
S	1.028	1.007
$\Delta\rho_{min}$, $\Delta\rho_{max}$ / *e*·Å^{-3}	−0.15, 0.42	−0.61, 0.65

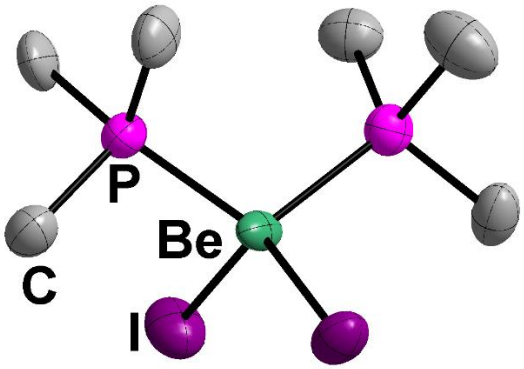

Fig. S1 Solid state structures of $[(PMe_3)_2BeI_2]$ (**1c**). Ellipsoids are depicted at 70 % probability at 100 K. Hydrogen atoms are omitted for clarity.

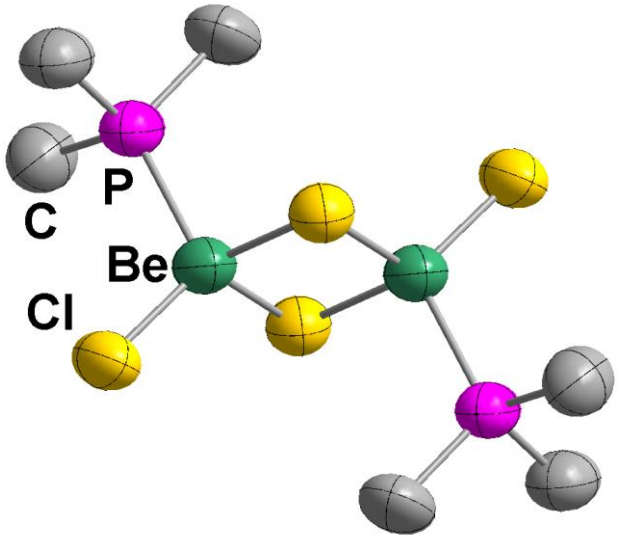

Fig. S2 Solid state structures of $[(PMe_3)BeCl_2]_2$ (**2a**). Ellipsoids are depicted at 70 % probability at 100 K. Hydrogen atoms are omitted for clarity.

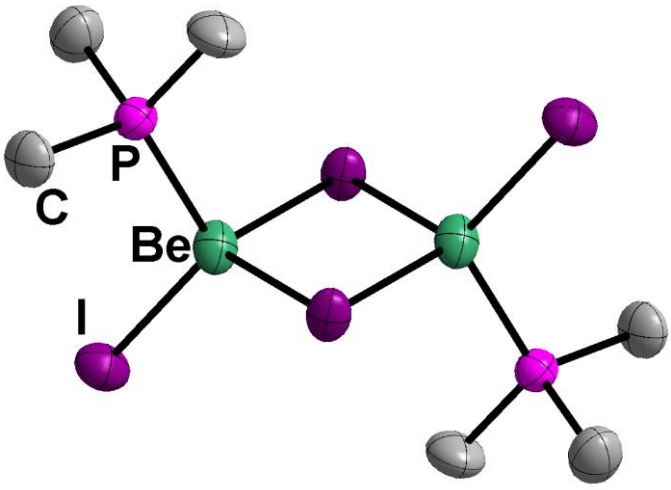

Fig. S3 Solid state structures of $[(PMe_3)BeI_2]_2$ (**2c**). Ellipsoids are depicted at 70 % probability at 100 K. Hydrogen atoms are omitted for clarity.

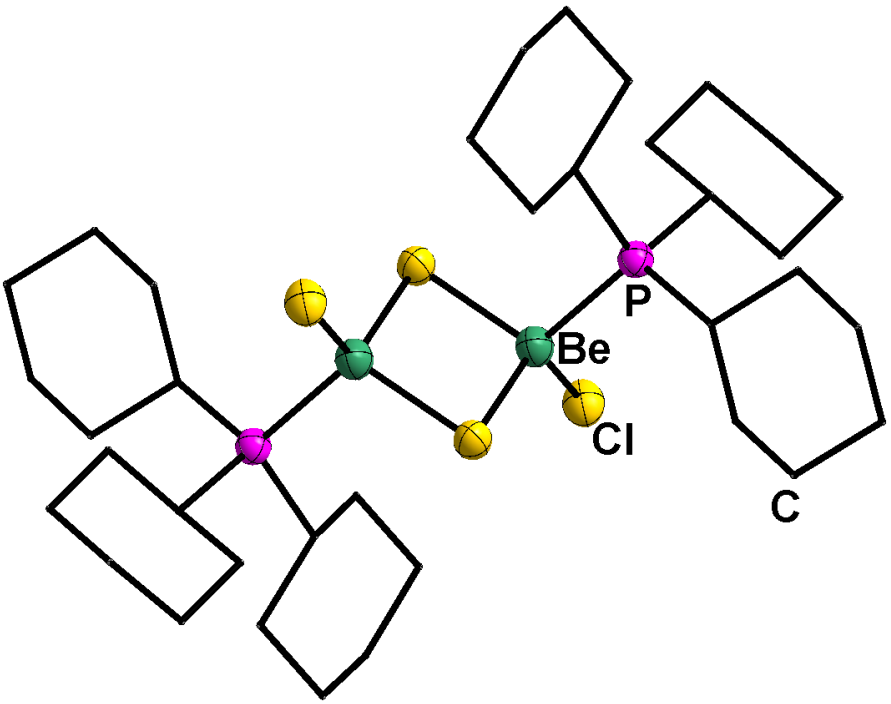

Fig. S4 Solid state structures of $[(PCy_3)BeCl_2]_2$ (**3a**). Ellipsoids are depicted at 70 % probability at 100 K. Carbon atoms are shown as wire frame and hydrogen atoms as well as crystal benzene are omitted for clarity.

Table S4: Selected atomic distances (Å) in $[(PMe_3)_2BeI_2]$ (**1c**).

Be1—P1	2.129(18)	Be1—I1	2.397(16)
Be1—P2	2.124(18)	Be1—I2	2.401(16)
Be2—P3	2.144(19)	Be2—I3	2.368(17)
Be2—P4	2.196(19)	Be2—I4	2.380(17)
Be3—P5	2.153(17)	Be3—I5	2.402(16)
Be3—P6	2.137(18)	Be3—I6	2.377(16)
Be4—P7	2.170(18)	Be4—I7	2.374(16)
Be4—P8	2.160(17)	Be4—I8	2.386(17)

NMR spectra

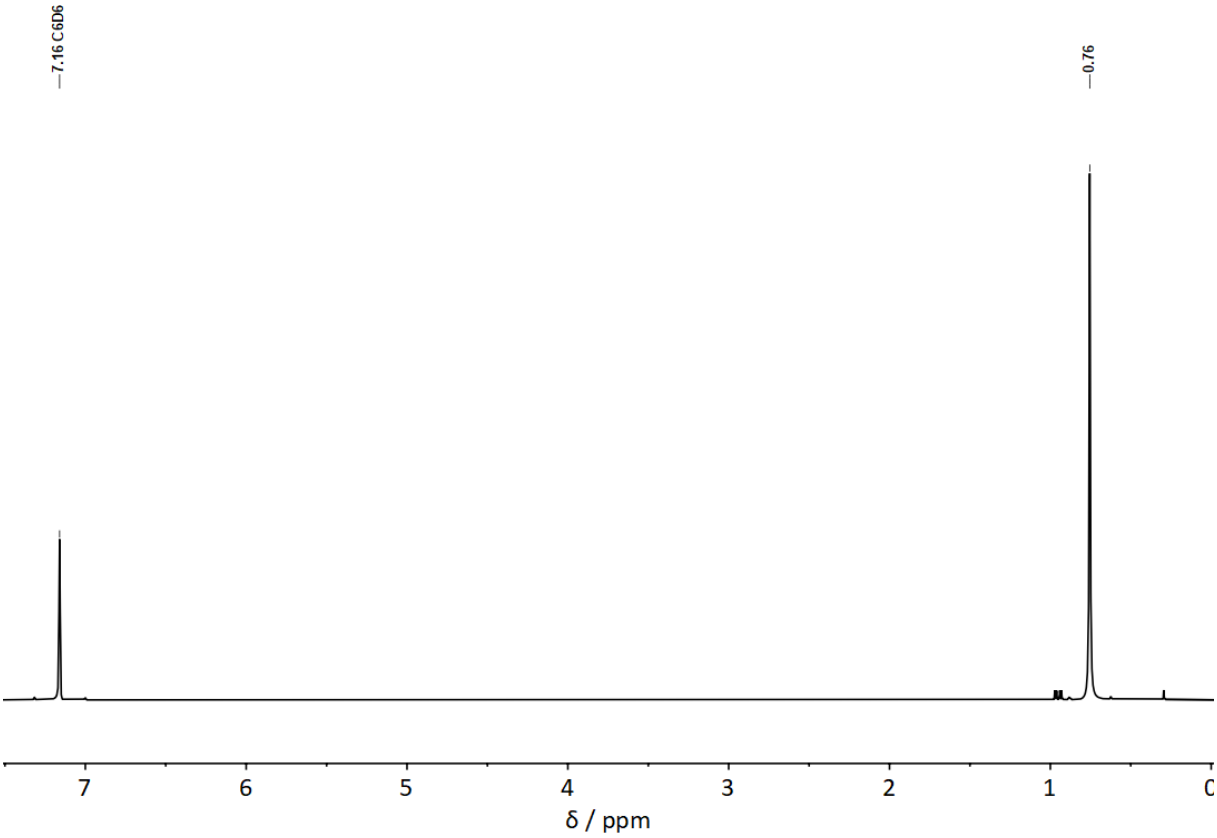

Fig. S5 ^{1}H NMR spectrum of [$(PMe_3)_2BeCl_2$] (**1a**) in C_6D_6.

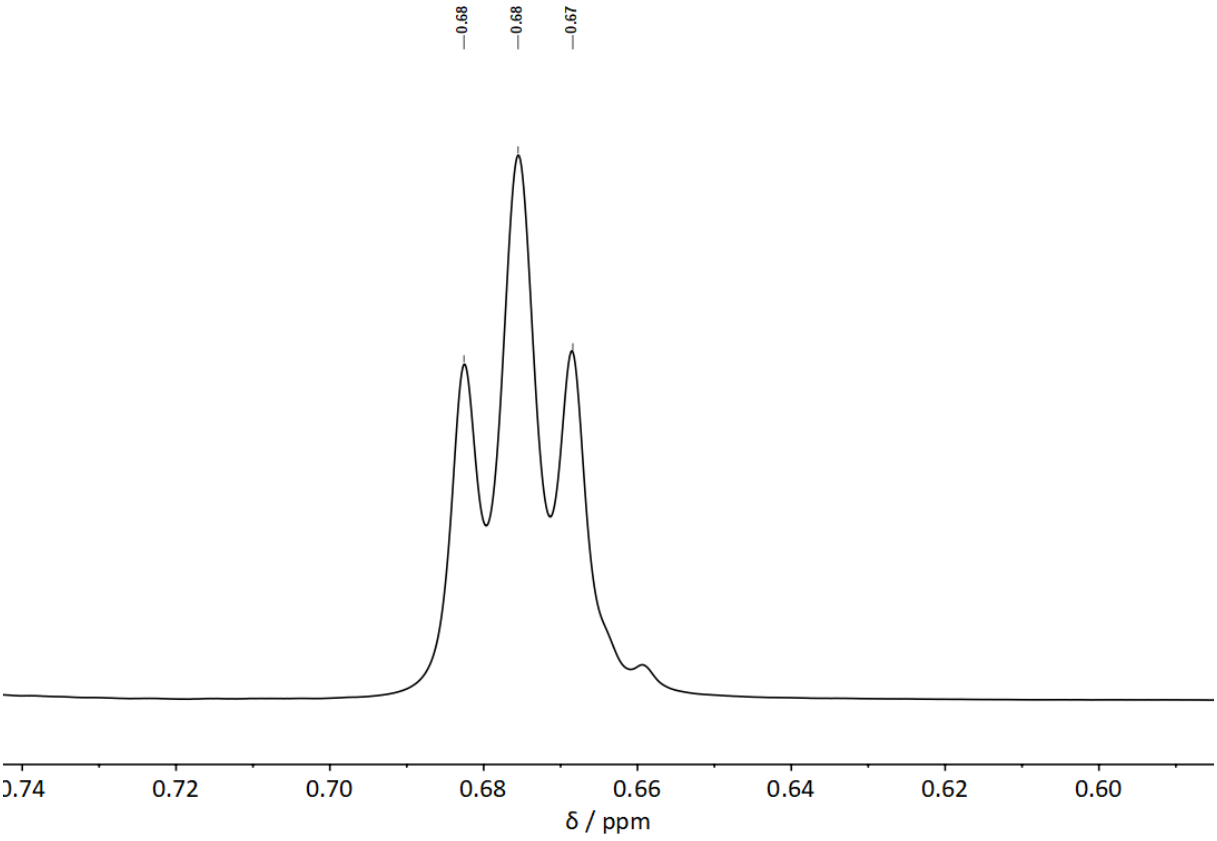

Fig. S6 ^{1}H NMR spectrum of [$(PMe_3)_2BeCl_2$] (**1a**) in Tol-d_8.

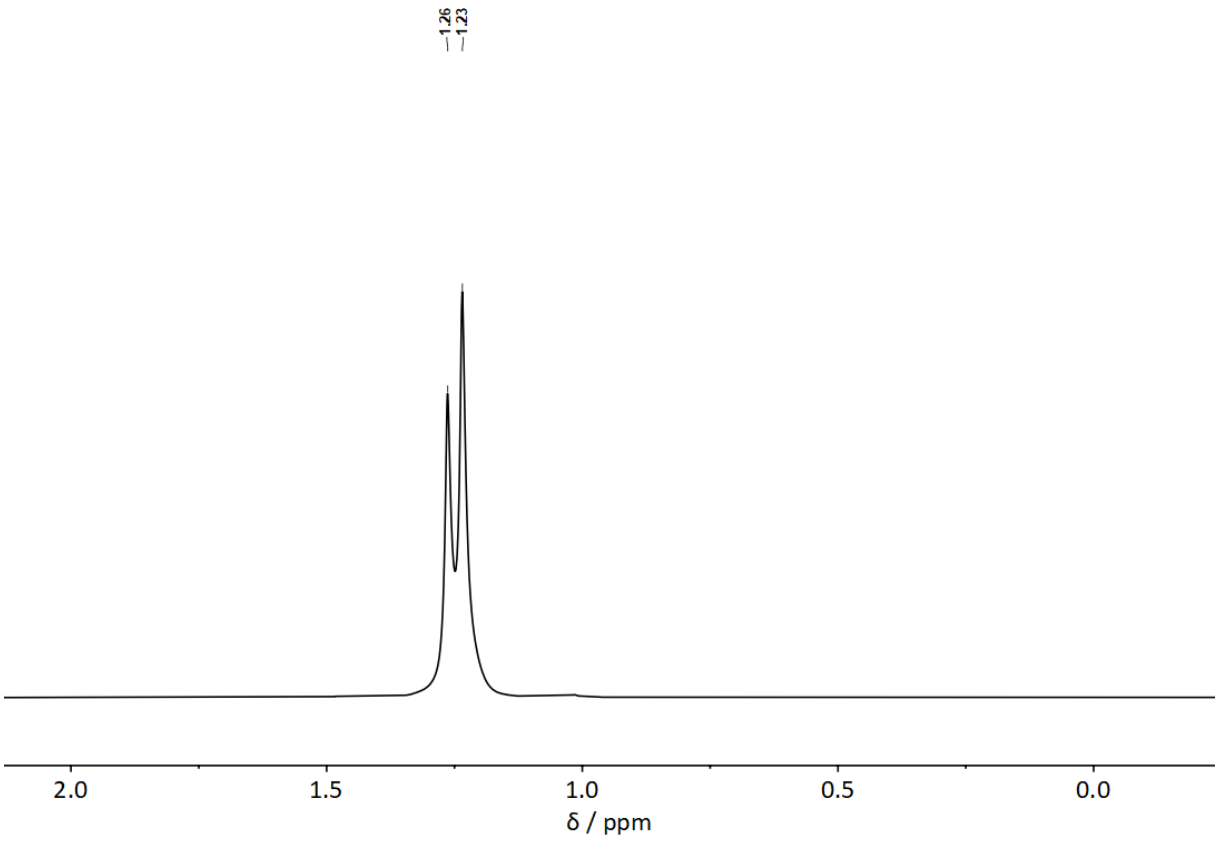

Fig. S7 ^{1}H NMR spectrum of [$(PMe_3)_2BeCl_2$] (**1a**) in $CDCl_3$.

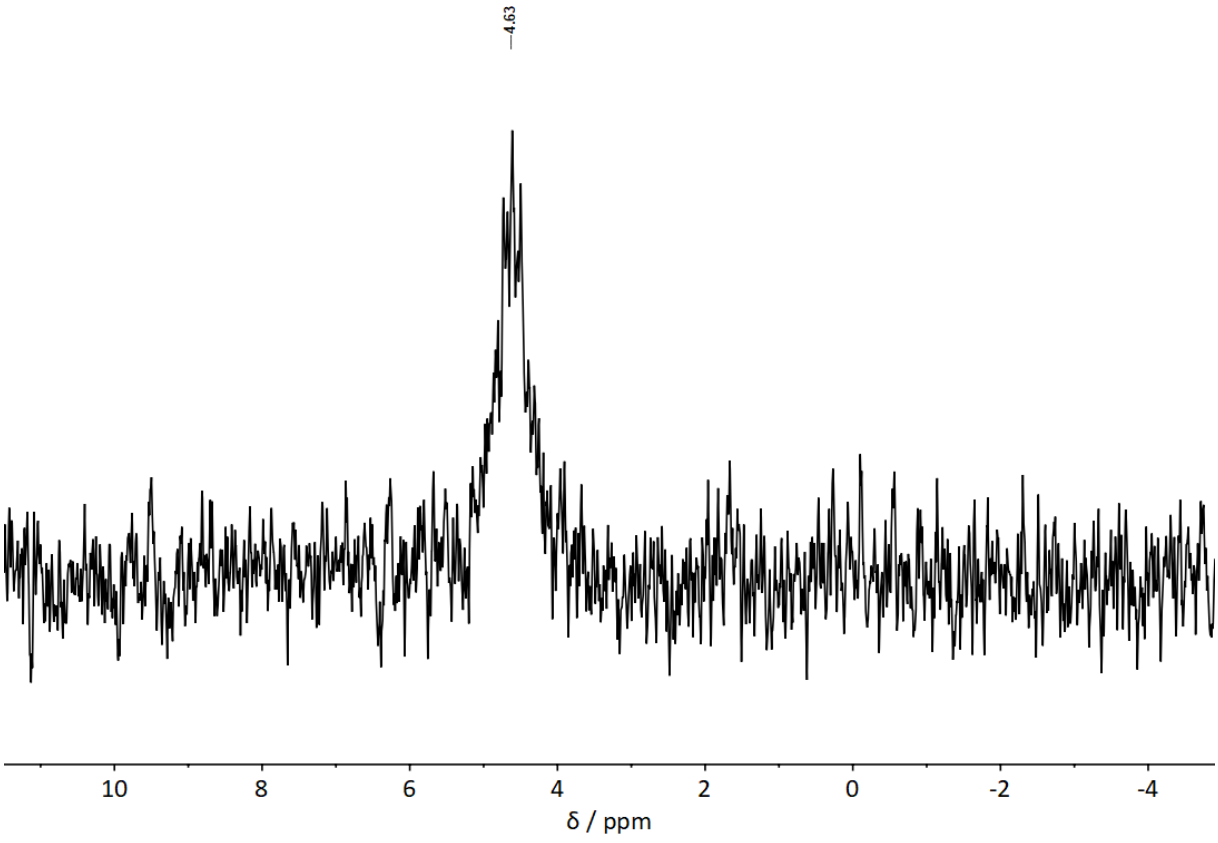

Fig. S8 ^{9}Be NMR spectrum of [$(PMe_3)_2BeCl_2$] (**1a**) in C_6D_6.

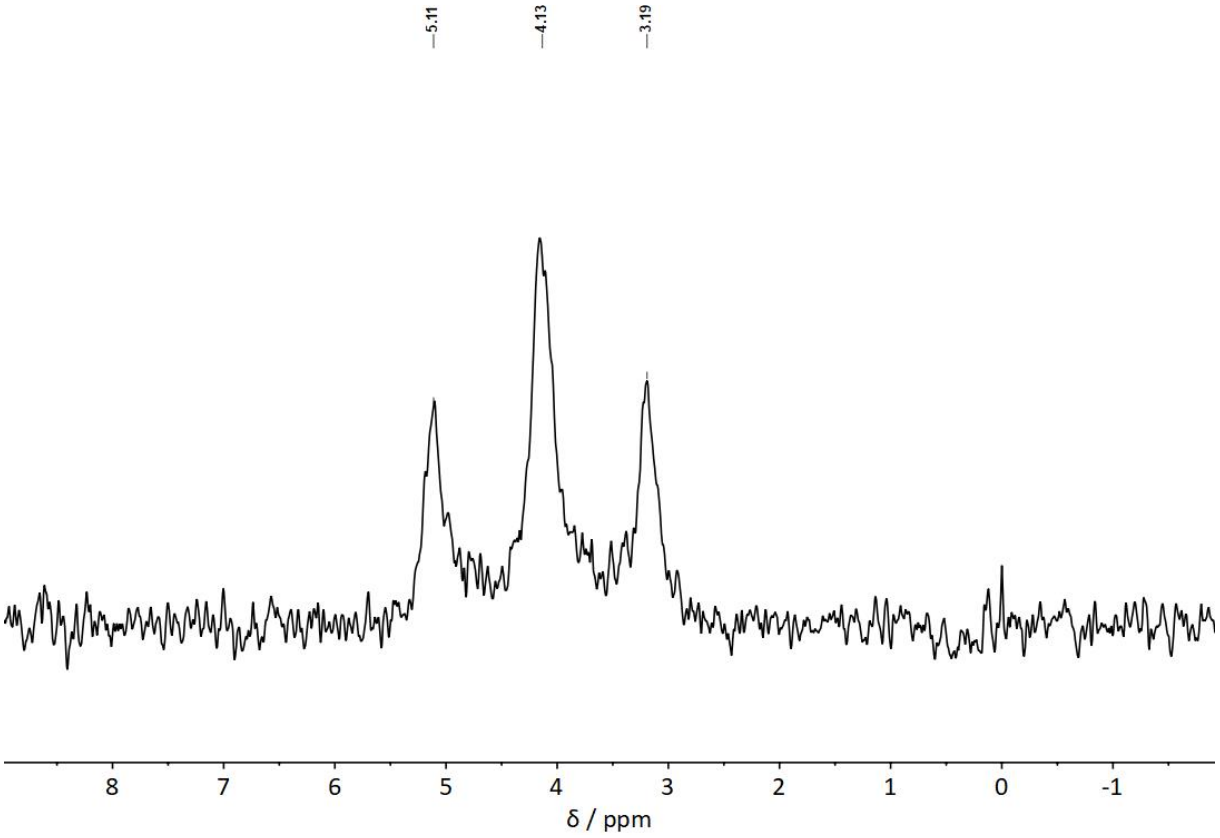

Fig. S9 ^{9}Be NMR spectrum of [$(PMe_3)_2BeCl_2$] (**1a**) in $CDCl_3$.

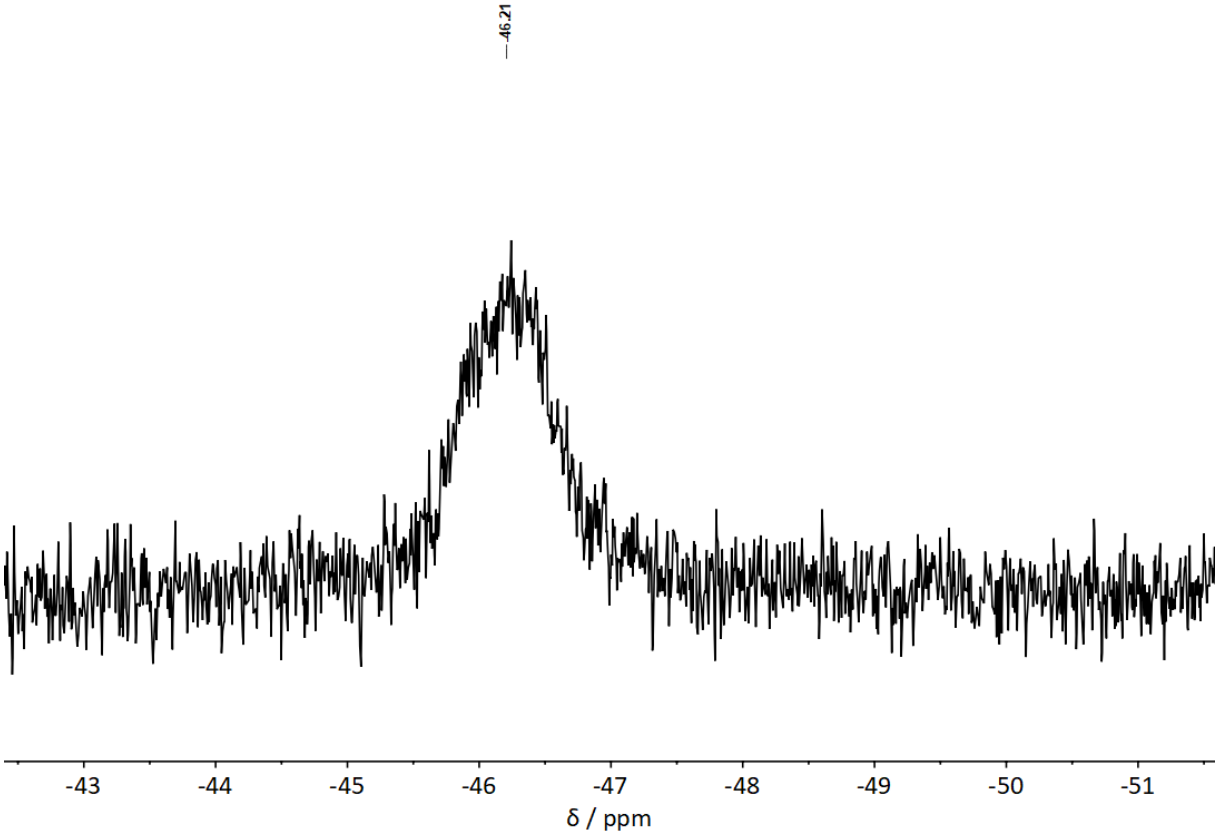

Fig. S10 ^{31}P NMR spectrum of [$(PMe_3)_2BeCl_2$] (**1a**) in C_6D_6.

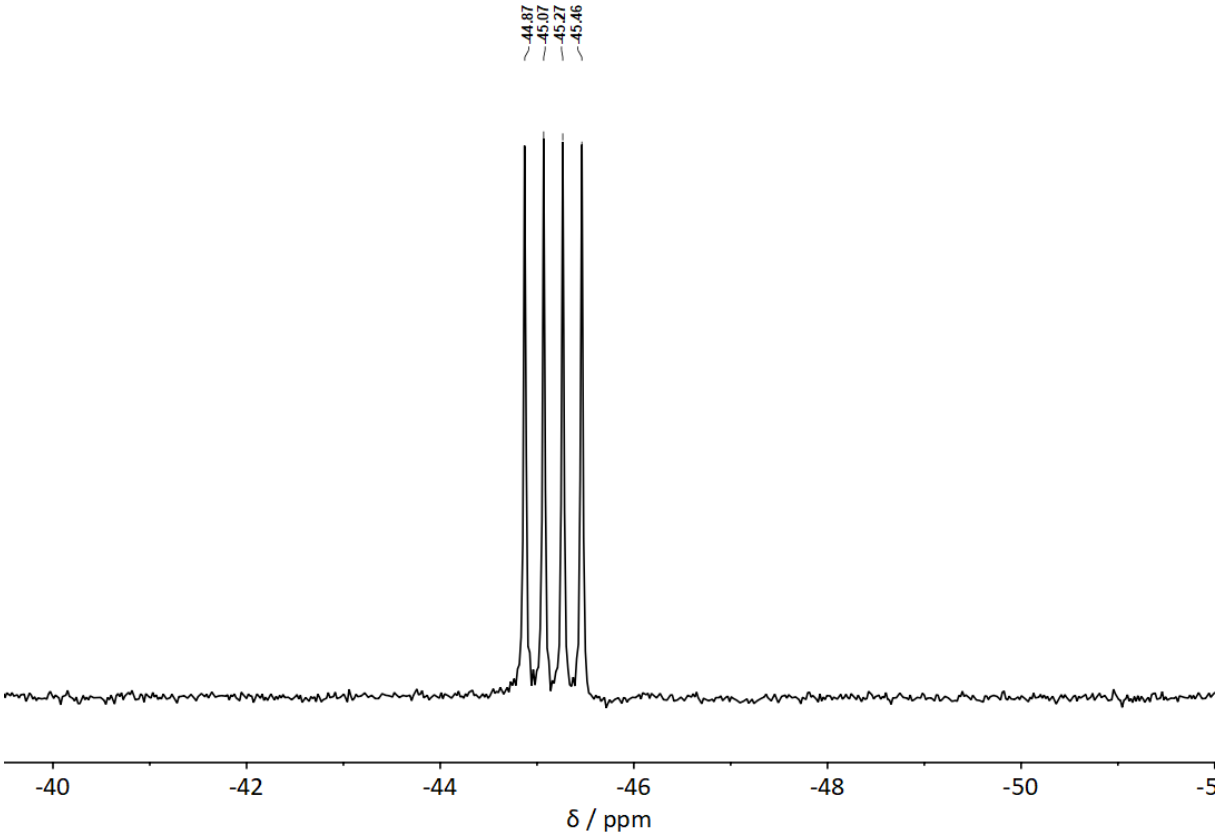

Fig. S11 ^{31}P NMR spectrum of [$(PMe_3)_2BeCl_2$] (**1a**) in Tol-d_8.

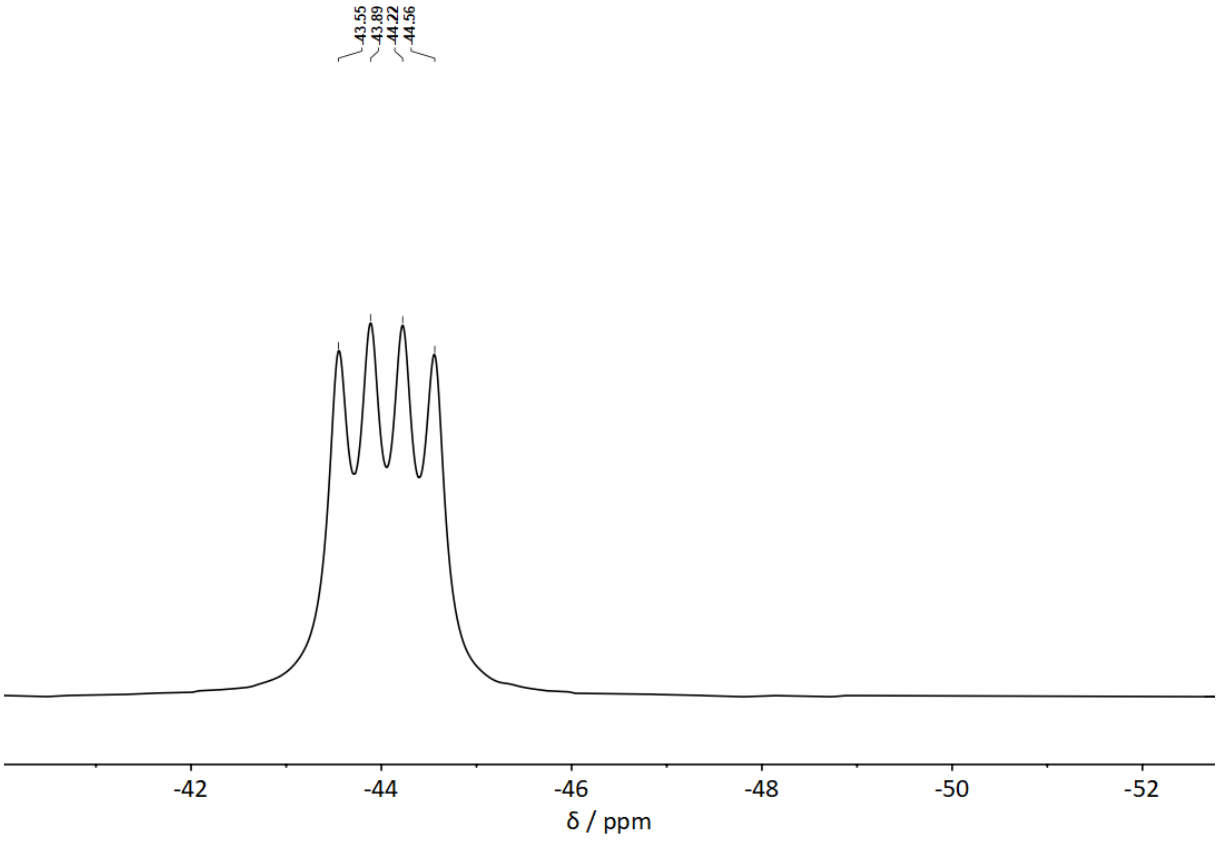

Fig. S12 ^{31}P NMR spectrum of [$(PMe_3)_2BeCl_2$] (**1a**) in $CDCl_3$.

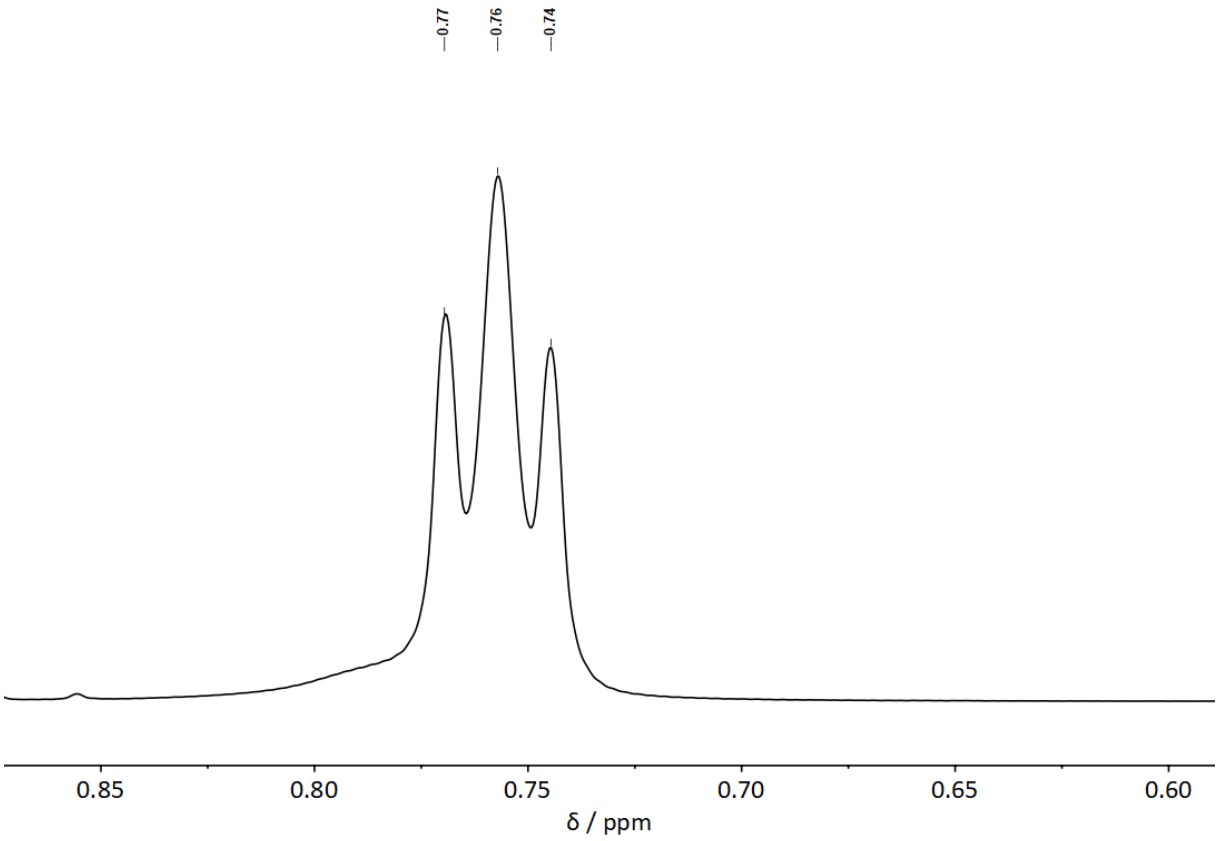

Fig. S13 ^{1}H NMR spectrum of [$(PMe_3)_2BeBr_2$] (**1b**) in C_6D_6.

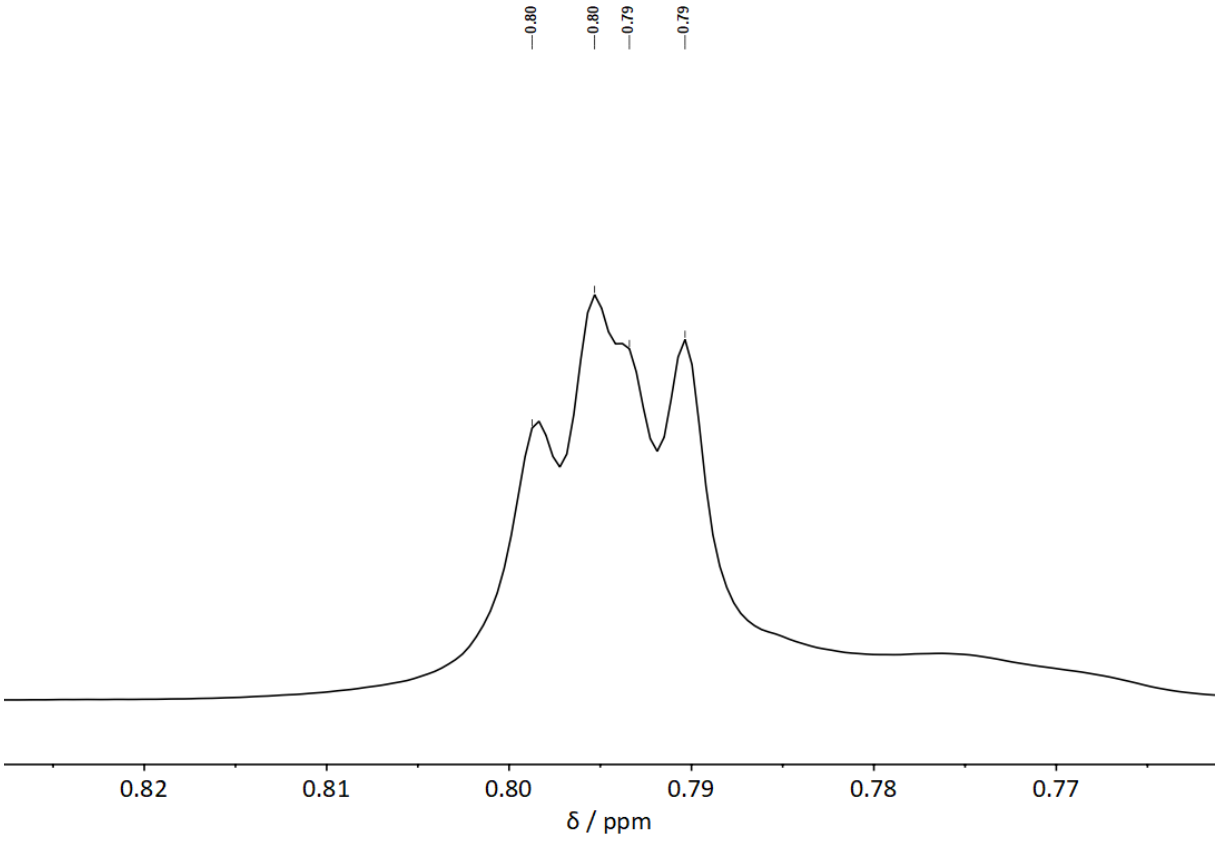

Fig. S14 ^{1}H NMR spectrum of [$(PMe_3)_2BeBr_2$] (**1b**) in Tol-d_8.

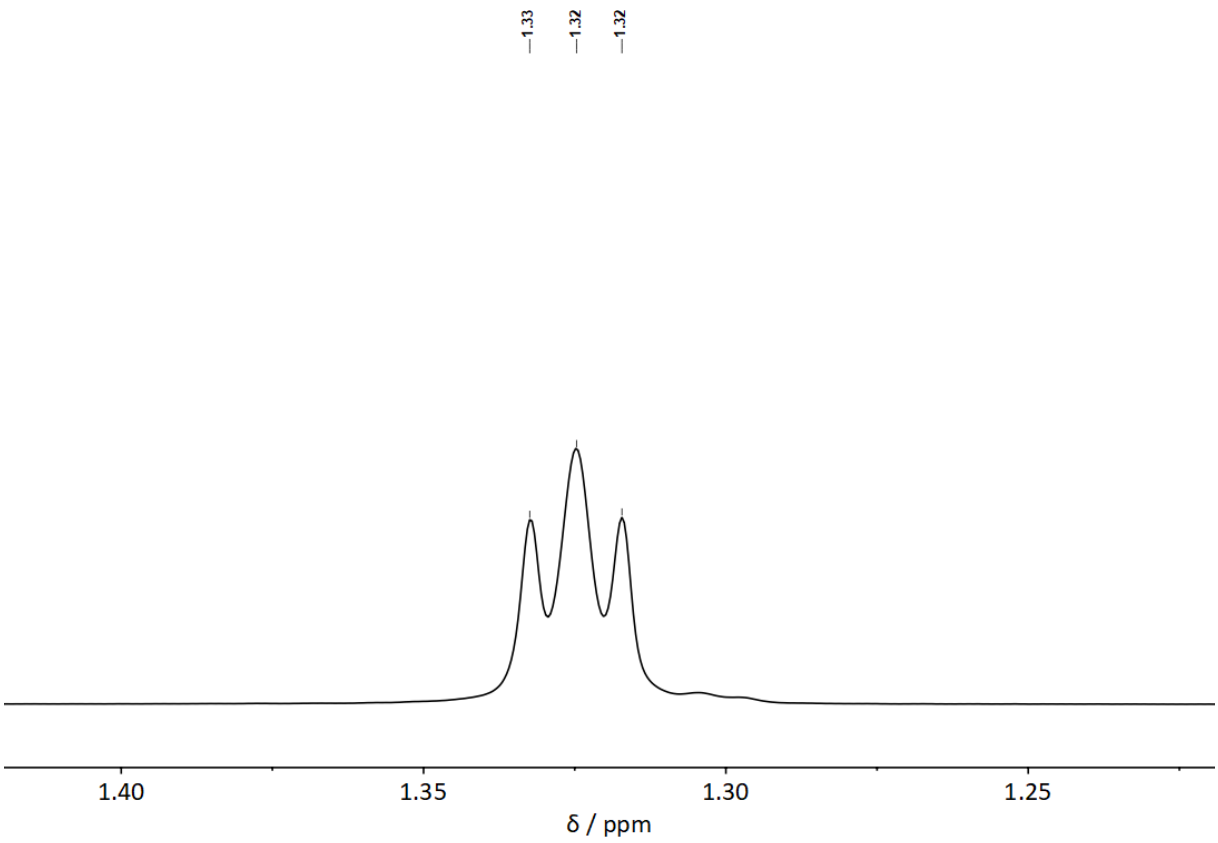

Fig. S15 ^{1}H NMR spectrum of [$(PMe_3)_2BeBr_2$] (**1b**) in $CDCl_3$.

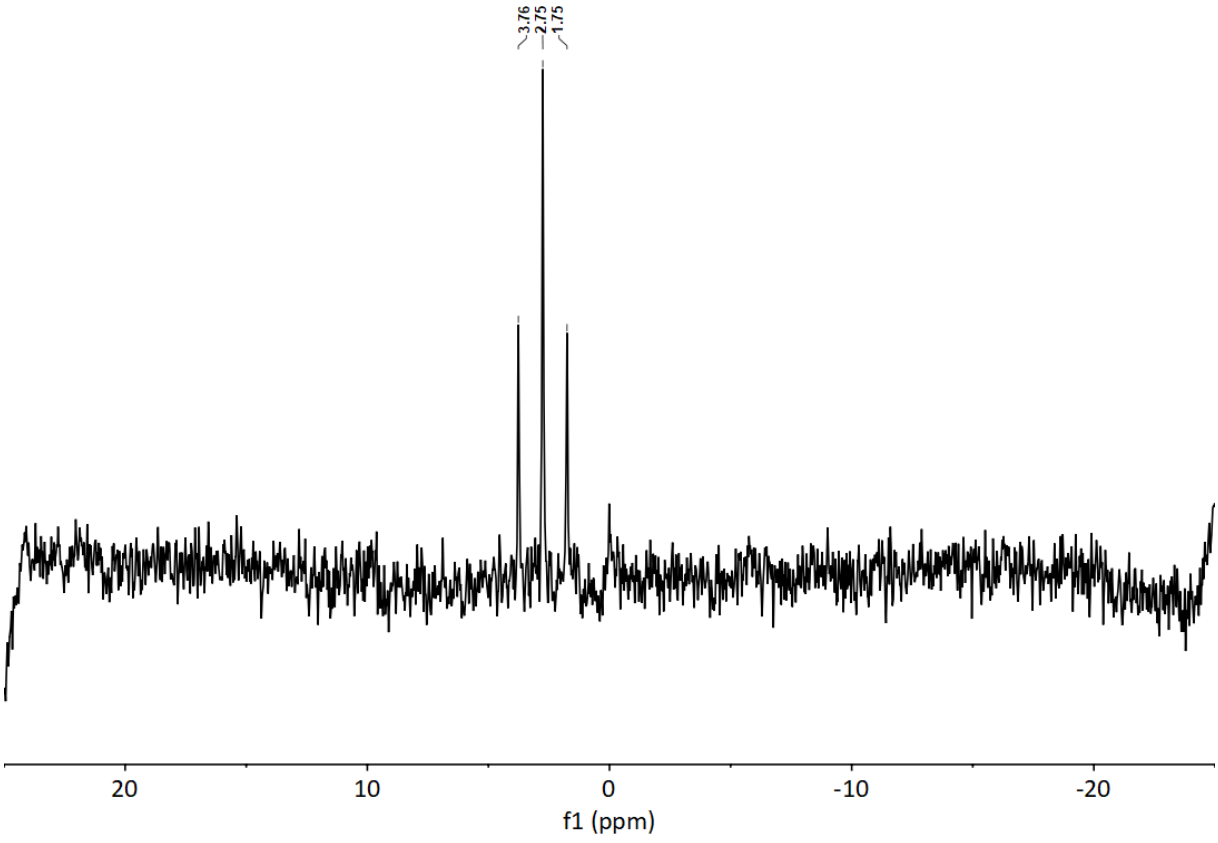

Fig. S16 ^{9}Be NMR spectrum of [$(PMe_3)_2BeBr_2$] (**1b**) in C_6D_6.

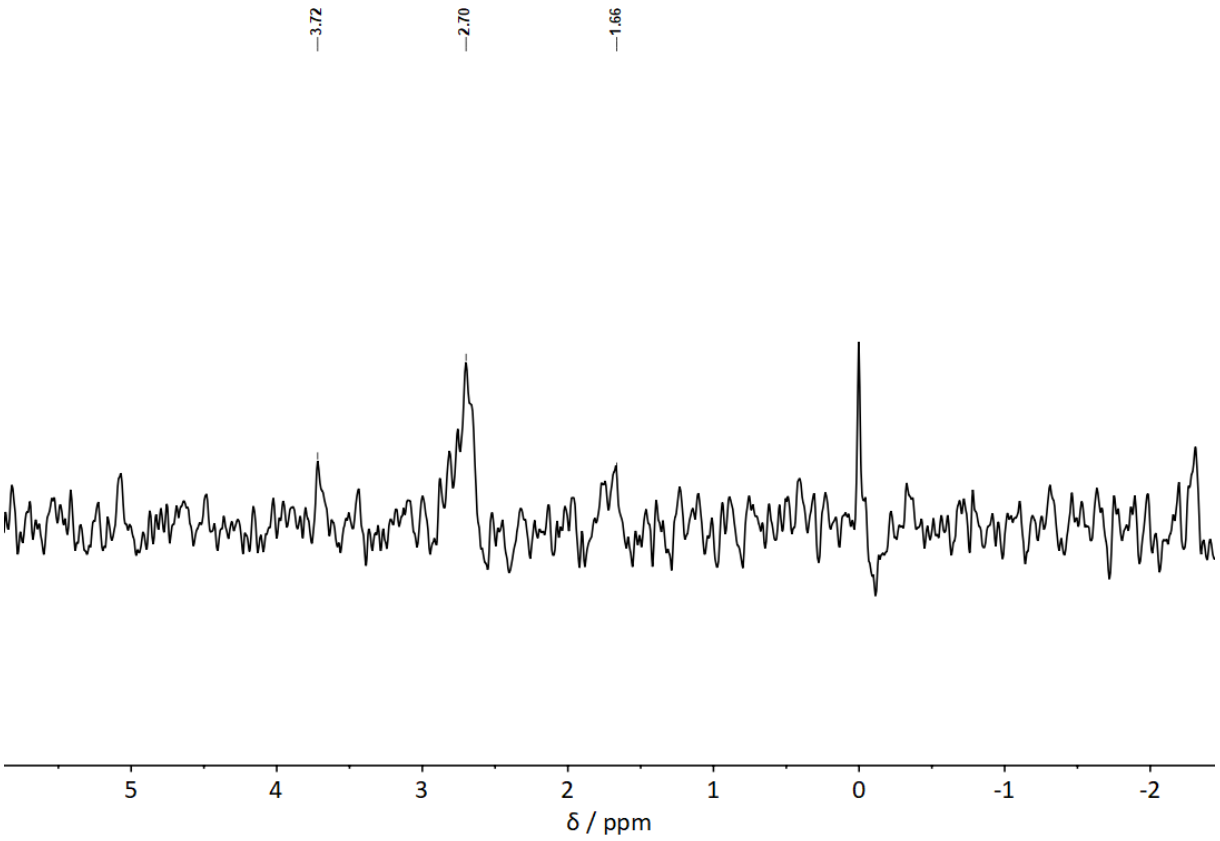

Fig. S17 ^{9}Be NMR spectrum of [$(PMe_3)_2BeBr_2$] (**1b**) in Tol-d_8.

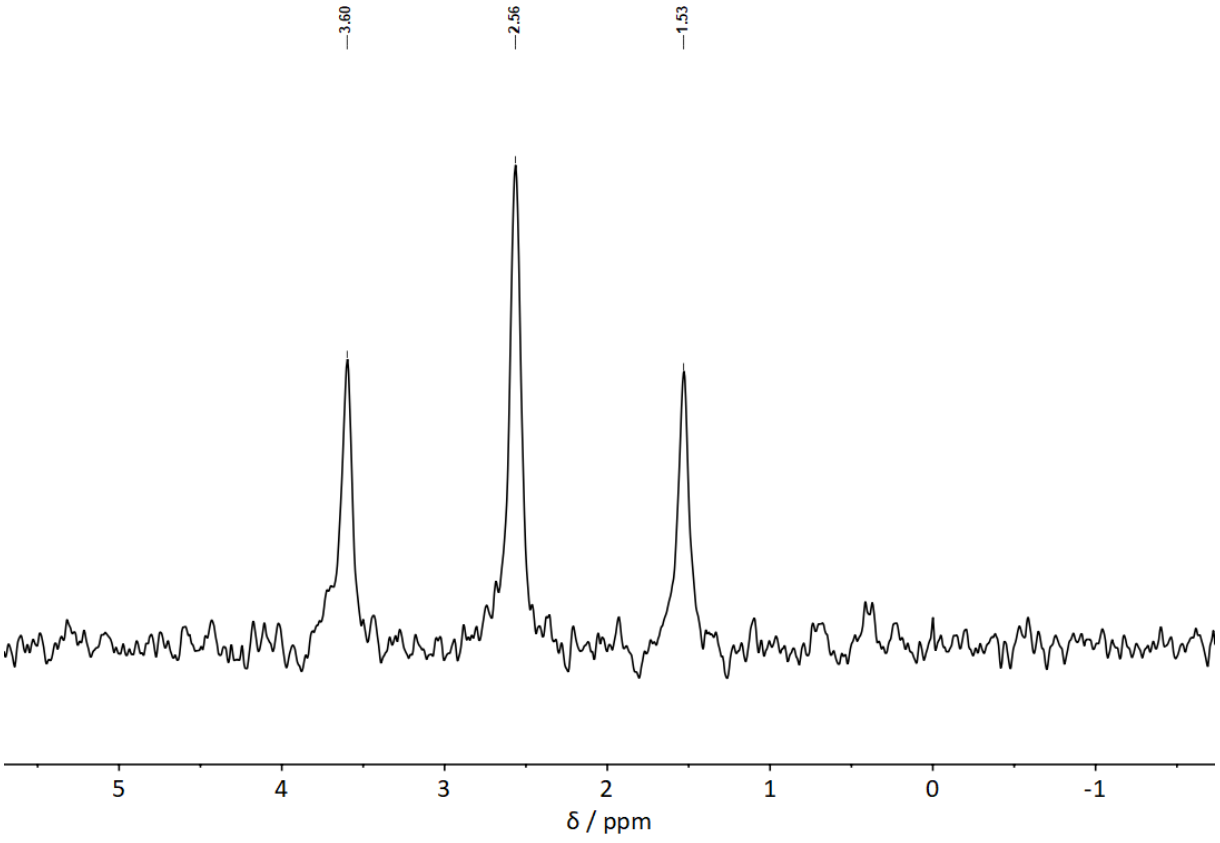

Fig. S18 ^{9}Be NMR spectrum of [$(PMe_3)_2BeBr_2$] (**1b**) in $CDCl_3$.

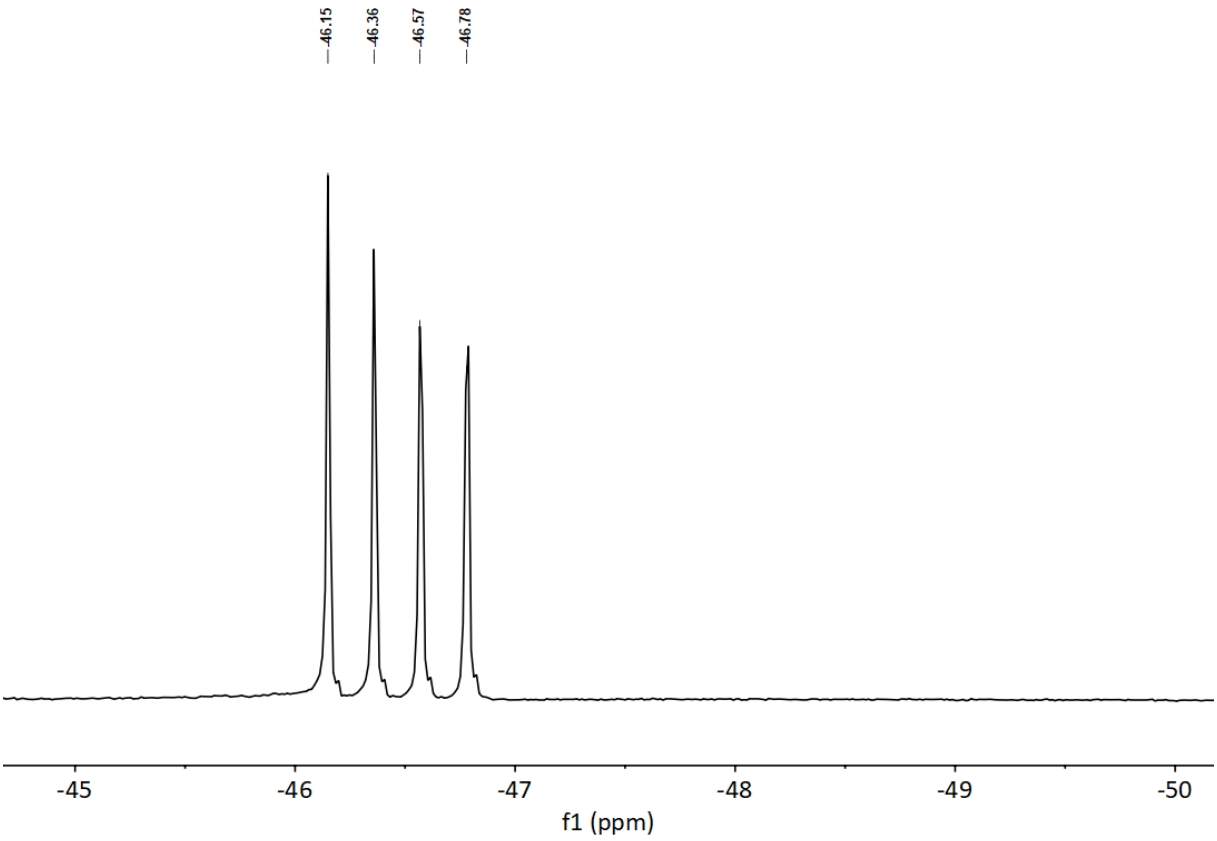

Fig. S19 ^{31}P NMR spectrum of [$(PMe_3)_2BeBr_2$] (**1b**) in C_6D_6.

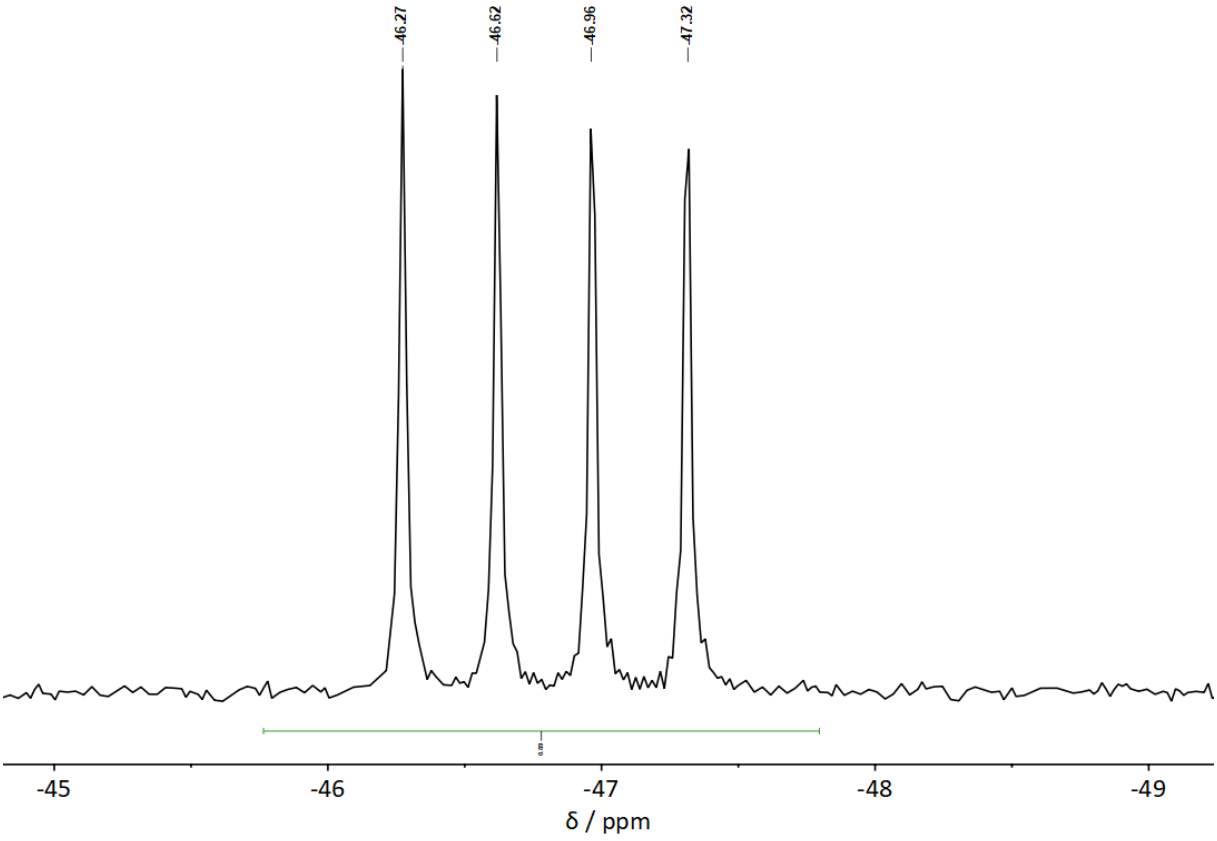

Fig. S20 ^{31}P NMR spectrum of [$(PMe_3)_2BeBr_2$] (**1b**) in Tol-d_8.

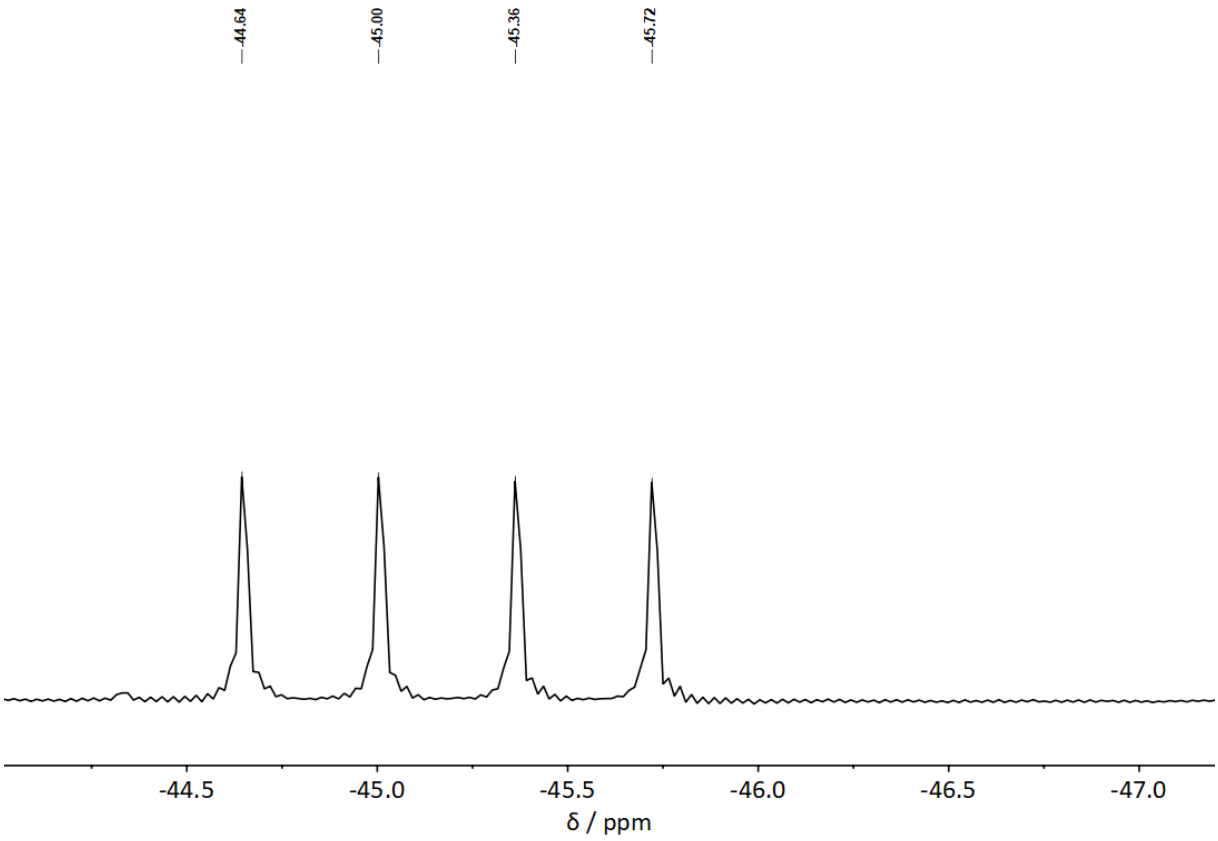

Fig. S21 ^{31}P NMR spectrum of $[(PMe_3)_2BeBr_2]$ (**1b**) in $CDCl_3$.

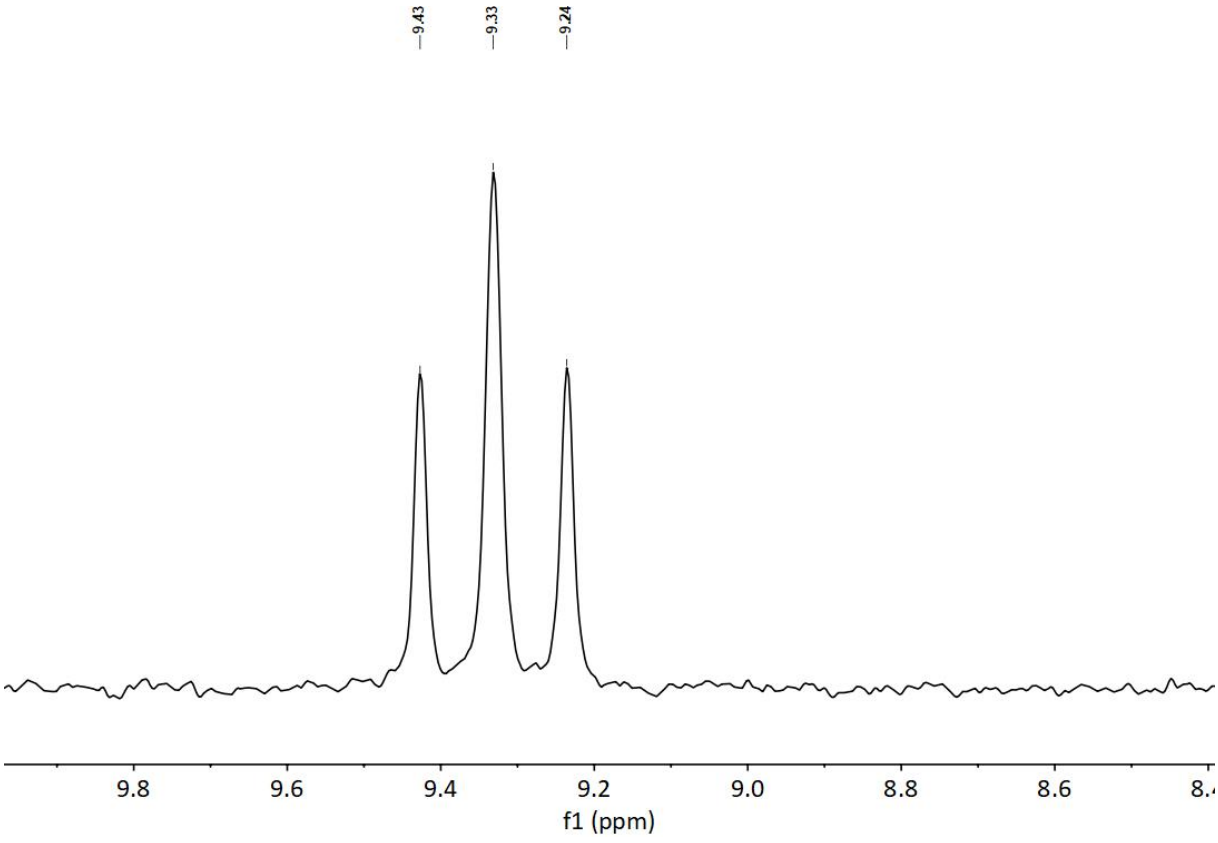

Fig. S22 ^{13}C NMR spectrum of $[(PMe_3)_2BeBr_2]$ (**1b**) in C_6D_6.

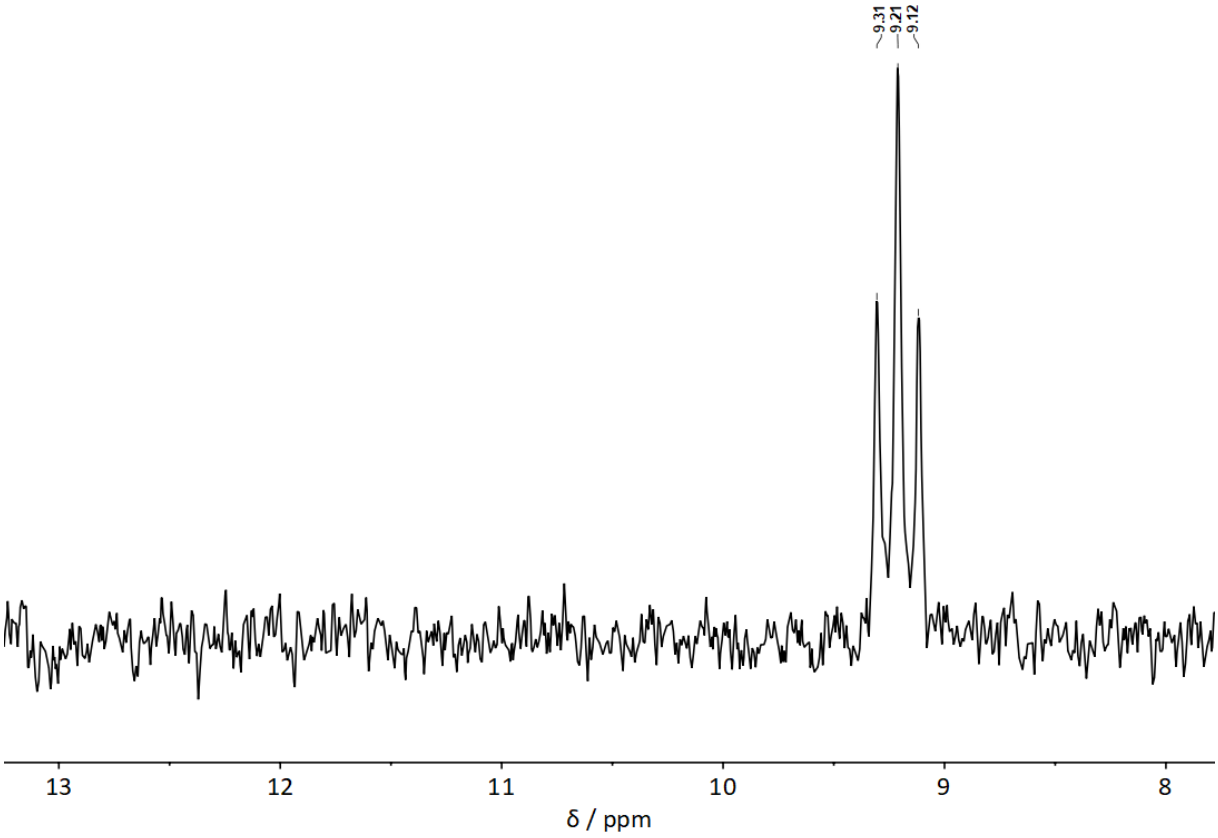

Fig. S23 ^{13}C NMR spectrum of $[(PMe_3)_2BeBr_2]$ (**1b**) in Tol-d_8.

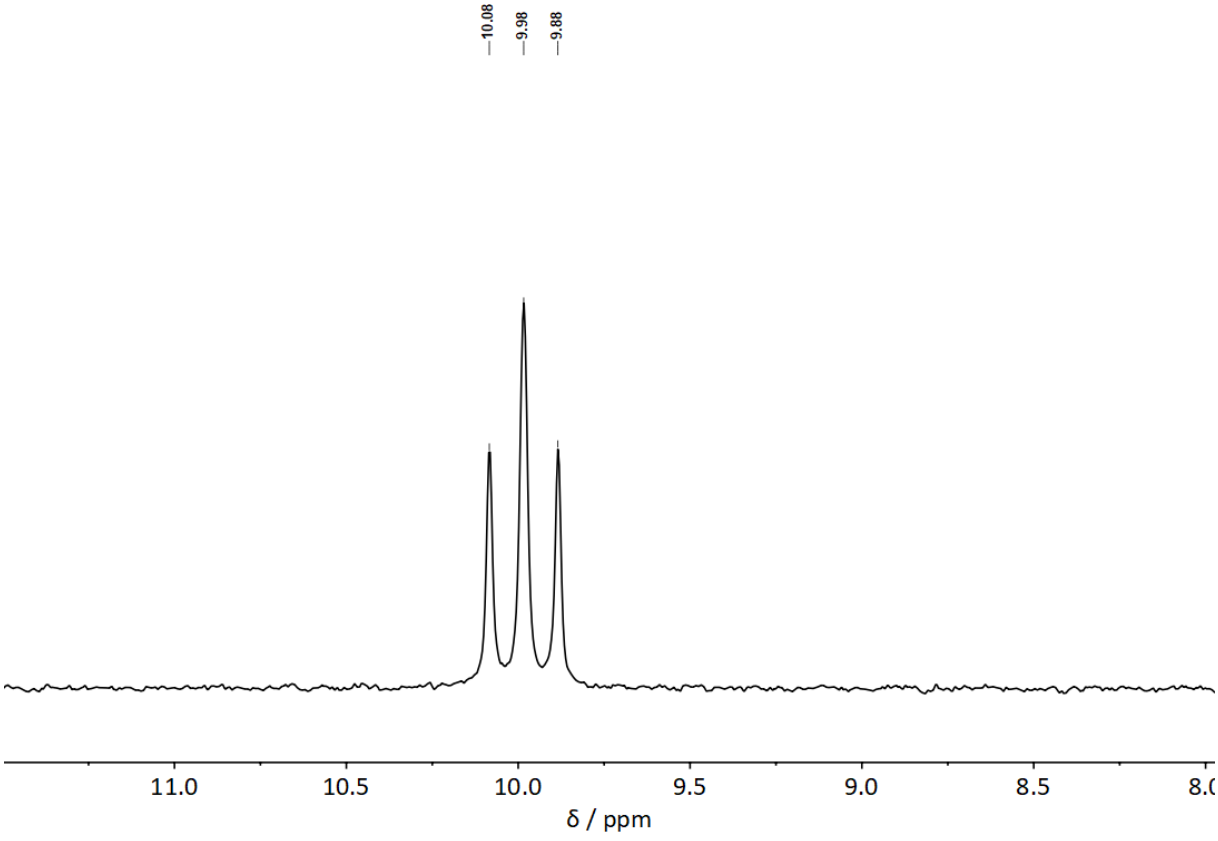

Fig. S24 ^{13}C NMR spectrum of $[(PMe_3)_2BeBr_2]$ (**1b**) in $CDCl_3$.

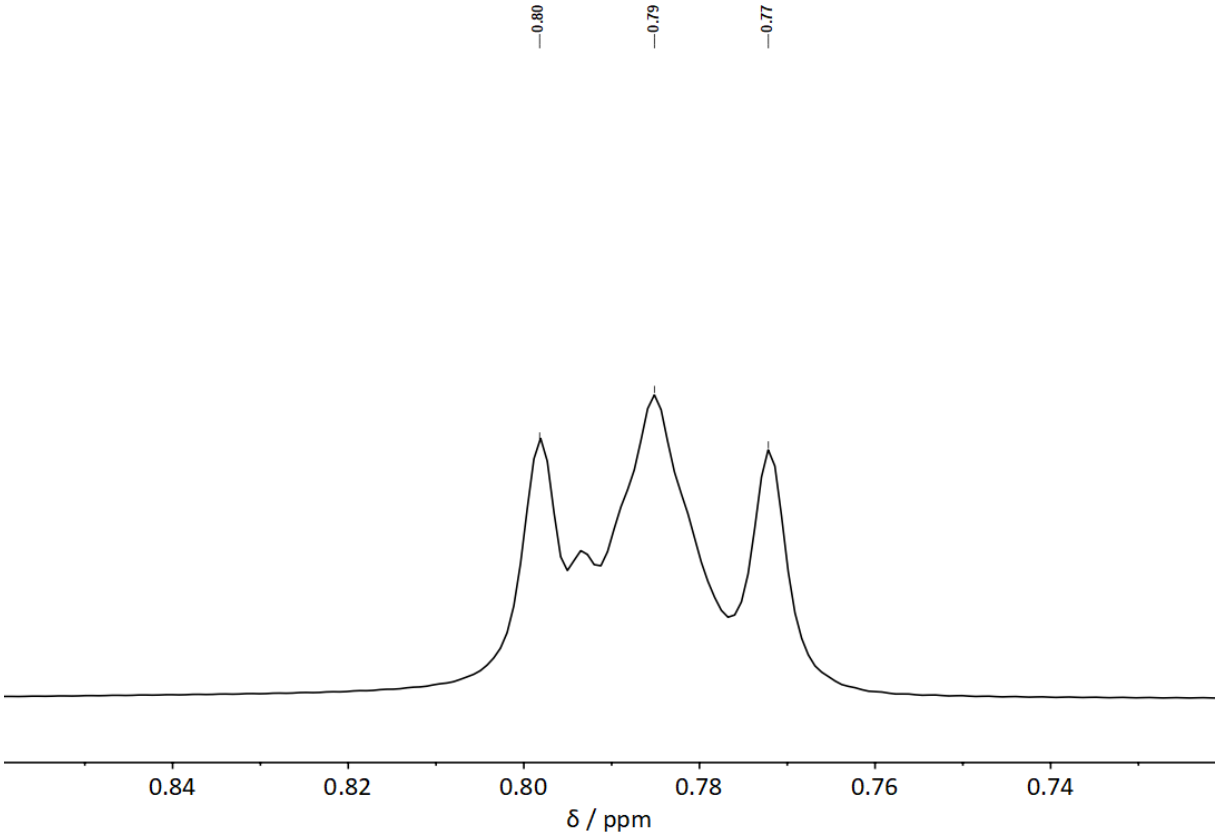

Fig. S25 ^{1}H NMR spectrum of [$(PMe_3)_2BeI_2$] (**1c**) in C_6D_6.

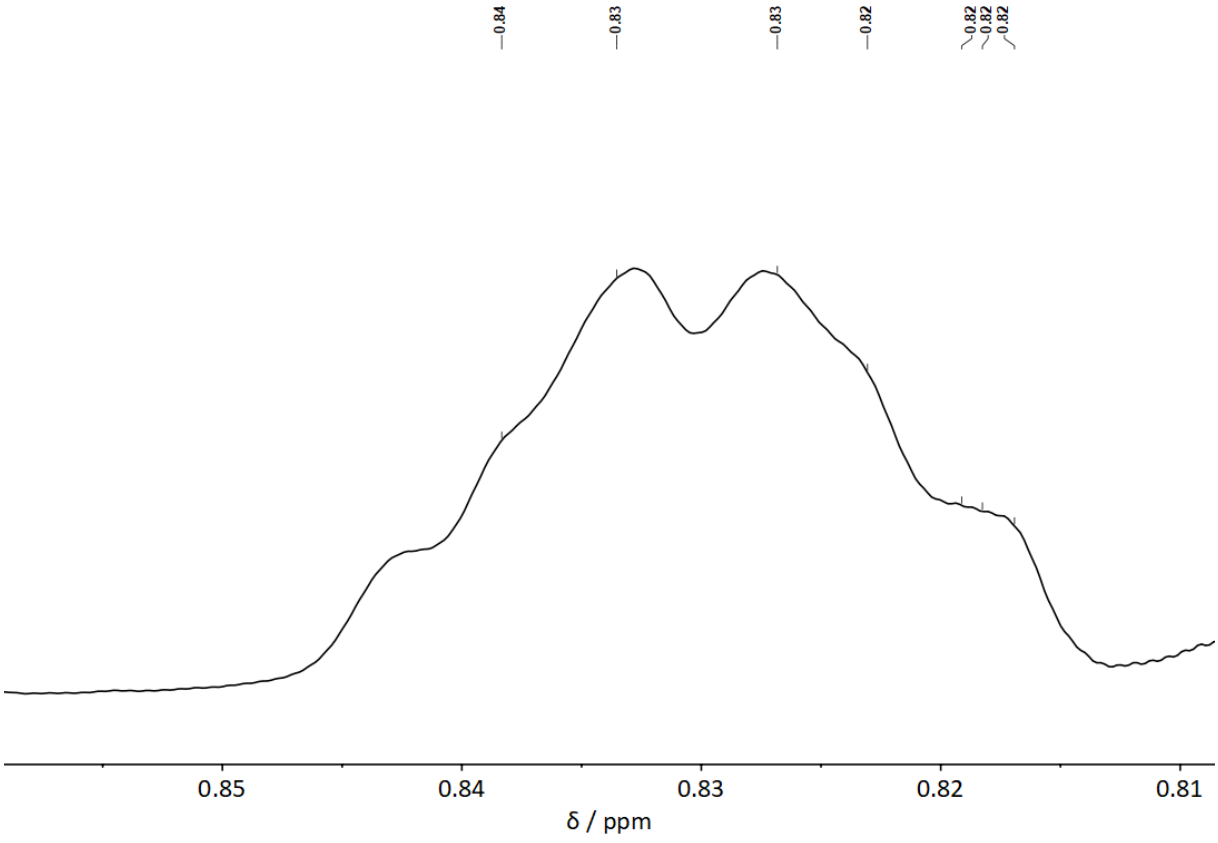

Fig. S26 ^{1}H NMR spectrum of [$(PMe_3)_2BeI_2$] (**1c**) in Tol-d_8.

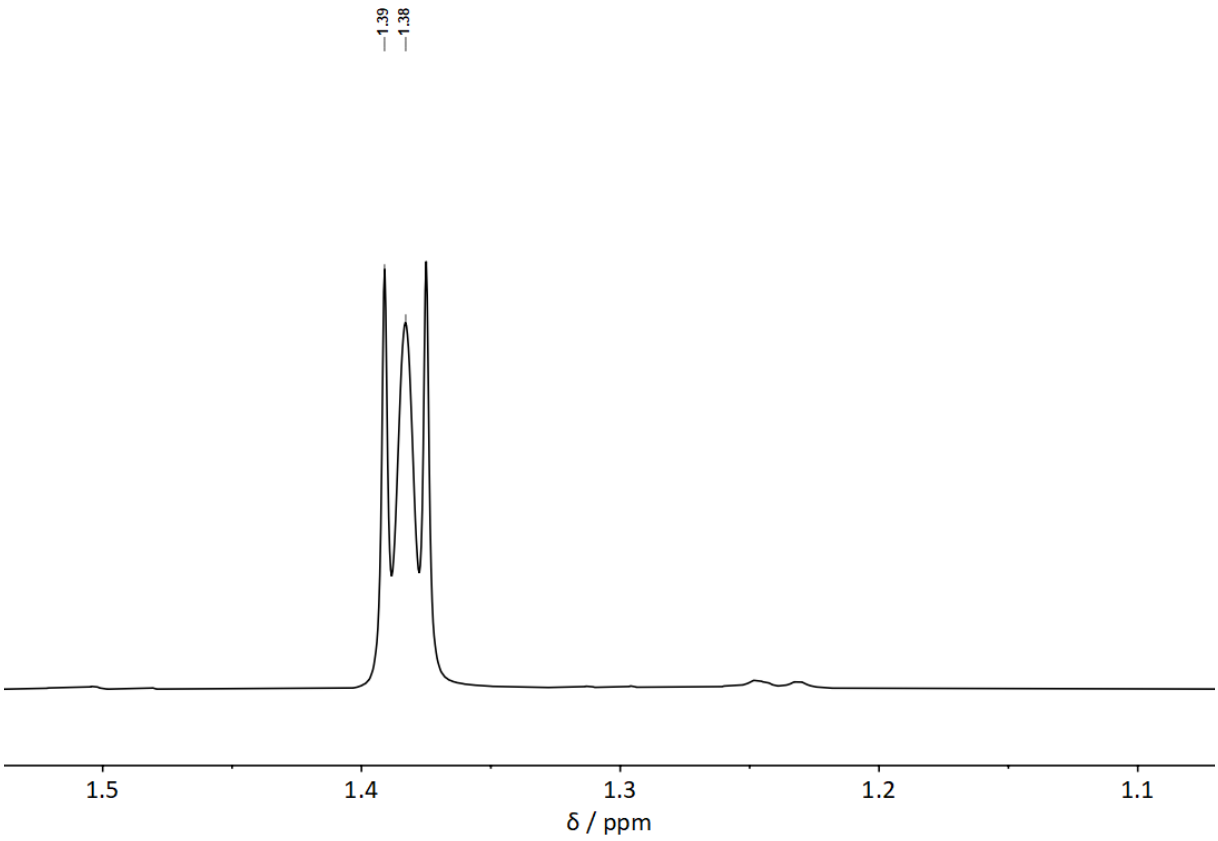

Fig. S27 ^{1}H NMR spectrum of [$(PMe_3)_2BeI_2$] (**1c**) in CD_2Cl_2.

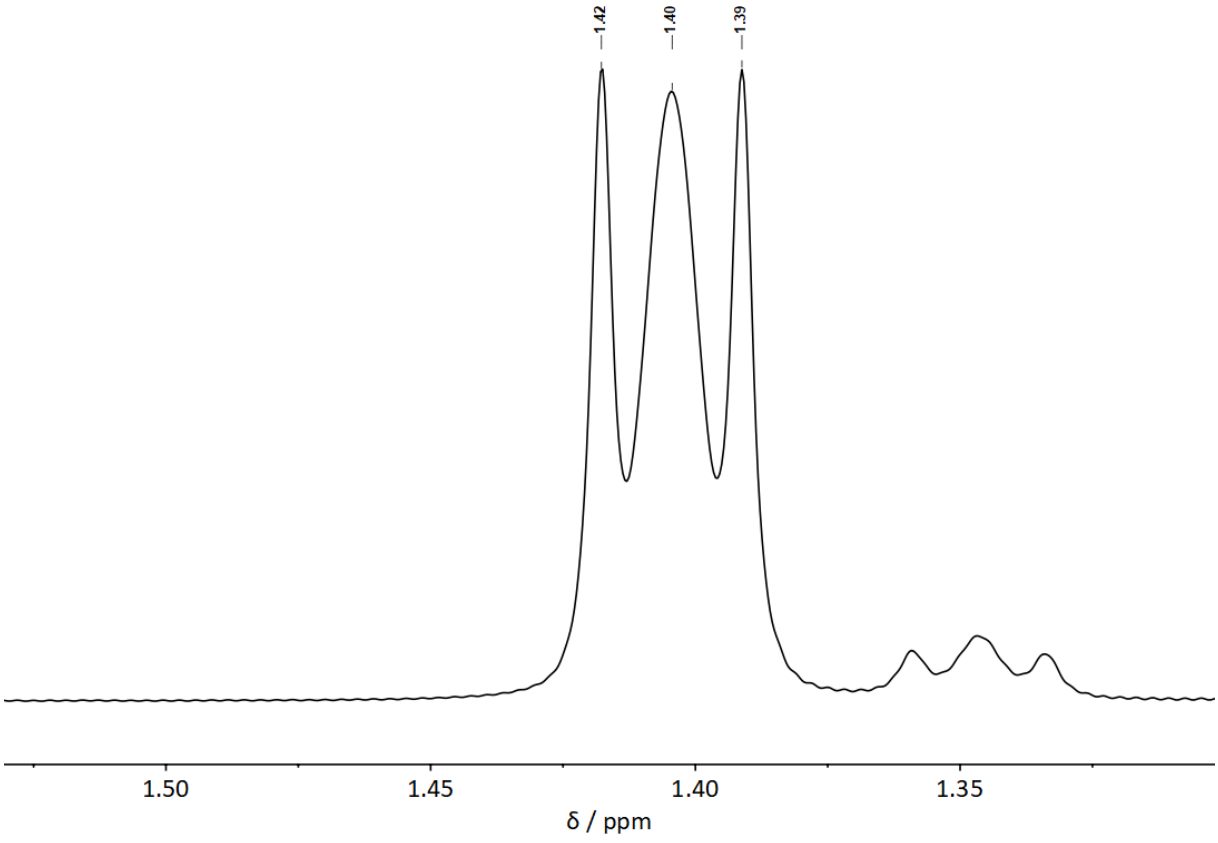

Fig. S28 ^{1}H NMR spectrum of [$(PMe_3)_2BeI_2$] (**1c**) in $CDCl_3$.

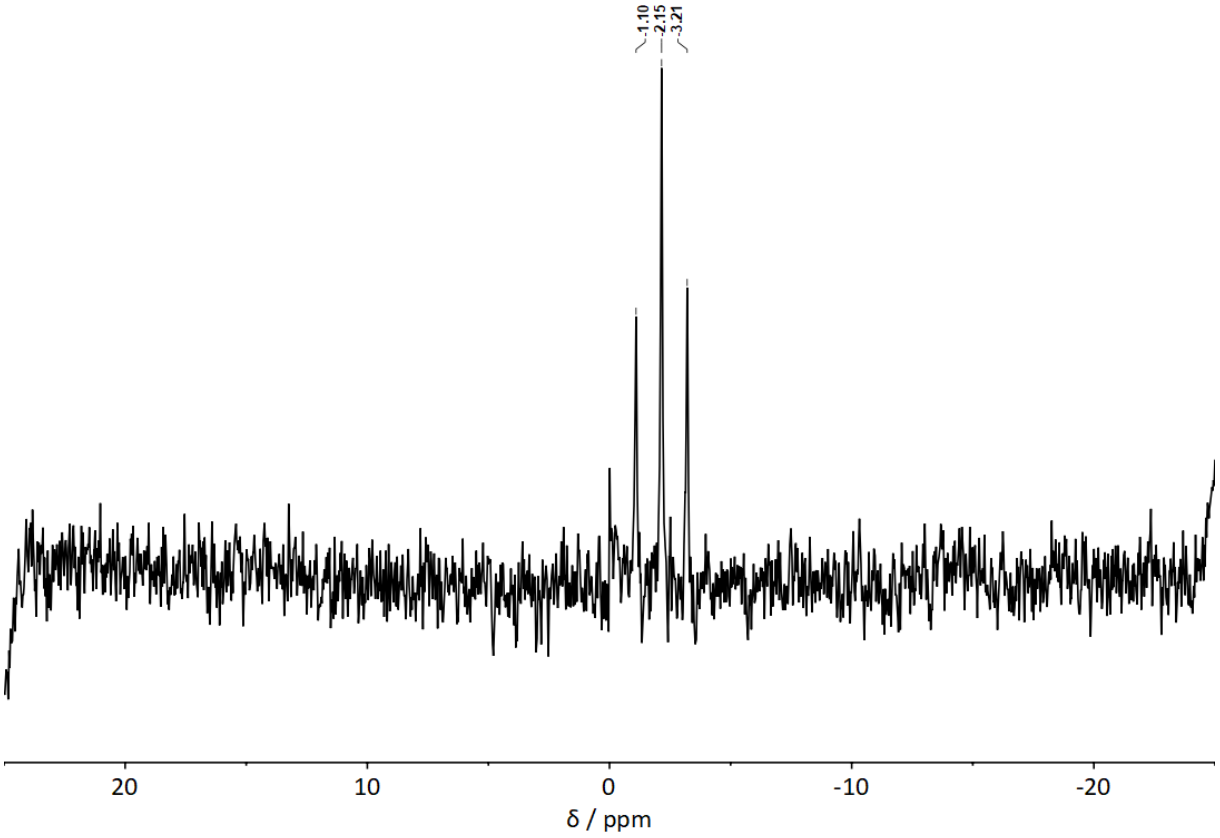

Fig. S29 ^{9}Be NMR spectrum of [$(PMe_3)_2BeI_2$] (**1c**) in C_6D_6.

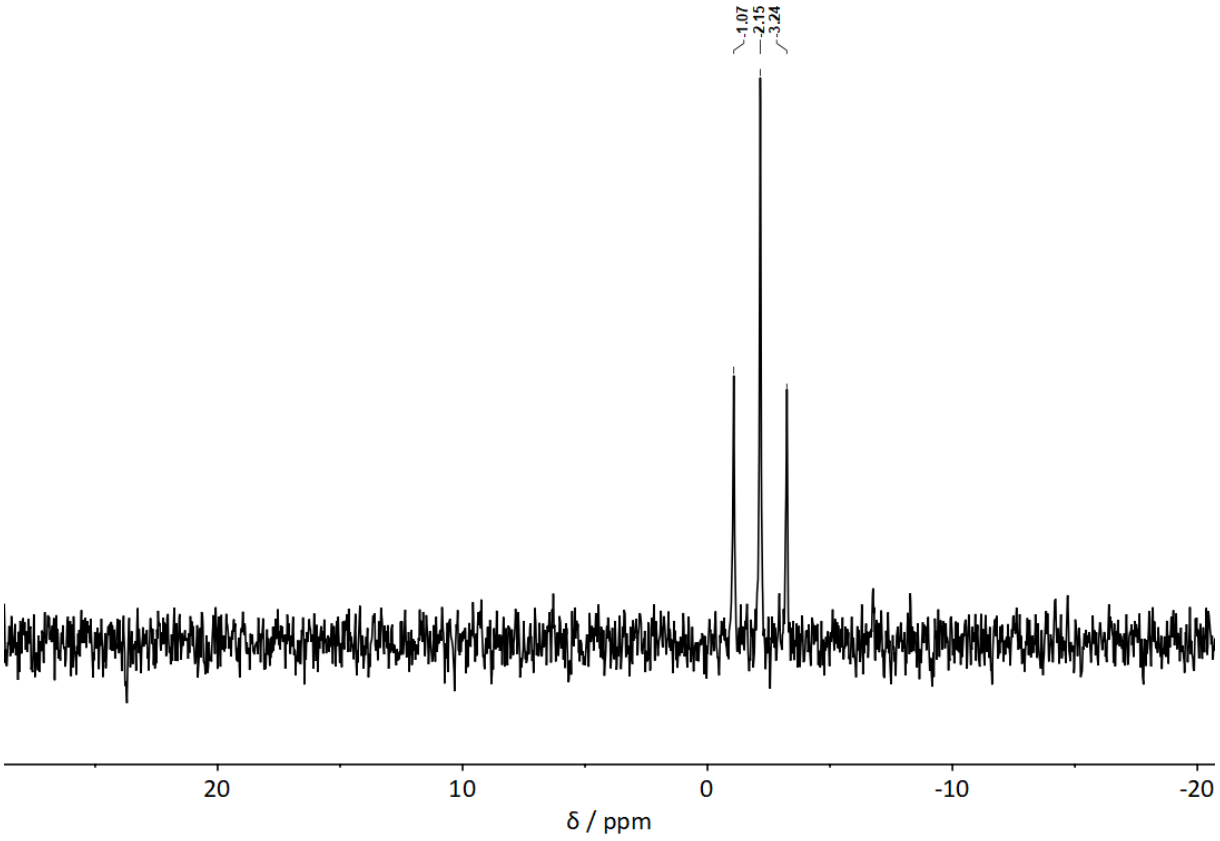

Fig. S30 ^{9}Be NMR spectrum of [$(PMe_3)_2BeI_2$] (**1c**) in CD_2Cl_2.

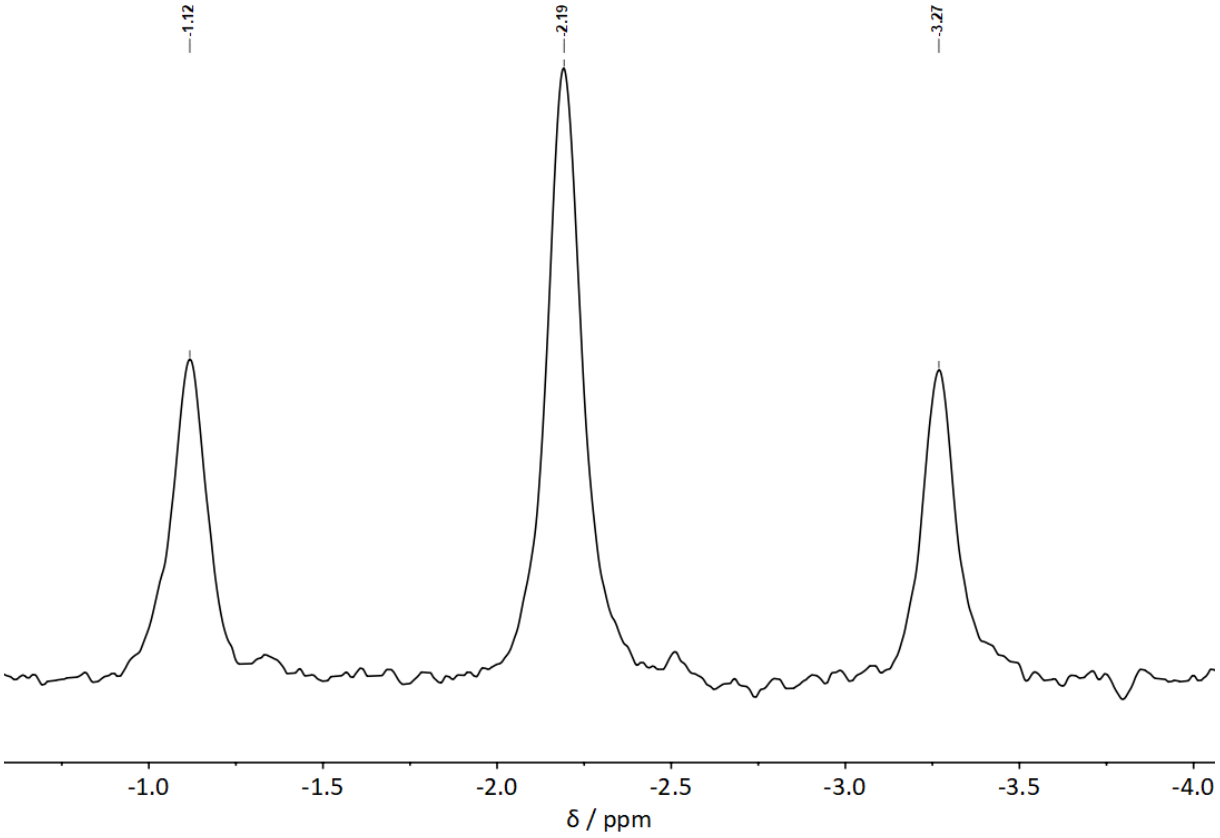

Fig. S31 ^{9}Be NMR spectrum of [$(PMe_3)_2BeI_2$] (**1c**) in $CDCl_3$.

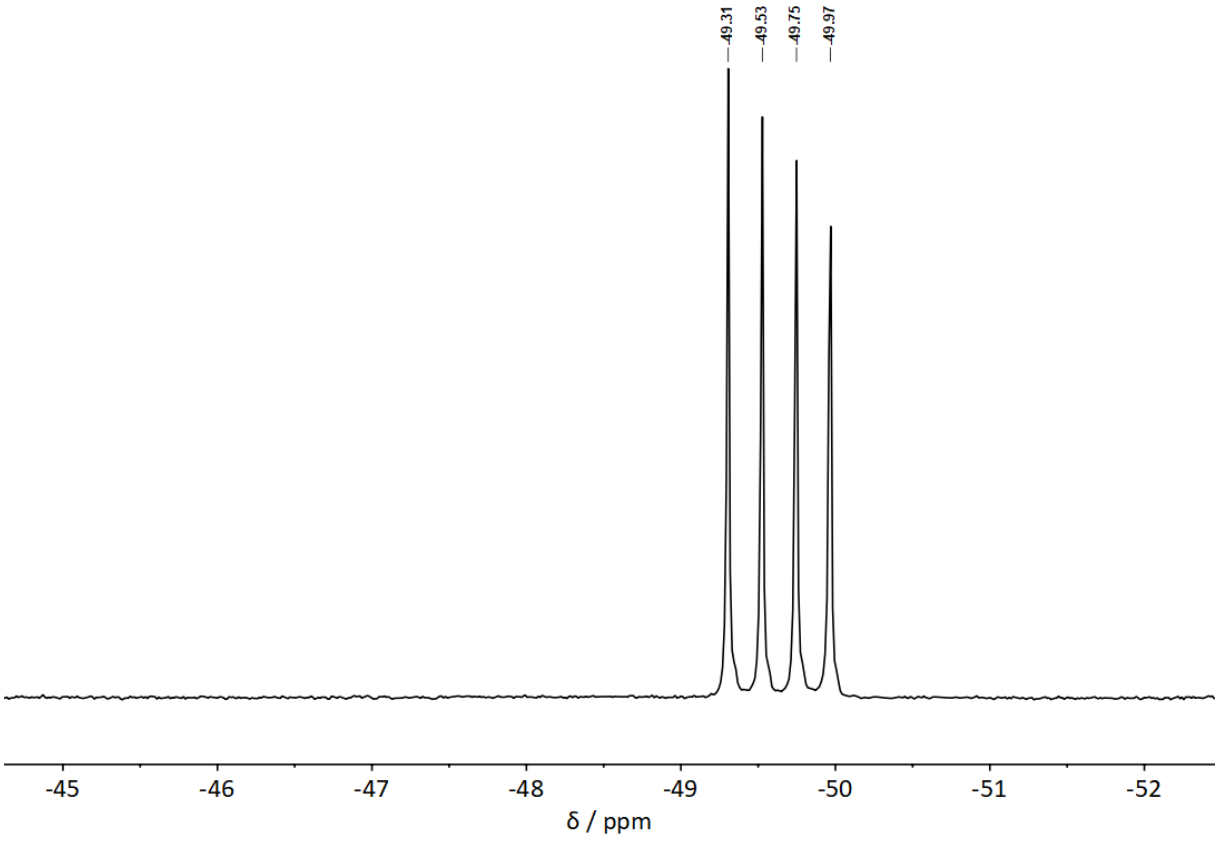

Fig. S32 ^{31}P NMR spectrum of [$(PMe_3)_2BeI_2$] (**1c**) in C_6D_6.

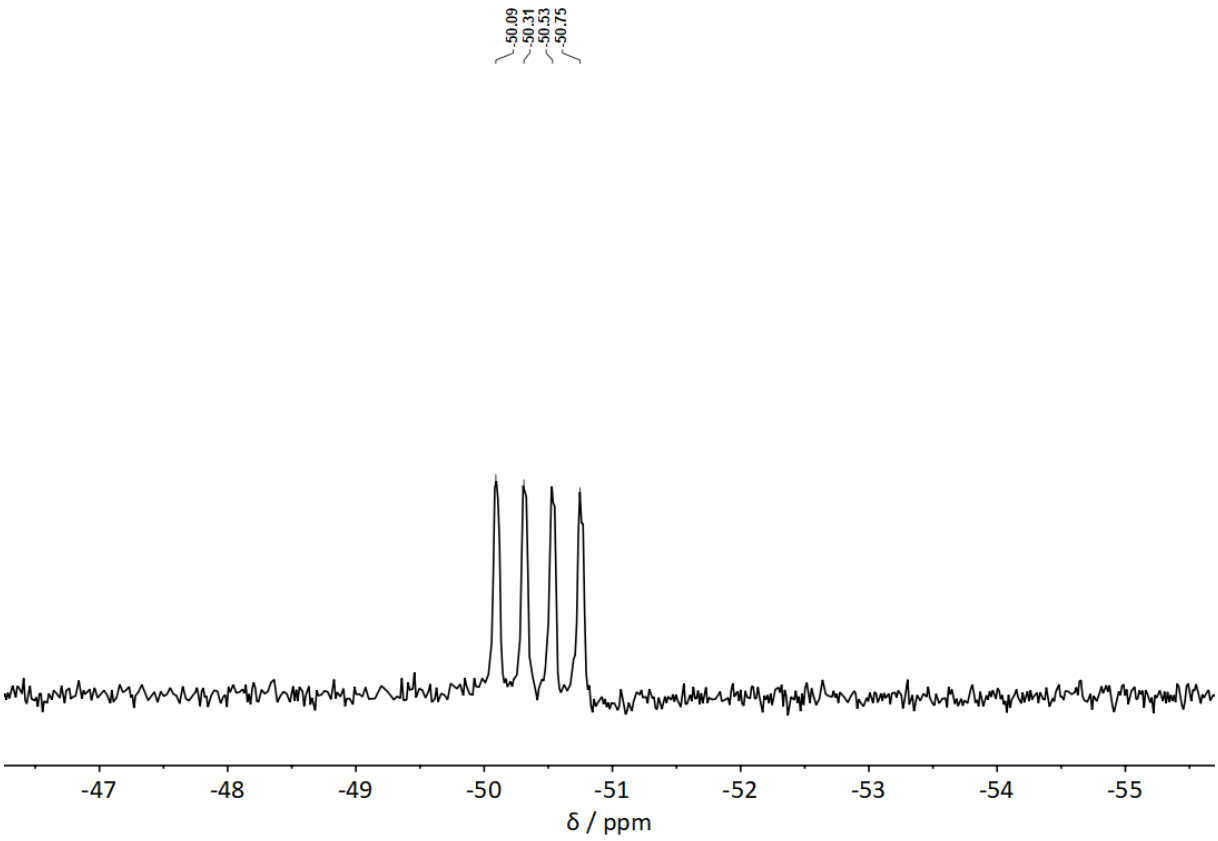

Fig. S33 ^{31}P NMR spectrum of [$(PMe_3)_2BeI_2$] (**1c**) in Tol-d_8.

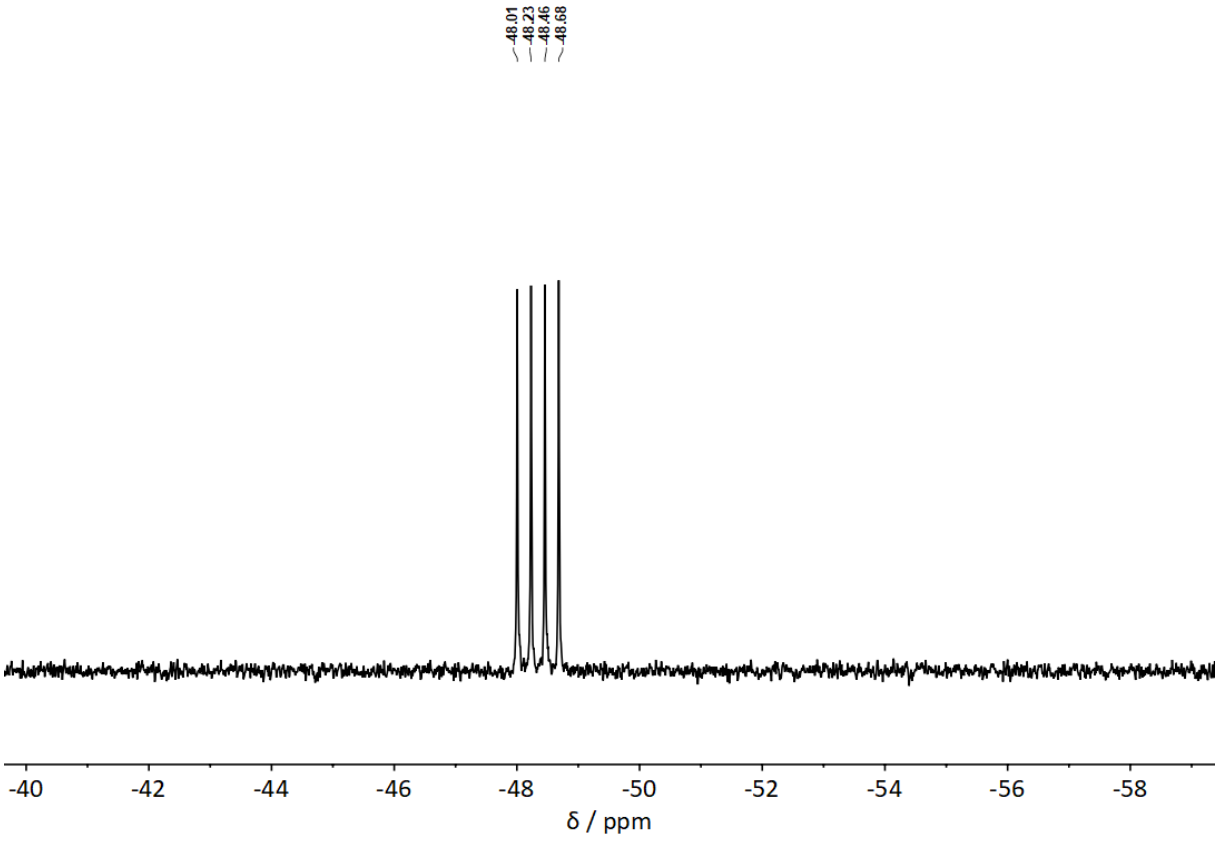

Fig. S34 ^{31}P NMR spectrum of [$(PMe_3)_2BeI_2$] (**1c**) in CD_2Cl_2.

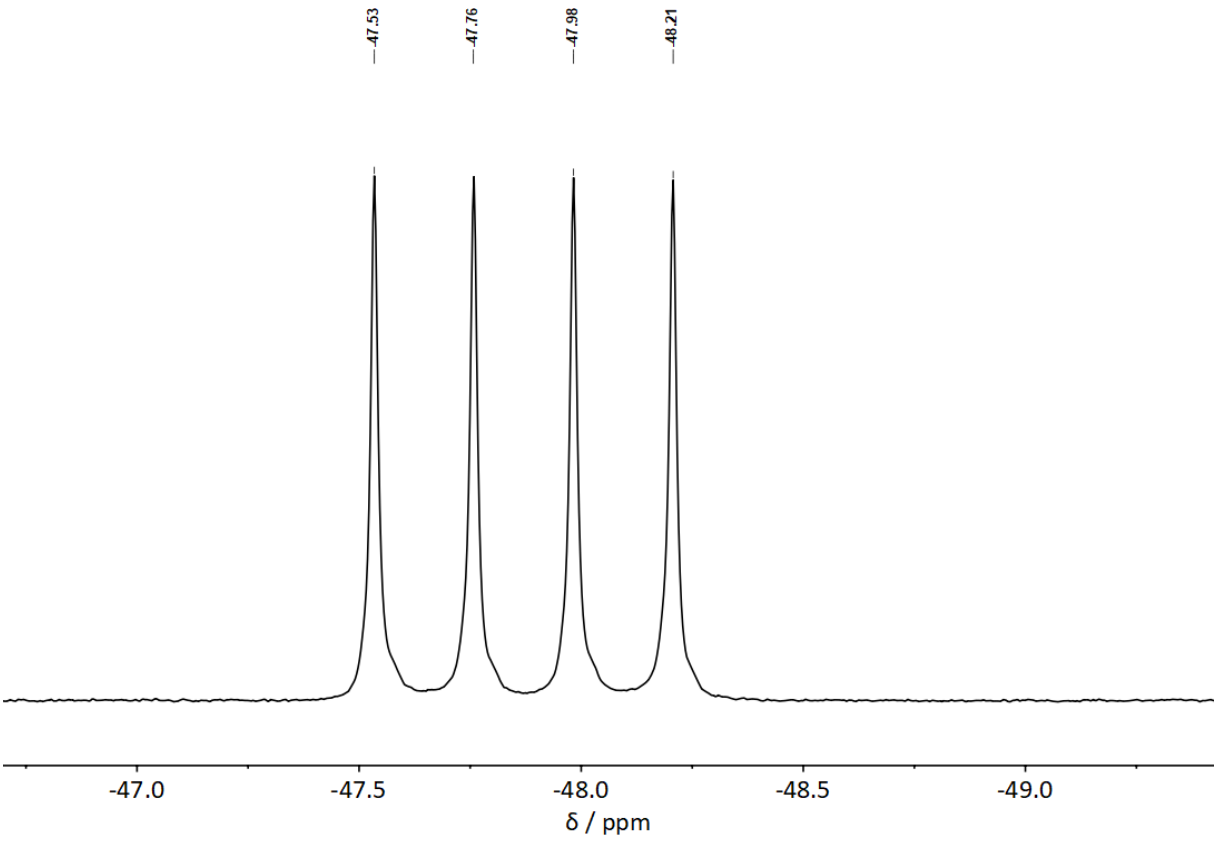

Fig. S35 ^{31}P NMR spectrum of [$(PMe_3)_2BeI_2$] (**1c**) in $CDCl_3$.

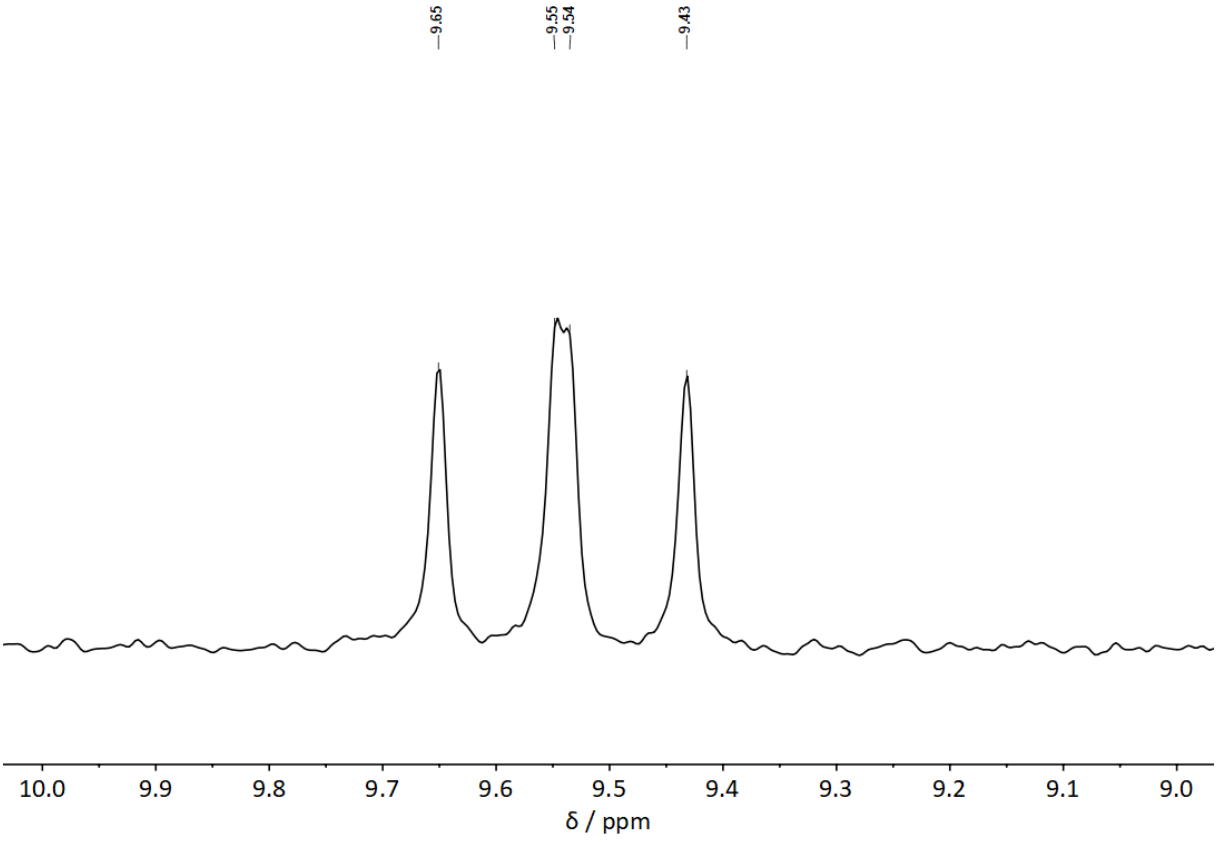

Fig. S36 ^{13}C NMR spectrum of [$(PMe_3)_2BeI_2$] (**1c**) in C_6D_6.

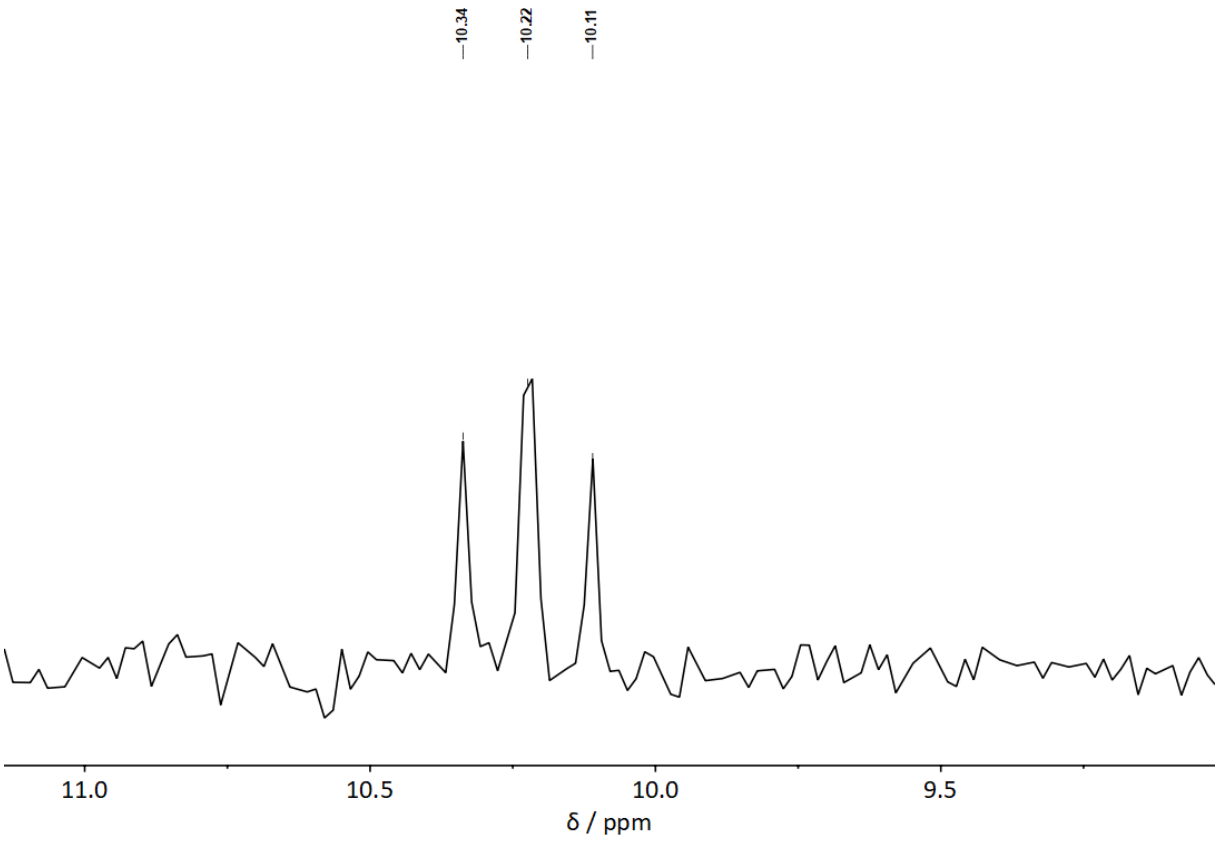

Fig. S37 ^{13}C NMR spectrum of $[(PMe_3)_2BeI_2]$ (**1c**) in CD_2Cl_2.

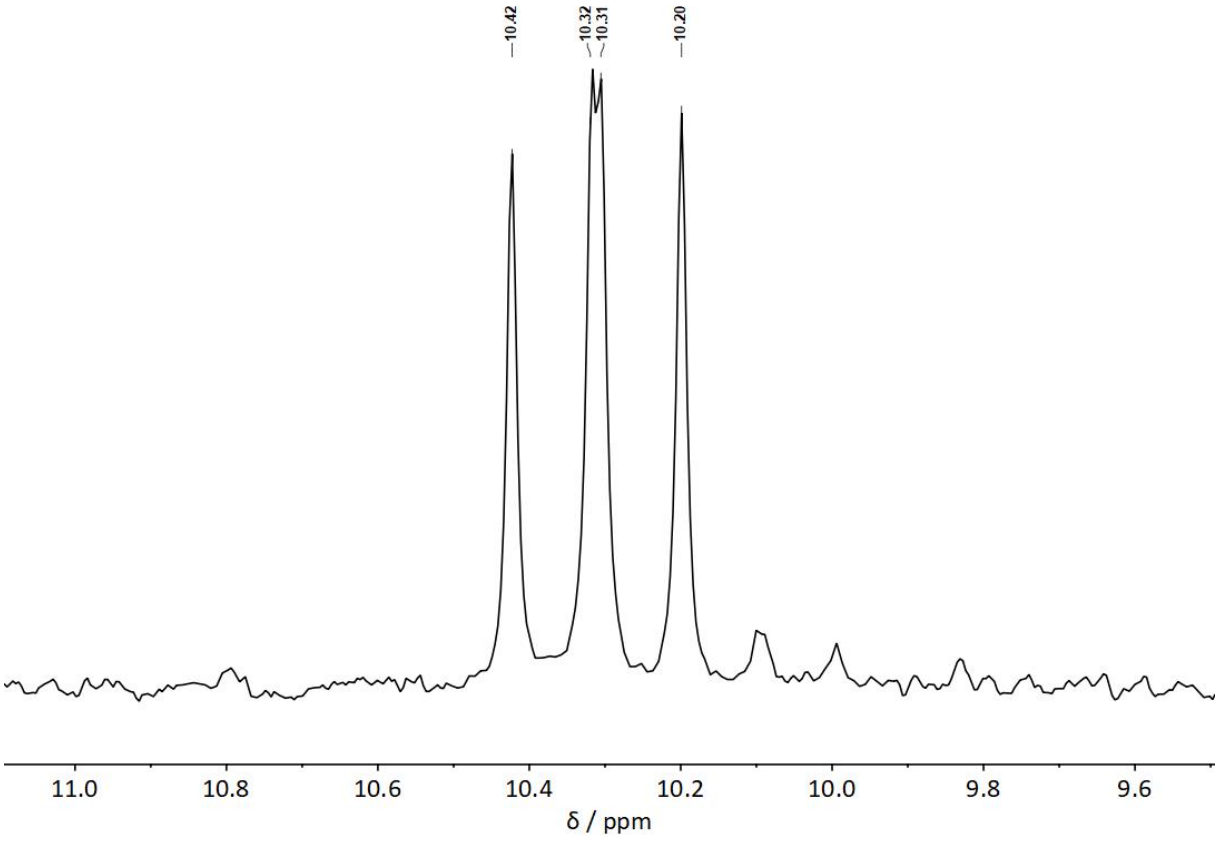

Fig. S38 ^{13}C NMR spectrum of $[(PMe_3)_2BeI_2]$ (**1c**) in $CDCl_3$.

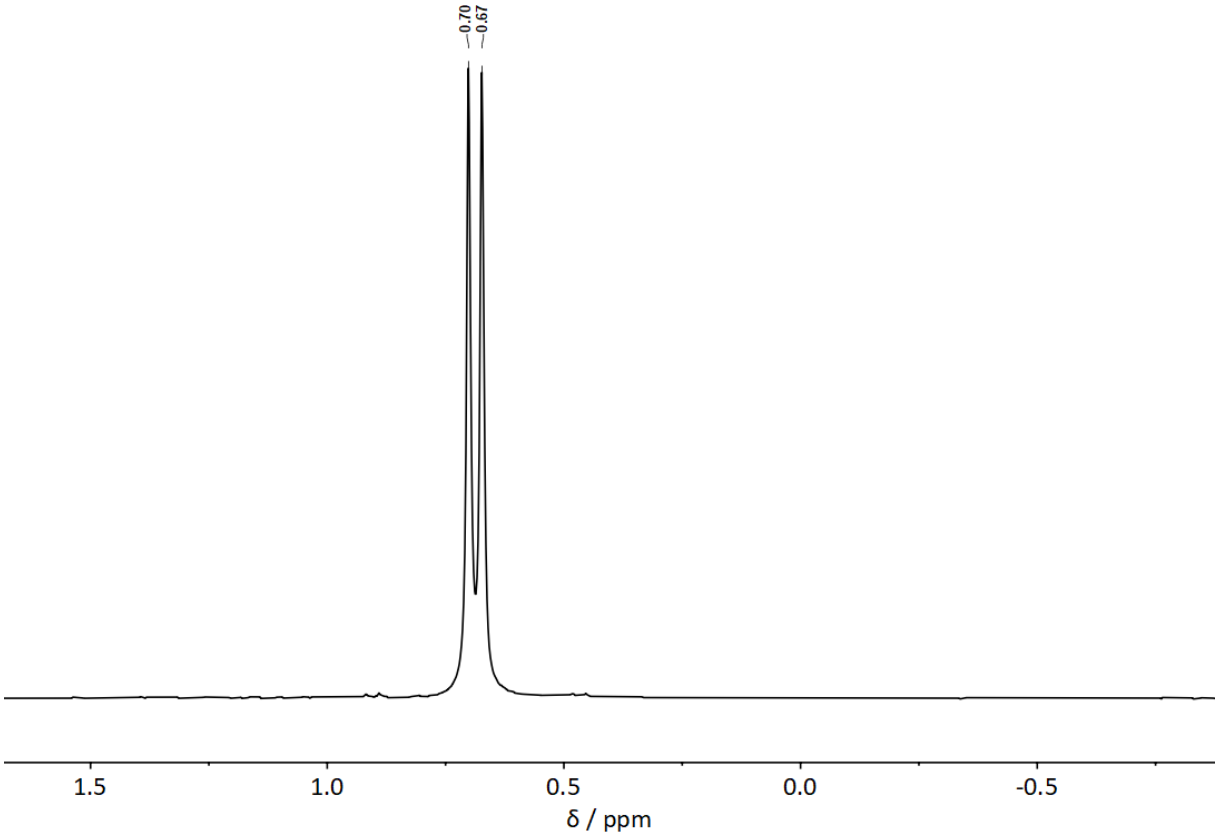

Fig. S39 ^{1}H NMR spectrum of $[(PMe_3)BeCl_2]_2$ (**2a**) in C_6D_6.

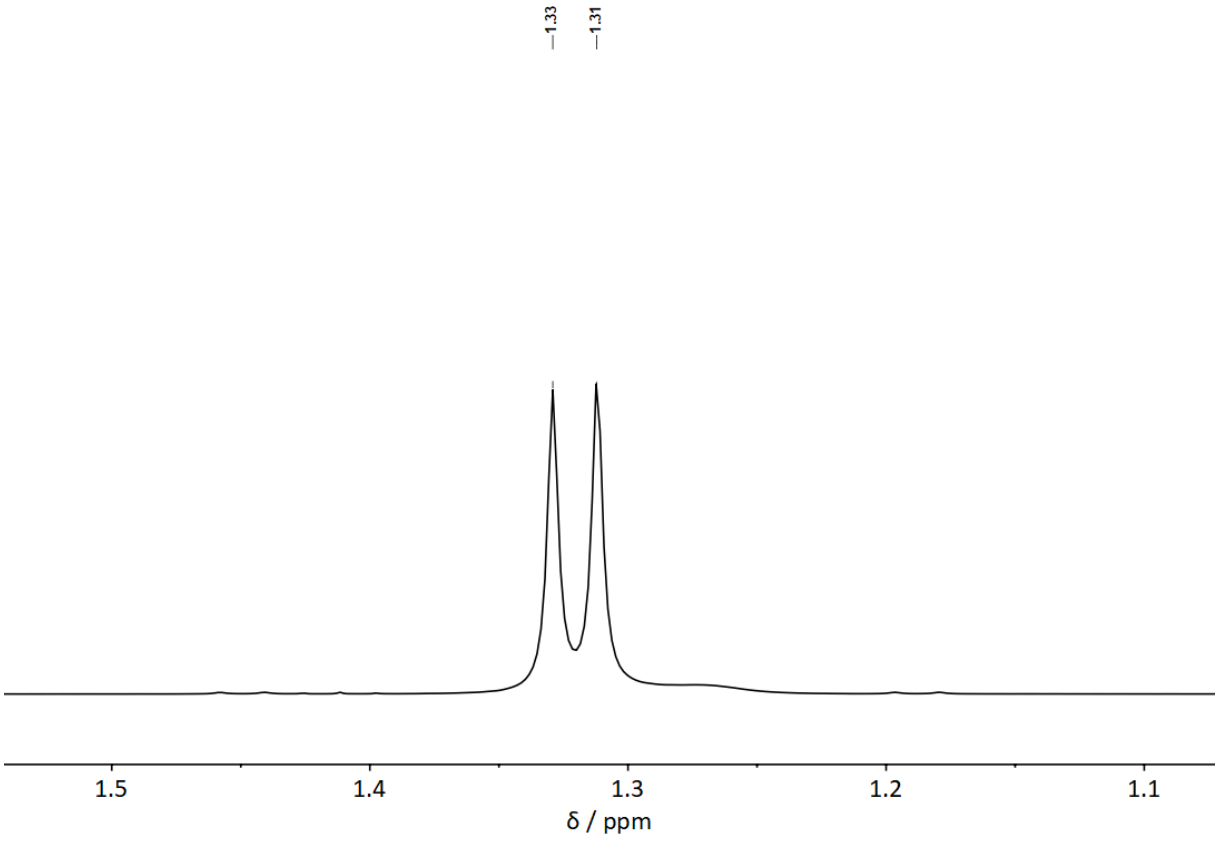

Fig. S40 ^{1}H NMR spectrum of $[(PMe_3)BeCl_2]_2$ (**2a**) in CD_2Cl_2.

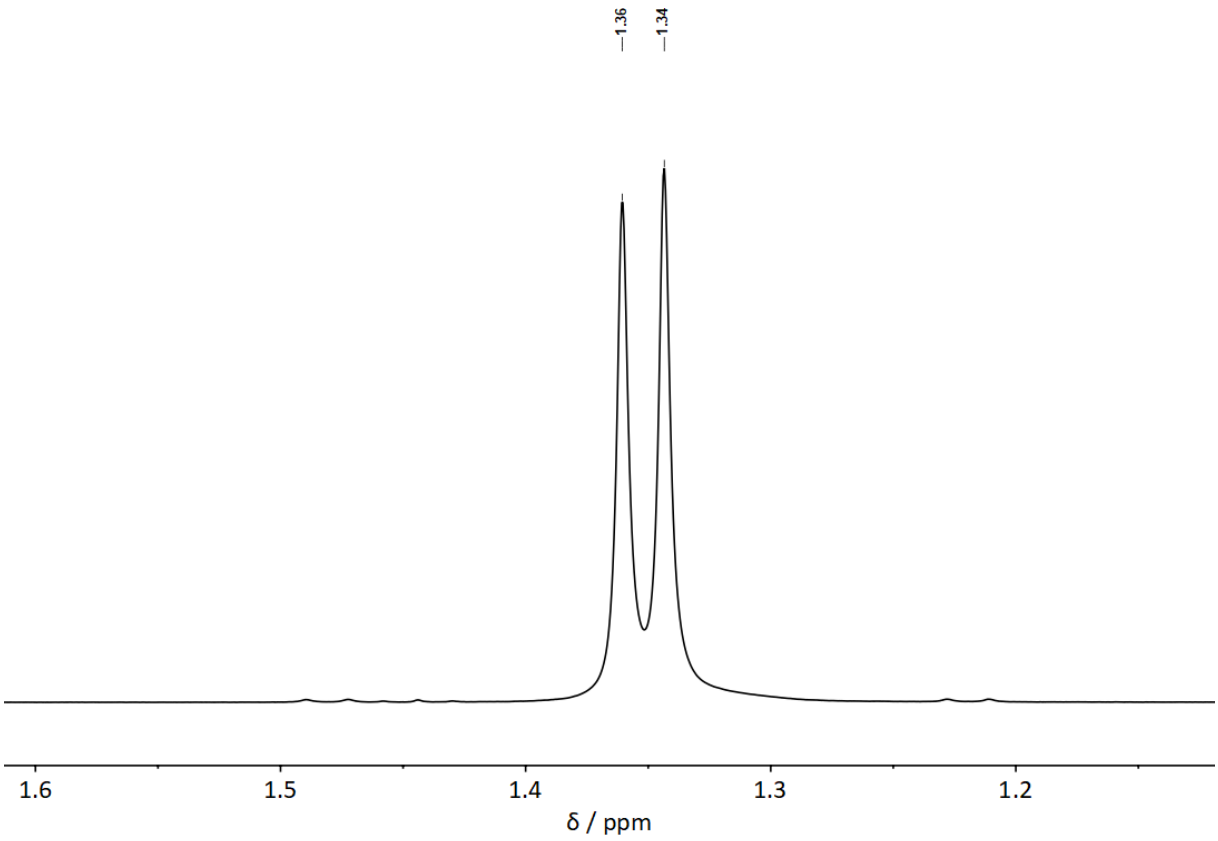

Fig. S41 ^{1}H NMR spectrum of $[(PMe_3)BeCl_2]_2$ (**2a**) in $CDCl_3$.

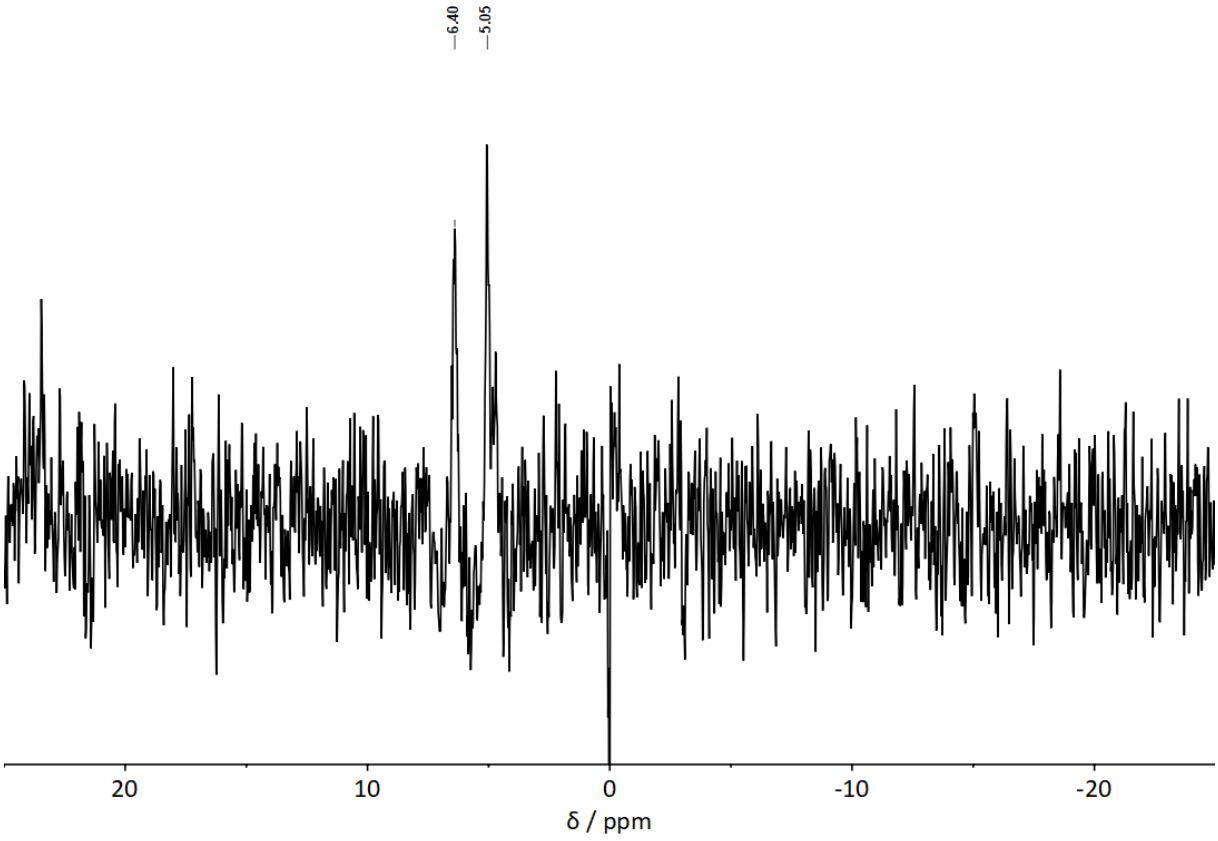

Fig. S42 ^{9}Be NMR spectrum of $[(PMe_3)BeCl_2]_2$ (**2a**) in C_6D_6.

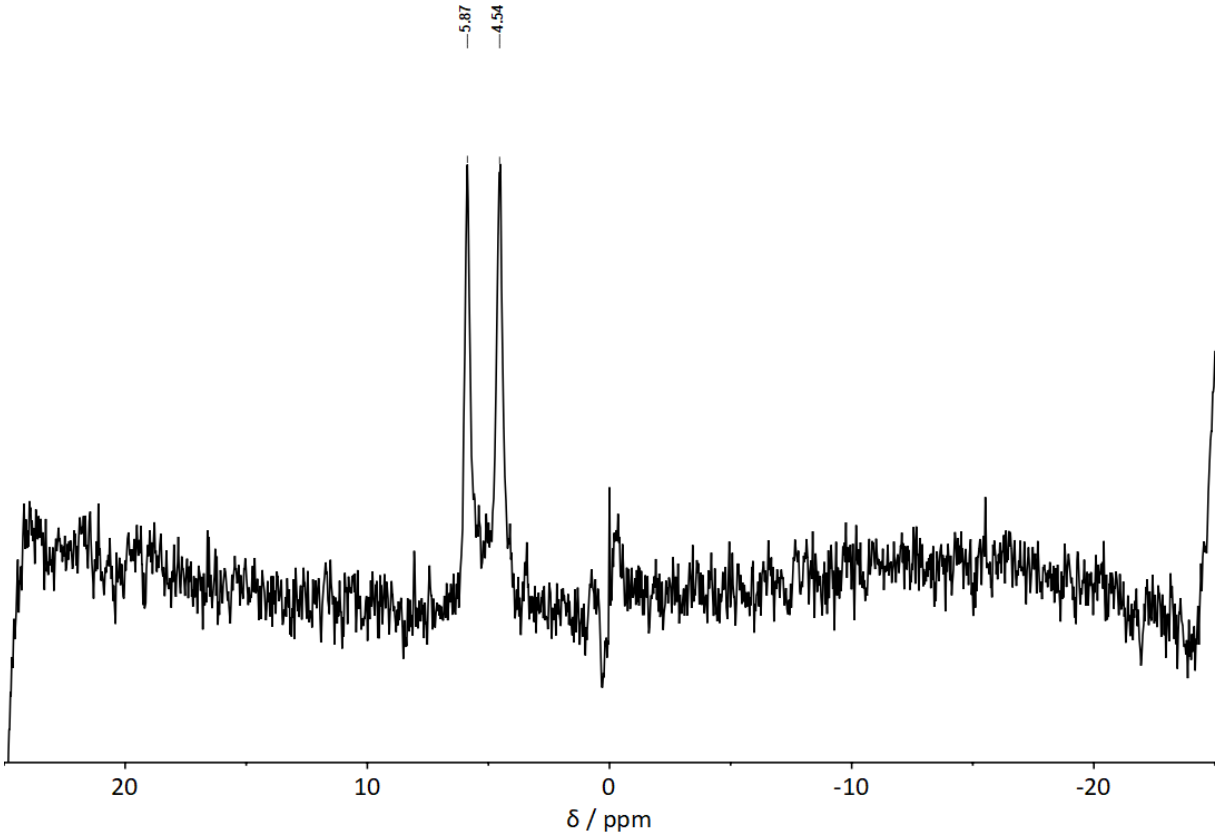

Fig. S43 ^{9}Be NMR spectrum of $[(PMe_3)BeCl_2]_2$ (**2a**) in CD_2Cl_2.

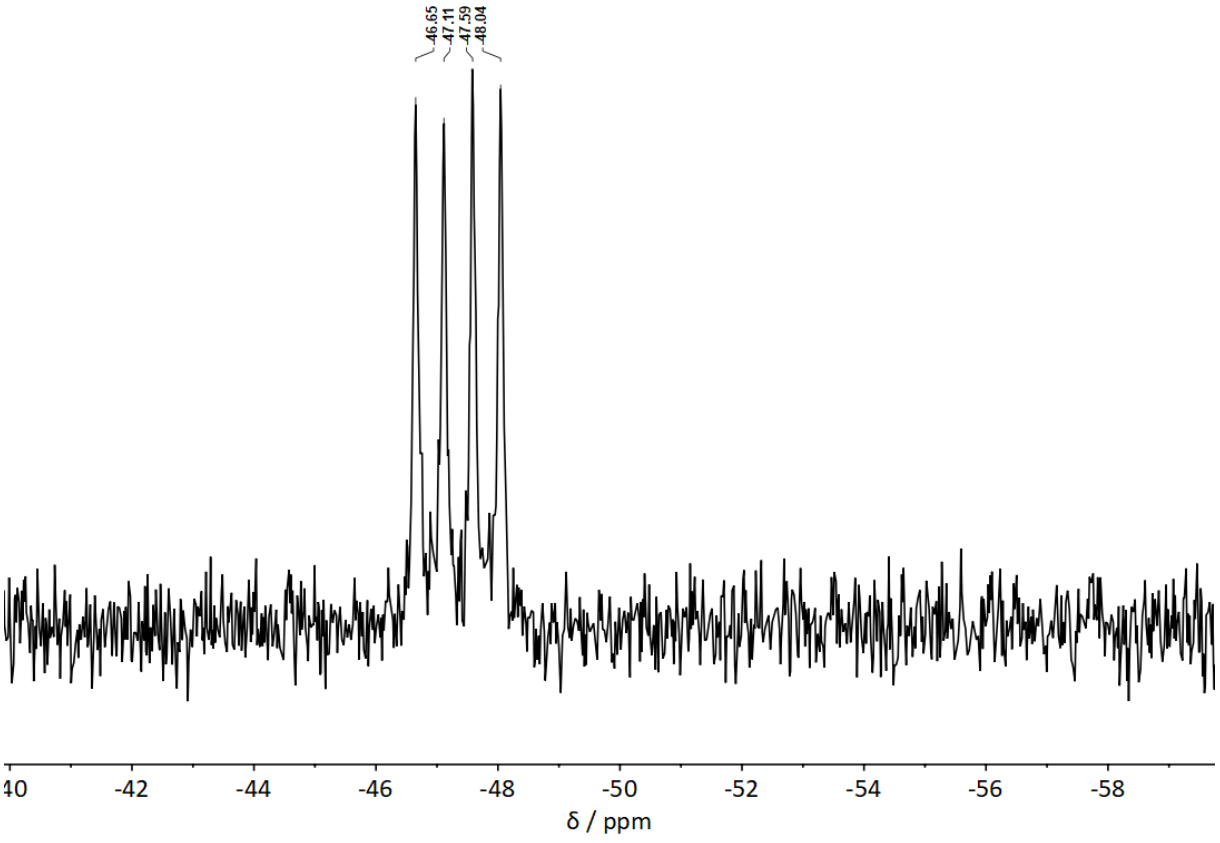

Fig. S44 ^{31}P NMR spectrum of $[(PMe_3)BeCl_2]_2$ (**2a**) in C_6D_6.

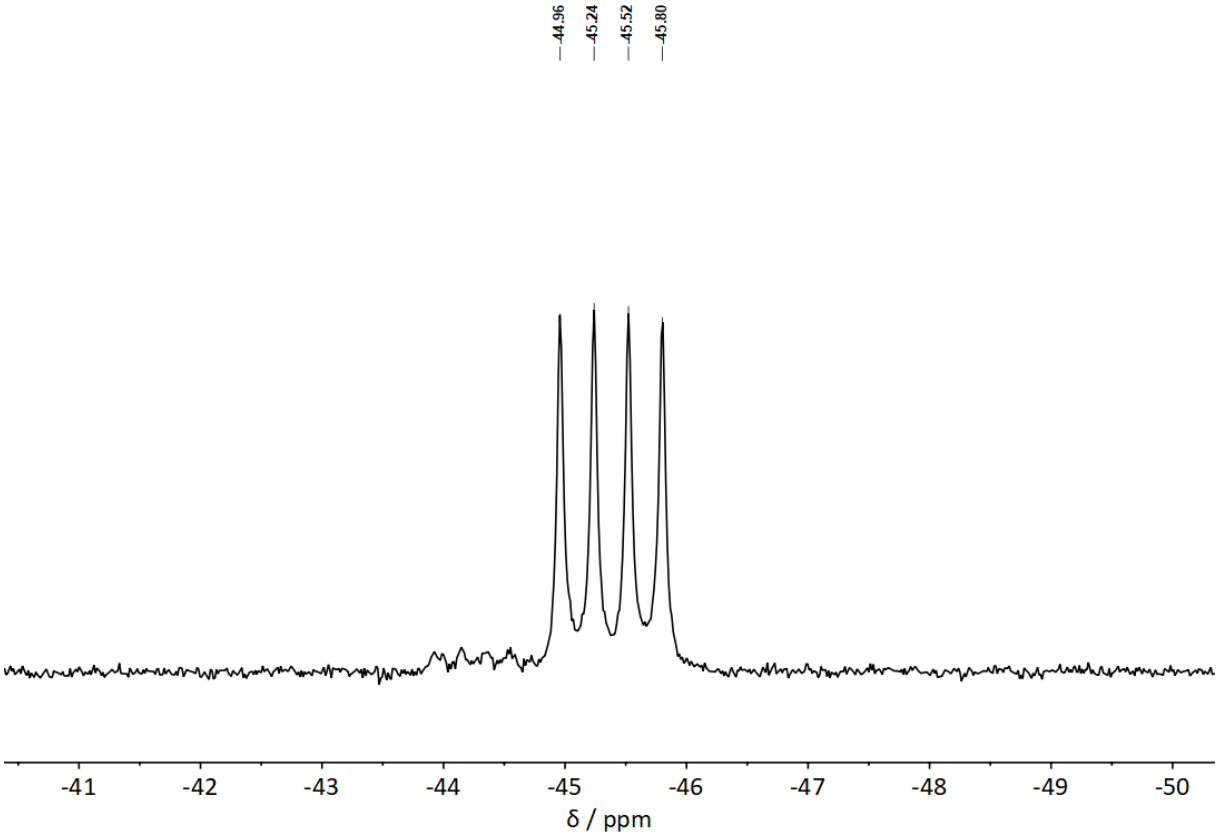

Fig. S45 ^{31}P NMR spectrum of $[(PMe_3)BeCl_2]_2$ (**2a**) in CD_2Cl_2.

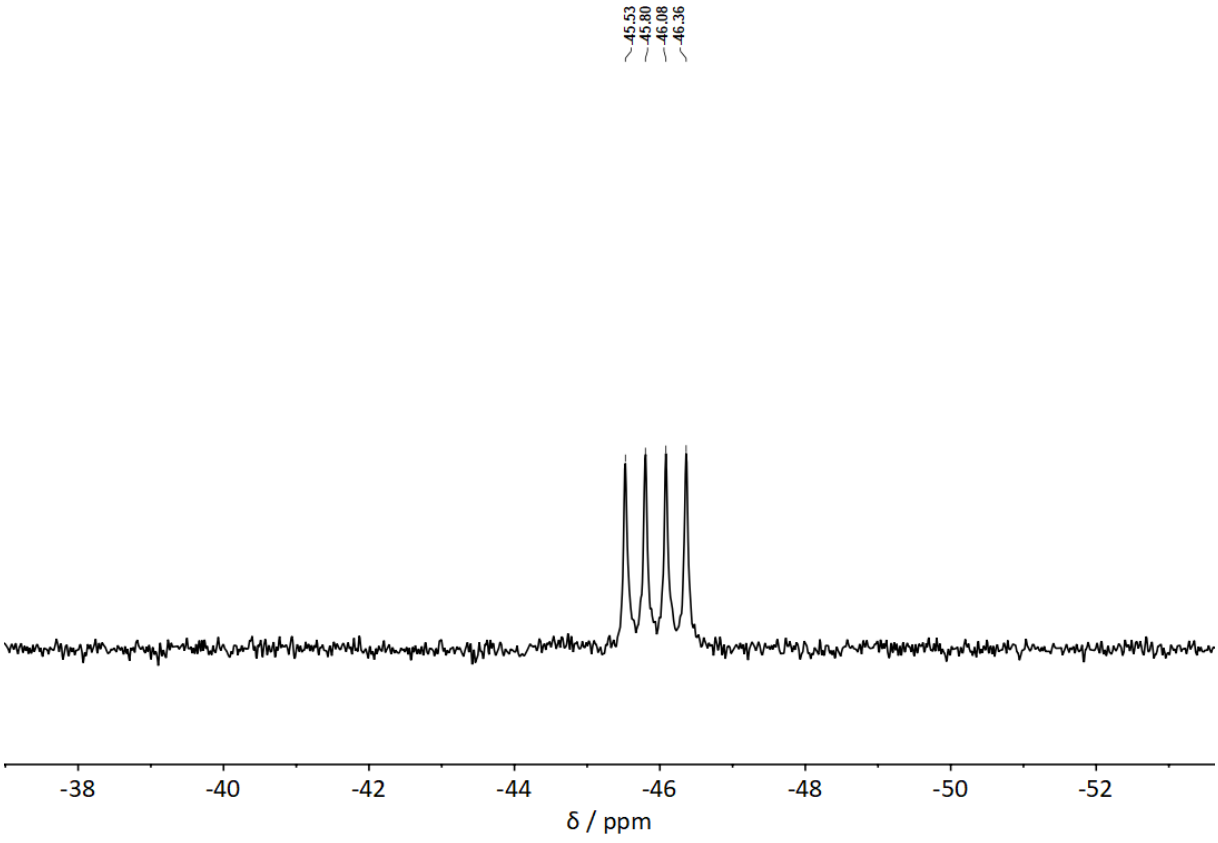

Fig. S46 ^{31}P NMR spectrum of $[(PMe_3)BeCl_2]_2$ (**2a**) in $CDCl_3$.

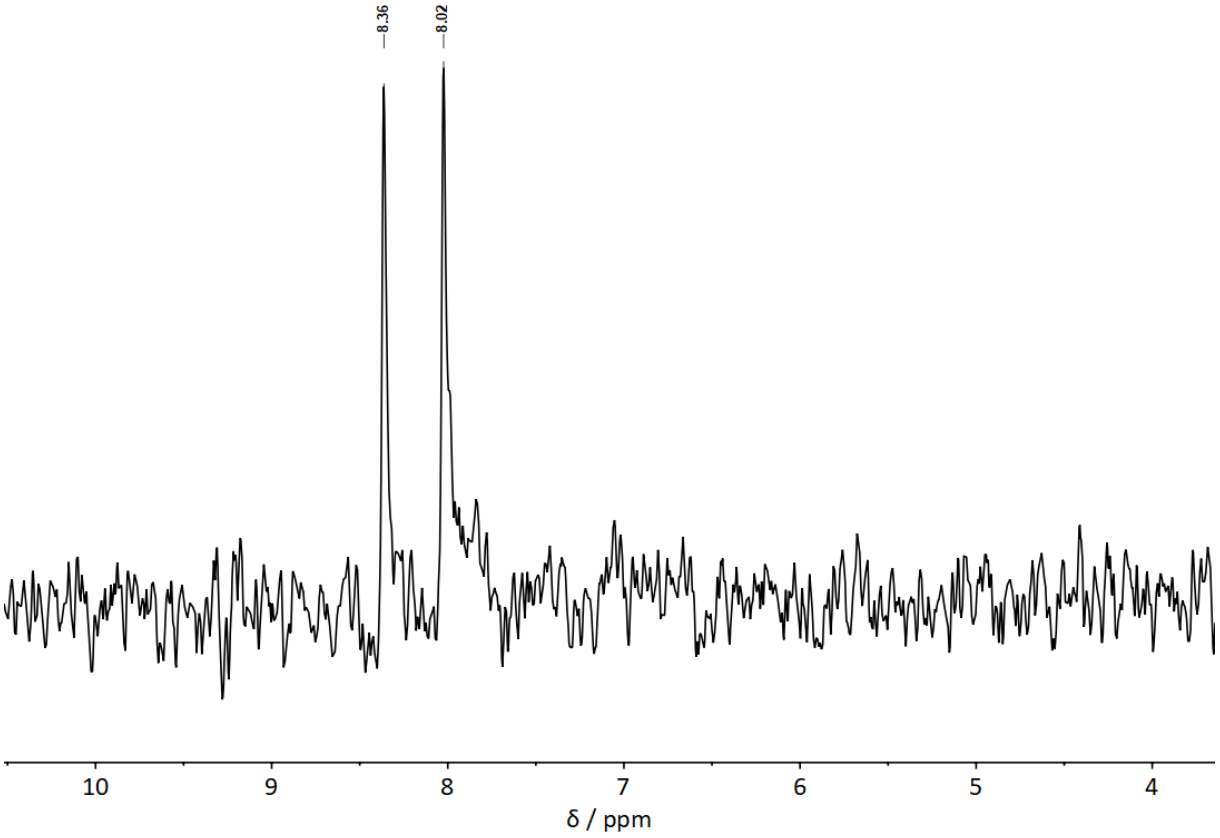

Fig. S47 ^{13}C NMR spectrum of $[(PMe_3)BeCl_2]_2$ (**2a**) in C_6D_6.

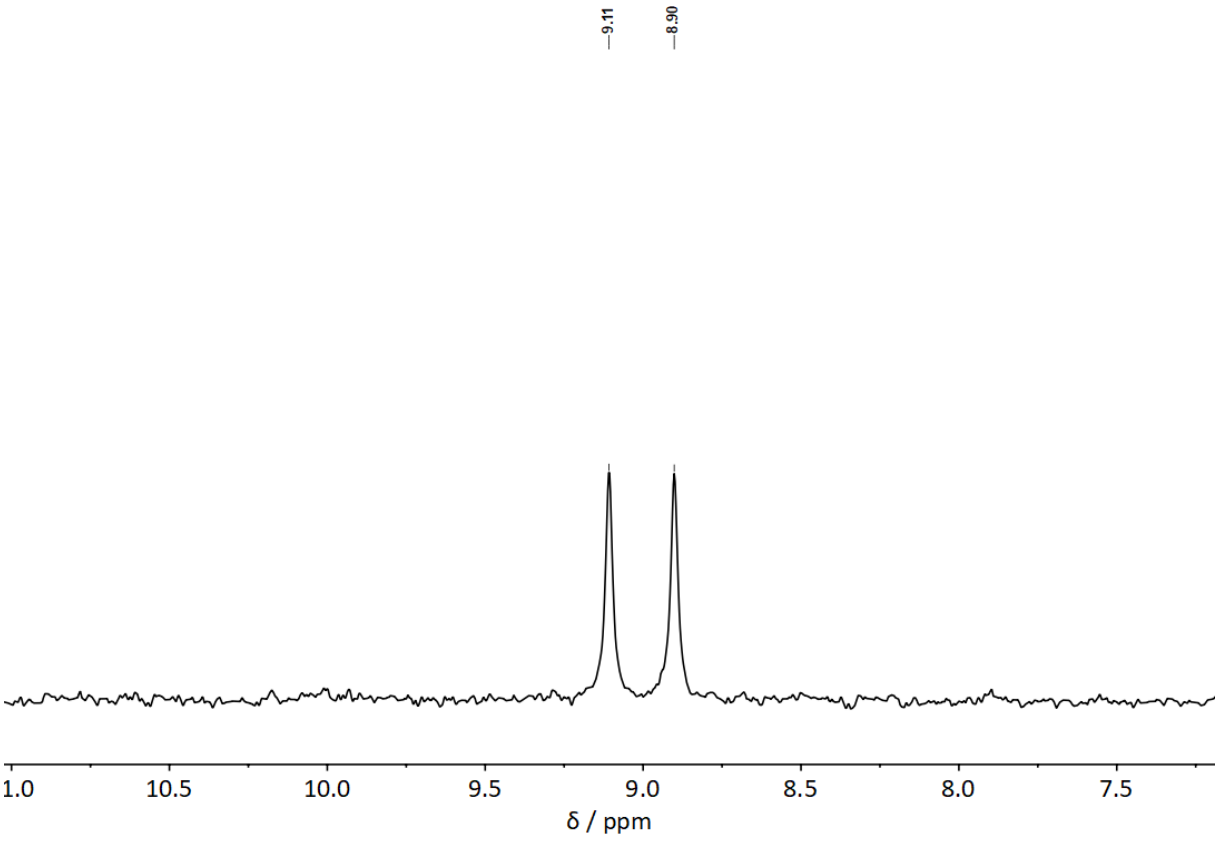

Fig. S48 ^{13}C NMR spectrum of $[(PMe_3)BeCl_2]_2$ (**2a**) in CD_2Cl_2.

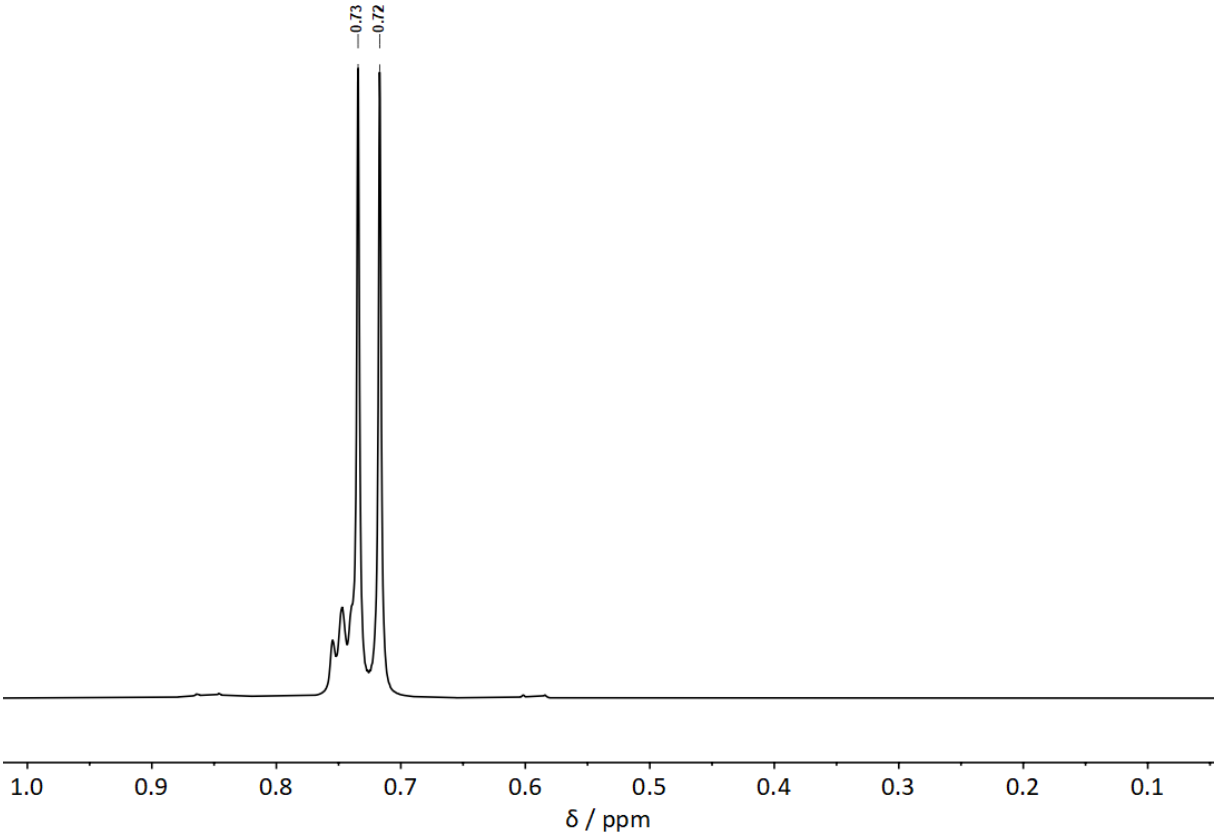

Fig. S49 ^{1}H NMR spectrum of $[(PMe_3)BeBr_2]_2$ (**2b**) in C_6D_6.

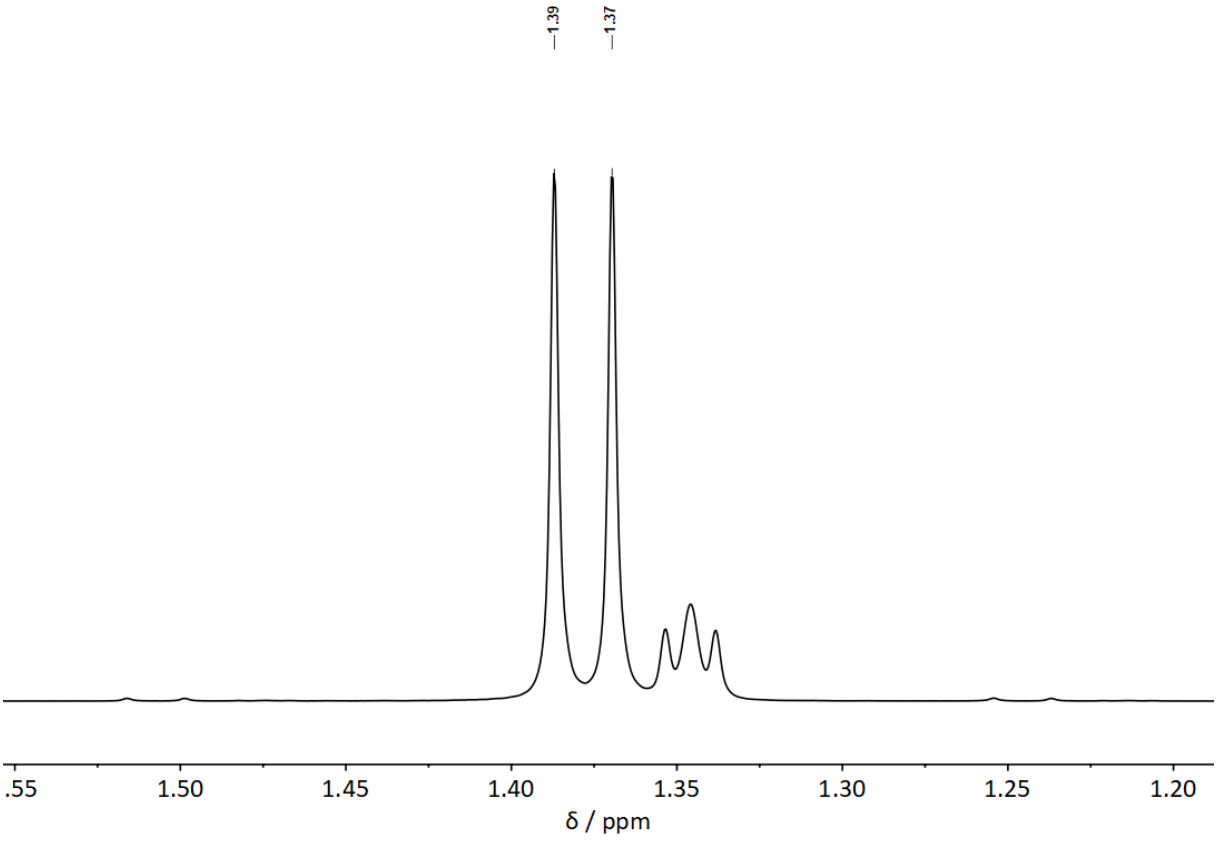

Fig. S50 ^{1}H NMR spectrum of $[(PMe_3)BeBr_2]_2$ (**2b**) in $CDCl_3$.

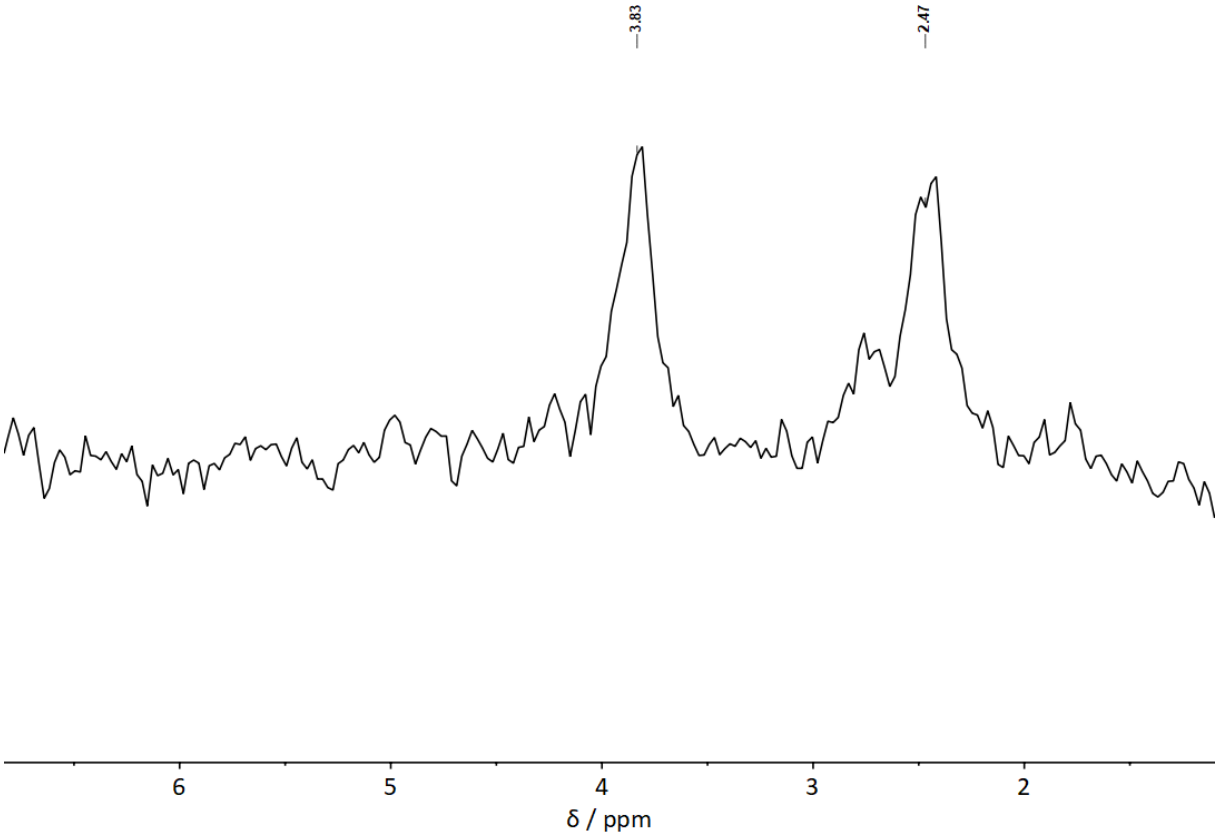

Fig. S51 ^{9}Be NMR spectrum of $[(PMe_3)BeBr_2]_2$ (**2b**) in C_6D_6.

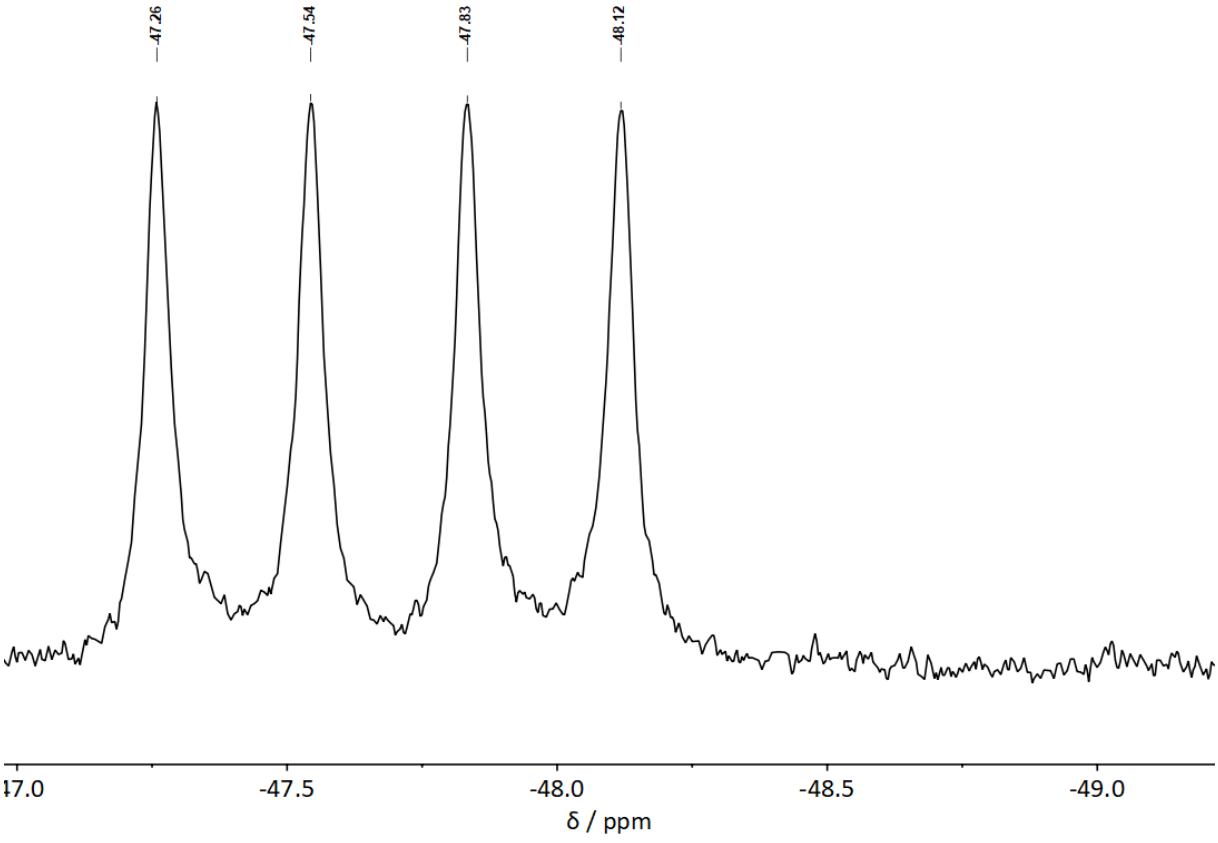

Fig. S52 ^{31}P NMR spectrum of $[(PMe_3)BeBr_2]_2$ (**2b**) in C_6D_6.

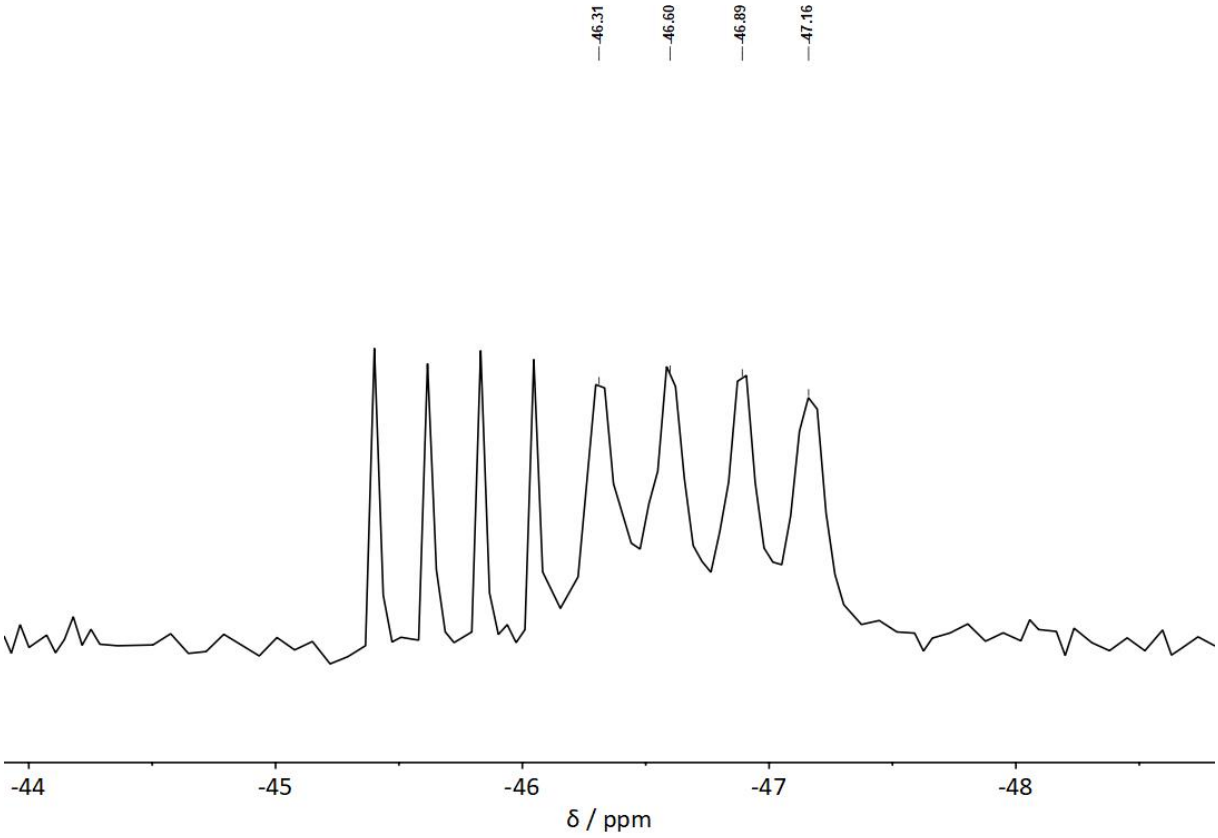

Fig. S53 ^{31}P NMR spectrum of $[(PMe_3)BeBr_2]_2$ (**2b**) in $CDCl_3$.

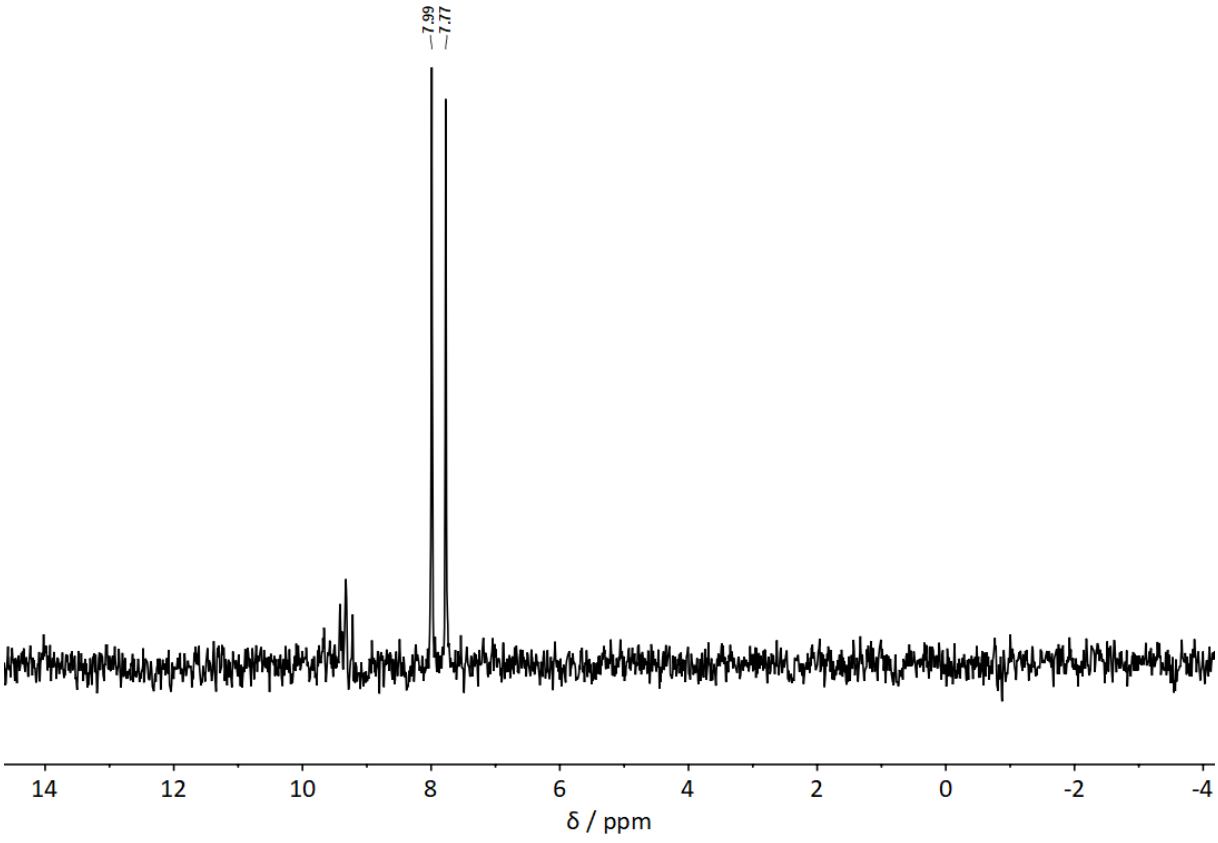

Fig. S54 ^{13}C NMR spectrum of $[(PMe_3)BeBr_2]_2$ (**2b**) in C_6D_6.

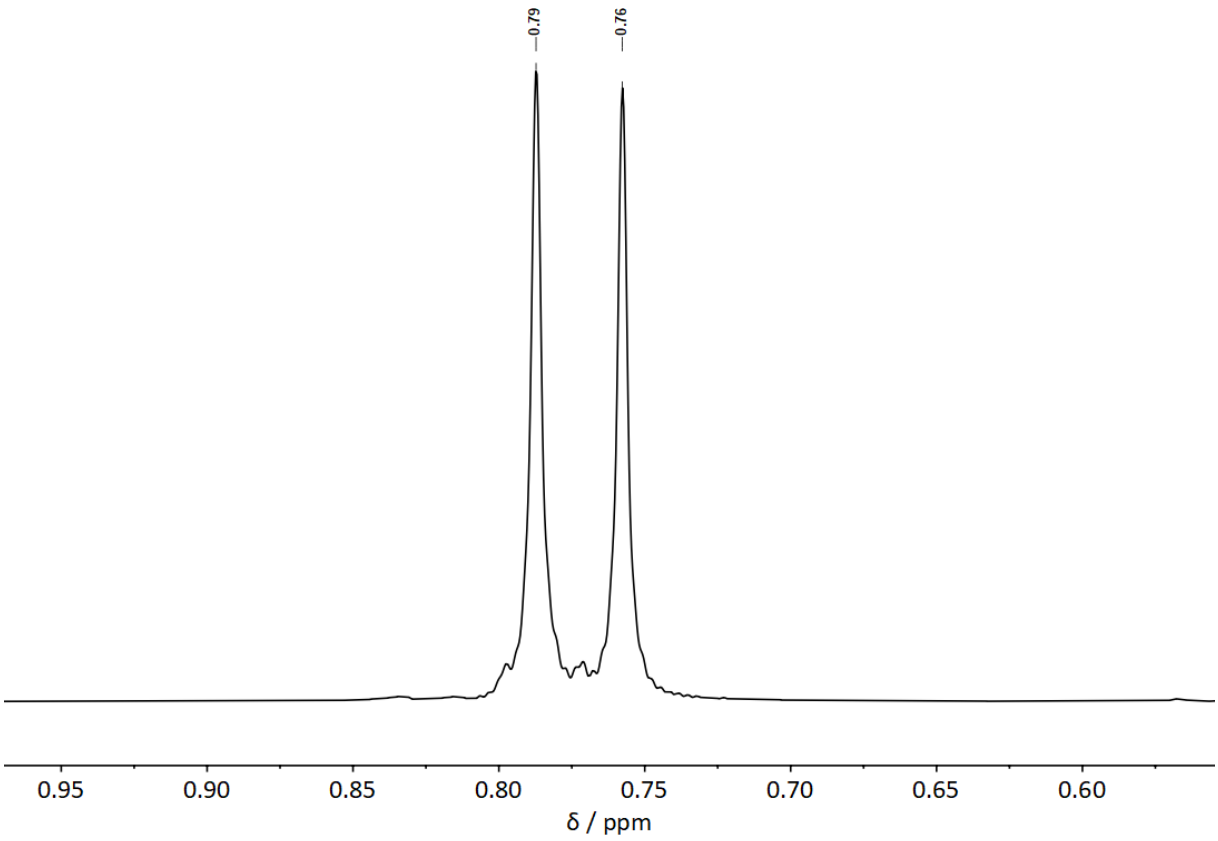

Fig. S55 ^{1}H NMR spectrum of $[(PMe_3)BeI_2]_2$ (**2c**) in C_6D_6.

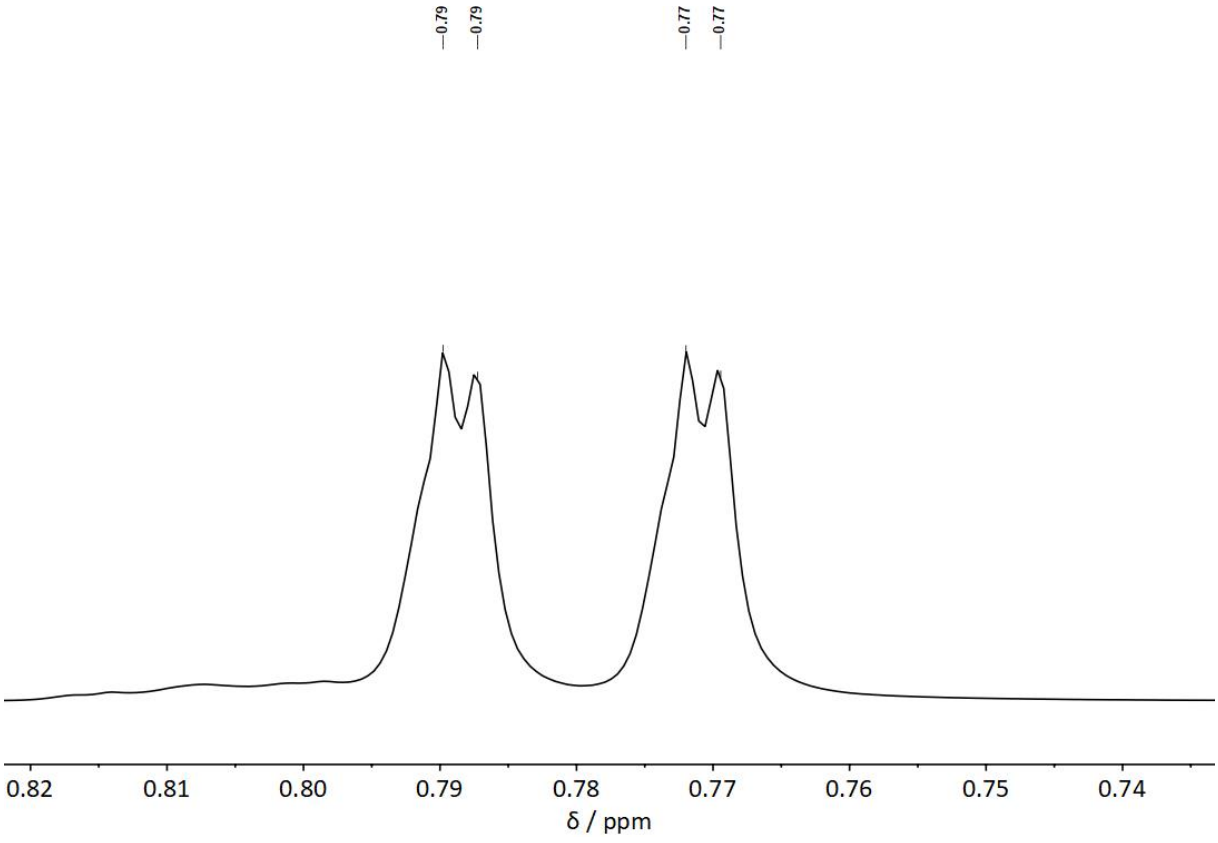

Fig. S56 ^{1}H NMR spectrum of $[(PMe_3)BeI_2]_2$ (**2c**) in Tol-d_8.

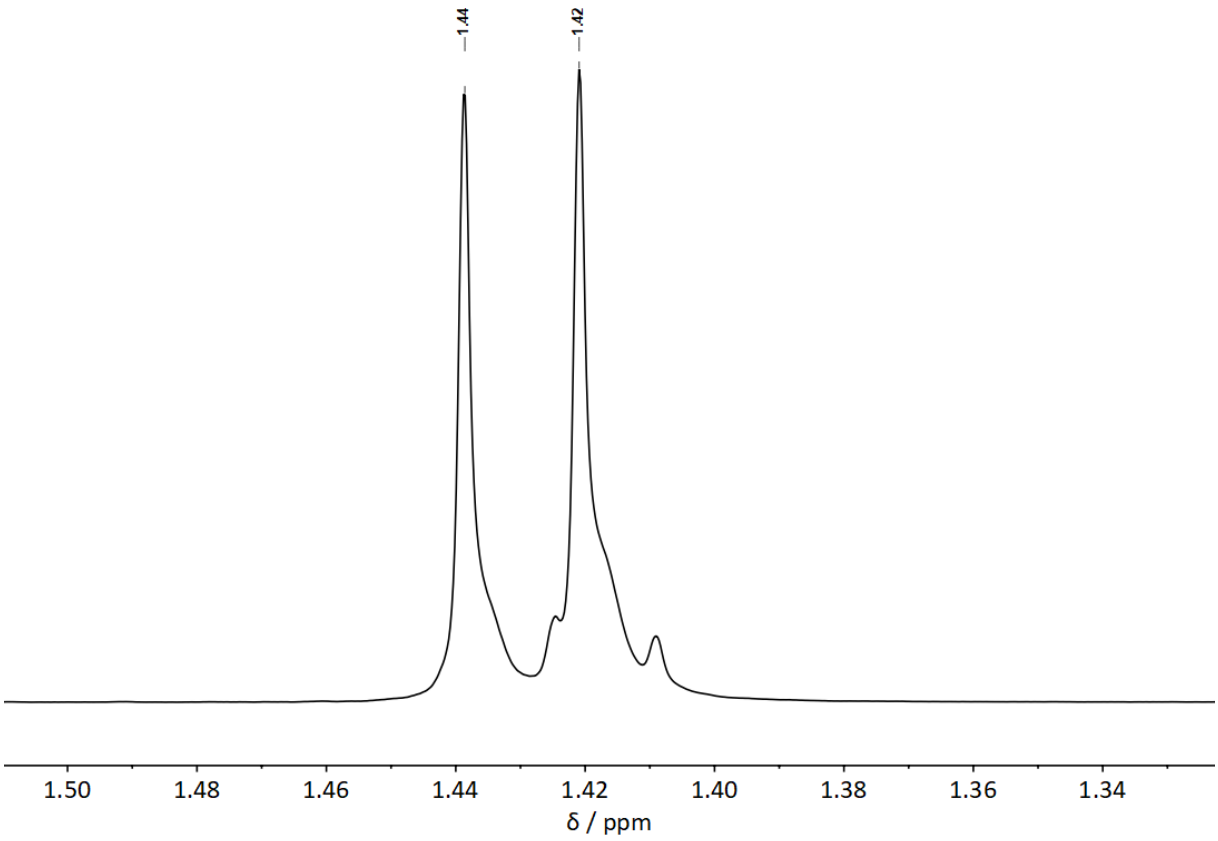

Fig. S57 ^{1}H NMR spectrum of $[(PMe_3)BeI_2]_2$ (**2c**) in $CDCl_3$.

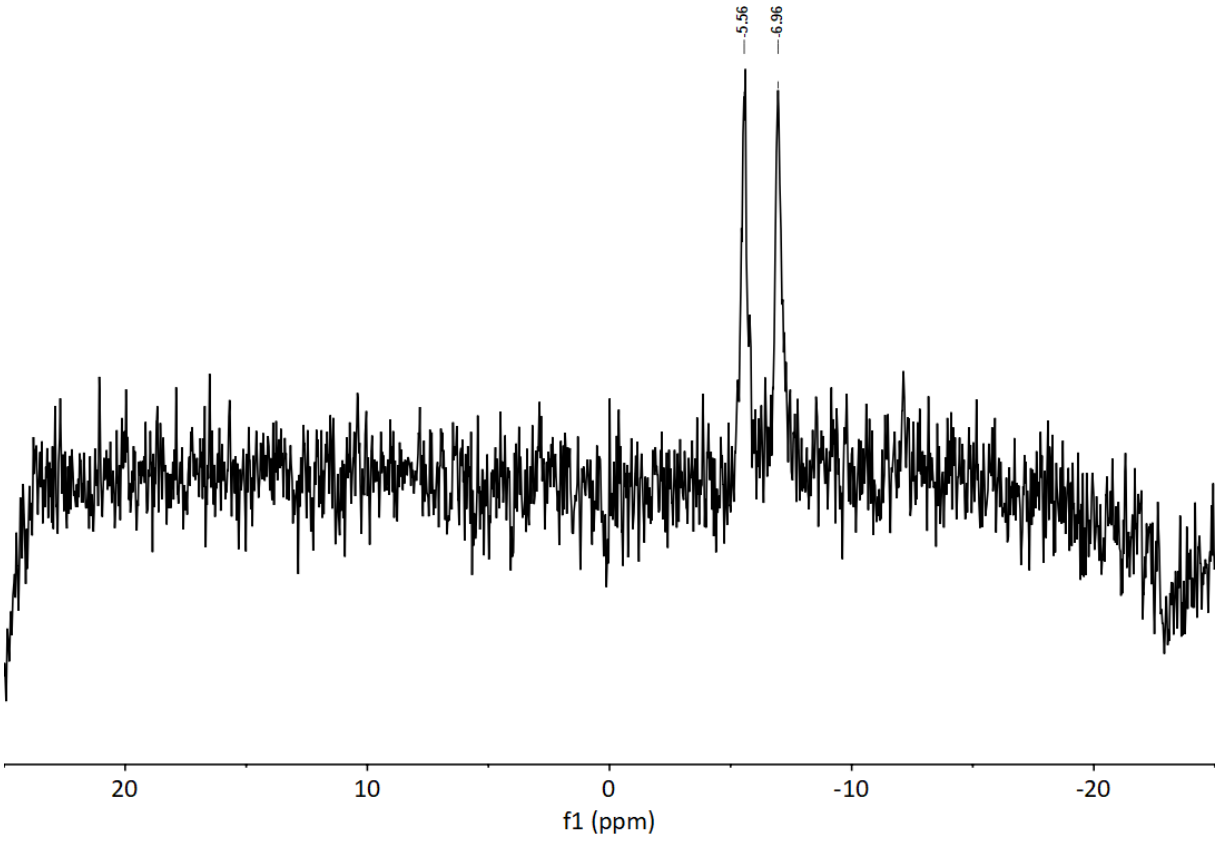

Fig. S58 ^{9}Be NMR spectrum of $[(PMe_3)BeI_2]_2$ (**2c**) in C_6D_6.

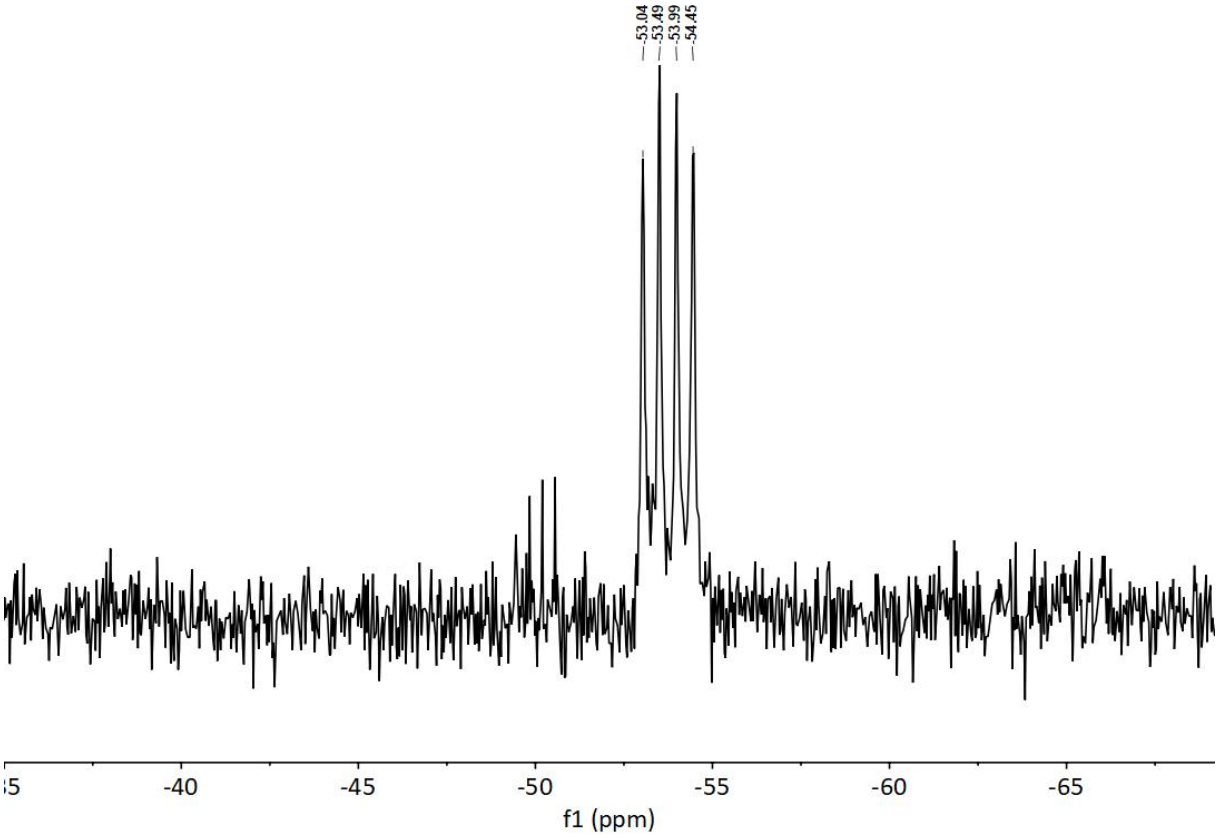

Fig. S59 ^{31}P NMR spectrum of $[(PMe_3)BeI_2]_2$ (**2c**) in C_6D_6.

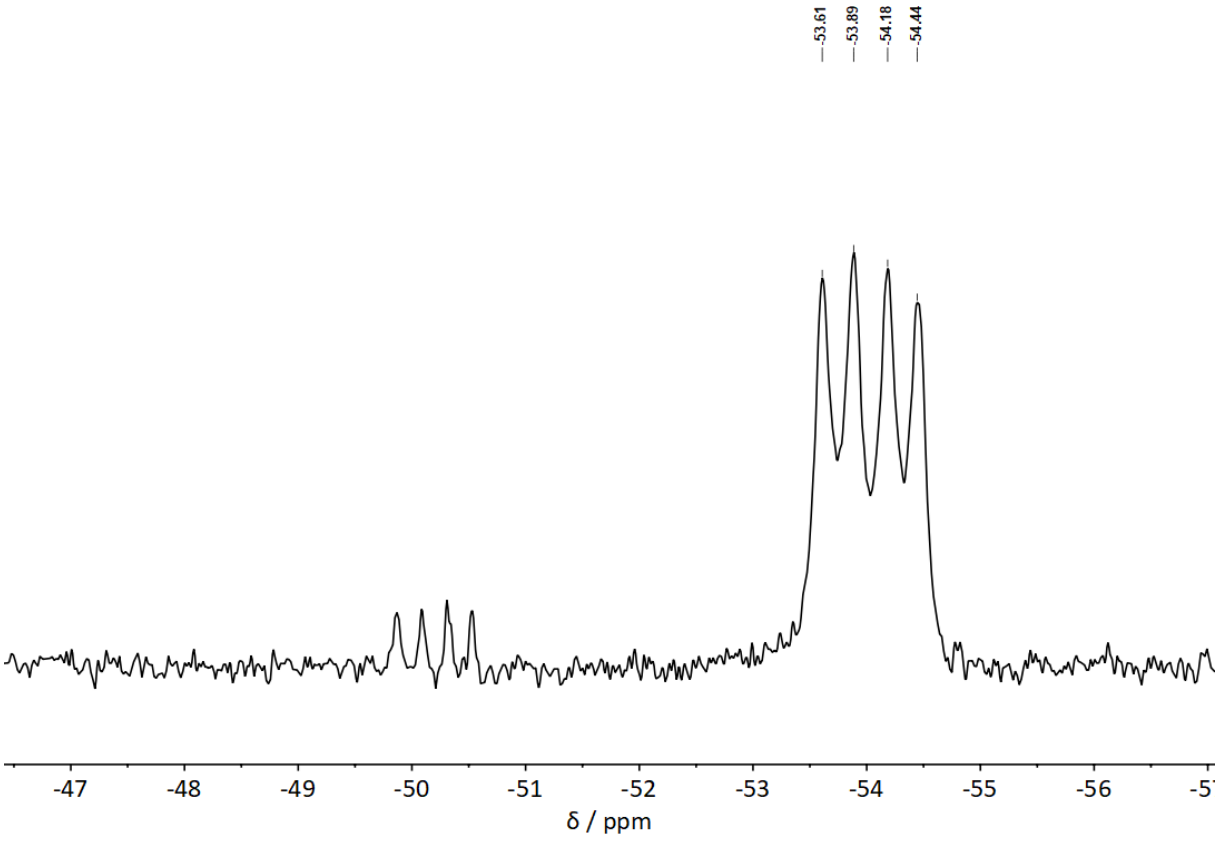

Fig. S60 ^{31}P NMR spectrum of $[(PMe_3)BeI_2]_2$ (**2c**) in Tol-d_8.

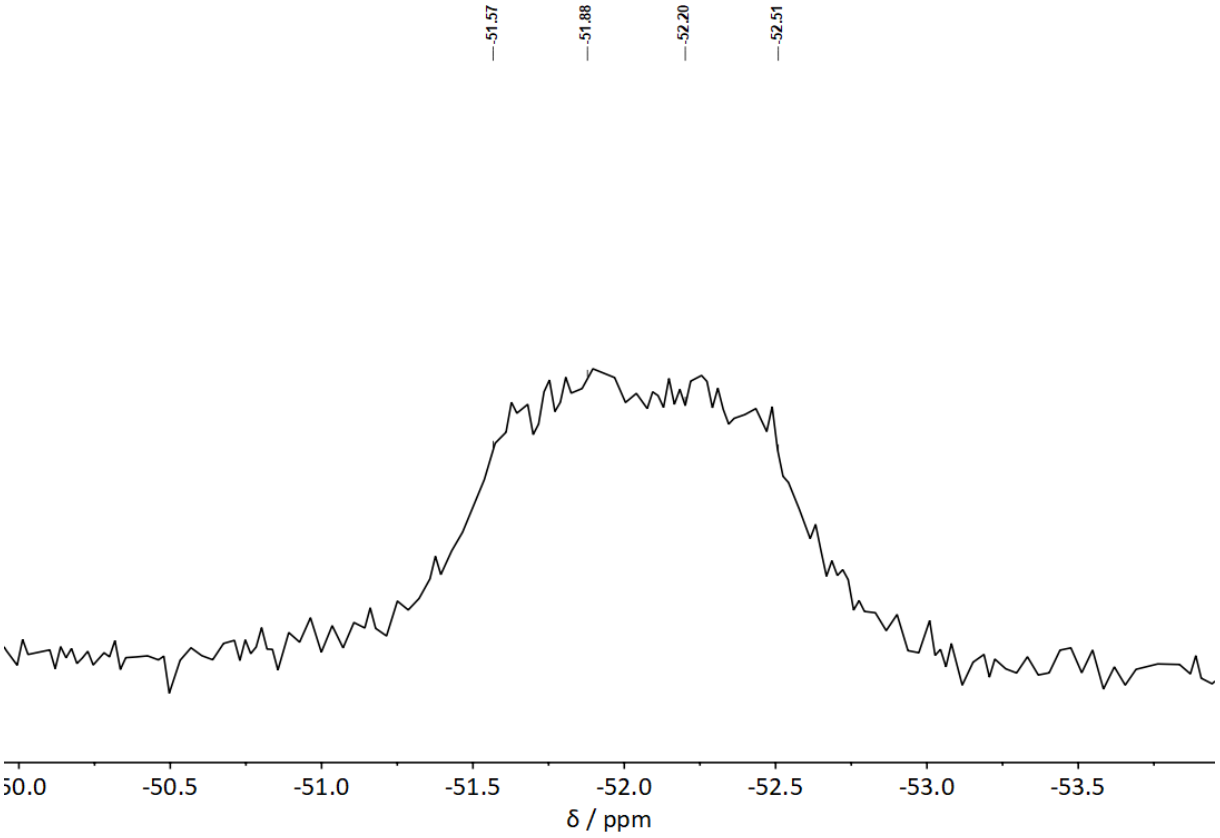

Fig. S61 ^{31}P NMR spectrum of $[(PMe_3)BeI_2]_2$ (**2c**) in $CDCl_3$.

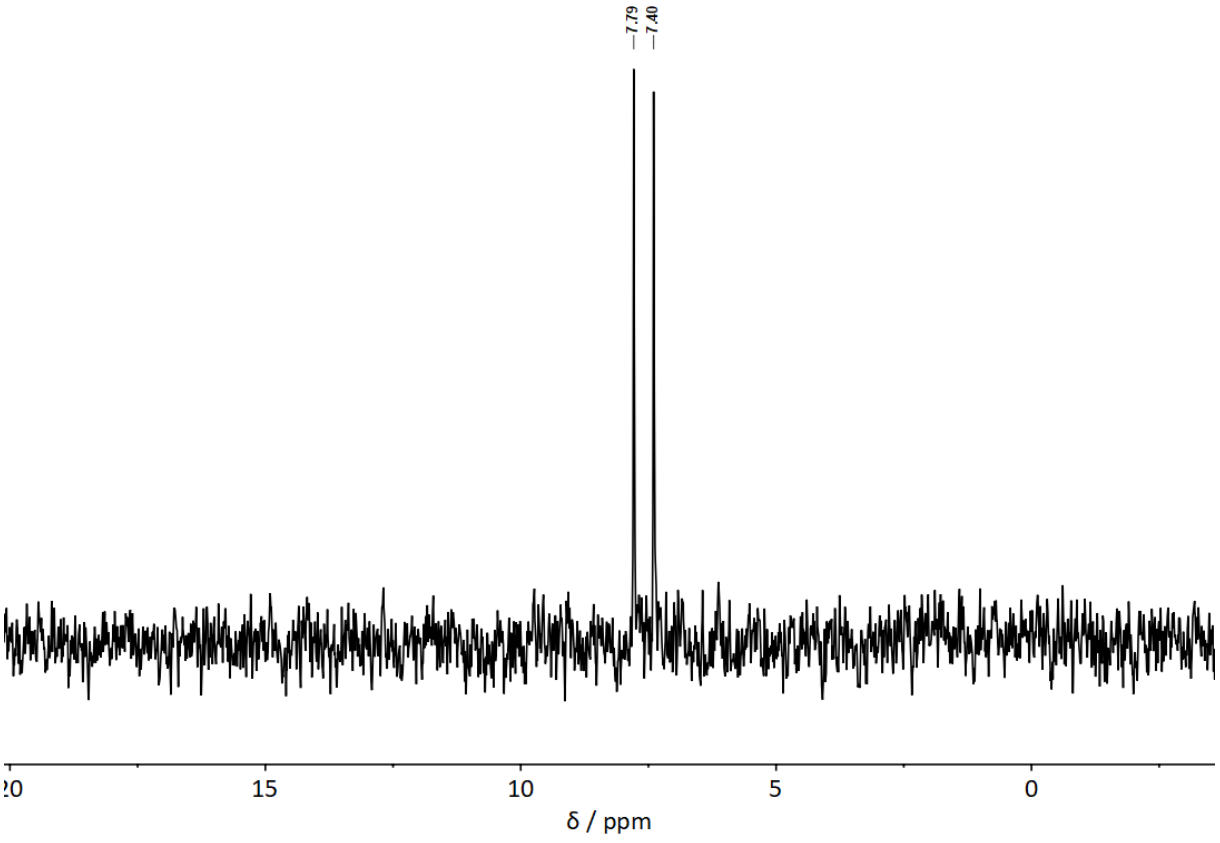

Fig. S62 ^{13}C NMR spectrum of $[(PMe_3)BeI_2]_2$ (**2c**) in C_6D_6.

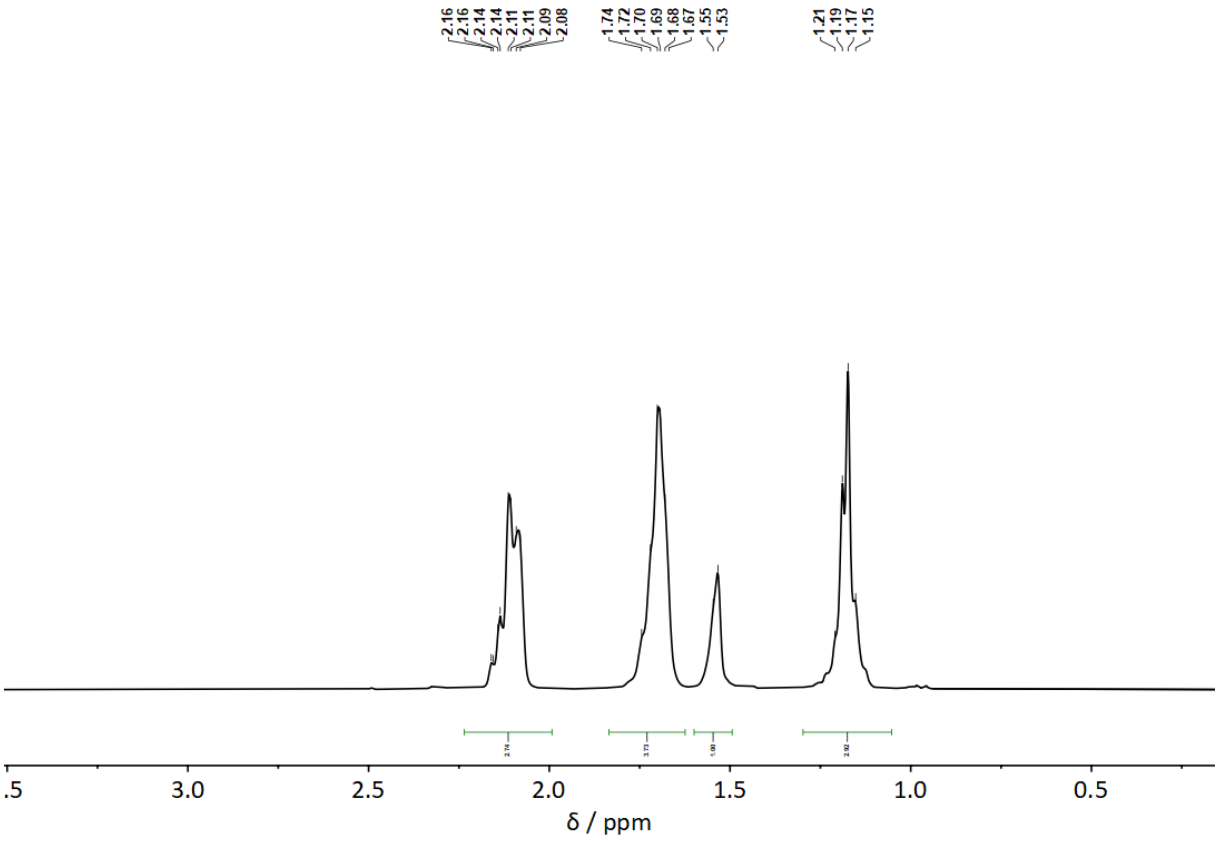

Fig. S63 ^{1}H NMR spectrum of $[(PCy_3)BeCl_2]_2$ (**3a**) in C_6D_6.

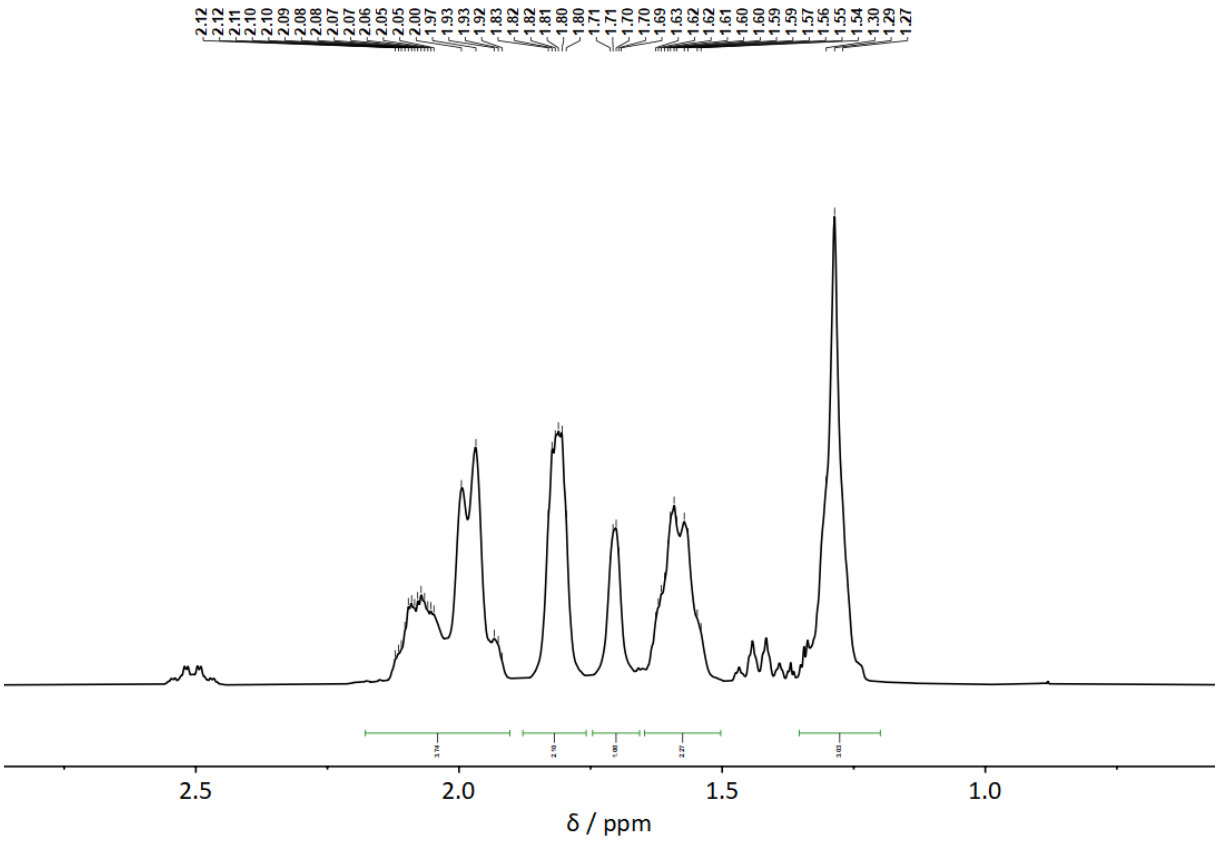

Fig. S64 ^{1}H NMR spectrum of $[(PCy_3)BeCl_2]_2$ (**3a**) in CD_2Cl_2.

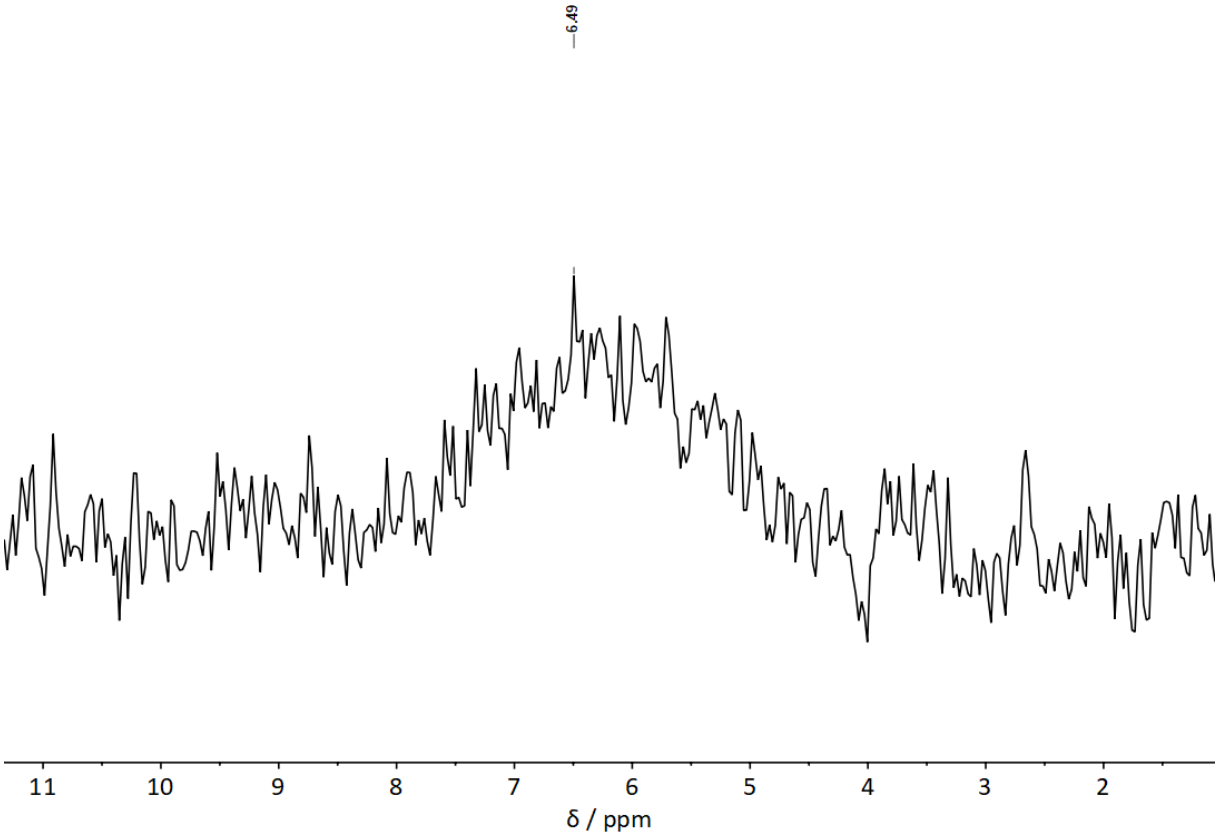

Fig. S65 ^{9}Be NMR spectrum of $[(PCy_3)BeCl_2]_2$ (**3a**) in C_6D_6.

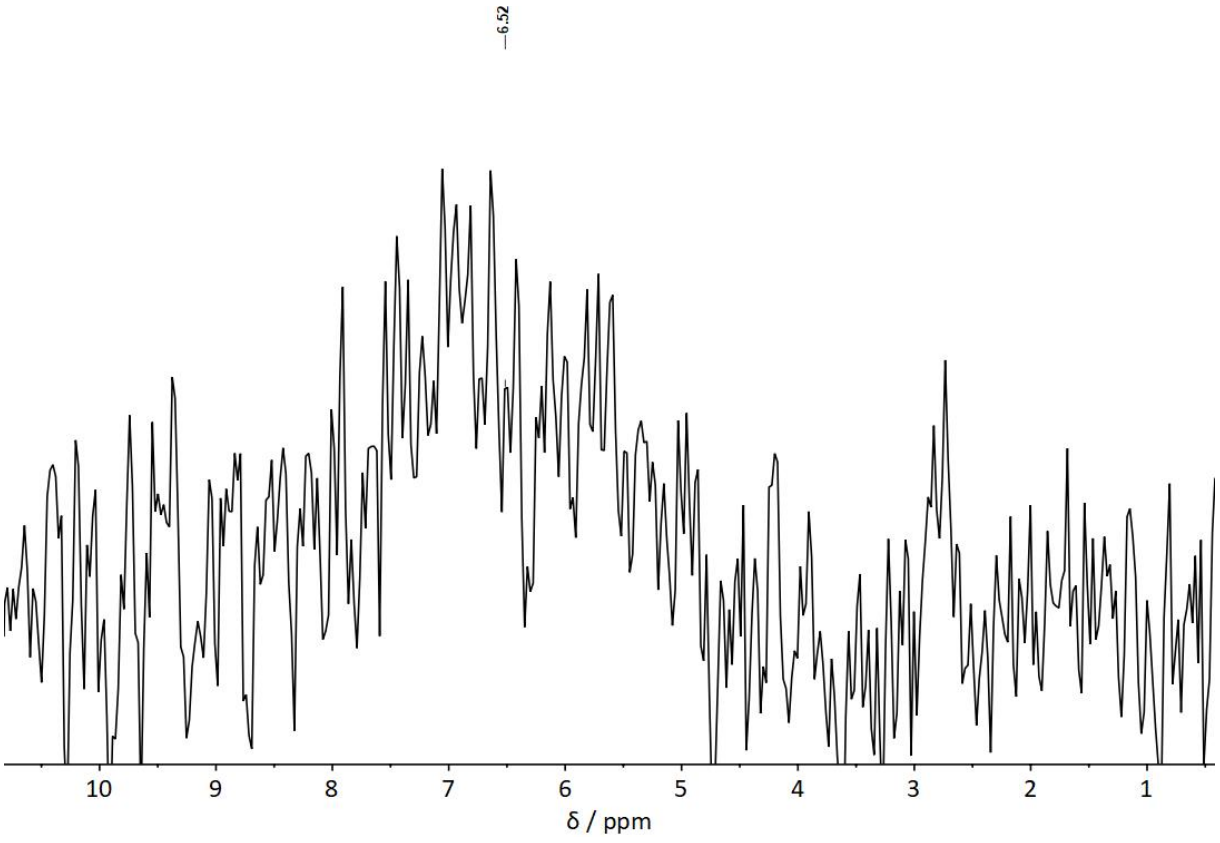

Fig. S66 ^{9}Be NMR spectrum of $[(PCy_3)BeCl_2]_2$ (**3a**) in CD_2Cl_2.

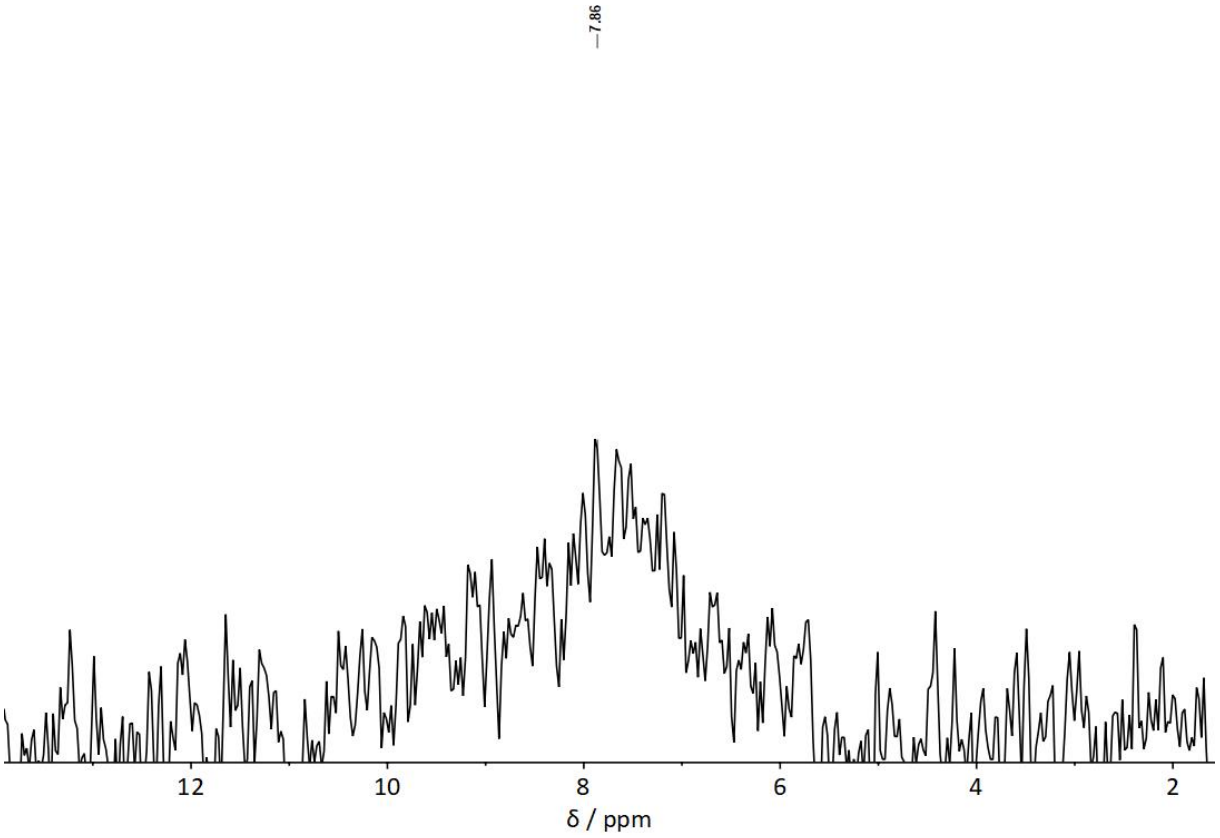

Fig. S67 ^{9}Be NMR spectrum of $[(PCy_3)BeCl_2]_2$ (**3a**) in $CDCl_3$.

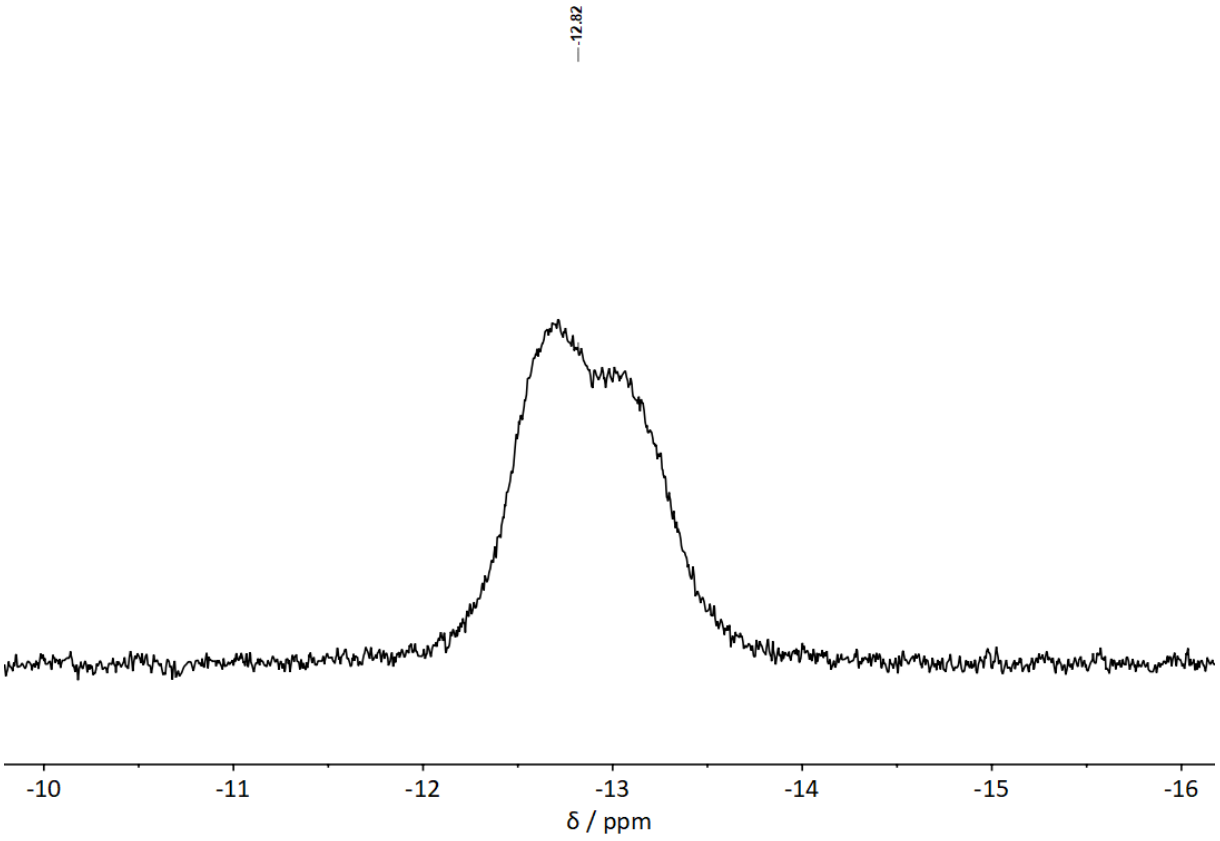

Fig. S68 ^{31}P NMR spectrum of $[(PCy_3)BeCl_2]_2$ (**3a**) in C_6D_6.

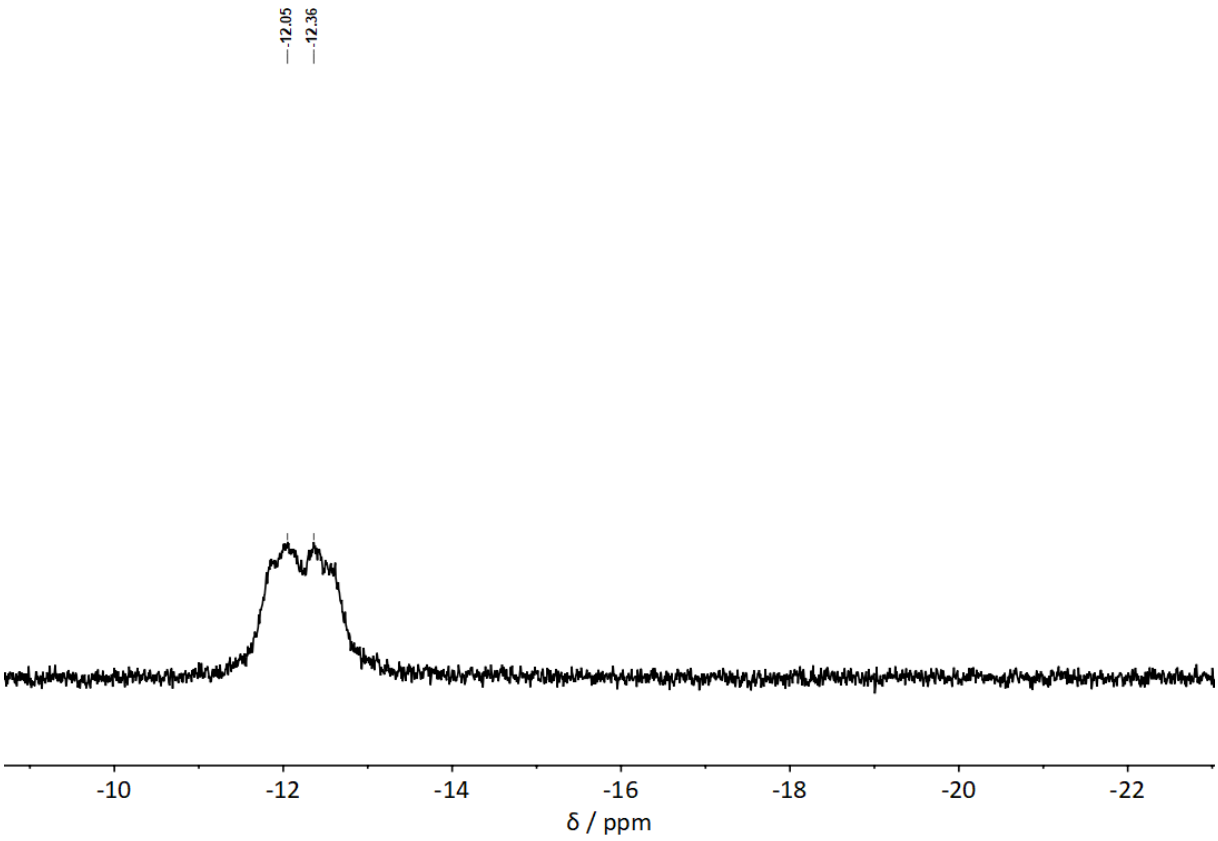

Fig. S69 ^{31}P NMR spectrum of $[(PCy_3)BeCl_2]_2$ (**3a**) in CD_2Cl_2.

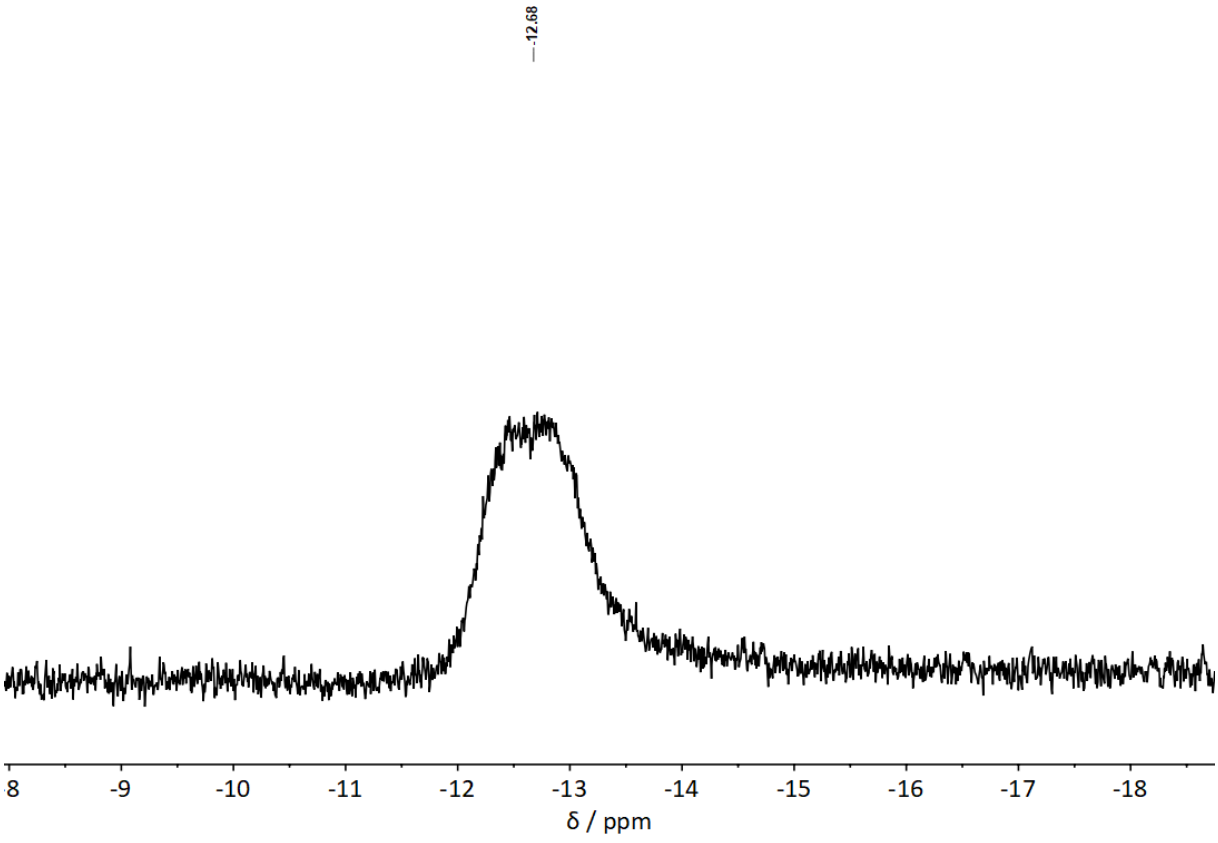

Fig. S70 ^{31}P NMR spectrum of $[(PCy_3)BeCl_2]_2$ (**3a**) in $CDCl_3$.

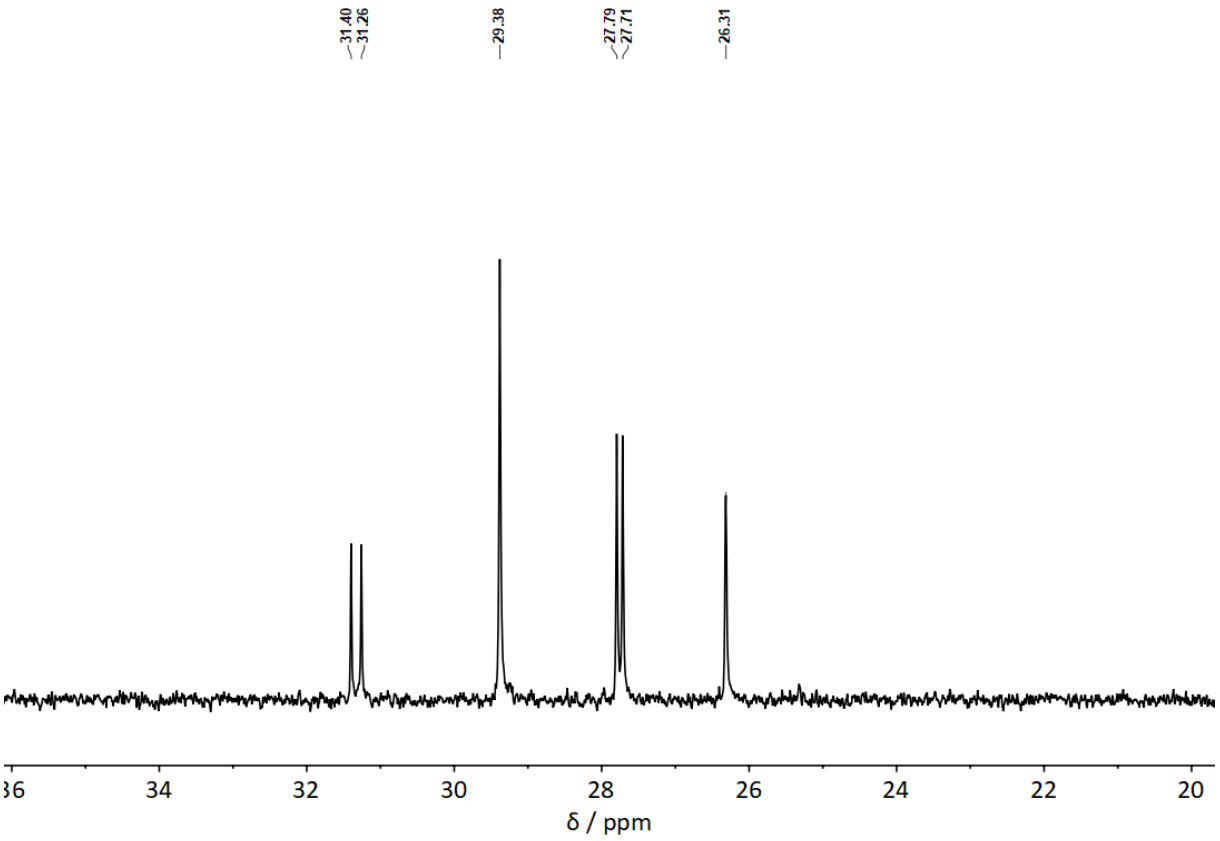

Fig. S71 ^{13}C NMR spectrum of $[(PCy_3)BeCl_2]_2$ (**3a**) in C_6D_6.

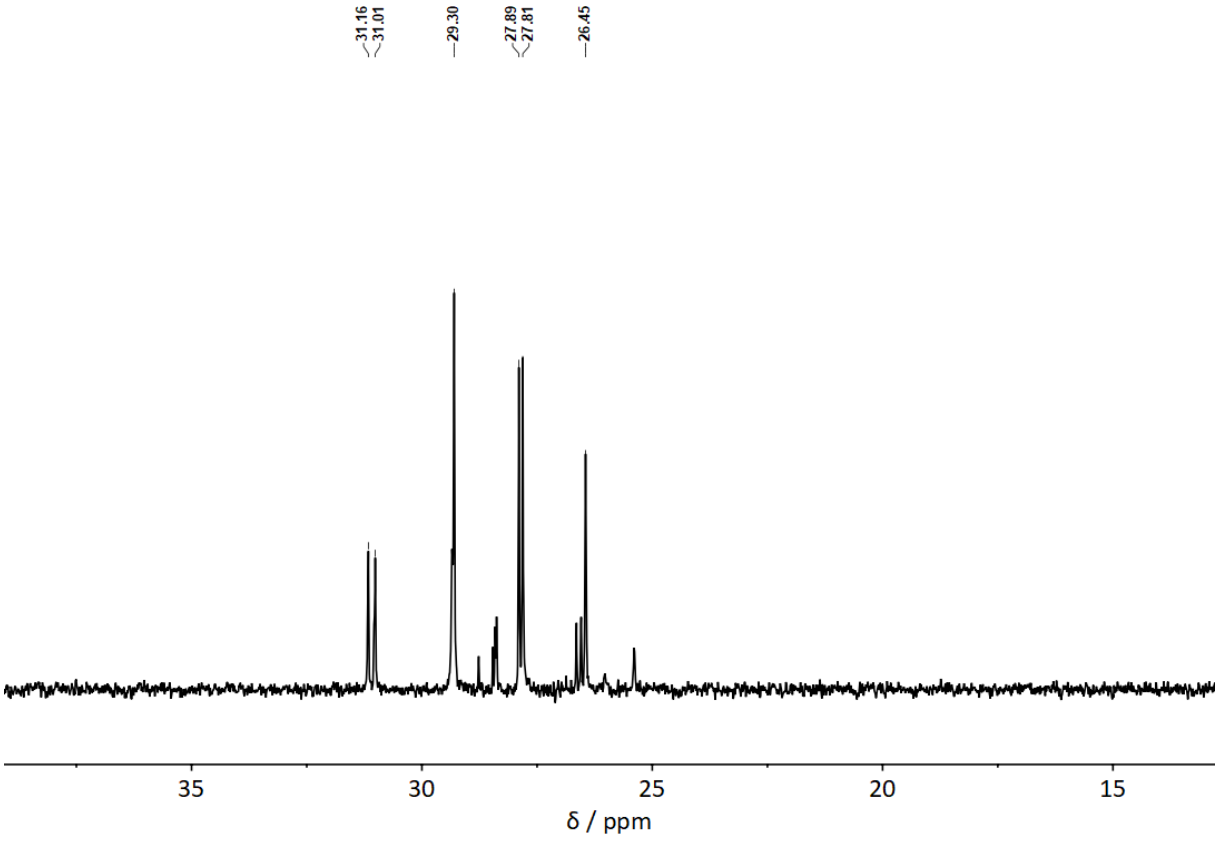

Fig. S72 ^{13}C NMR spectrum of $[(PCy_3)BeCl_2]_2$ (**3a**) in CD_2Cl_2.

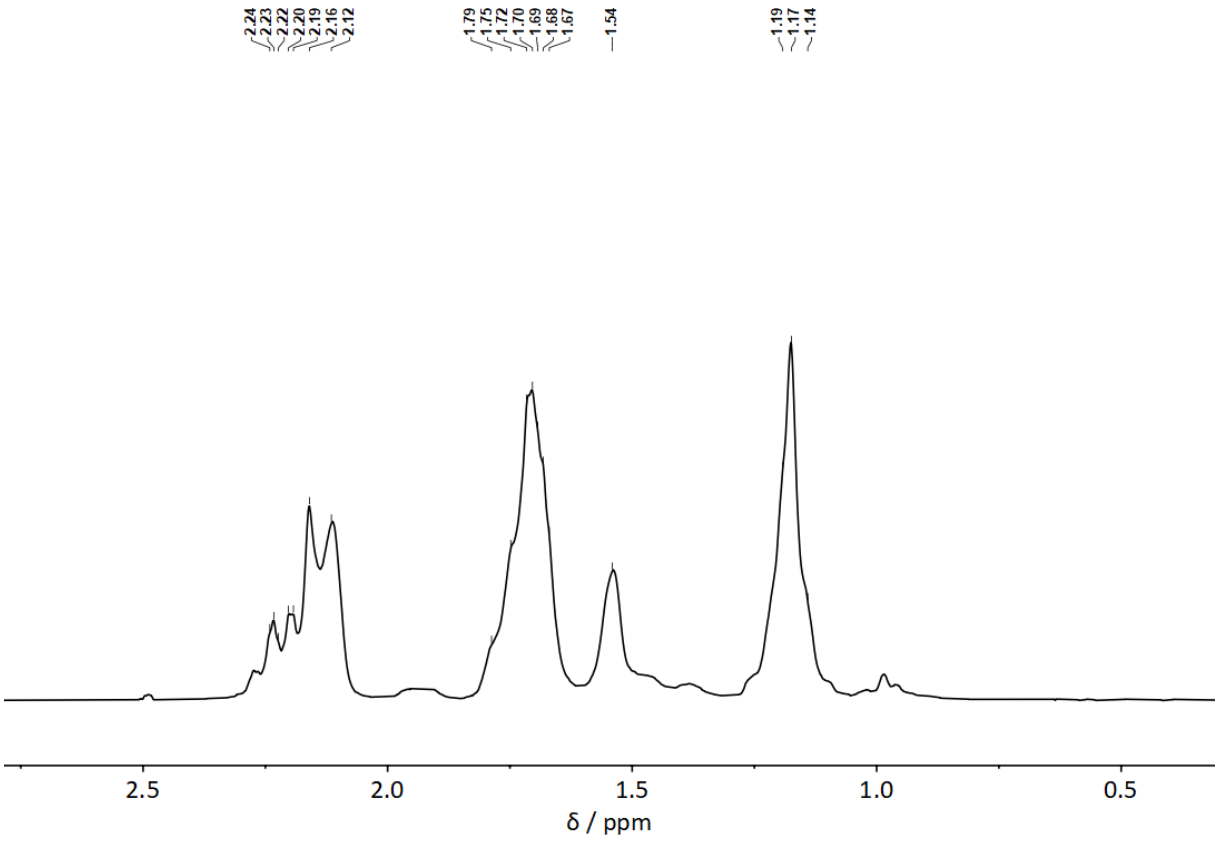

Fig. S73 ^{1}H NMR spectrum of $[(PCy_3)BeBr_2]_2$ (**3b**) in C_6D_6.

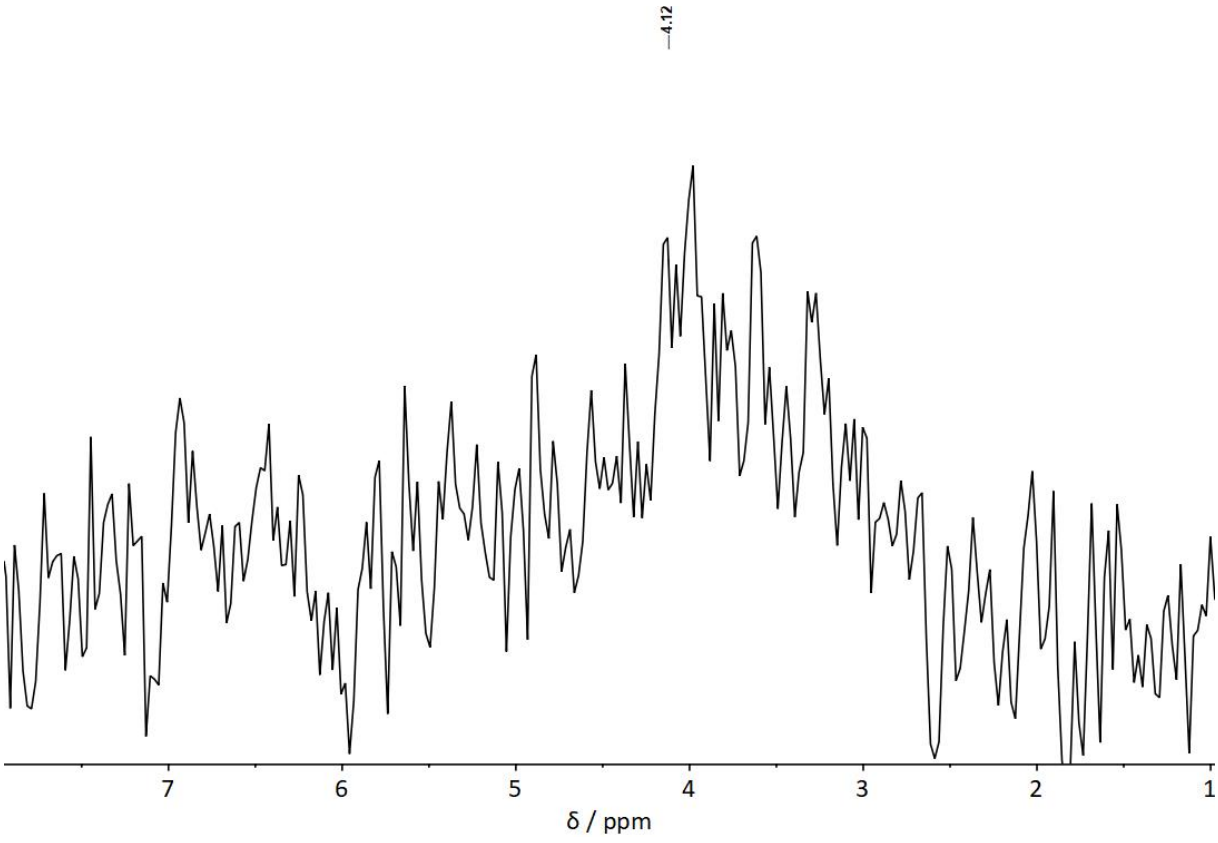

Fig. S74 ^{9}Be NMR spectrum of $[(PCy_3)BeBr_2]_2$ (**3b**) in C_6D_6.

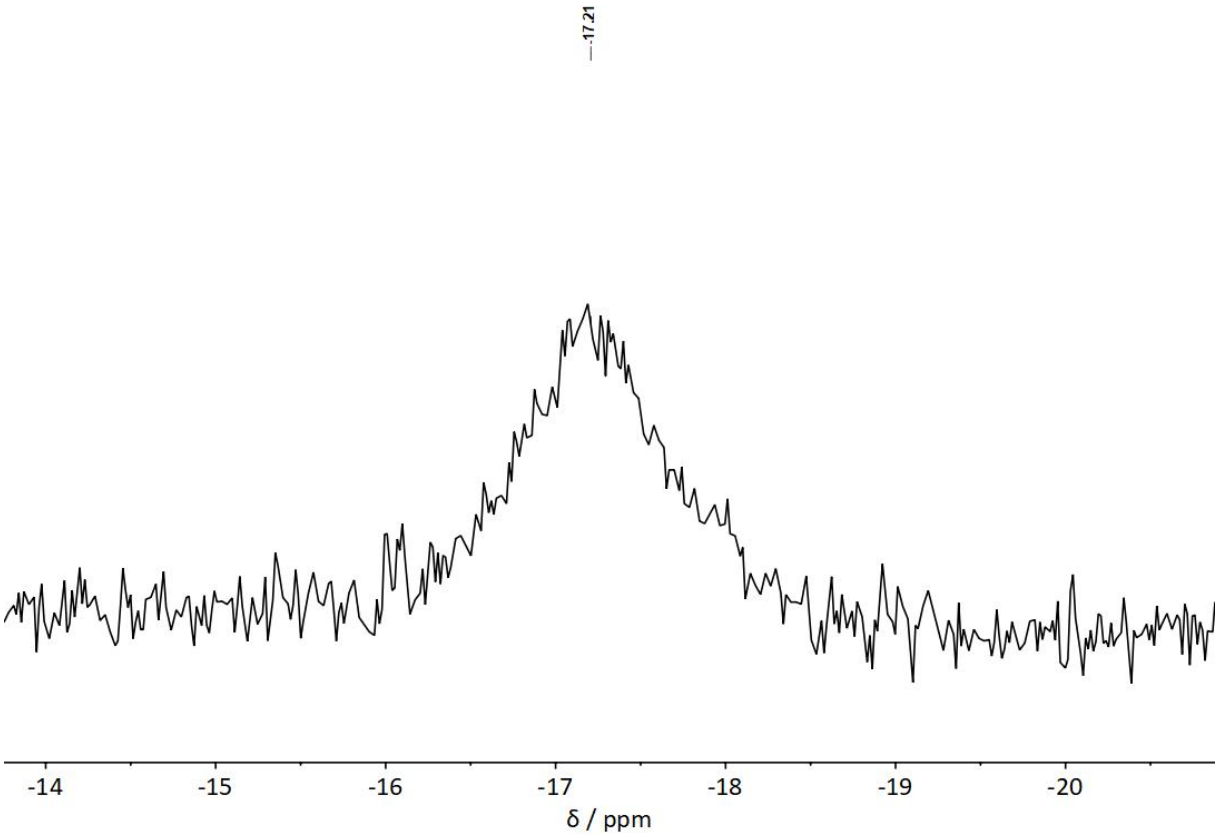

Fig. S75 ^{31}P NMR spectrum of $[(PCy_3)BeBr_2]_2$ (**3b**) in C_6D_6.

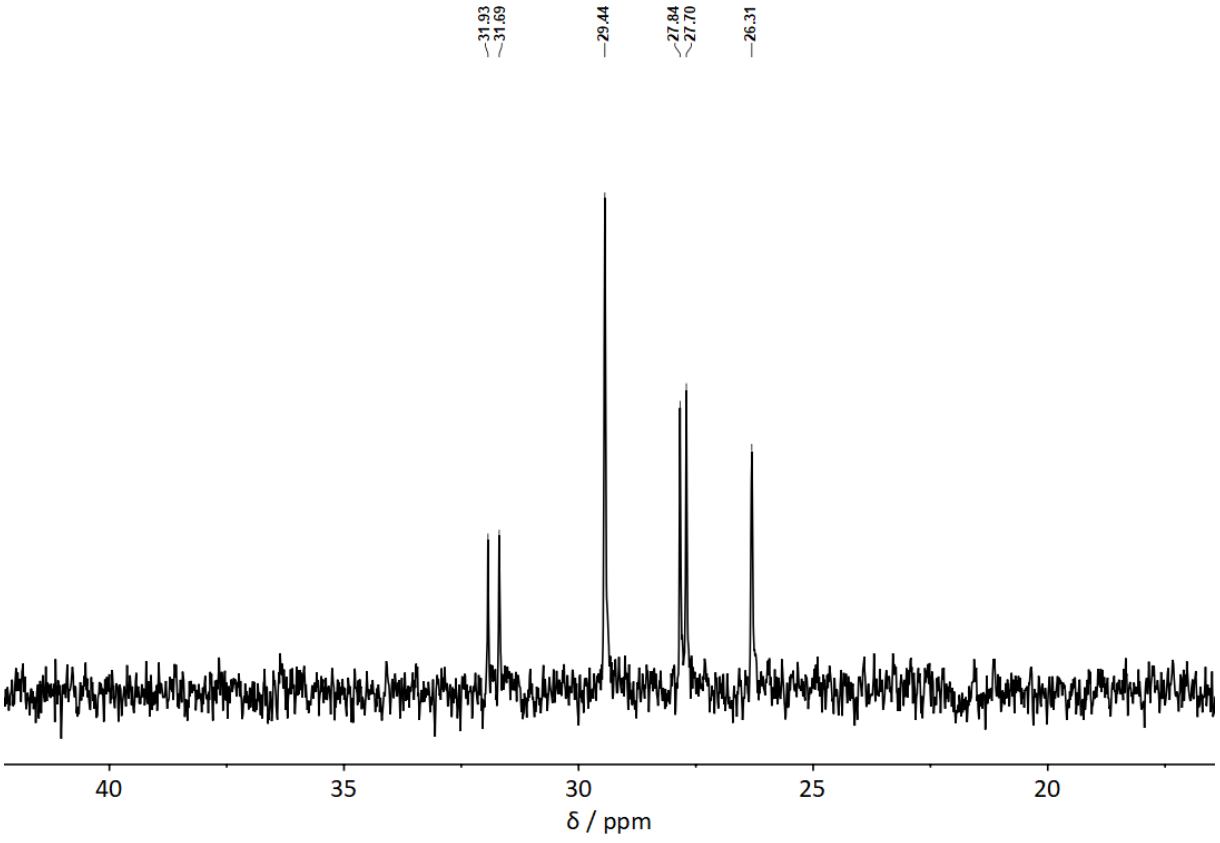

Fig. S76 ^{13}C NMR spectrum of $[(PCy_3)BeBr_2]_2$ (**3b**) in C_6D_6.

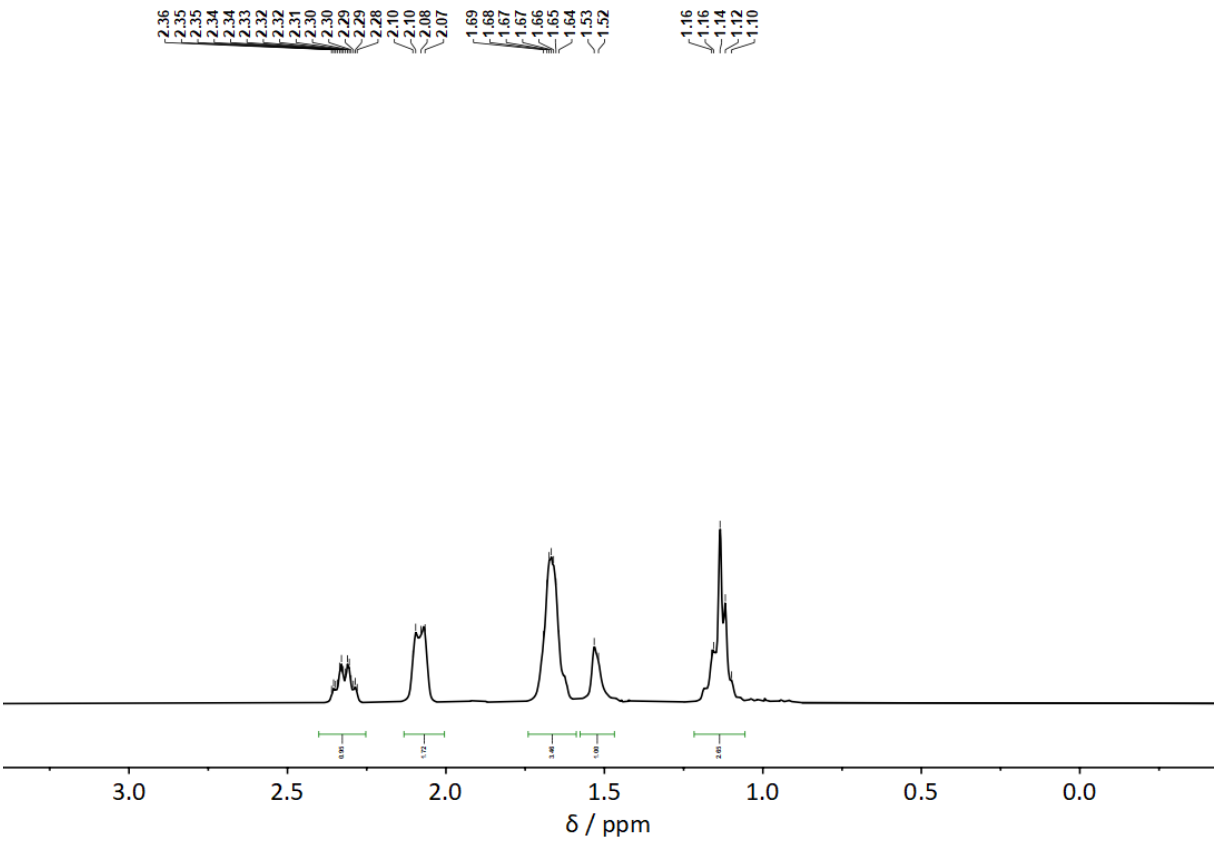

Fig. S77 ^{1}H NMR spectrum of $[(PCy_3)BeI_2]_2$ (**3c**) in C_6D_6.

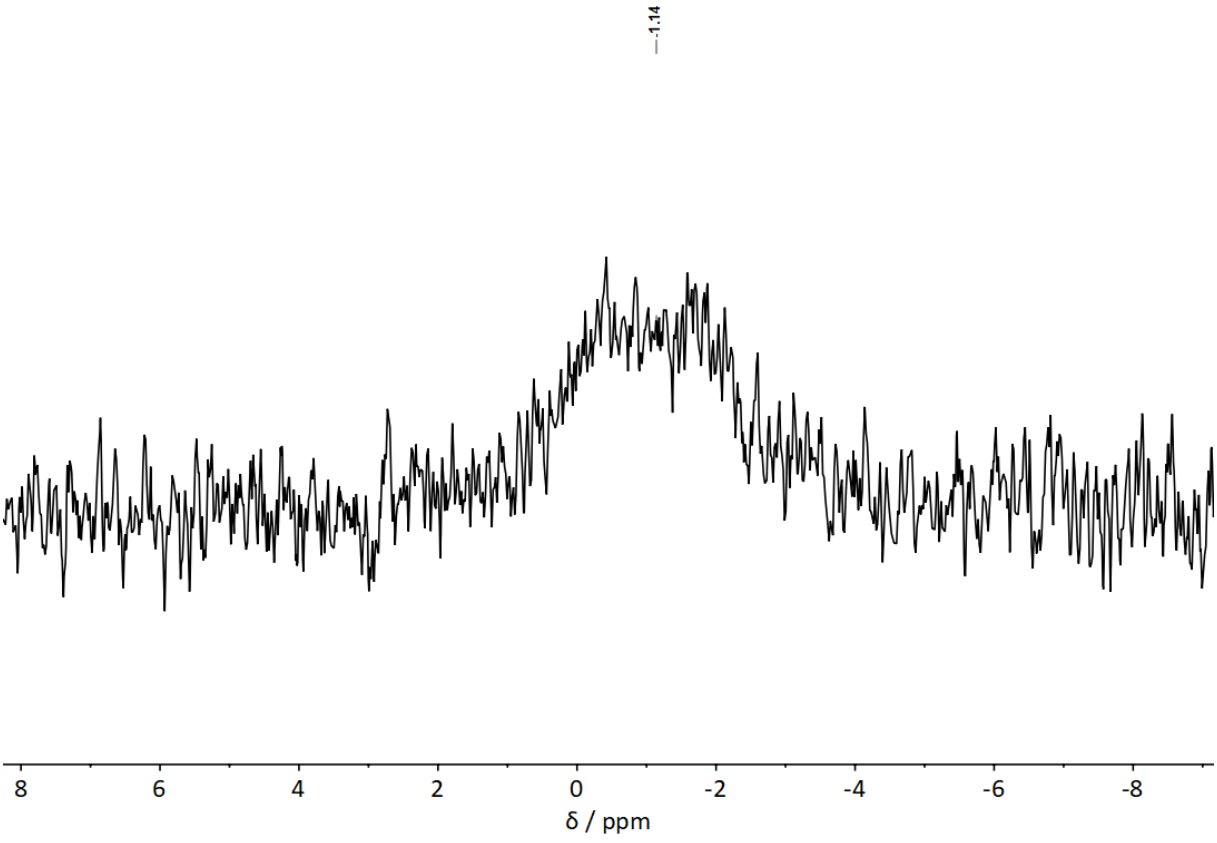

Fig. S78 ^{9}Be NMR spectrum of $[(PCy_3)BeI_2]_2$ (**3c**) in C_6D_6.

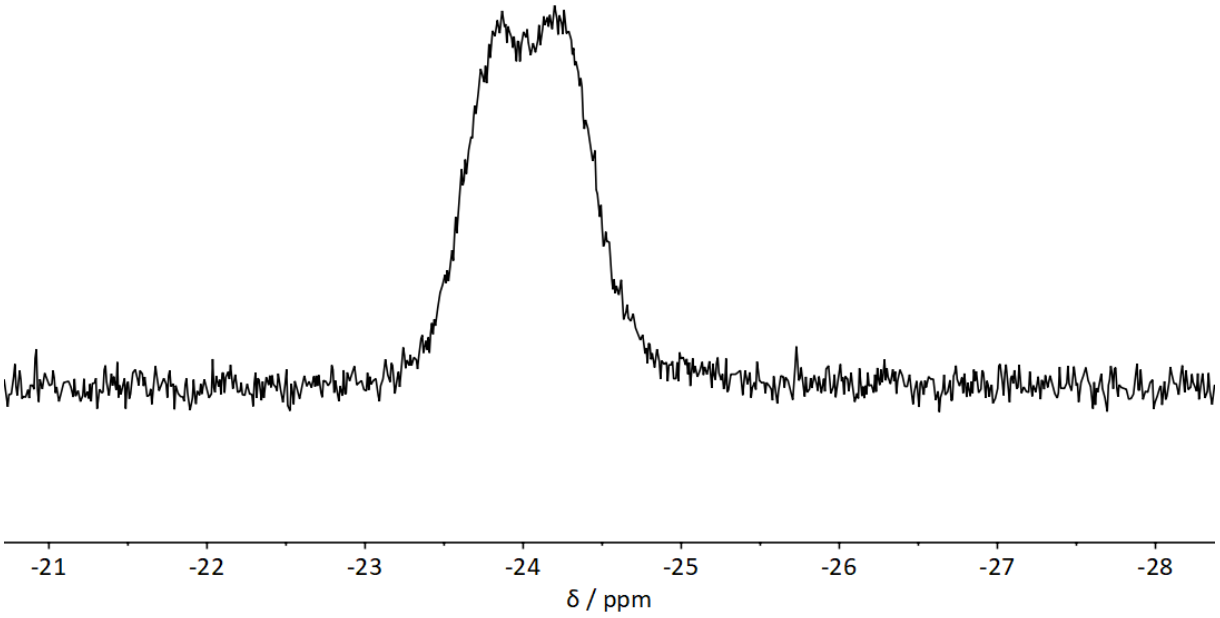

Fig. S79 ^{31}P NMR spectrum of $[(PCy_3)BeI_2]_2$ (**3c**) in C_6D_6.

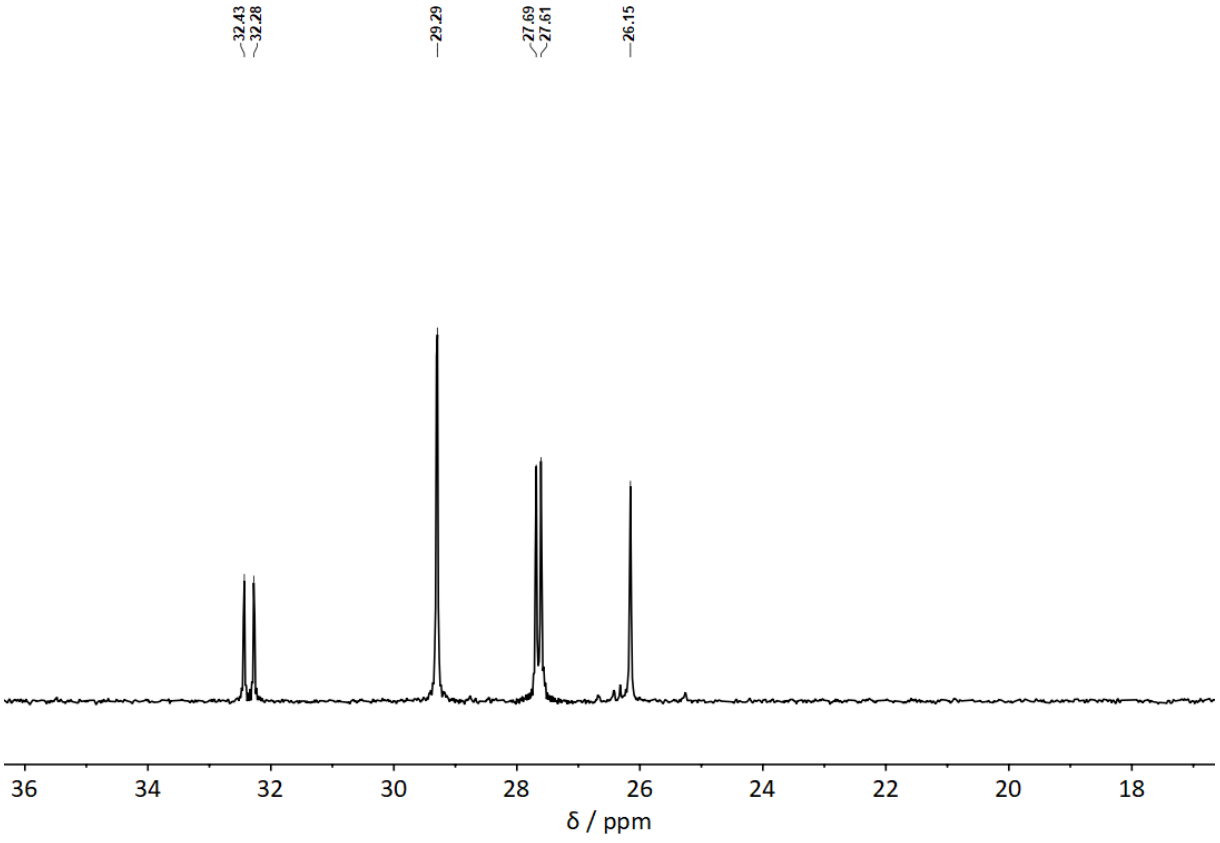

Fig. S80 ^{13}C NMR spectrum of $[(PCy_3)BeI_2]_2$ (**3c**) in C_6D_6.

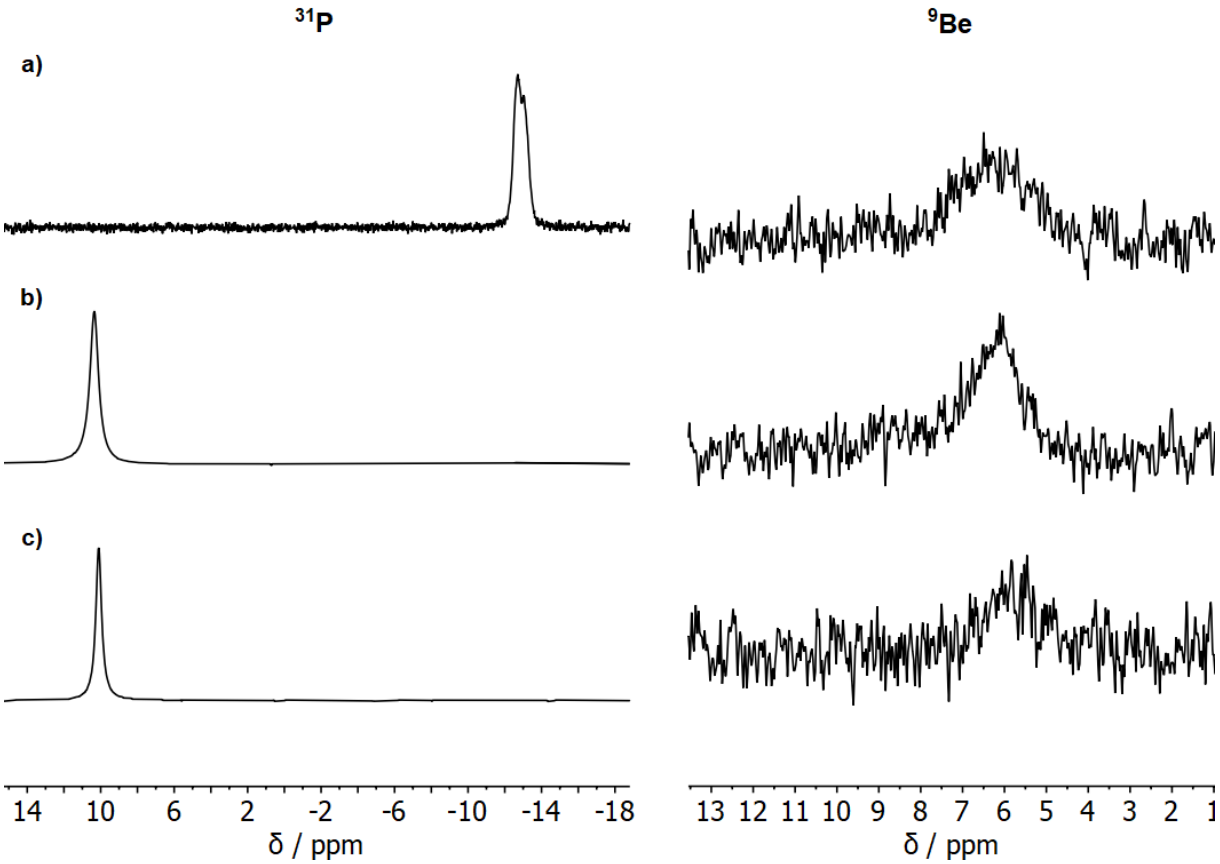

Fig. S81 ^{31}P (left) and ^{9}Be (right) NMR spectra of $[(PCy_3)BeCl_2]_2$ (**3a**) with the addition of a) zero, b) one and c) two equivalents of PCy_3 in C_6D_6.

NMR line shape analysis

Phospine dissociation

Table S5: Activation energies for PMe_3 dissociation from compounds **1a-c** in toluene and chloroform.

	E_A [kJ / mol]	
solvent	C_7D_8	$CDCl_3$
1a	22.18 ± 3.73	69.62 ± 4.22
1b	—[a]	—[a]
1c	—[a]	—[a]

[a] Too high for determination via VT NMR experiments.

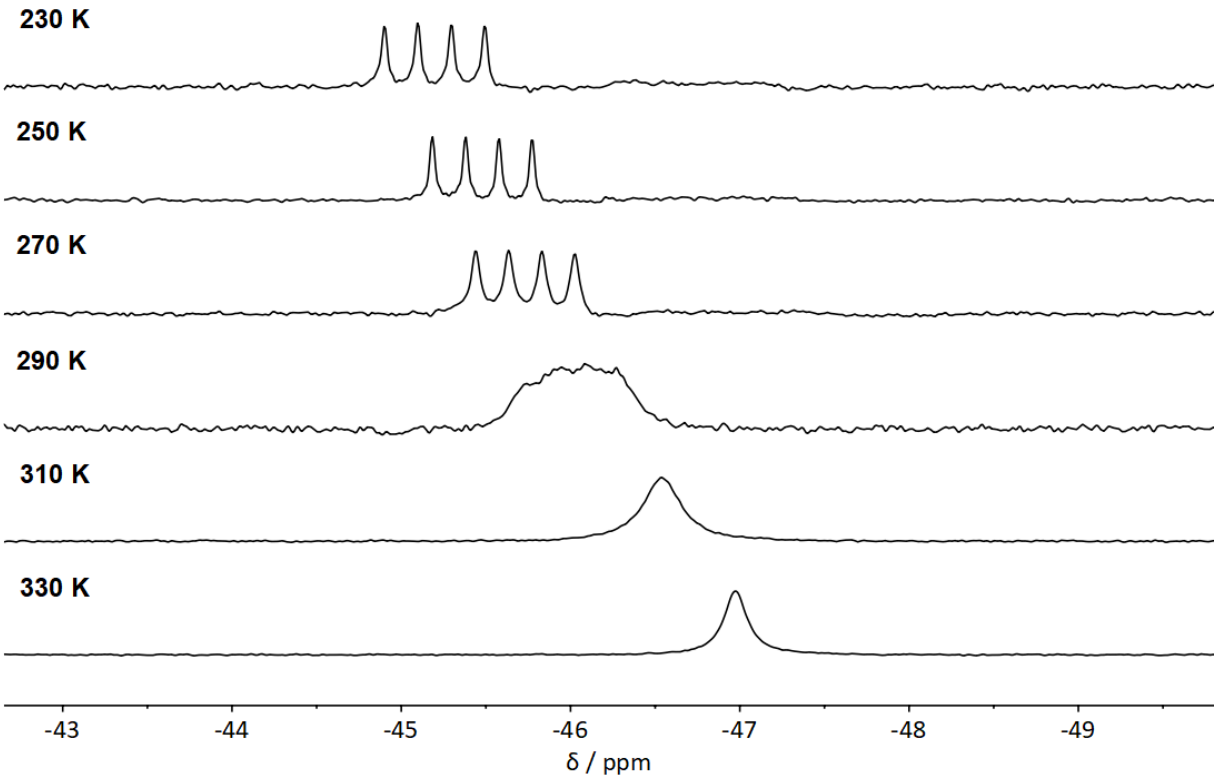

Fig. S82 Temperature dependent ^{31}P NMR spectra of $(PMe_3)_2BeCl_2$ (**1a**) in C_7D_8.

Table S6: Temperature dependent linewidths and derived parameters for **1a** in C_7D_8.

T [K]	$\omega_{1/2}$ [Hz]	k	ln k
250	8.0	25.1	3.22
270	13.3	41.8	3.73
290	42.8	134.5	4.90
310	53.5	168.1	5.12

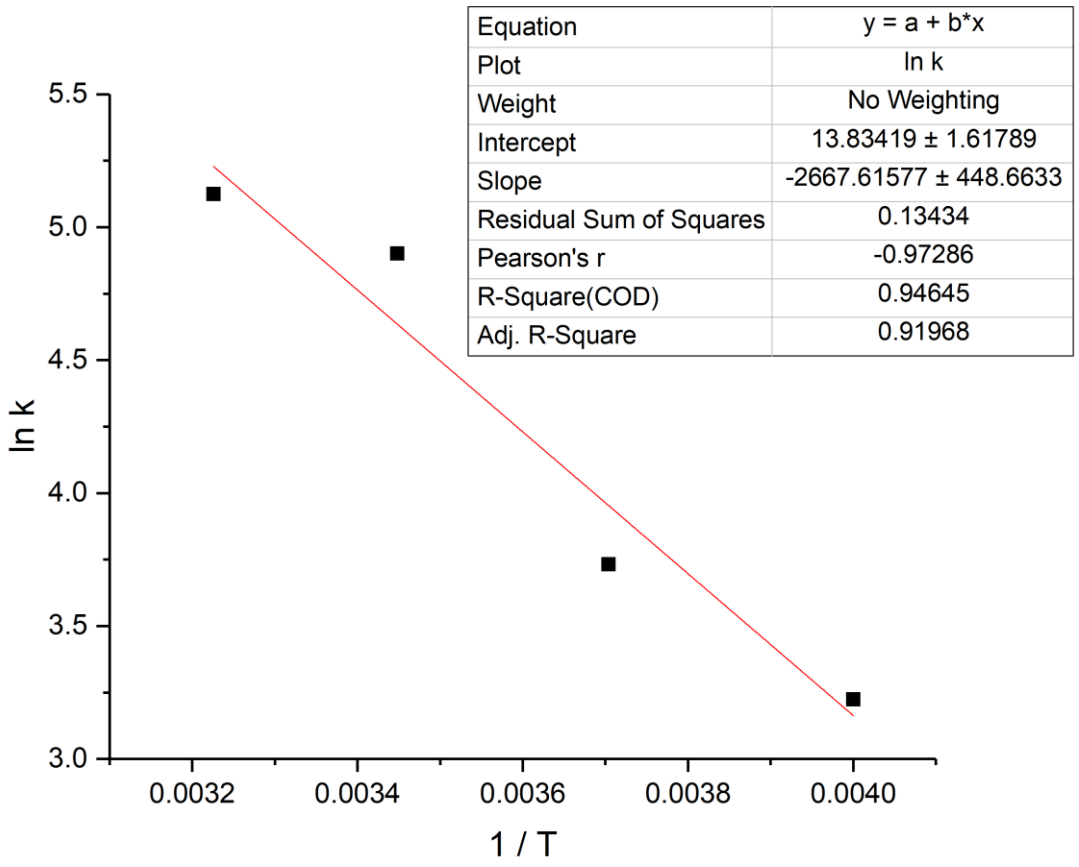

Fig. S83 Arrhenius plot for $(PMe_3)_2BeCl_2$ (**1a**) in C_7D_8.

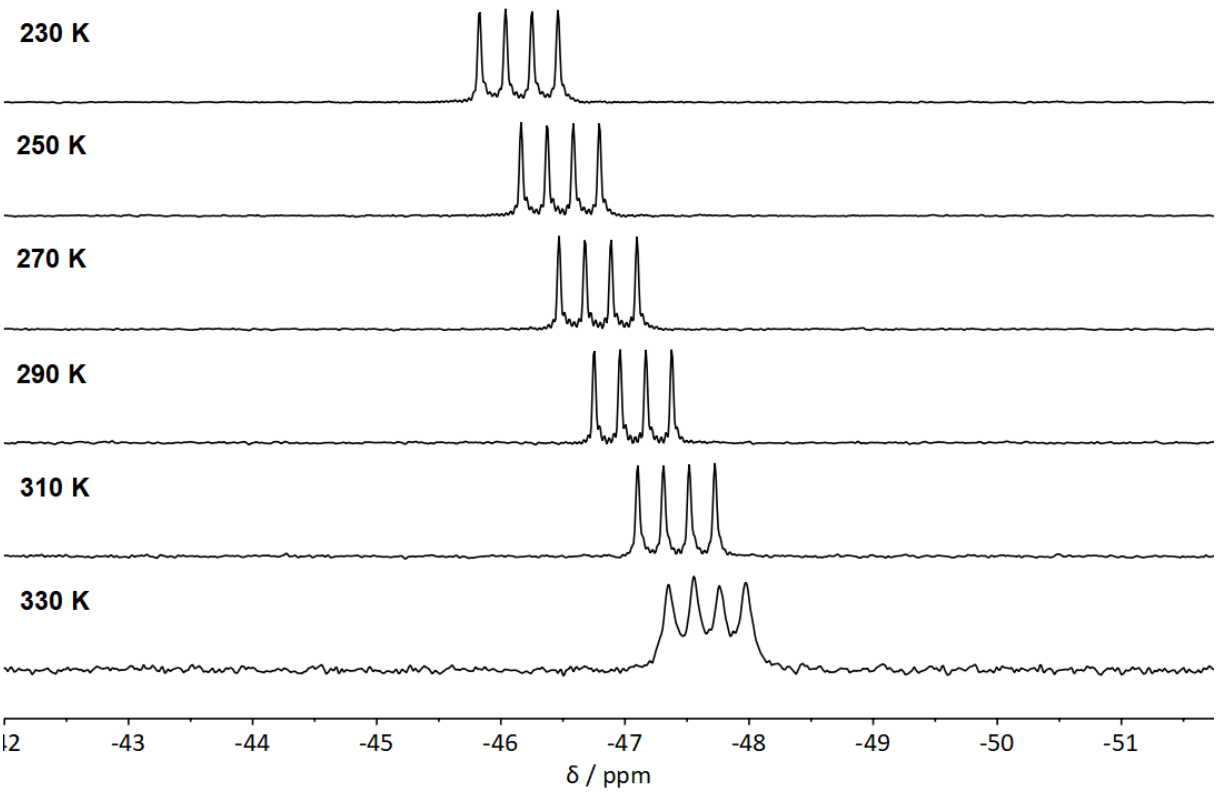

Fig. S84 Temperature dependent ^{31}P NMR spectra of $(PMe_3)_2BeBr_2$ (**1b**) in C_7D_8.

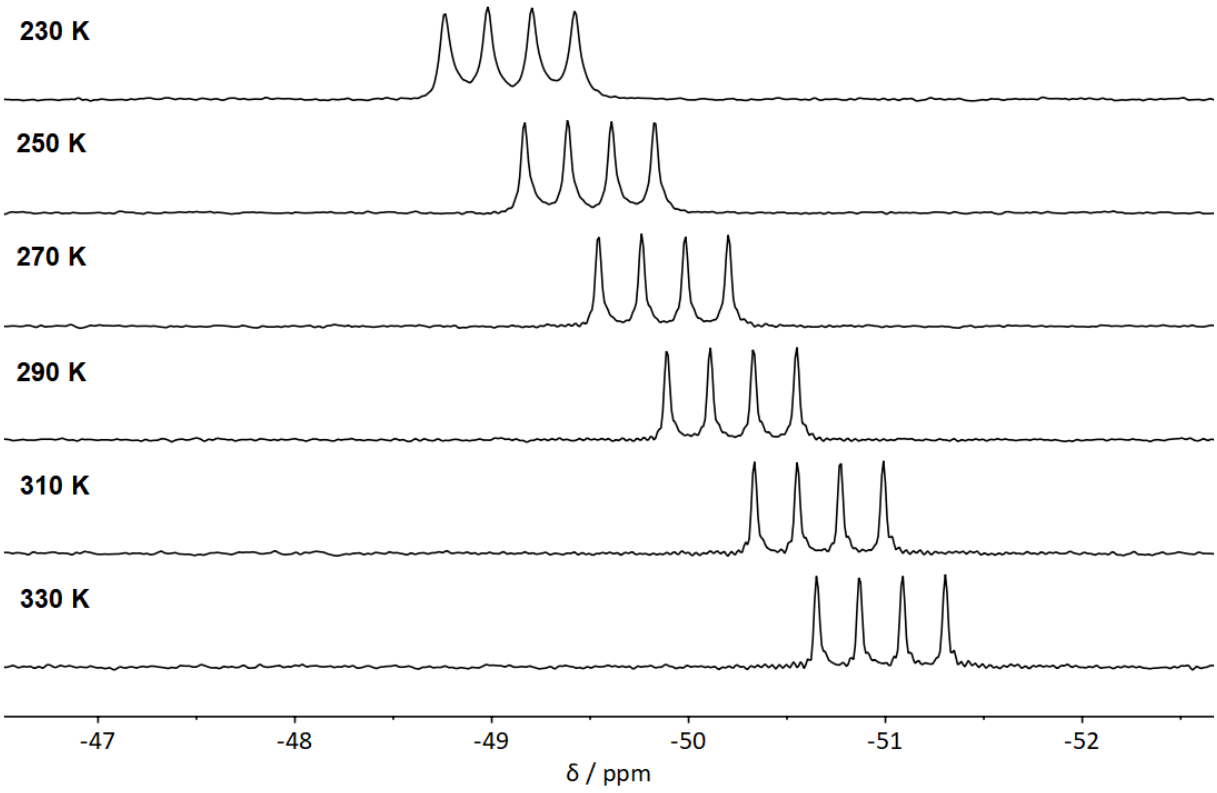

Fig. S85 Temperature dependent ^{31}P NMR spectra of $(PMe_3)_2BeI_2$ (**1c**) in C_7D_8.

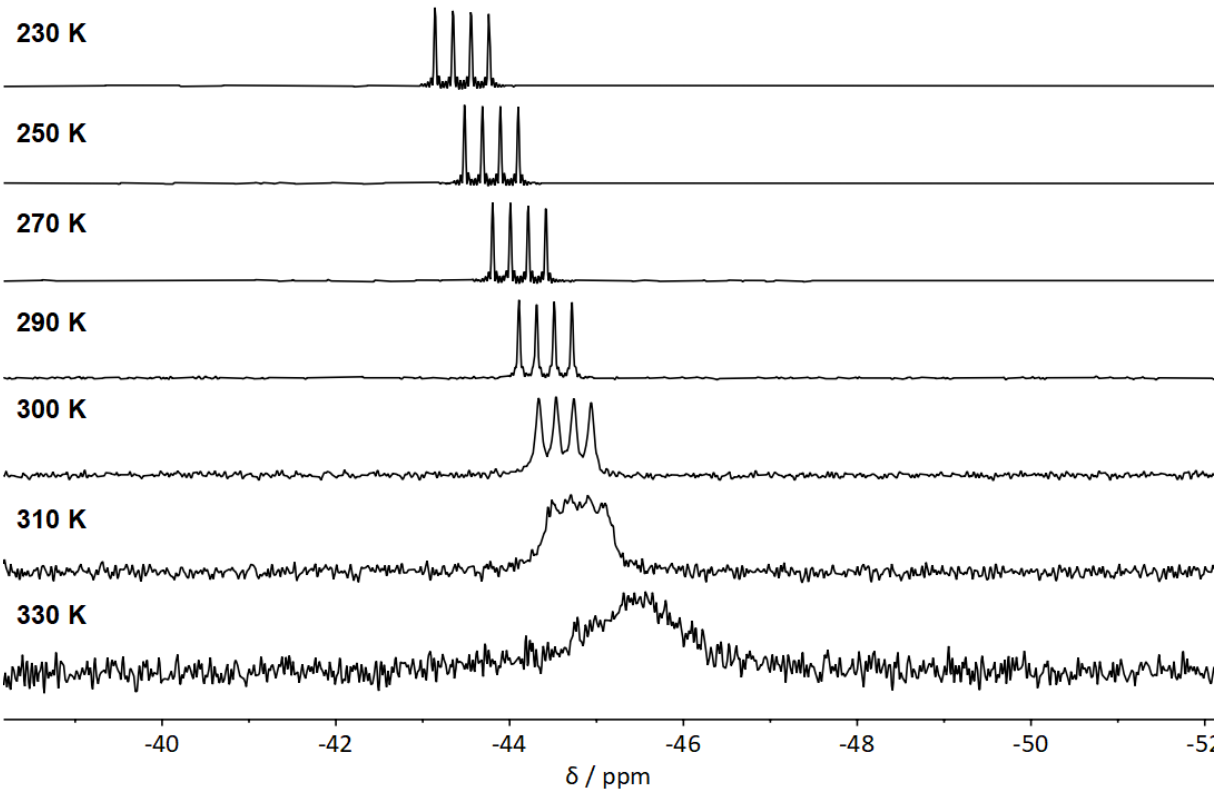

Fig. S86 Temperature dependent ^{31}P NMR spectra of $(PMe_3)_2BeCl_2$ (**1a**) in $CDCl_3$.

Table S7: Temperature dependent linewidths and derived parameters for **1a** in $CDCl_3$.

T [K]	$\omega_{1/2}$ [Hz]	k	ln k
290	6.8	21.4	3.06
300	18.0	56.5	4.04
310	56.0	175.9	5.17
330	218.0	684.9	6.53

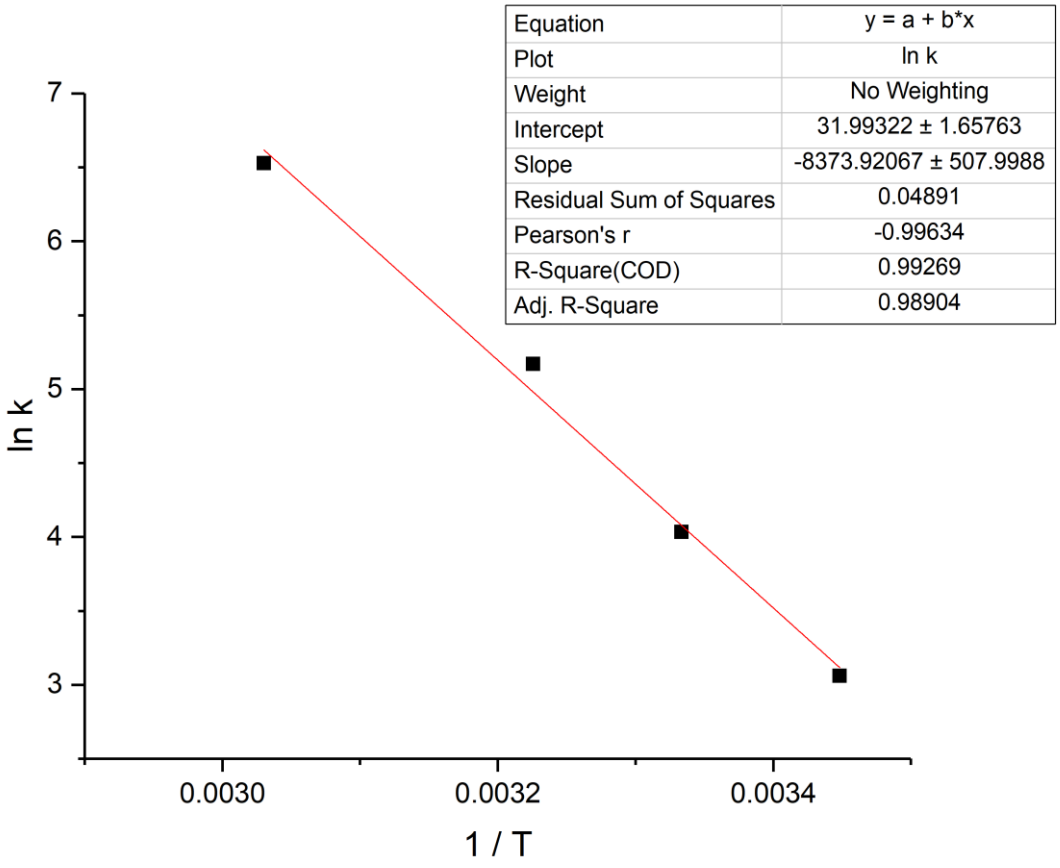

Fig. S87 Arrhenius plot for $(PMe_3)_2BeBr_2$ (**1a**) in $CDCl_3$.

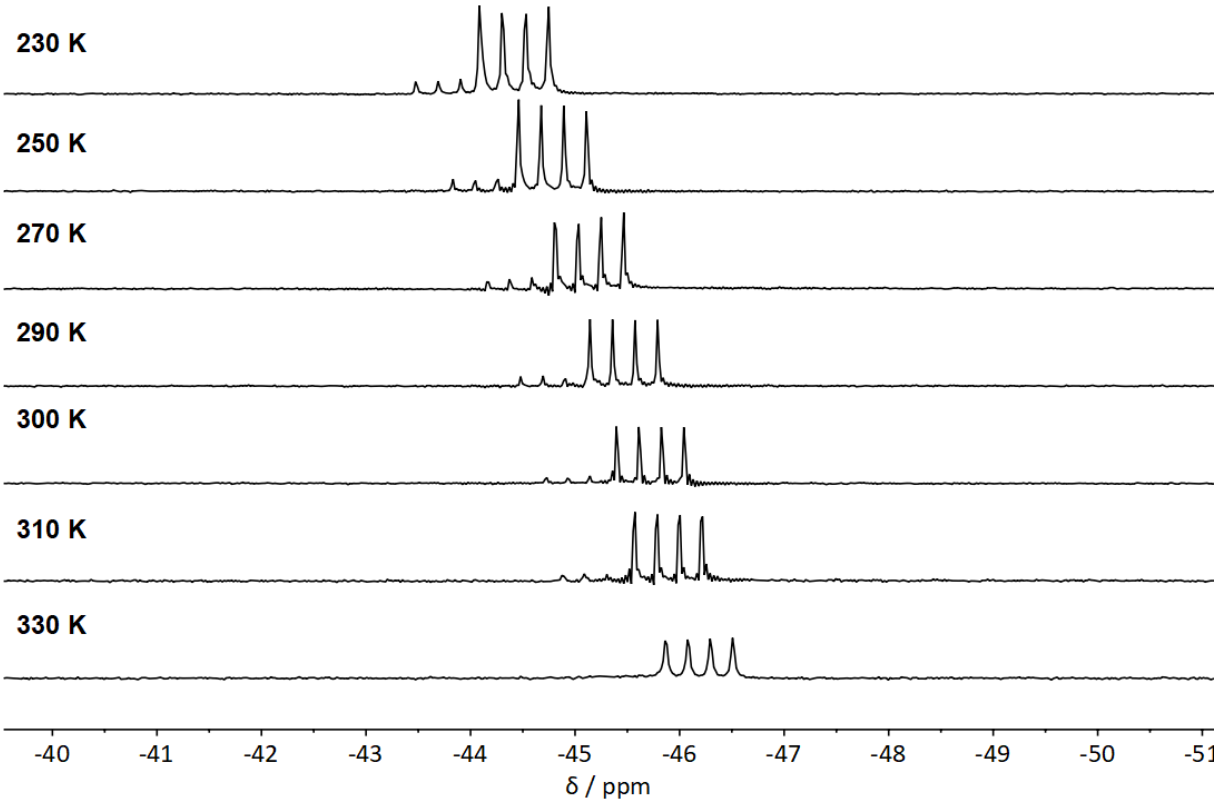

Fig. S88 Temperature dependent ^{31}P NMR spectra of $(PMe_3)_2BeBr_2$ (**1b**) in $CDCl_3$.

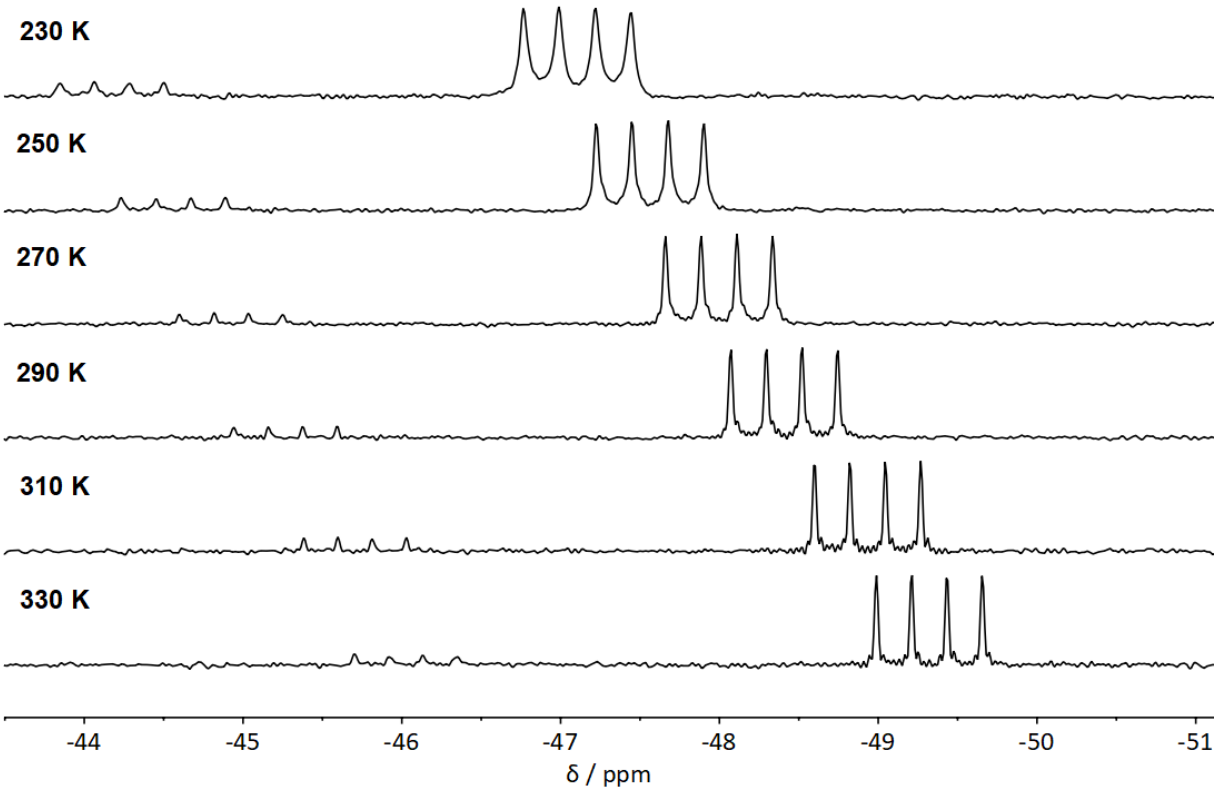

Fig. S89 Temperature dependent ^{31}P NMR spectra of $(PMe_3)_2BeI_2$ (**1c**) in $CDCl_3$.

Phosphine exchange

Table S8: Activation energies for the exchange of PMe_3 at compounds **1a-c** in toluene and chloroform with complex to ligand ration in parenthesis.

	E_A [kJ / mol]	
solvent	C_7D_8	$CDCl_3$
1a	31.38 ± 9.44 (1 / 8.4)	38.92 ± 4.60 (1 / 0.5)
		32.80 ± 4.55 (1 / 1.9)
		37.24 ± 2.26 (1 / 25.5)
1b	28.98 ± 3.14 (1 / 7.9)	77.66 ± 20.07 (1 / 3.8)
1c	19.99 ± 0.50 (1 / 6.1)	50.23 ± 9.25 (1 / 5.2)

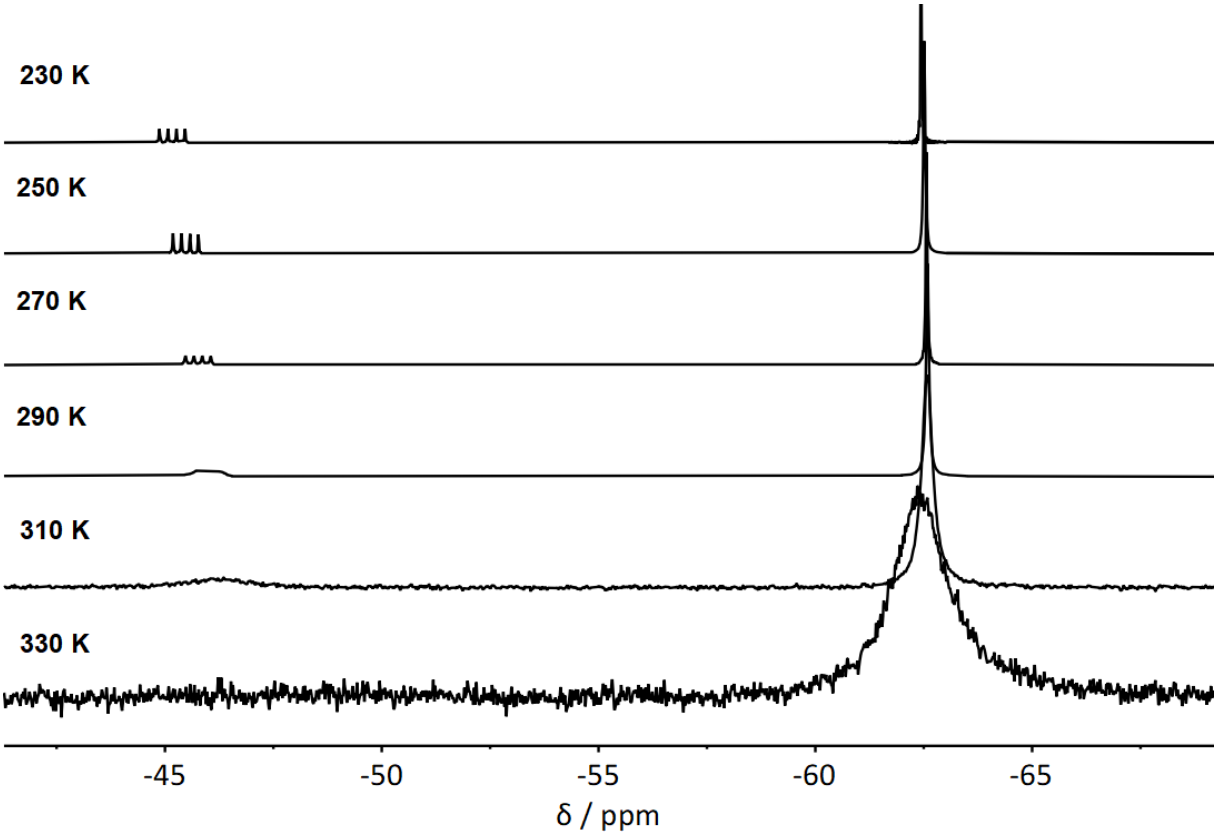

Fig. S90 Temperature dependent ^{31}P NMR spectra of a 1 / 8.4 mixture of $[(PMe_3)_2BeCl_2]$ (**1a**) and PMe_3 in C_7D_8.

Table S9: Temperature dependent linewidths and derived parameters of a 1 / 8.4 mixture of $[(PMe_3)_2BeCl_2]$ (**1a**) and PMe_3 in C_7D_8.

T [K]	$\omega_{1/2}$ [Hz]	k	ln k
250	3.1	10	2.28
270	3.4	11	2.37
290	11.3	35	3.57
310	58.1	183	5.21
330	326.8	1027	6.93

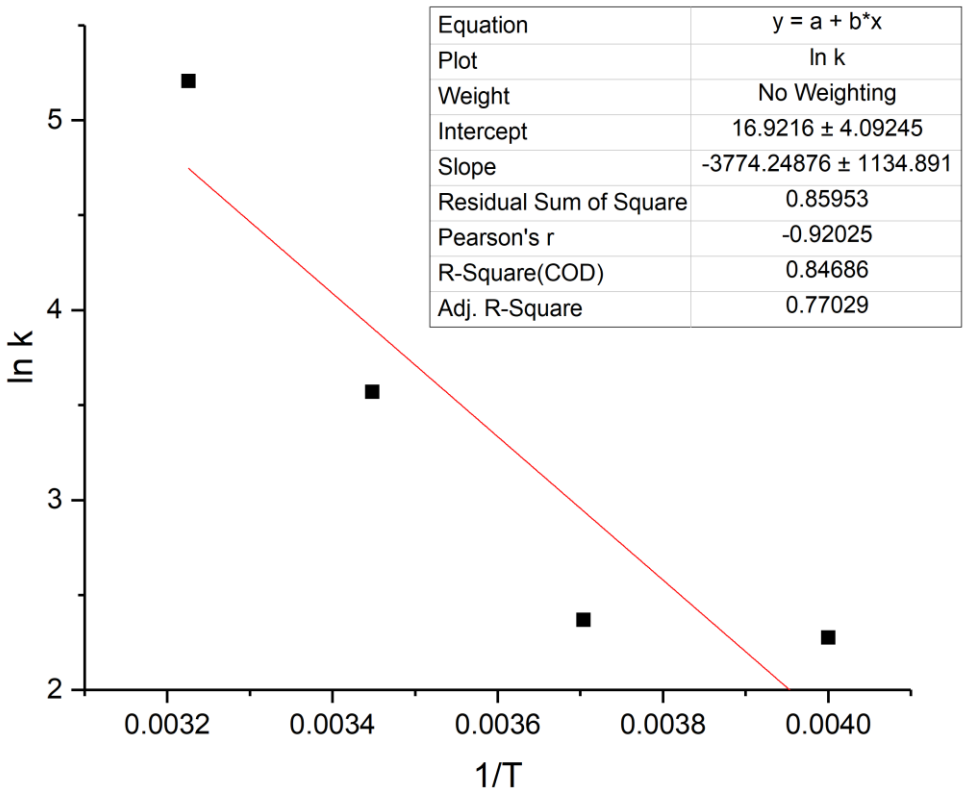

Fig. S91 Arrhenius plot for a 1 / 8.4 mixture of $[(PMe_3)_2BeCl_2]$ (**1a**) and PMe_3 in C_7D_8.

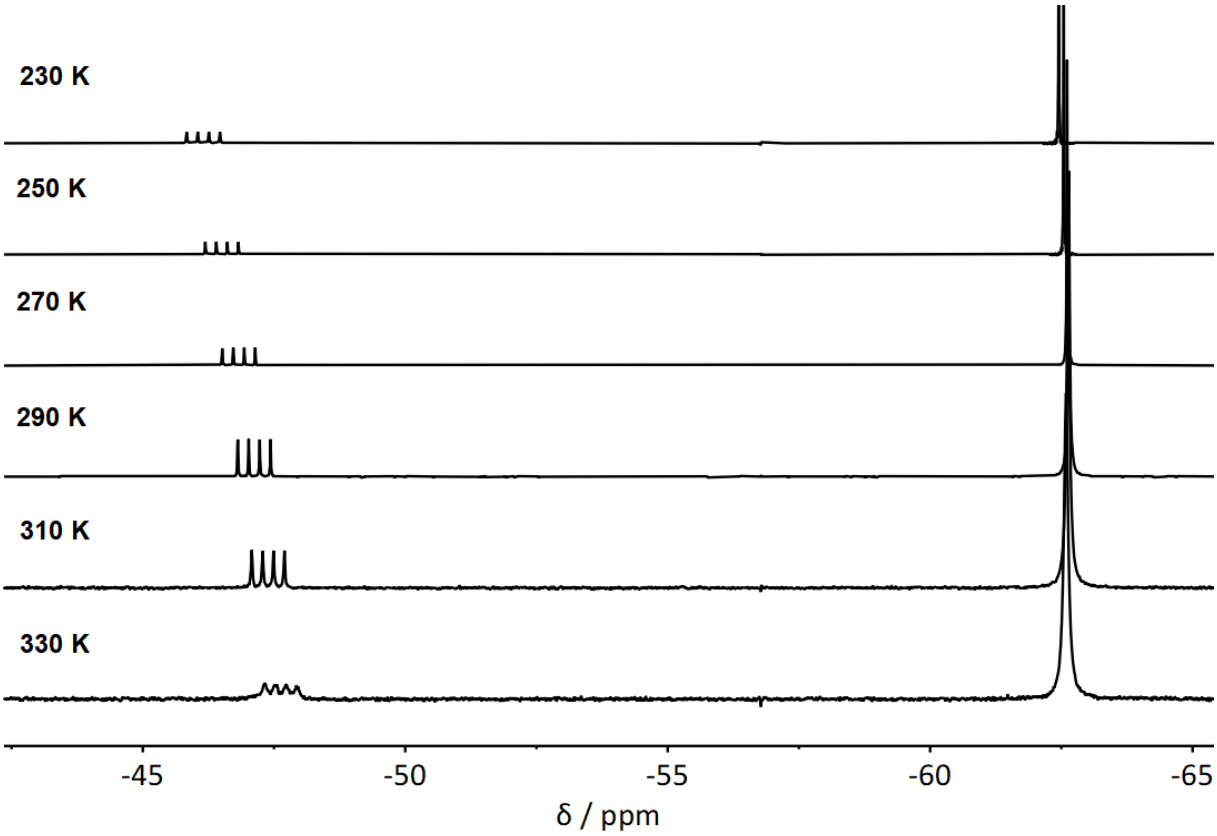

Fig. S92 Temperature dependent ^{31}P NMR spectra of a 1 / 7.9 mixture of $[(PMe_3)_2BeBr_2]$ (**1b**) and PMe_3 in C_7D_8.

Table S 10: Temperature dependent linewidths and derived parameters of a 1 / 7.9 mixture of $[(PMe_3)_2BeBr_2]$ (**1b**) and PMe_3 in C_7D_8.

T [K]	$\omega_{1/2}$ [Hz]	k	ln k
250	0.8	3	0.92
270	1.6	5	1.61
290	6.5	20	3.02
310	14.4	45	3.81
330	17.6	55	4.01

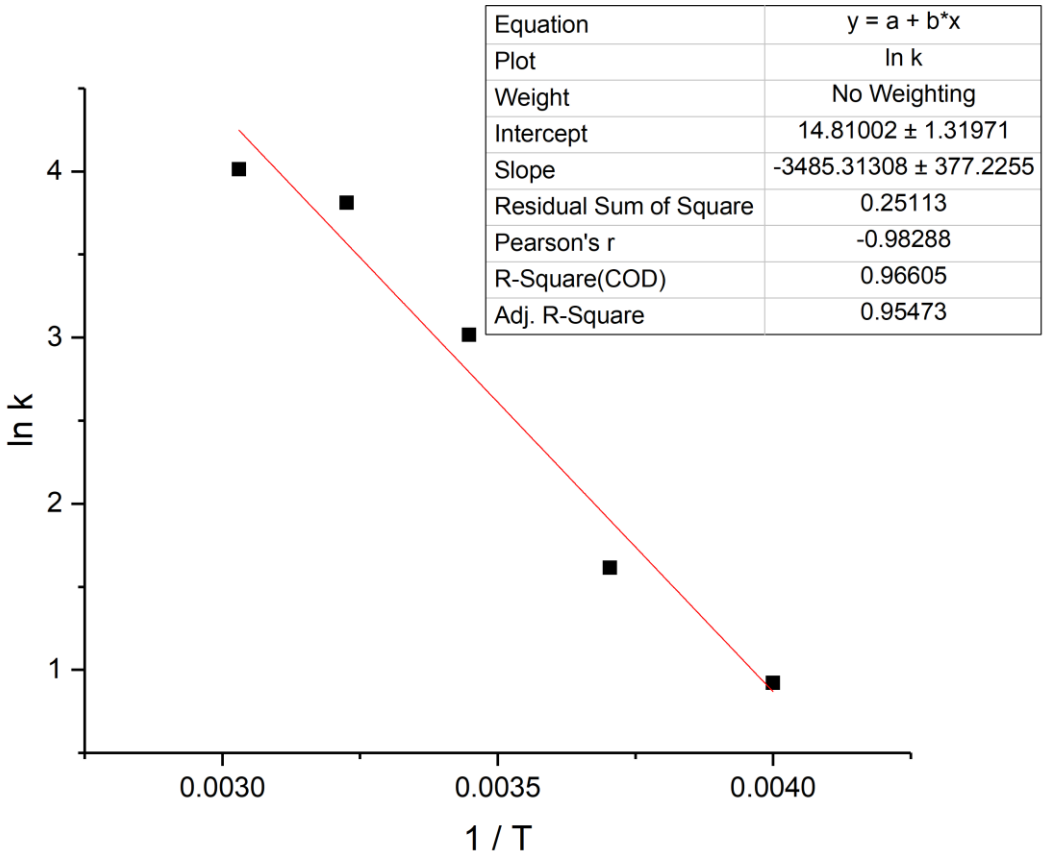

Fig. S93 Arrhenius plot for a 1 / 7.9 mixture of $[(PMe_3)_2BeBr_2]$ (**1b**) and PMe_3 in C_7D_8.

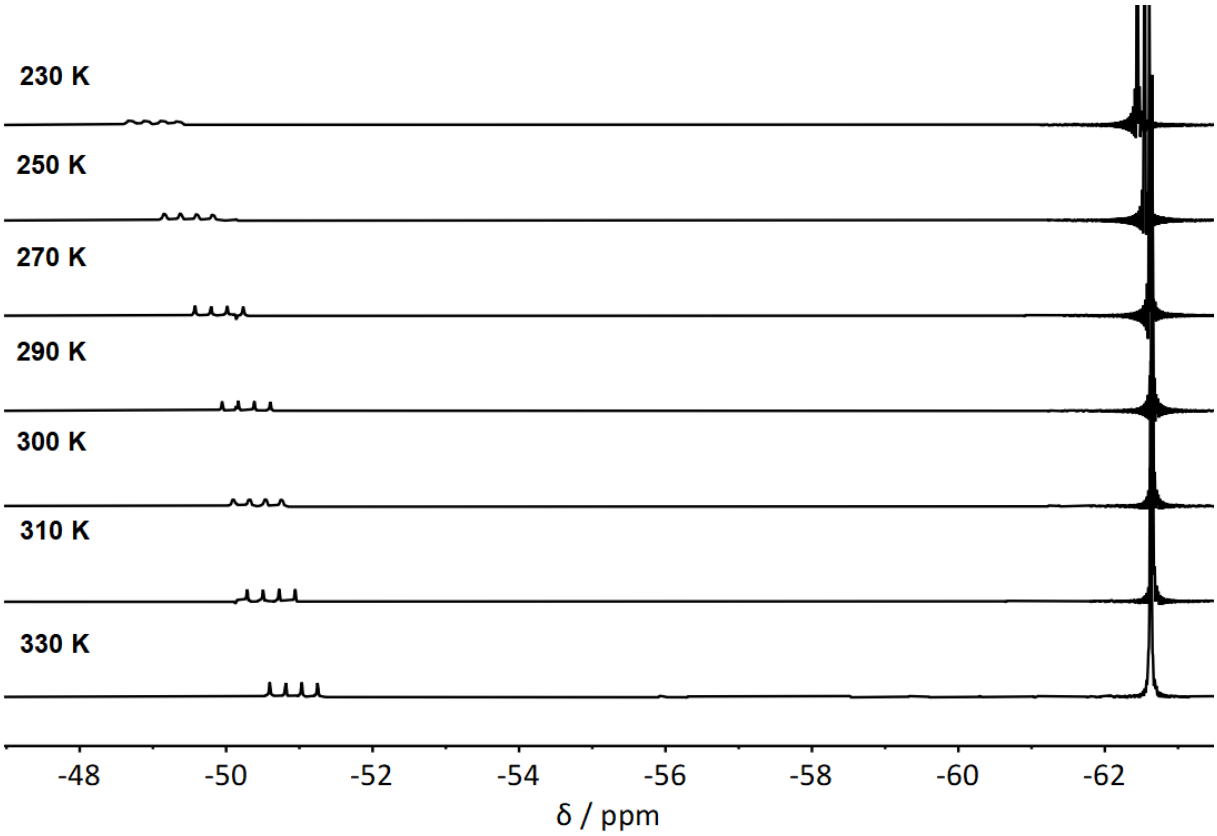

Fig. S94 Temperature dependent ^{31}P NMR spectra of a 1 / 6.1 mixture of $[(PMe_3)_2BeI_2]$ (**1c**) and PMe_3 in C_7D_8.

Table S11: Temperature dependent linewidths and derived parameters of a 1 / 6.1 mixture of $[(PMe_3)_2BeI_2]$ (**1c**) and PMe_3 in C_7D_8.

T [K]	$\omega_{1/2}$ [Hz]	k	ln k
290	0.7	2.2	0.78
300	0.9	2.8	1.04
330	1.9	6.0	1.78

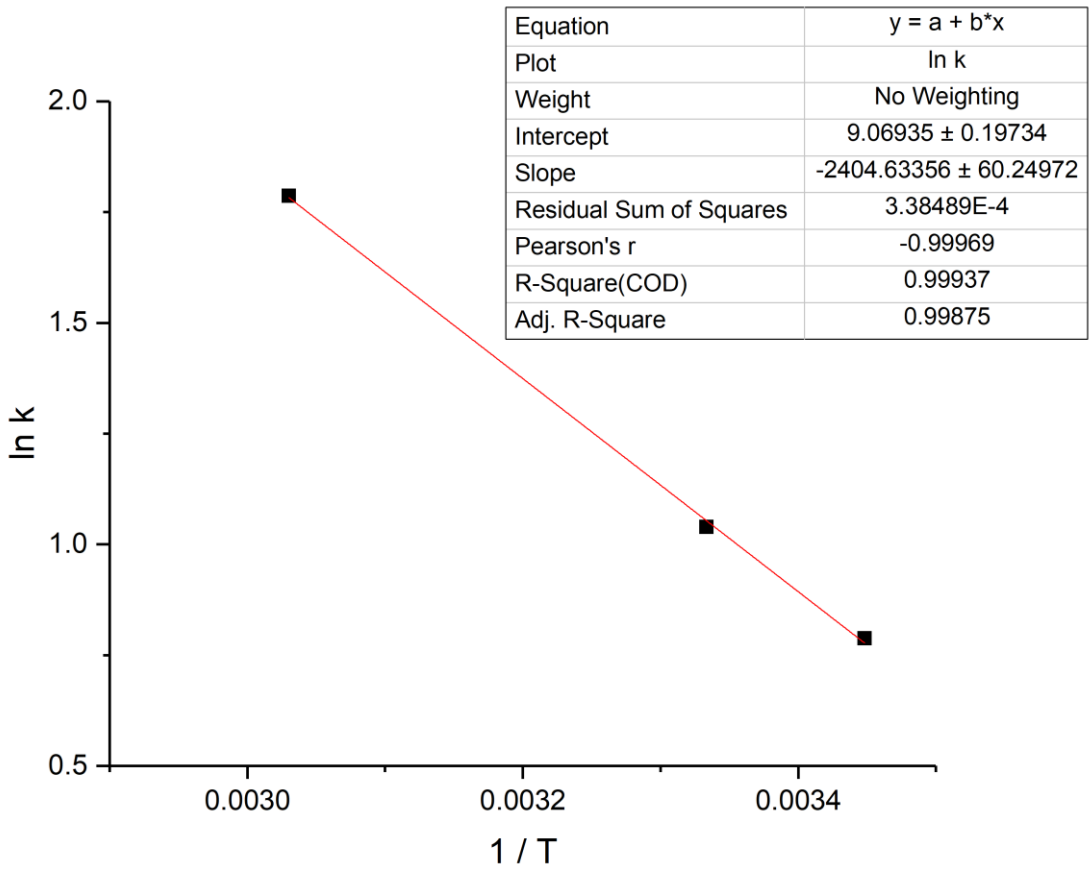

Fig. S95 Arrhenius plot for a 1 / 6.1 mixture of $[(PMe_3)_2BeI_2]$ (**1c**) and PMe_3 in C_7D_8.

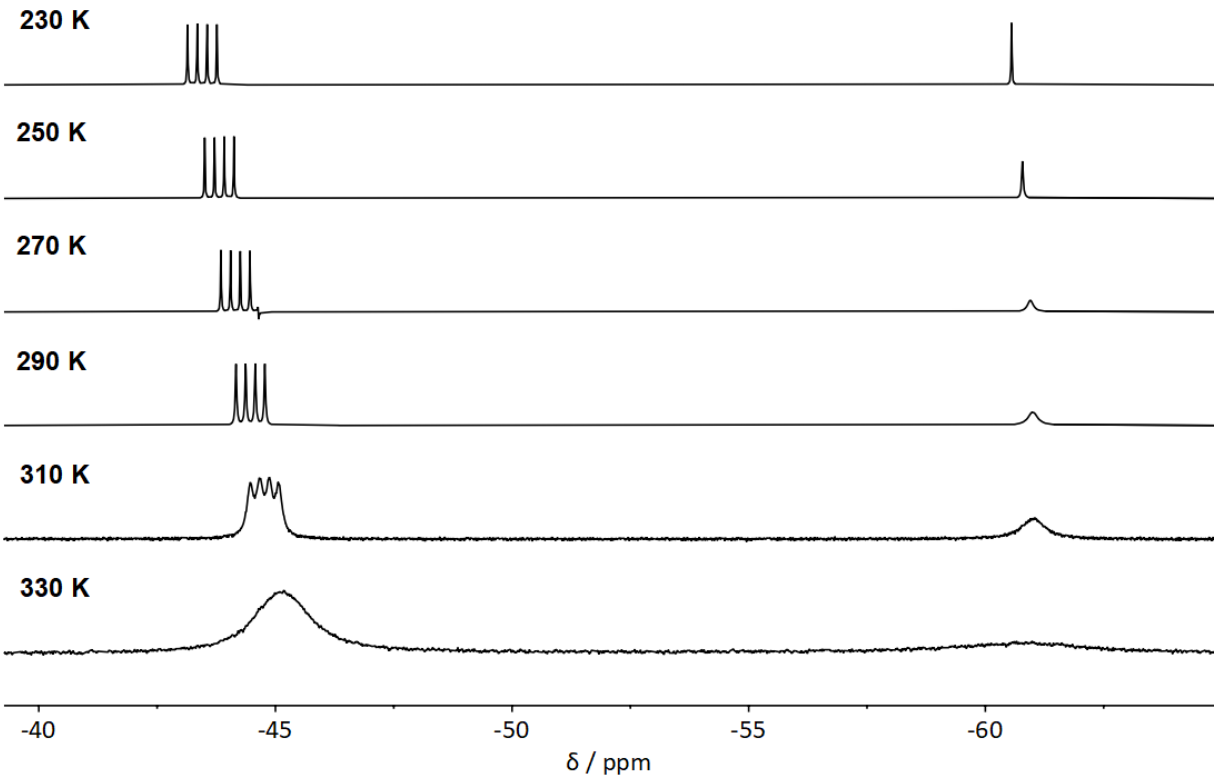

Fig. S96 Temperature dependent ^{31}P NMR spectra of a 1 / 0.5 mixture of $[(PMe_3)_2BeCl_2]$ (**1a**) and PMe_3 in $CDCl_3$.

Table S12: Temperature dependent linewidths and derived parameters of a 1 / 0.5 mixture of $[(PMe_3)_2BeCl_2]$ (**1a**) and PMe_3 in $CDCl_3$.

T [K]	$\omega_{1/2}$ [Hz]	k	ln k
250	4.1	13	2.56
270	26.6	84	4.43
290	44.2	139	4.93
310	111.2	349	5.86
330	593.5	1865	7.53

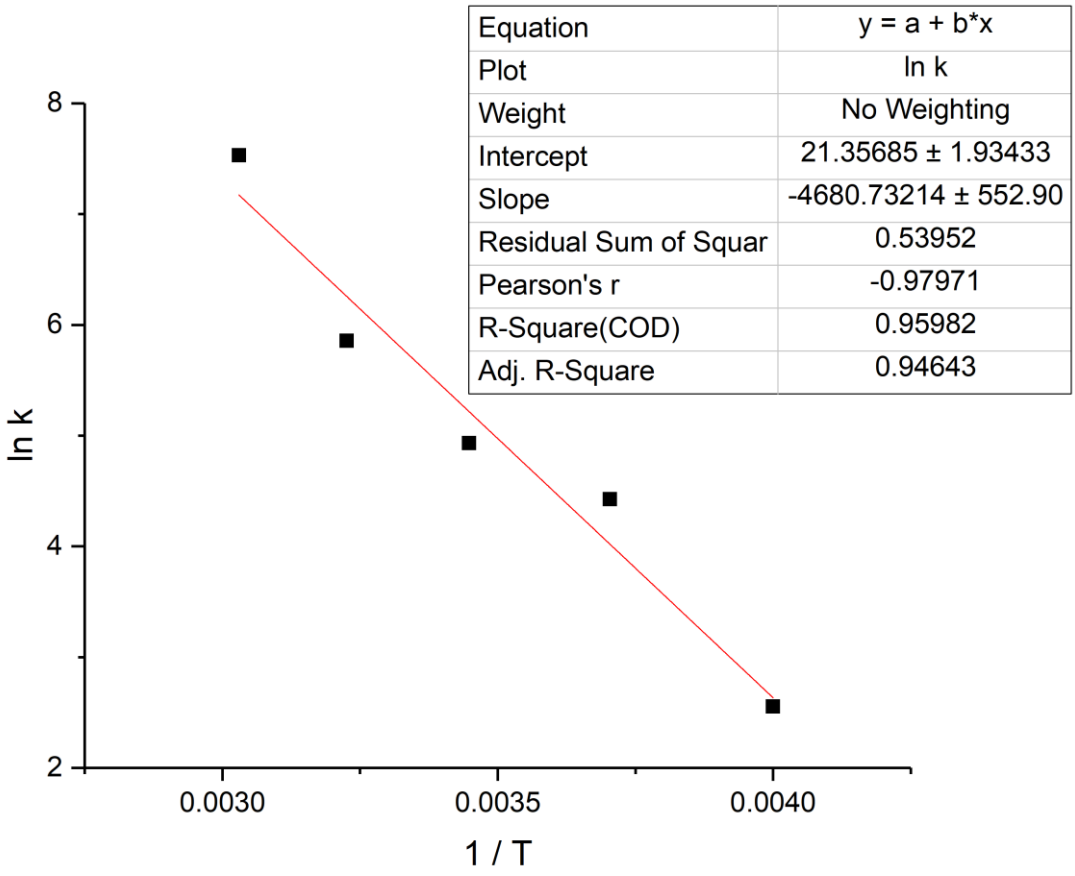

Fig. S97 Arrhenius plot for a 1 / 0.5 mixture of [$(PMe_3)_2BeCl_2$] (**1a**) and PMe_3 in $CDCl_3$.

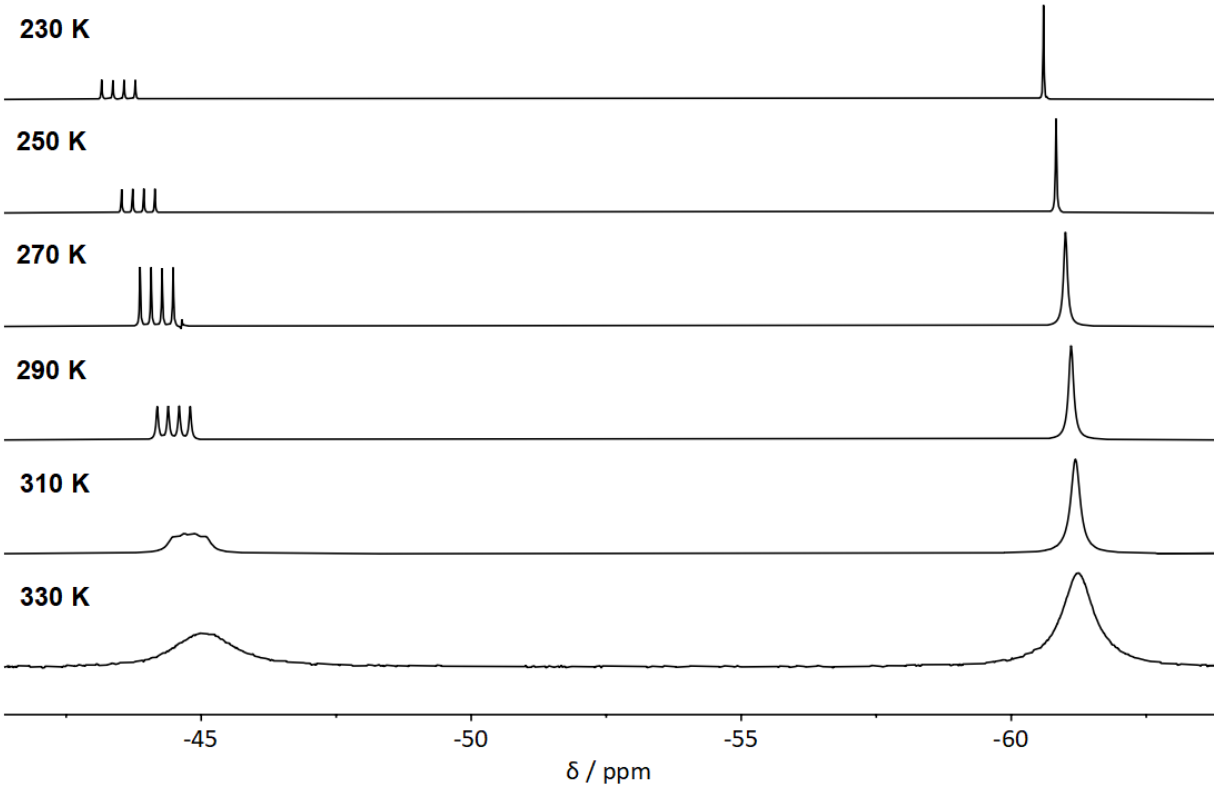

Fig. S98 Temperature dependent ^{31}P NMR spectra of a 1 / 1.9 mixture of $[(PMe_3)_2BeCl_2]$ (**1a**) and PMe_3 in $CDCl_3$.

Table S13: Temperature dependent linewidths and derived parameters of a 1 / 1.9 mixture of $[(PMe_3)_2BeCl_2]$ (**1a**) and PMe_3 in $CDCl_3$.

T [K]	$\omega_{1/2}$ [Hz]	k	ln k
250	2.0	6	1.84
270	14.4	45	3.81
290	18.6	58	4.07
310	40.3	127	4.84
330	139.7	438	6.08

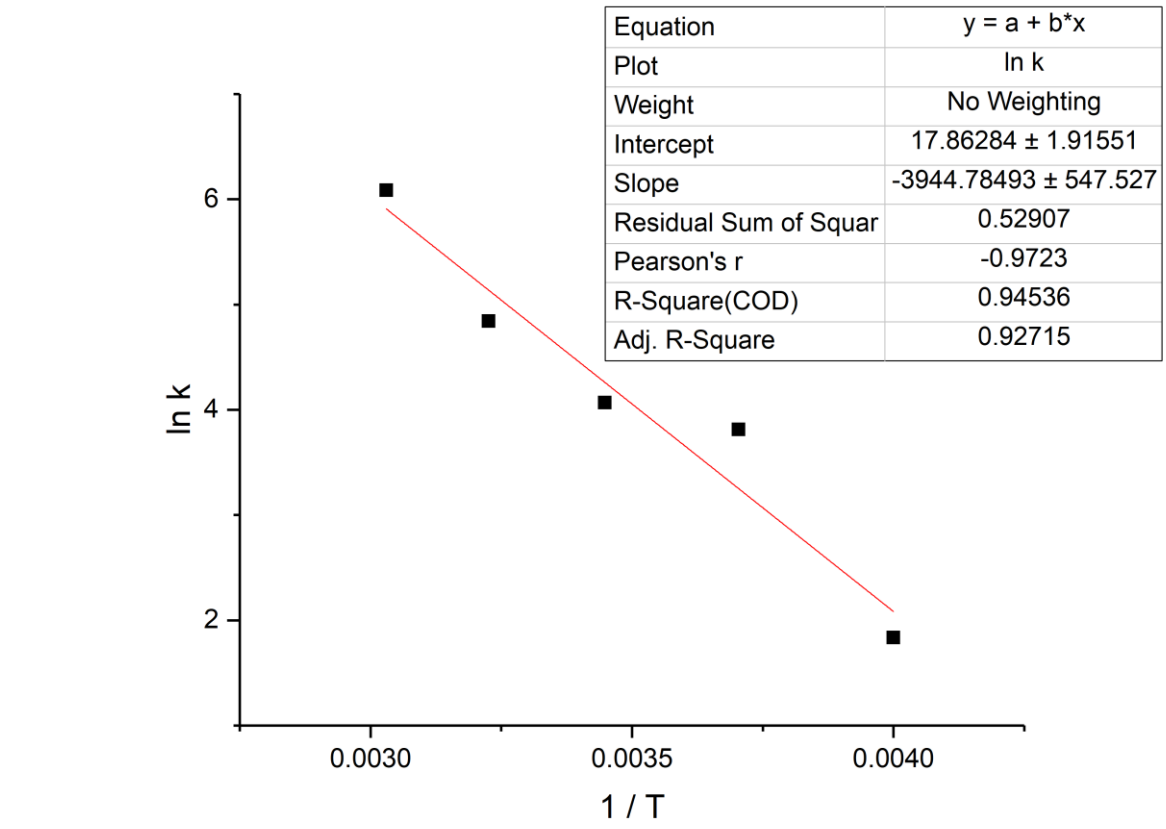

Fig. S99 Arrhenius plot for a 1 / 1.9 mixture of $[(PMe_3)_2BeCl_2]$ (**1a**) and PMe_3 in $CDCl_3$.

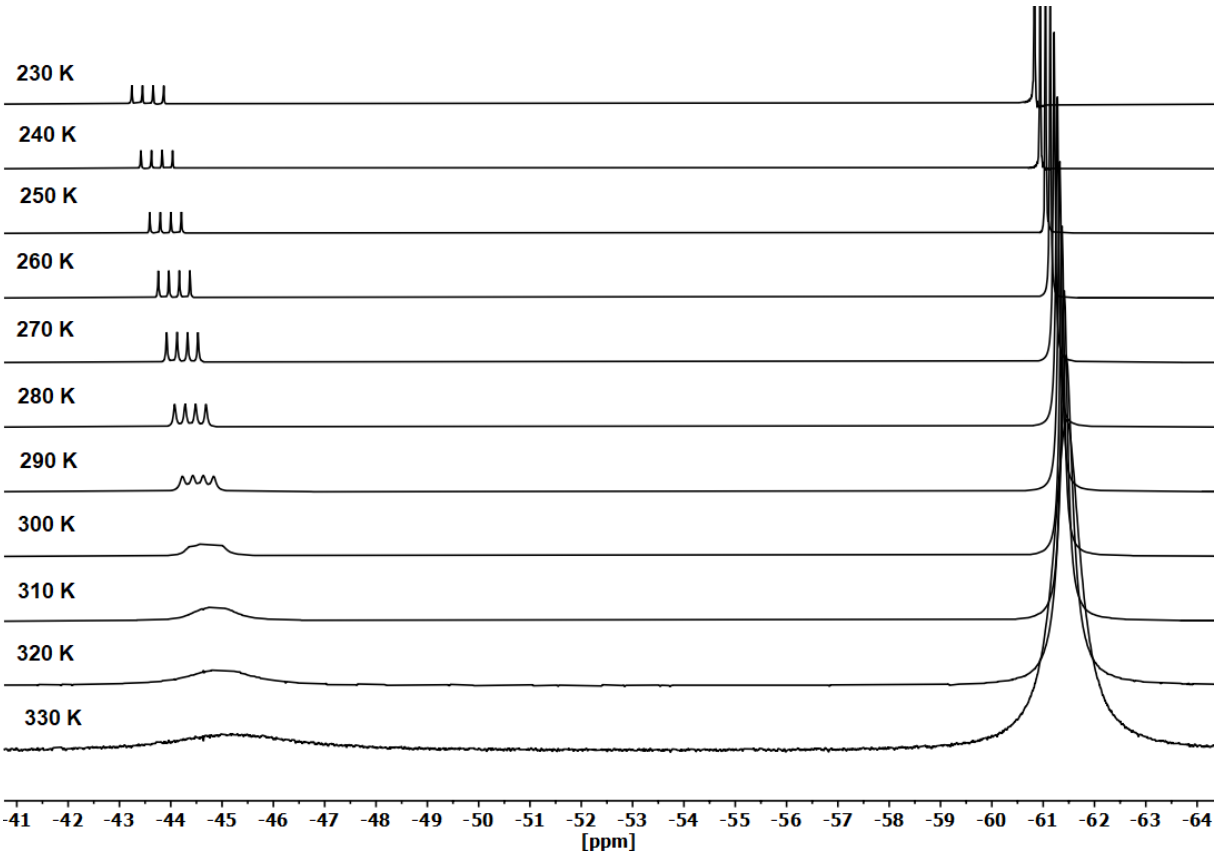

Fig. S100 Temperature dependent ^{31}P NMR spectra of a 1 / 25.5 mixture of $[(PMe_3)_2BeCl_2]$ (**1a**) and PMe_3 in $CDCl_3$.

Table S14: Temperature dependent linewidths and derived parameters of a 1 / 25.5 mixture of $[(PMe_3)_2BeCl_2]$ (**1a**) and PMe_3 in $CDCl_3$.

T [K]	$\omega_{1/2}$ [Hz]	k	ln k
240	0.4	1	0.23
250	1.2	4	1.33
260	3.4	11	2.37
270	7.5	24	3.16
280	11.4	36	3.58
290	15.0	47	3.85
300	18.8	59	4.08
310	29.2	92	4.52
320	58.5	184	5.21
330	117.1	368	5.91

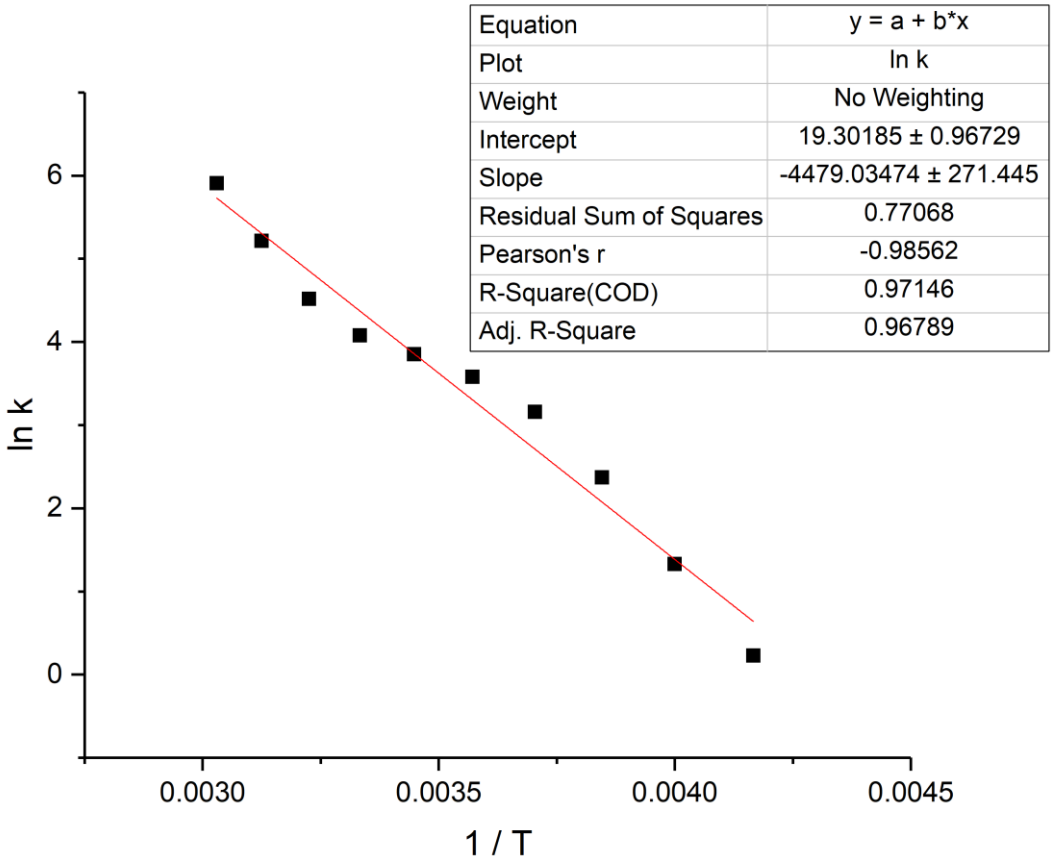

Fig. S101 Arrhenius plot for a 1 / 25.5 mixture of $[(PMe_3)_2BeCl_2]$ (**1a**) and PMe_3 in $CDCl_3$.

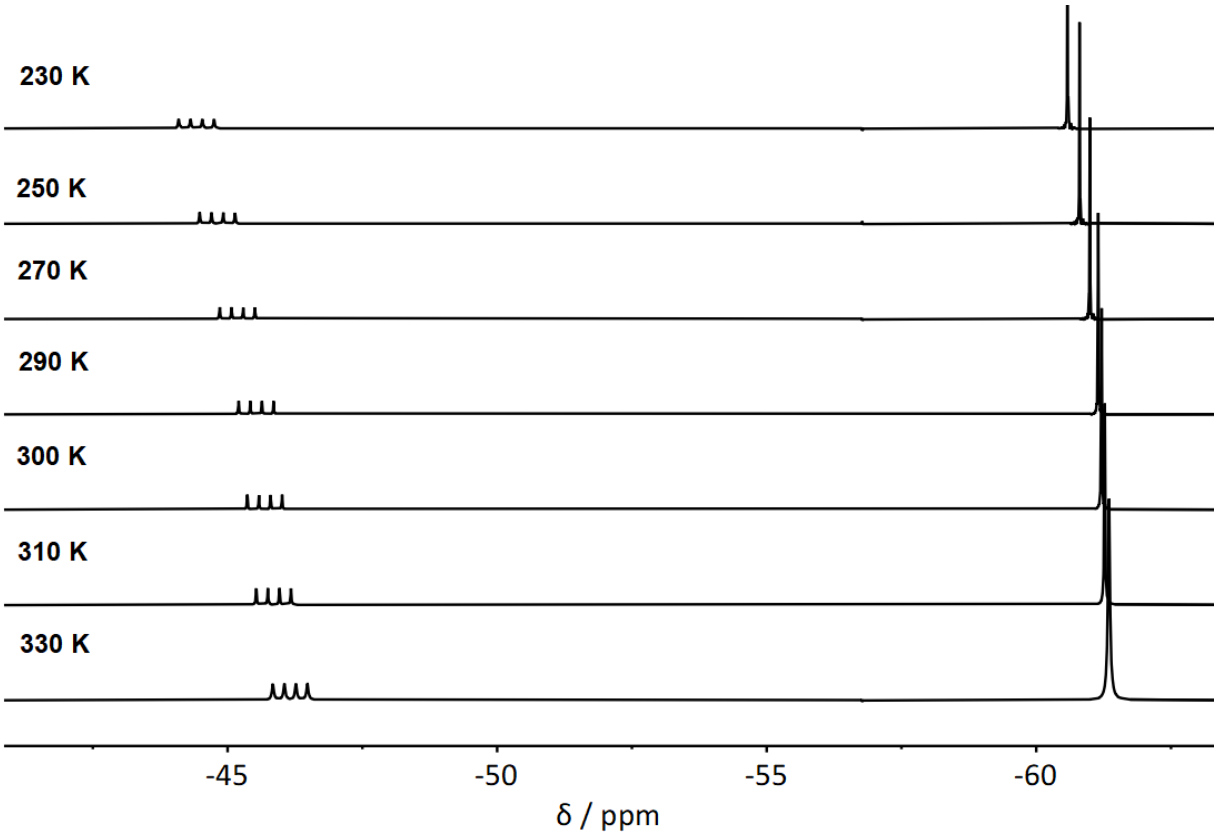

Fig. S102 Temperature dependent ^{31}P NMR spectra of a 1 / 3.8 mixture of $[(PMe_3)_2BeBr_2]$ (**1b**) and PMe_3 in $CDCl_3$.

Table S15: Temperature dependent linewidths and derived parameters of a 1 / 3.8 mixture of $[(PMe_3)_2BeBr_2]$ (**1b**) and PMe_3 in $CDCl_3$.

T [K]	$\omega_{1/2}$ [Hz]	k	ln k
290	0.1	0.3	−1.16
300	1.2	3.8	1.33
310	1.7	5.3	1.68
330	7	22.0	3.09

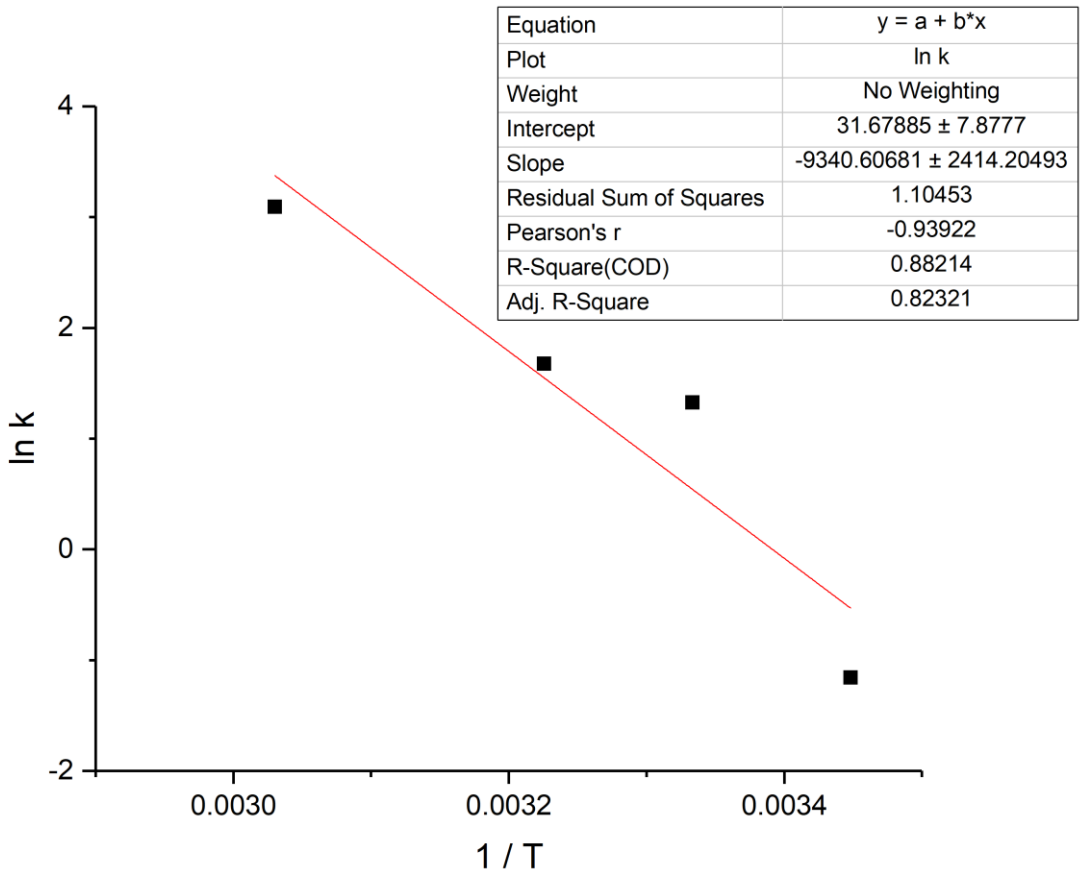

Fig. S103 Arrhenius plot for a 1 / 3.8 mixture of $[(PMe_3)_2BeBr_2]$ (**1b**) and PMe_3 in $CDCl_3$.

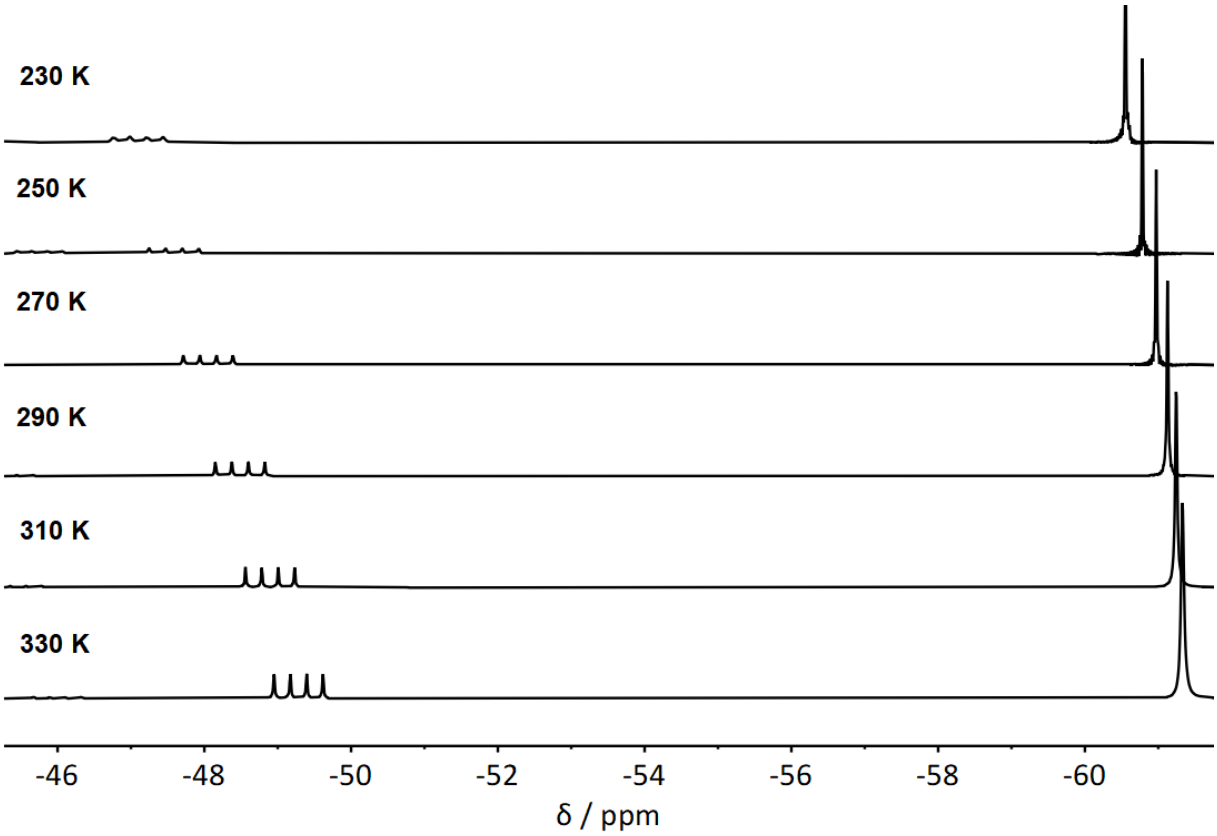

Fig. S104 Temperature dependent ^{31}P NMR spectra of a 1 / 5.2 mixture of $[(PMe_3)_2BeI_2]$ (**1c**) and PMe_3 in $CDCl_3$.

Table S16: Temperature dependent linewidths and derived parameters of a 1 / 5.2 mixture of $[(PMe_3)_2BeI_2]$ (**1c**) and PMe_3 in $CDCl_3$.

T [K]	$\omega_{1/2}$ [Hz]	k	ln k
270	0.1	0.3	−1.16
290	1.2	3.8	1.33
310	3.3	10.4	2.34
330	6.1	19.2	2.95

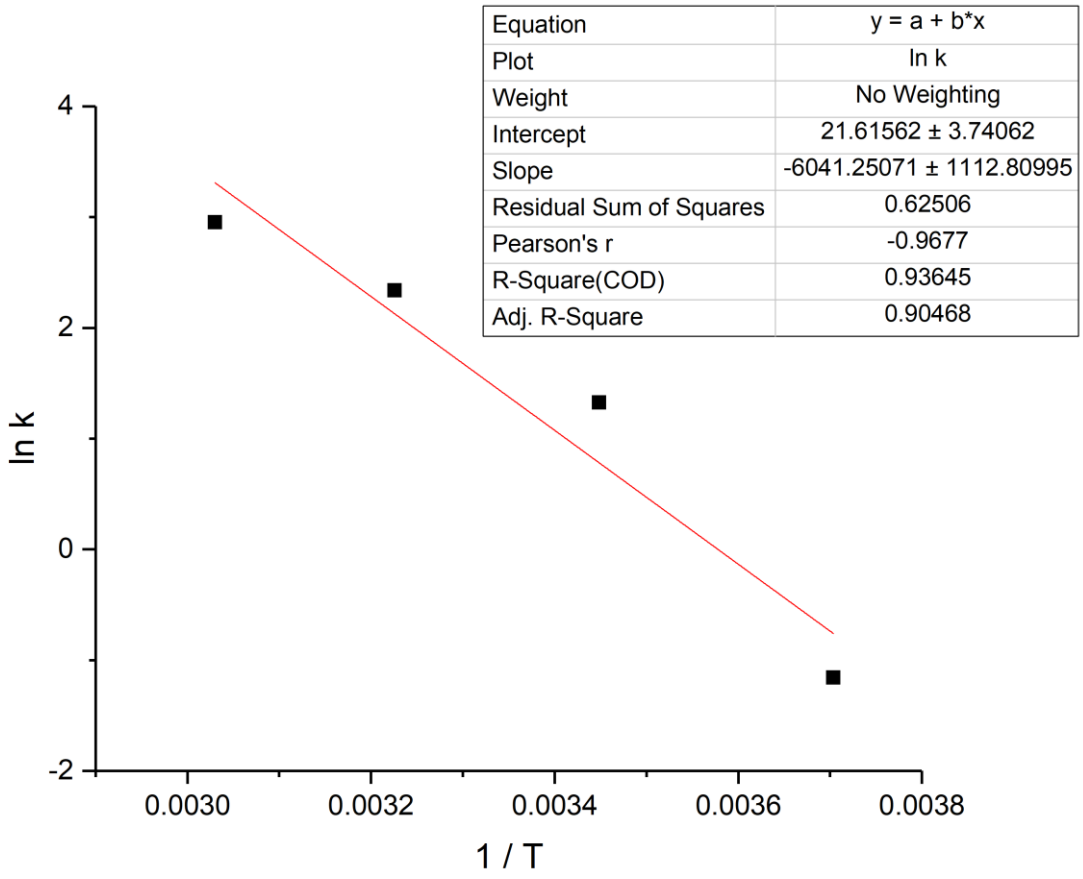

Fig. S105 Arrhenius plot for a 1 / 5.2 mixture of $[(PMe_3)_2BeI_2]$ (**1c**) and PMe_3 in $CDCl_3$.

Dimer Dissoziation

Table S17: Activation energies for the dissociation of compounds **2a-c** in toluene and chloroform.

	E_A [kJ / mol]	
solvent	C_7D_8	$CDCl_3$
2a	—[a]	—[a]
2b	—[a]	—[a]
2c	—[a]	50.32 ± 26.52

[a] Too high for determination via VT NMR experiments.

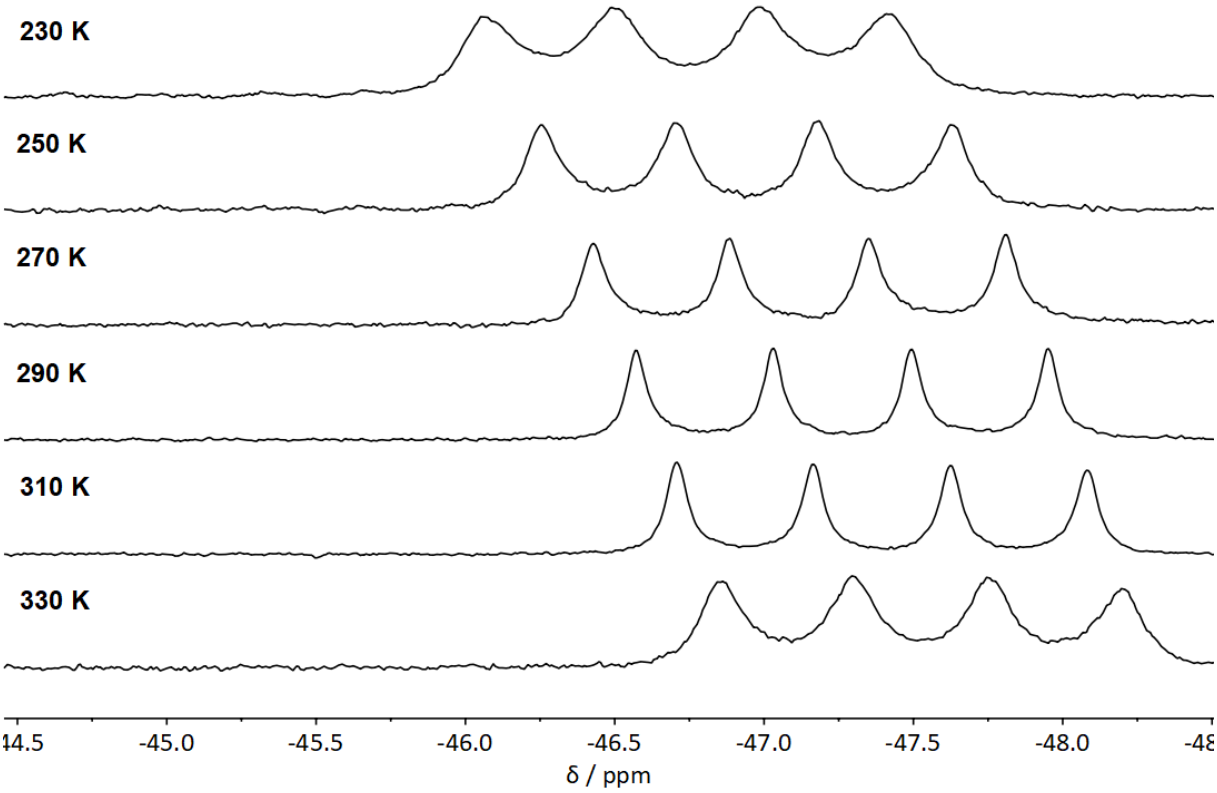

Fig. S106 Temperature dependent ^{31}P NMR spectra of $[(PMe_3)BeCl_2]_2$ (**2a**) in C_7D_8.

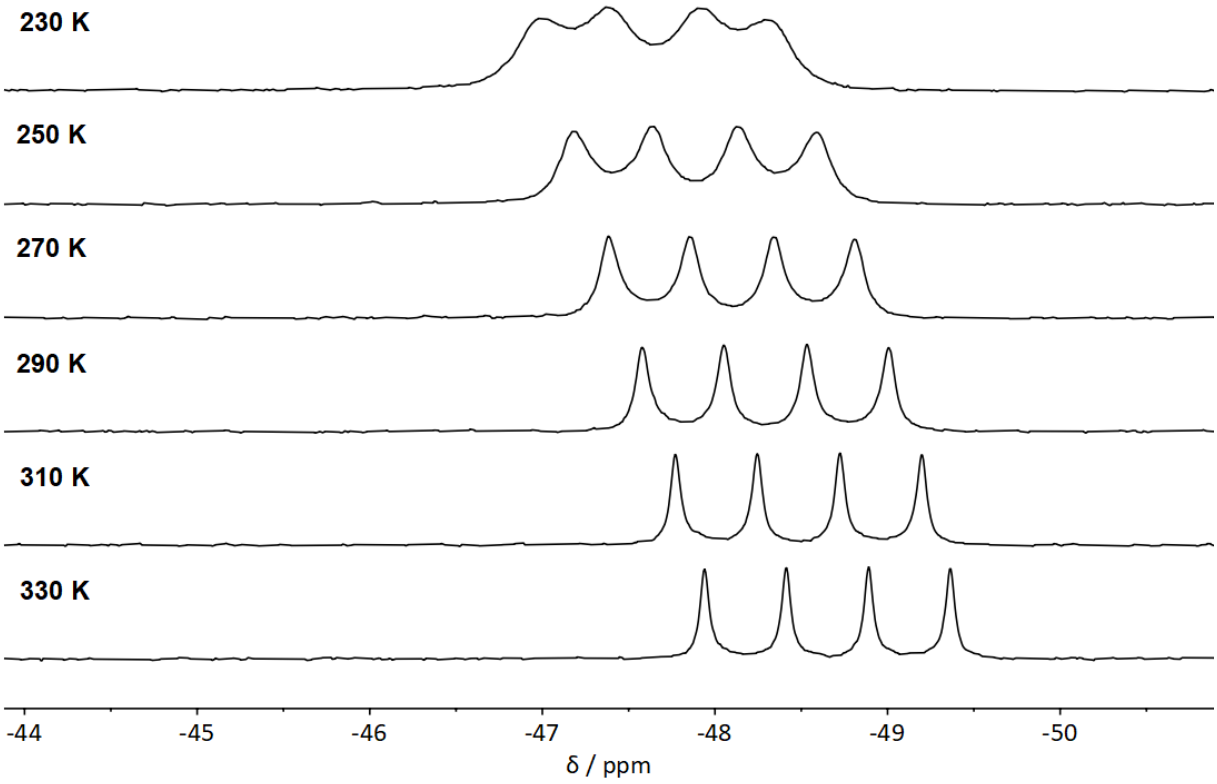

Fig. S107 Temperature dependent ^{31}P NMR spectra of $[(PMe_3)BeBr_2]_2$ (**2b**) in C_7D_8.

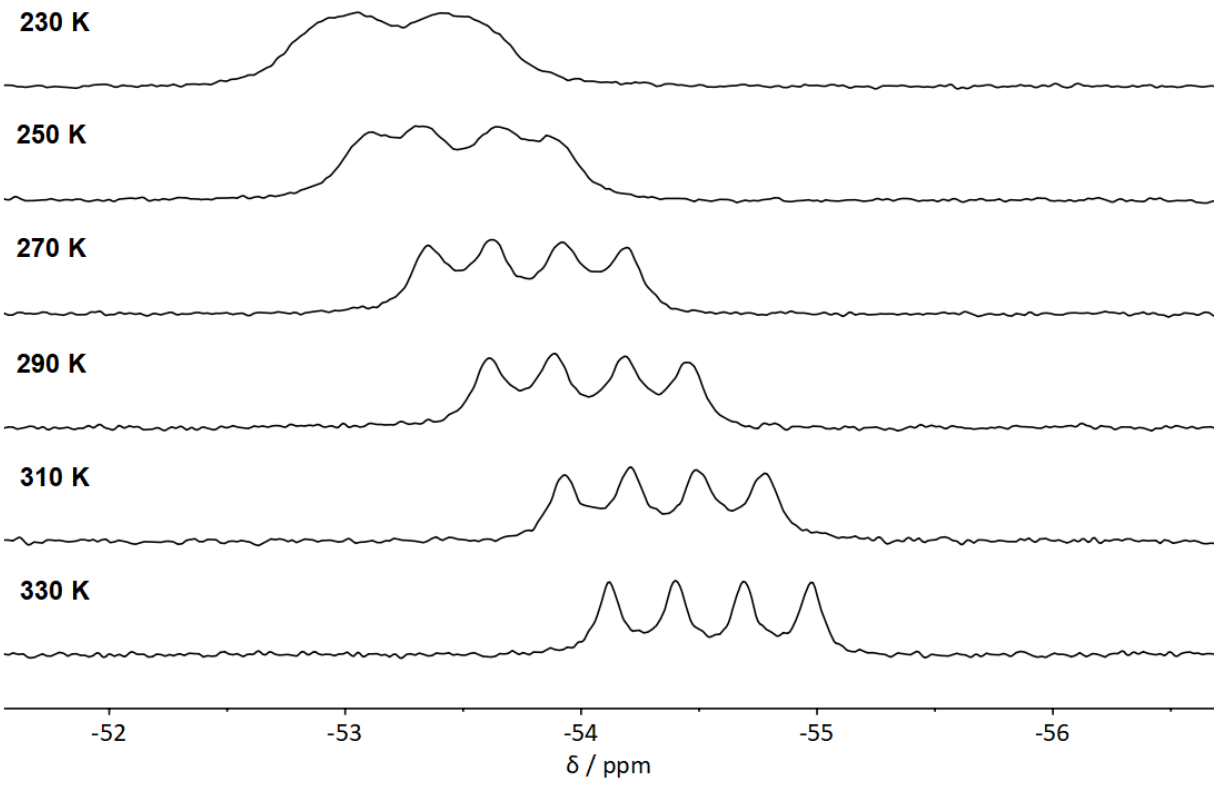

Fig. S108 Temperature dependent ^{31}P NMR spectra of $[(PMe_3)BeI_2]_2$ (**2c**) in C_7D_8.

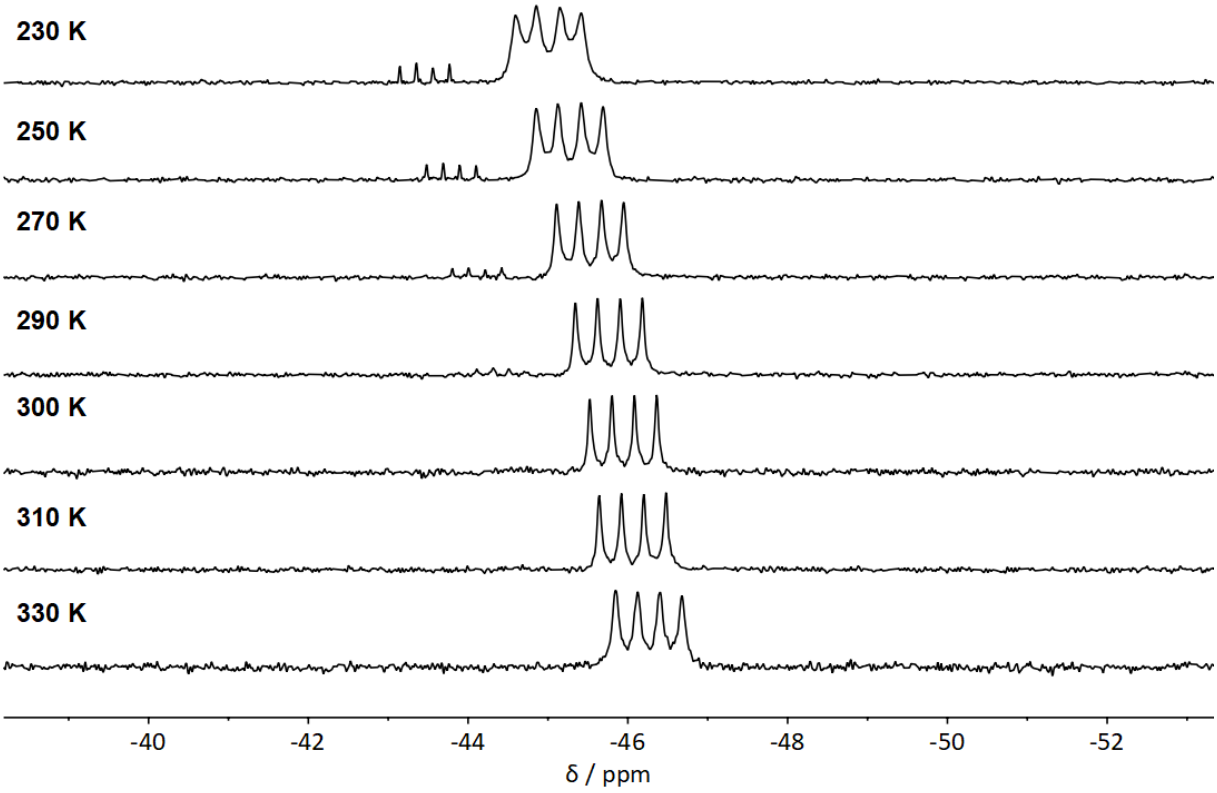

Fig. S109 Temperature dependent ^{31}P NMR spectra of $[(PMe_3)BeCl_2]_2$ (**2a**) in $CDCl_3$.

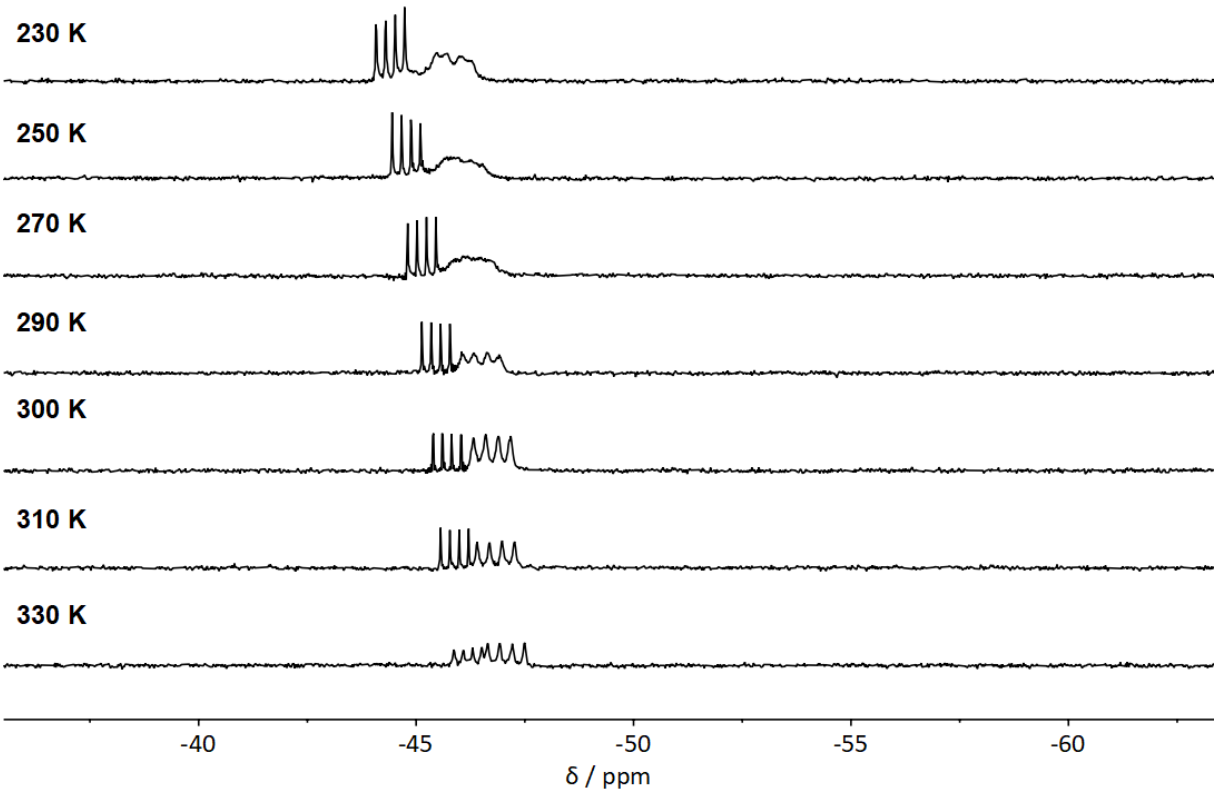

Fig. S110 Temperature dependent ^{31}P NMR spectra of $[(PMe_3)BeBr_2]_2$ (**2b**) in $CDCl_3$.

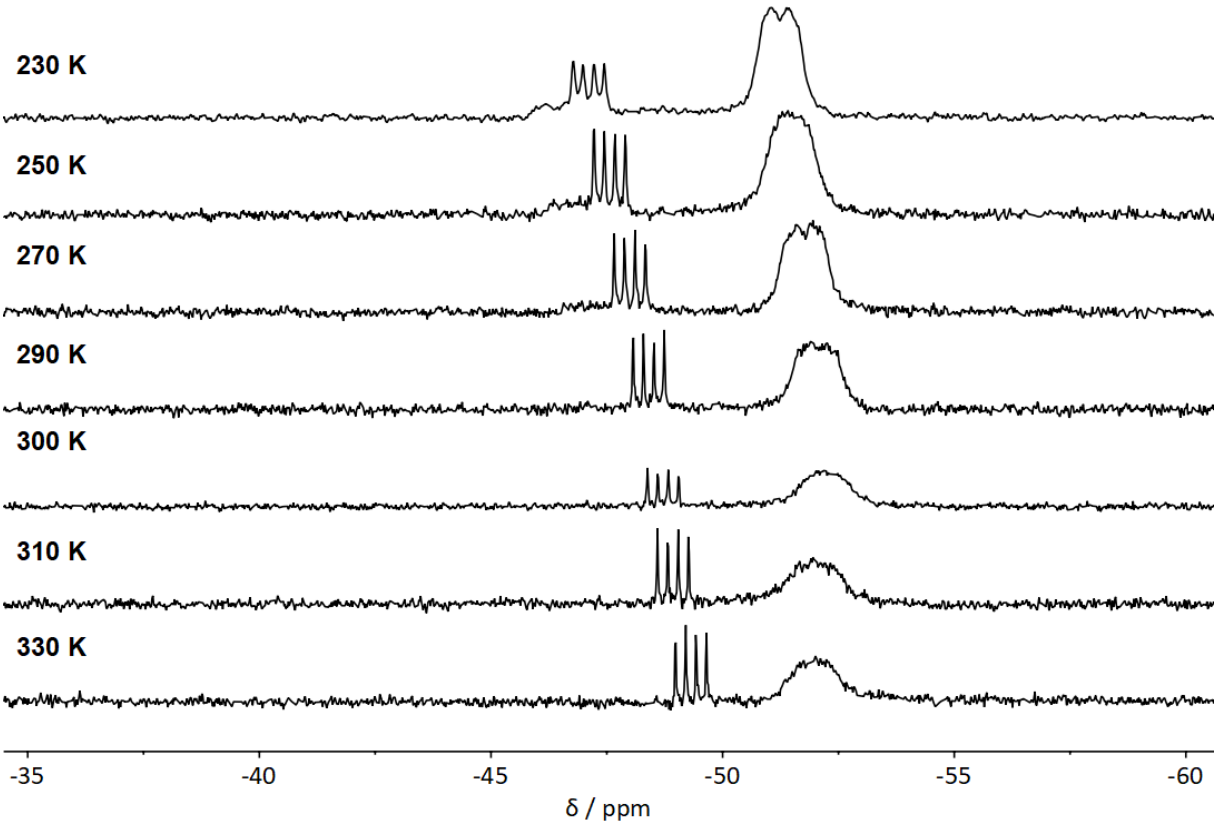

Fig. S111 Temperature dependent ^{31}P NMR spectra of $[(PMe_3)BeI_2]_2$ (**2c**) in $CDCl_3$.

Table S18: Temperature dependent linewidths and derived parameters for **2c** in $CDCl_3$.

T [K]	$\omega_{1/2}$ [Hz]	k	ln k
290	37	199	5.29
300	237	733	6.60
310	244	755	6.63

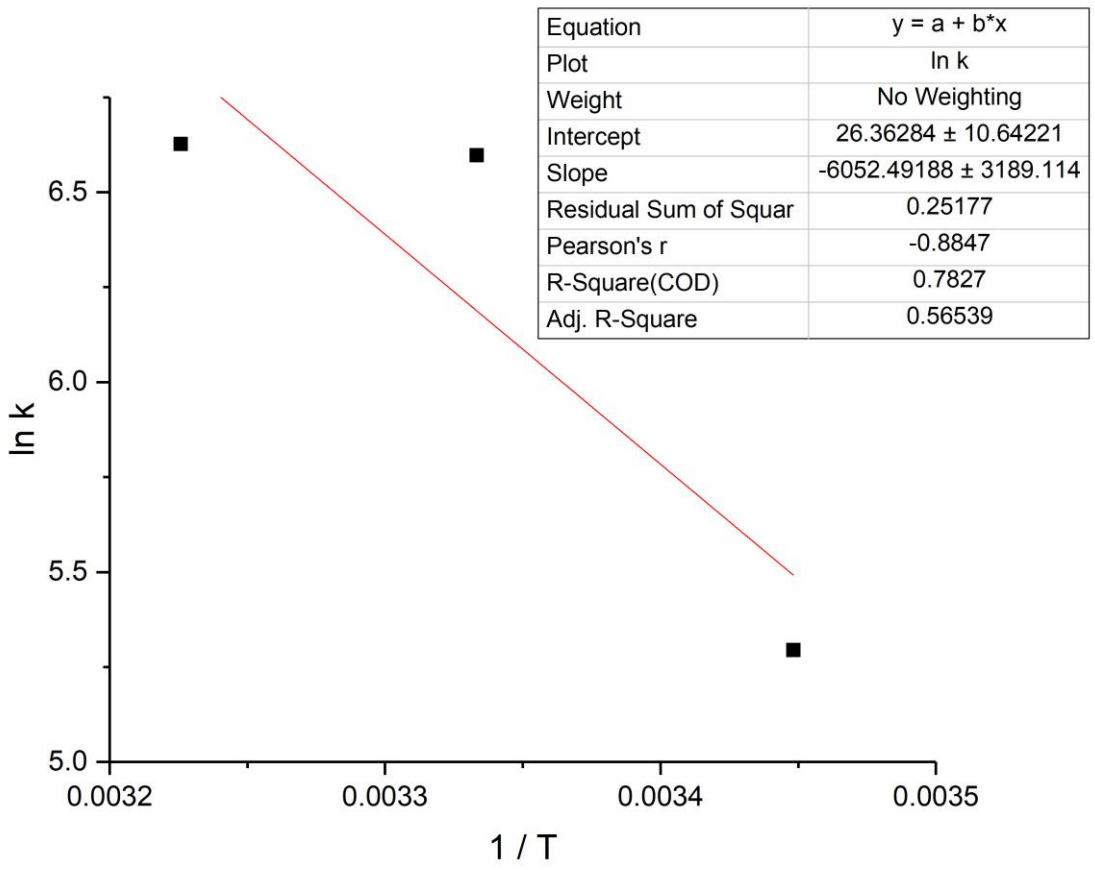

Fig. S112 Arrhenius plot for $[(PMe_3)BeI_2]_2$ (2c) in $CDCl_3$

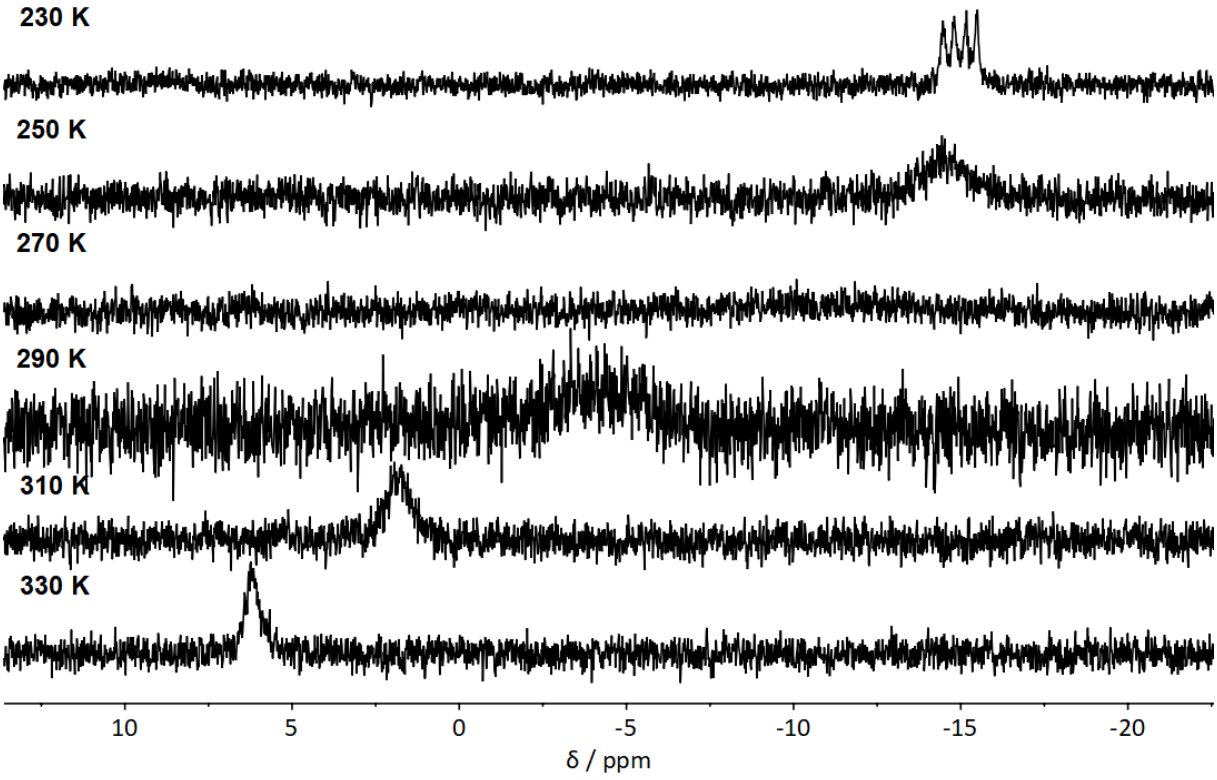

Fig. S113 Temperature dependent ^{31}P NMR spectra of $[(PCy_3)BeCl_2]_2$ (**3a**) in C_7D_8.

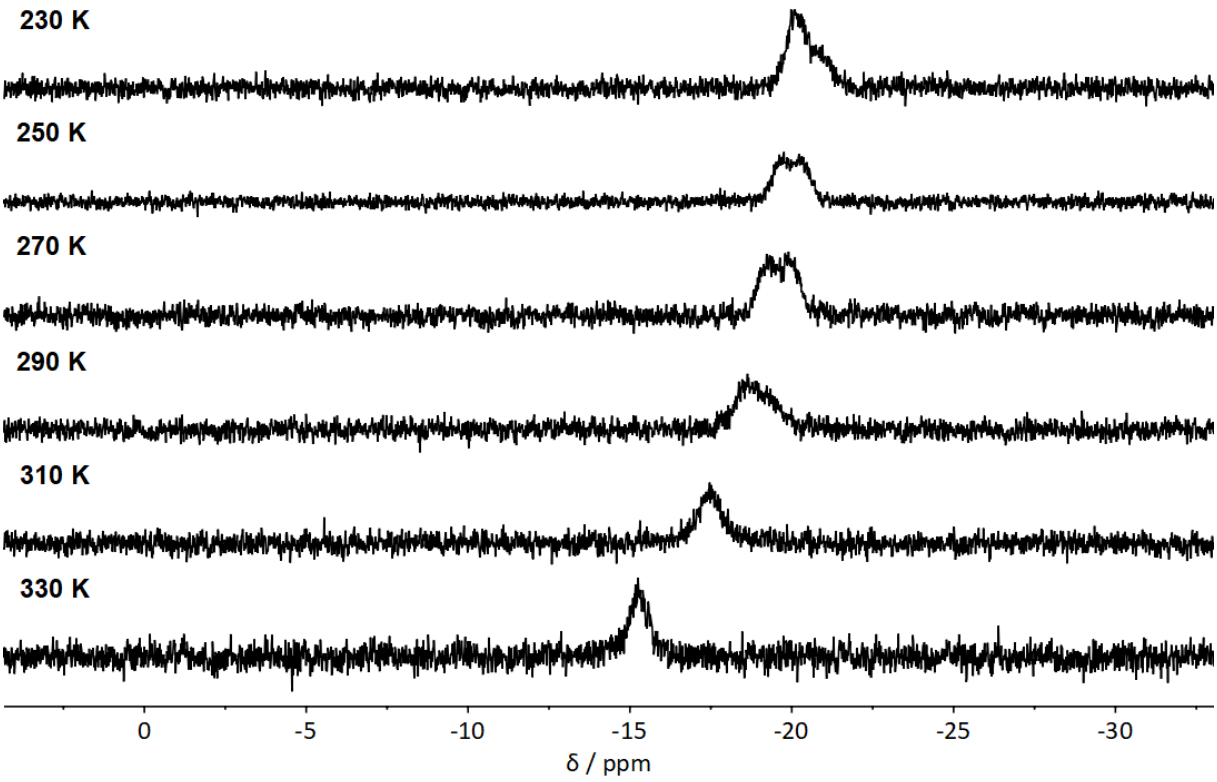

Fig. S114 Temperature dependent ^{31}P NMR spectra of $[(PCy_3)BeBr_2]_2$ (**3b**) in C_7D_8.

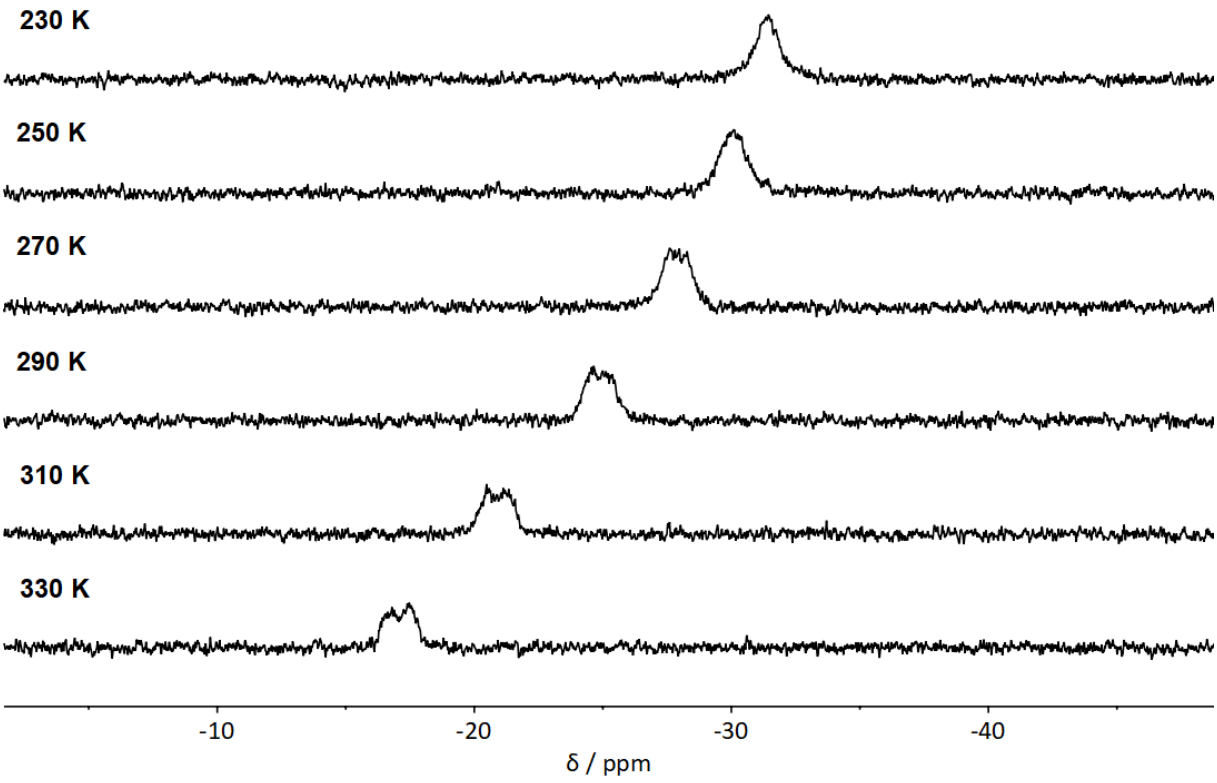

Fig. S115 Temperature dependent ^{31}P NMR spectra of $[(PCy_3)BeI_2]_2$ (**3c**) in C_7D_8.

IR spectra

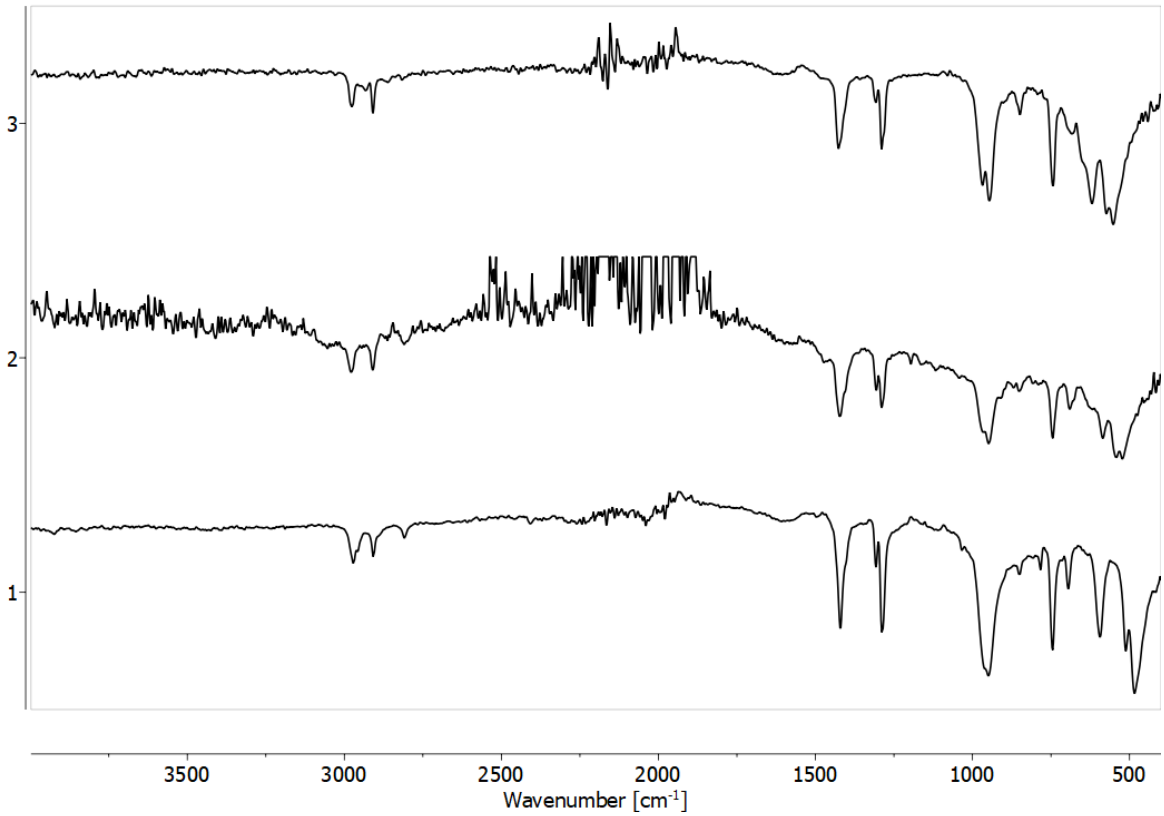

Fig. S116 IR spectra of $[(PMe_3)_2BeCl_2]$ (**1a**), $[(PMe_3)_2BeBr_2]$ (**1b**) and $[(PMe_3)_2BeI_2]$ (**1c**) (from top to bottom).

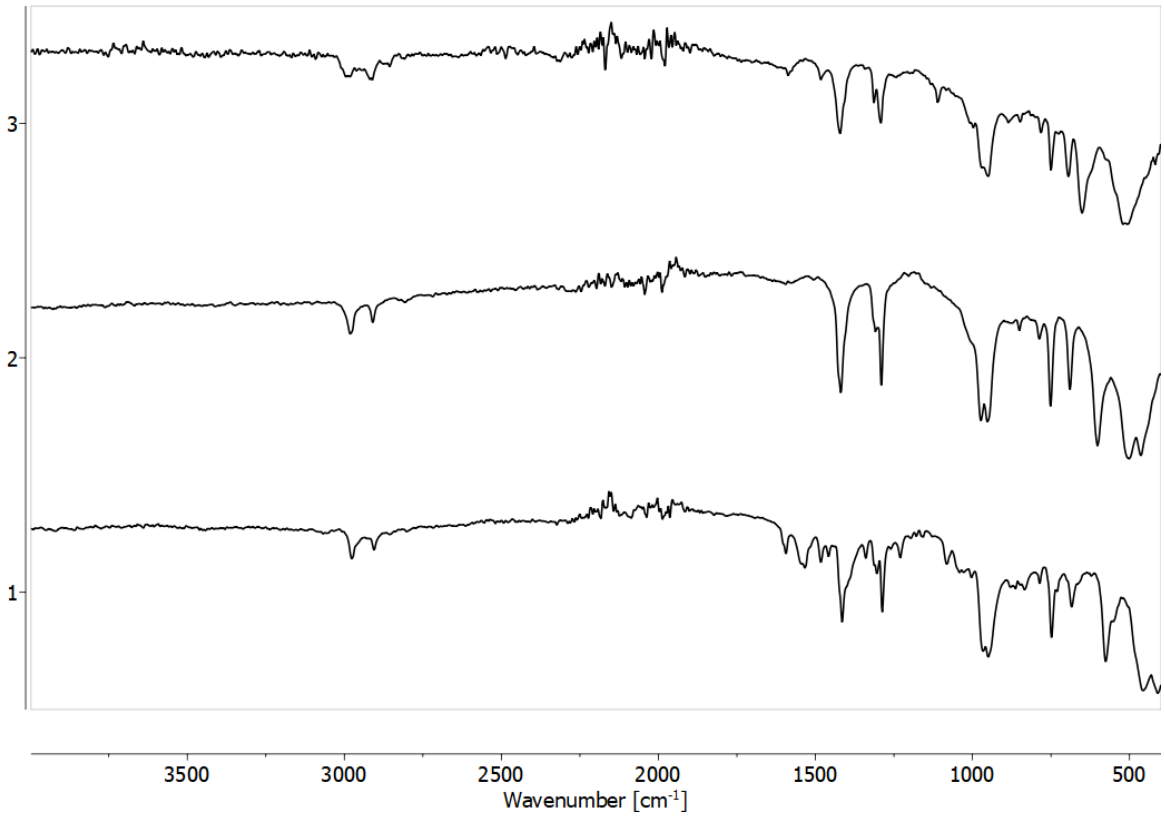

Fig. S117 IR spectra of $[(PMe_3)BeCl_2]_2$ (**2a**), $[(PMe_3)BeBr_2]_2$ (**2b**) and $[(PMe_3)BeI_2]_2$ (**2c**) (from top to bottom).

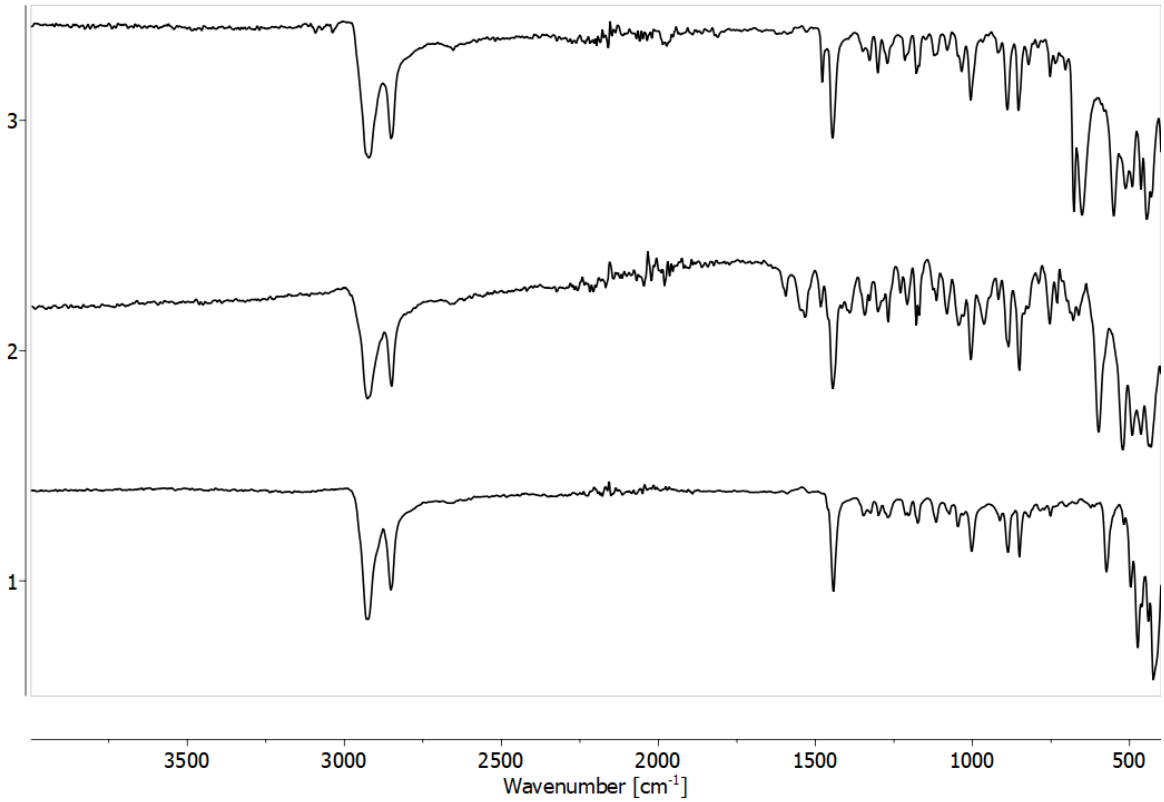

Fig. S118 IR spectra of $[(PCy_3)BeCl_2]_2$ (**3a**), $[(PCy_3)BeBr_2]_2$ (**3b**) and $[(PCy_3)BeI_2]_2$ (**3c**) (from top to bottom).

Computational details

All computational calculations were performed using the ωB97XD[13][ChaiHead-Gordon2008] theory level in combination with the def2tzvp[14, 15][AhlrichsWeigendHaeserEtAl1998,WeigendAhlrichs2005] basis set. All structures were characterized as local minima or true transition states by computation of vibration frequencies at the same level of theory (ωB97XD/def2tzvp). The reactions were followed along with the IRC (IRC = ξ), which determines the minimum energy path connecting the transition state to reactant and product states.[16][FukuiKatoFujimoto1975] Reaction work was calculated and examine as previously described.[17][CocicPetrovicPuchtaEtAl2022] The influence of bulk solvent was evaluated via single point calculations using the CPCM formalism[18, 19][BaroneCossi1998,CossiRegaScalmaniEtAl2003] on the same theory level (ωB97XD/def2tzvp) and with chloroform and toluene as a solvent. Additionally different computation methods B3LYP,[20-22][Becke1993,LeeYangParr1988,StephensDevlinChabalowskiEtAl1994] B3LYP with the extension by Grimme's dispersion correction[23][GrimmeAntonyEhrlichEtAl2010] and MP2[24-28][FrischHead-GordonPople1990,FrischHead-GordonPople1990a,Head-GordonPopleFrisch1988,SaeboAlmloef1989,Head-GordonHead-Gordon1994] for comparison reasons were used. All calculations were performed using the Gaussian 09 program package.[29][Frischextitetal.2009] Hydrogen bond strength[30][EspinosaMolinsLecomte1998] evaluation was performed using the Multiwfn program package.[31][TianChen2012]

Relative cis/trans stability

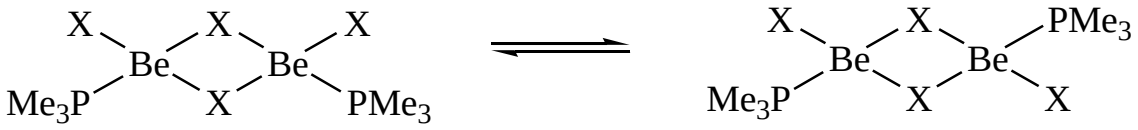

Fig. S119 Potential quilibrium between *cis*- and *trans*-isomer (X = Cl, Br, I).

Table S19: Calculated relative cis/trans stabilities of [(PMe$_3$)BeX_2]$_2$ (**2**) in the gas phase using wb97xd/def2tzvp method.

		cis-		*trans*-	
X	E (kcal/mol)	*d*(Be-Be) /Å	dipole moment /D	*d*(Be-Be) /Å	dipole moment /D
Cl	-5.28	2.74	11.531	2.75	0.128
Br	-5.07	2.90	11.889	2.90	0.463
I	-4.90	3.11	12.175	3.12	1.296

Table S20: Calculated relative cis/trans stabilities of [(PMe$_3$)BeX_2]$_2$ (**2**) using wb97xd/def2tzvp method by applying the CPCM model in chlorophorm as a solvent.

		cis-		*trans*-	
X	E (kcal/mol)	*d*(Be-Be) /Å	dipole moment /D	*d*(Be-Be) /Å	dipole moment /D
Cl	-1.72	2.76	15.529	2.77	0.126
Br	-1.78	2.91	16.241	2.92	0.125
I	-2.17	3.10	16.905	3.14	0.335

Table S21: Calculated relative cis/trans stabilities of [(PMe$_3$)BeX_2]$_2$ (**2**) using wb97xd/def2tzvp method by applying the CPCM model in toluene as a solvent.

		cis-		*trans*-	
X	E (kcal/mol)	*d*(Be-Be) /Å	dipole moment /D	*d*(Be-Be) /Å	dipole moment /D
Cl	-3.05	2.75	14.203	2.76	0.139

Br	-3.01	2.91	14.769	2.92	0.187
I	-3.41	3.11	15.311	3.13	0.836

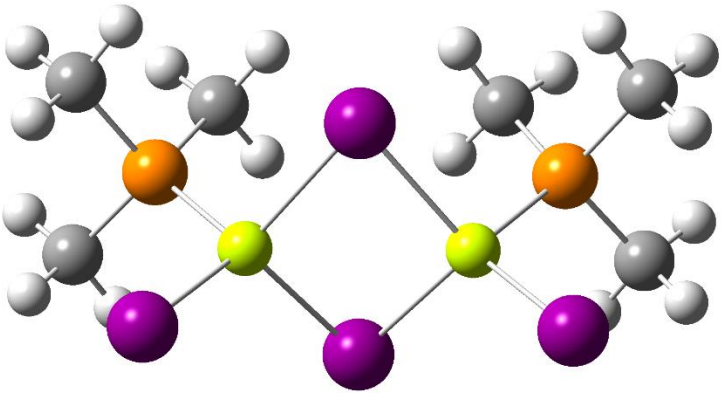

Fig. S120 Optimised gas phase structure of the *cis*-isomer of $[(PMe_3)BeI_2]_2$ (**2c**) at the wb97xd/def2tzvp level of theory.

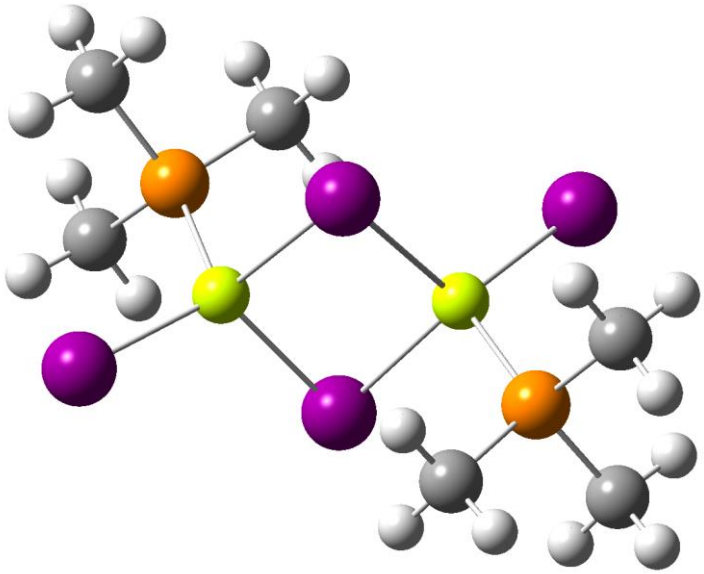

Fig. S121 Optimised gas phase structure of the *cis*-isomer of $[(PMe_3)BeI_2]_2$ (**2c**) at the wb97xd/def2tzvp level of theory.

Table S22: Calculated dipole moments of $BeX_2(PMe_3)_2$ (**1**) and *cis*-/*trans*-$[(PMe_3)BeX_2]_2$ (**2**) in the gas phase the wb97xd/def2tzvp level of theory

	1	*cis*-***2***	*trans*-***2***
X	dipole moment /D	dipole moment /D	dipole moment /D
Cl	7.382	11.531	0.128
Br	7.828	11.889	0.463
I	8.339	12.175	1.296

Table S23: Calculated dipole moments of $BeX_2(PMe_3)_2$ (**1**) and *cis*-/*trans*-$[(PMe_3)BeX_2]_2$ (**2**) at the wb97xd/def2tzvp level of theory with the CPCM model in chlorophorm as solvent

	1	*cis*-***2***	*trans*-***2***
X	dipole moment /D	dipole moment /D	dipole moment /D
Cl	10.518	15.529	0.126

Br	11.175	16.241	0.125
I	11.935	16.905	0.335

Table S24: Calculated dipole moments of $BeX_2(PMe_3)_2$ (**1**) and *cis-*/*trans*-$[(PMe_3)BeX_2]_2$ (**2**) at the wb97xd/def2tzvp level of theory with the CPCM model in toluene as solvent

	1	*cis-**2***	*trans-**2***
X	dipole moment /D	dipole moment /D	dipole moment /D
Cl	9.503	14.203	0.139
Br	10.070	14.769	0.187
I	10.732	15.311	0.836

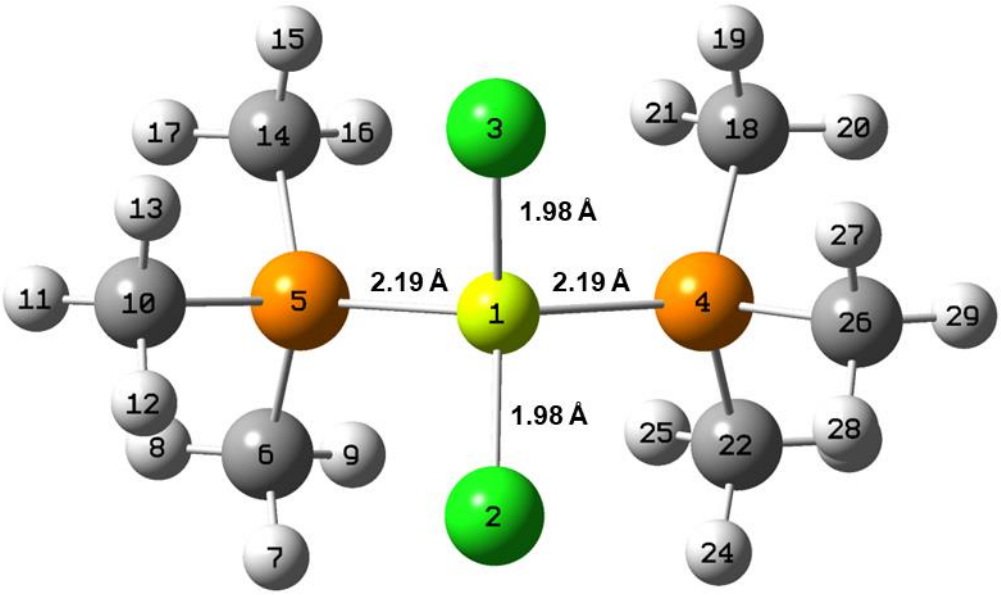

Fig. S122 Optimised gas phase structure of $(Me_3P)_2BeCl_2$ (**1a**) at the wb97xd/def2tzvp level of theory.

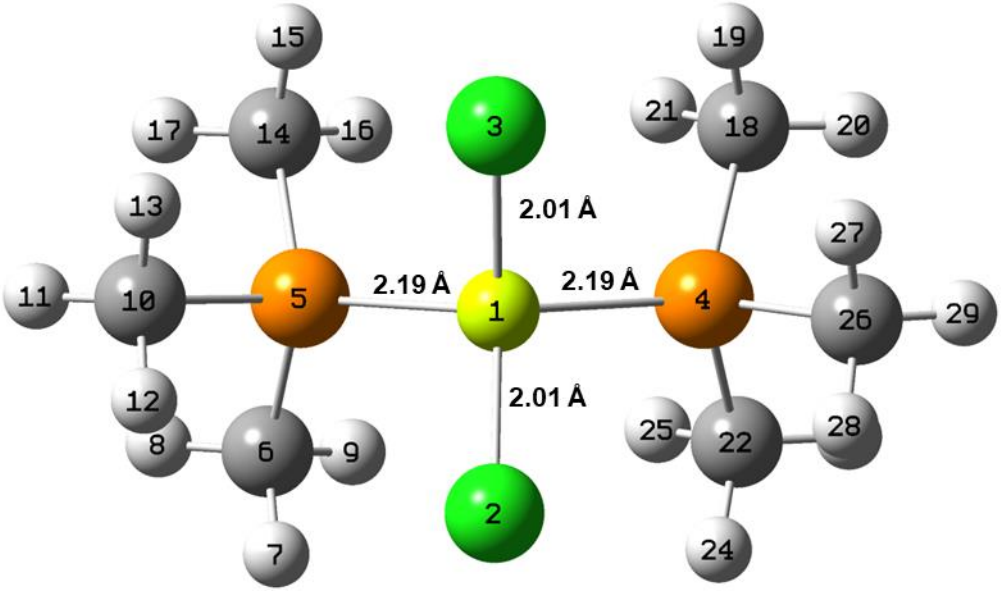

Fig. S123 Optimised structure of $(Me_3P)_2BeCl_2$ (**1a**) at the wb97xd/def2tzvp level of theory with application of CPCM to take solvation effects in chloroform into account.

H-bond evaluation of $(Me_3P)_2BeX_3$ molecule with three additional solvent molecules

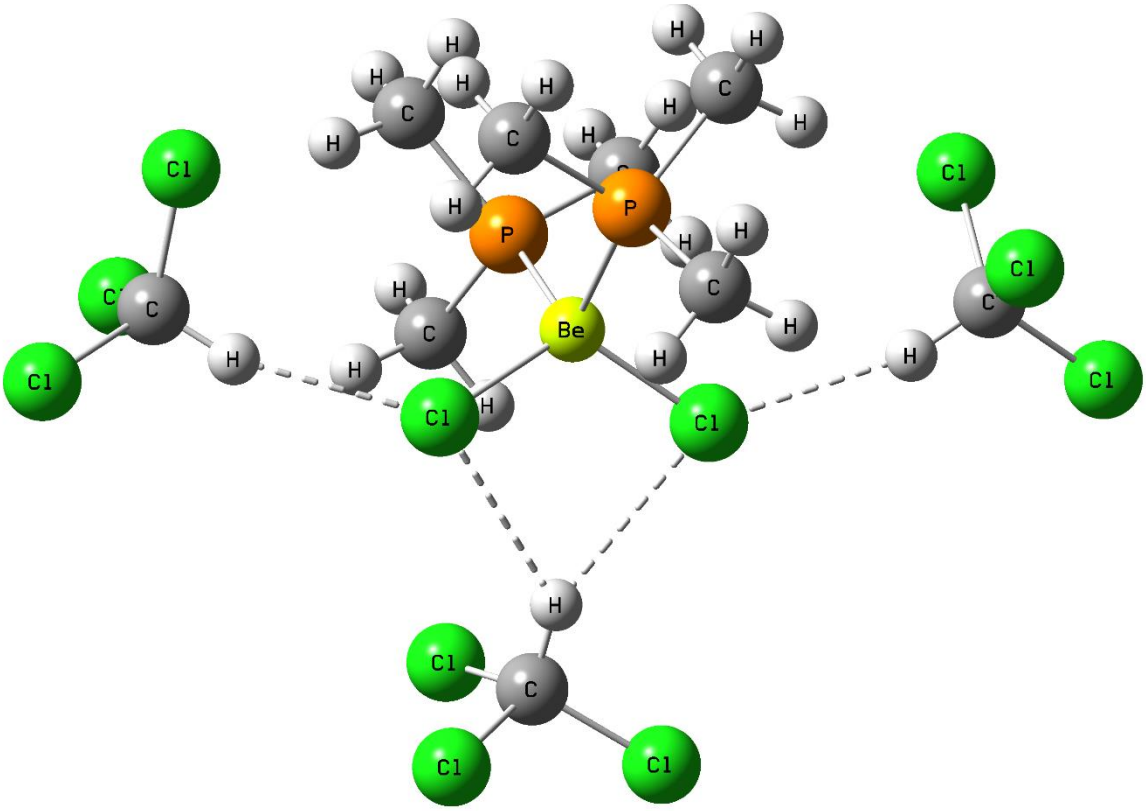

Fig. S124 Optimised gas phase structure of $(Me_3P)_2BeCl_2$ (**1a**) at the wb97xd/def2tzvp level of theory including three additional chloroform molecules to model solvent interactions.

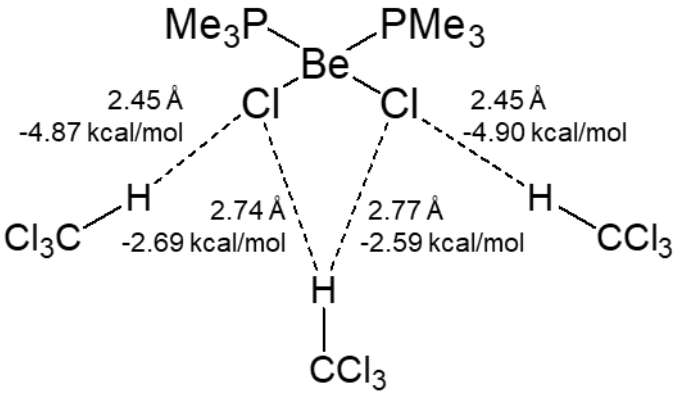

Fig. S125 Selected bond lengths and hydrogen bond strengths from the gas phase optimisation of $(Me_3P)_2BeCl_2$ (**1a**) at the wb97xd/def2tzvp level of theory including three additional chloroform molecules to model solvent interactions.

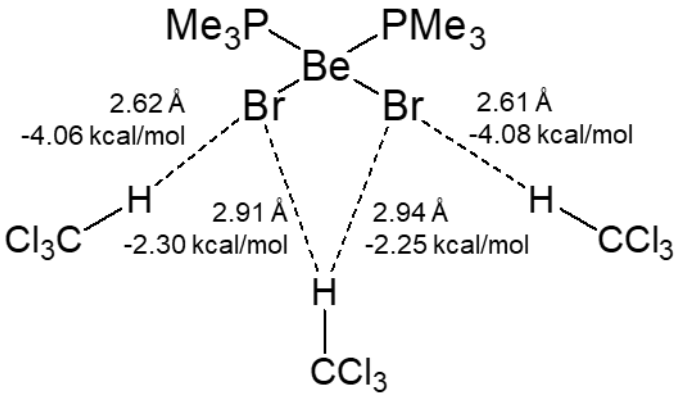

Fig. S126 Selected bond lengths and hydrogen bond strengths from the gas phase optimisation of $(Me_3P)_2BeBr_2$ (**1b**) at the wb97xd/def2tzvp level of theory including three additional chloroform molecules to model solvent interactions.

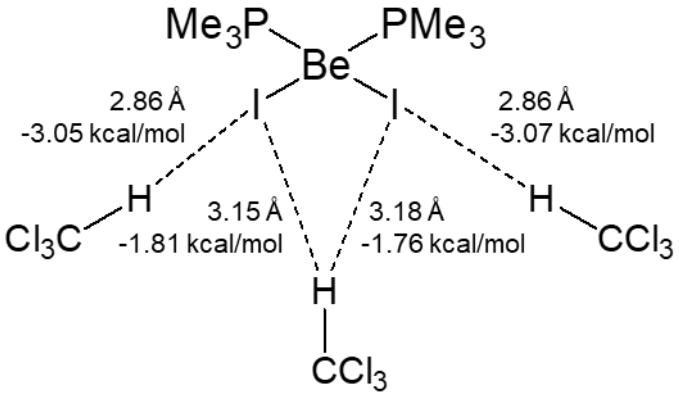

Fig. S127 Selected bond lengths and hydrogen bond strengths from the gas phase optimisation of $(Me_3P)_2BeI_2$ (**1c**) at the wb97xd/def2tzvp level of theory including three additional chloroform molecules to model solvent interactions.

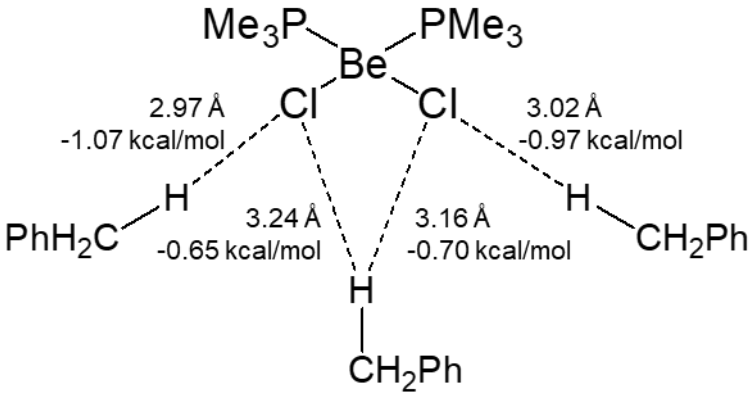

Fig. S128 Selected bond lengths and hydrogen bond strengths from the gas phase optimisation of $(Me_3P)_2BeCl_2$ (**1a**) at the wb97xd/def2tzvp level of theory including three additional toluene molecules to model solvent interactions.

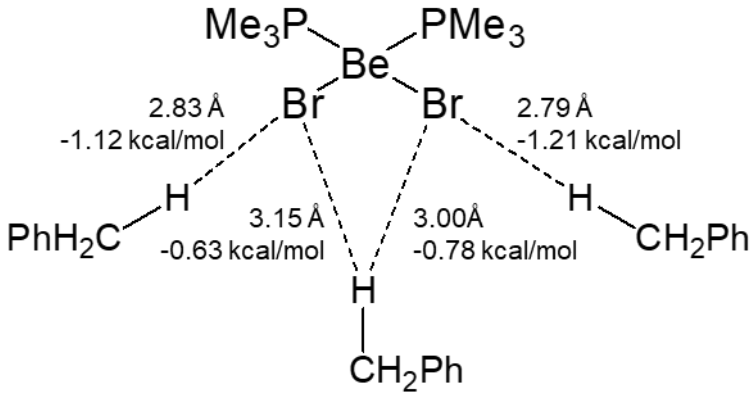

Fig. S129 Selected bond lengths and hydrogen bond strengths from the gas phase optimisation of $(Me_3P)_2BeBr_2$ (**1b**) at the wb97xd/def2tzvp level of theory including three additional toluene molecules to model solvent interactions.

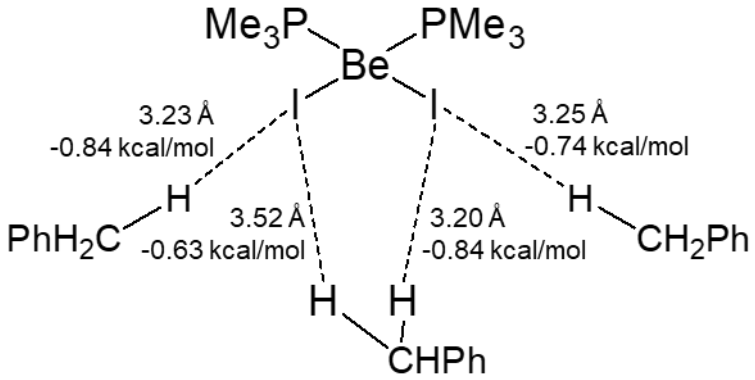

Fig. S130 Selected bond lengths and hydrogen bond strengths from the gas phase optimisation of $(Me_3P)_2BeI_2$ (**1c**) at the wb97xd/def2tzvp level of theory including three additional toluene molecules to model solvent interactions.

Trimethylphosphine dissociation

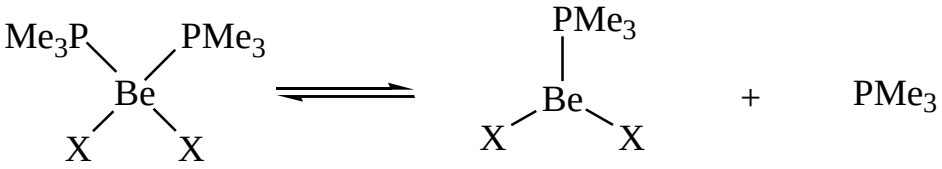

Fig. S131 Trimethylphosphine dissociation from $(PMe_3)_2BeX_2$ (**1**) (X = Cl, Br, I).

Table S25: Calculated dissociation energies of PMe_3 from $(PMe_3)_2BeX_2$ (**1**) (X = Cl, Br, I) in the **gas phase** at the wb97xd/def2tzvp level of theory.

X	E (kcal/mol)
Cl	+19.38
Br	+ 23.24
I	+ 26.39

Table S26: Calculated dissociation energies of PMe_3 from $(PMe_3)_2BeX_2$ (**1**) (X = Cl, Br, I) at the wb97xd/def2tzvp level of theory with a CPCM model of **chloroform** as the solvent.

X	E (kcal/mol)
Cl	+ 18.26
Br	+ 21.56
I	+ 25.18

Table S27: Calculated dissociation energies of PMe_3 from $(PMe_3)_2BeX_2$ (**1**) (X = Cl, Br, I) at the wb97xd/def2tzvp level of theory with a CPCM model of **toluene** as the solvent.

X	E (kcal/mol)
Cl	+ 18.44
Br	+ 21.76
I	+ 25.37

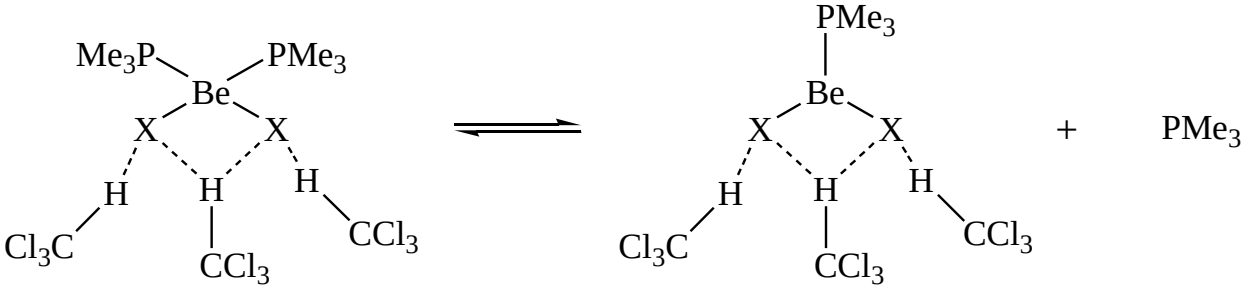

Fig. S132 Trimethylphosphine dissociation from $(PMe_3)_2BeX_2$ (**1**) (X = Cl, Br, I) with three additional chloroform molecules to model solvent interactions.

Table S28: Calculated dissociation energies of PMe_3 from $(PMe_3)_2BeX_2$ (**1**) (X = Cl, Br, I) with three additional chloroform molecules to model solvent interactions at the wb97xd/def2tzvp level of theory.

X	E (kcal/mol)
Cl	+18.08
Br	+17.47
I	+22.46

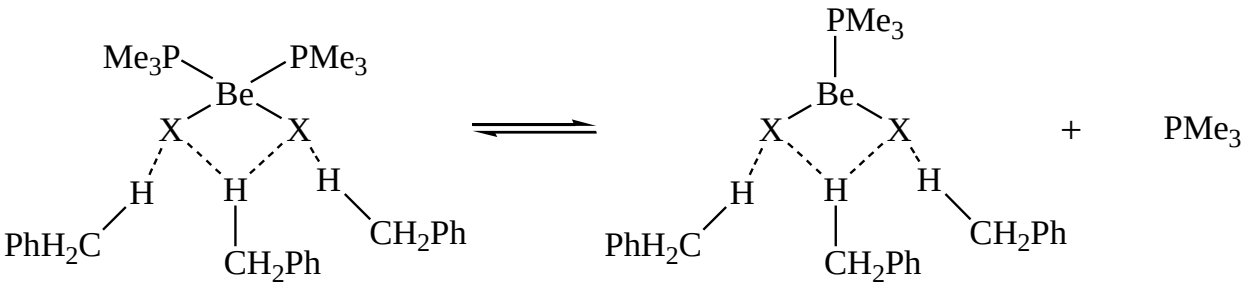

Fig. S133 Trimethylphosphine dissociation from $(PMe_3)_2BeX_2$ (**1**) (X = Cl, Br, I) with three additional toluene molecules to model solvent interactions.

Table S29: Calculated dissociation energies of PMe_3 from $(PMe_3)_2BeX_2$ (**1**) (X = Cl, Br, I) with three additional toluene molecules to model solvent interactions at the wb97xd/def2tzvp level of theory.

X	E (kcal/mol)
Cl	+11.96
Br	+15.70
I	+18.16

Solvent coordination

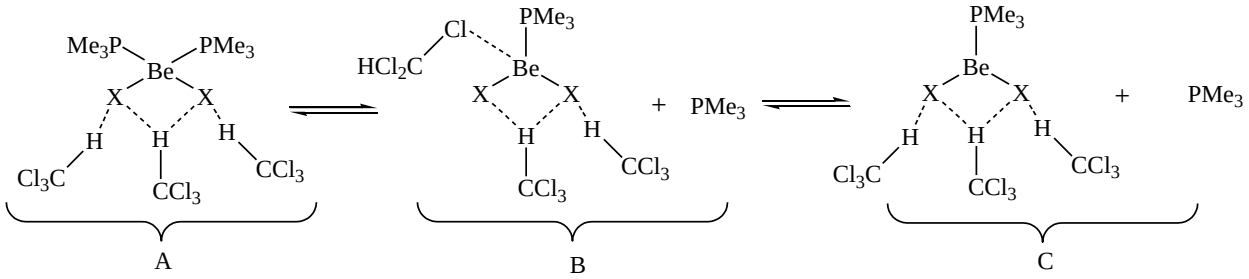

Fig. S134 Solvent molecule migration during trimethylphosphine dissociation from $(PMe_3)_2BeX_2$ (**1**) (X = Cl, Br, I) with three additional chloroform molecules to model solvent interactions.

Table S30: Comparison of the stabilities of species A, B and C (***Fig. S134***) in the gas phase at the wb97xd/def2tzvp level of theory.

X	A (kcal/mol)	B (kcal/mol)	C (kcal/mol)
Cl	0	+14.38	+18.08
Br	0	+19.54	+17.47
I	0	+21.15	+22.46

Chloroform trimethylphosphine exchange

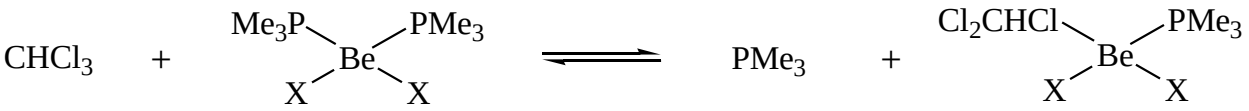

Fig. S135 Displacement of trimethylphosphine by chloroform in $(PMe_3)_2BeX_2$ (**1**) (X = Cl, Br, I).

Table S31: Calculated relative energies required for trimethylphosphine displeacement by chloroform in $(PMe_3)_2BeX_2$ (**1**) (X = Cl, Br, I) in the **gas phase** at the wb97xd/def2tzvp level of theory.

X	E (kcal/mol)	*d* (Å) [a]
Cl	+0.026	3.317
Br	+0.031	3.356
I	+0.033	3.404

[a] distance between the chloride from coordinated chloroform and the Be metal center

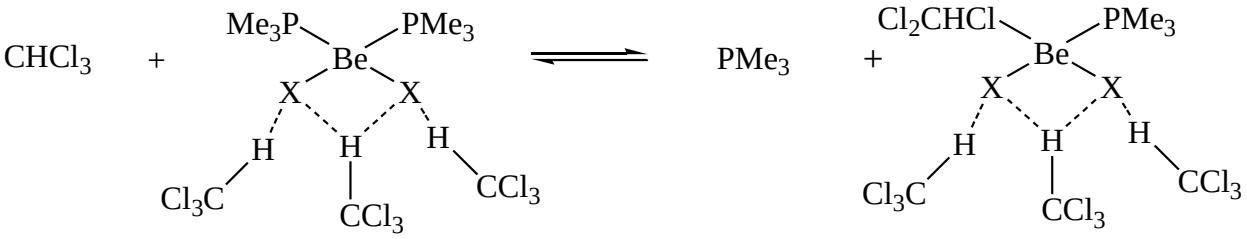

Fig. S136 Displacement of trimethylphosphine by chloroform in $(PMe_3)_2BeX_2$ (**1**) (X = Cl, Br, I) with three additional chloroform molecules to model solvent interactions.

Table S32: Calculated relative energies required for trimethylphosphine displacement by chloroform in $(PMe_3)_2BeX_2$ (**1**) (X = Cl, Br, I) in the **gas phase** at the wb97xd/def2tzvp level of theory with three additional chloroform molecules to model solvent interactions.

X	E (kcal/mol)	*d* (Å) [a]
Cl	+0.026	3.294
Br	+0.031	3.330
I	+0.037	3.124

[a] distance between the chloride from coordinated chloroform and the Be metal center

Halide Dissociation

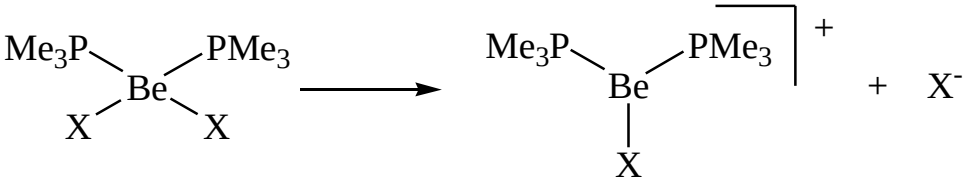

Fig. S137 Halide dissociation from $(PMe_3)_2BeX_2$ (**1**) (X = Cl, Br, I).

Table S33: Calculated dissociation energies of halide X from $(PMe_3)_2BeX_2$ (**1**) (X = Cl, Br, I) in the **gas phase** at the wb97xd/def2tzvp level of theory.

X	E (kcal/mol)
Cl	+49.98
Br	+46.83
I	+41.99

All species were calculated as a isomers to avoid the influence of the Coulomb term.

Table S34: Calculated dissociation energies of halide X from $(PMe_3)_2BeX_2$ (**1**) (X = Cl, Br, I) at the wb97xd/def2tzvp level of theory with a CPCM model of **chloroform** as the solvent.

X	E (kcal/mol)
Cl	+29.78
Br	+25.34
I	+20.86

All species were calculated as a isomers to avoid the influence of the Coulomb term.

Table S35: Calculated dissociation energies of halide X from $(PMe_3)_2BeX_2$ (**1**) (X = Cl, Br, I) at the wb97xd/def2tzvp level of theory with a CPCM model of **toöuene** as the solvent.

X	E (kcal/mol)
Cl	+36.06
Br	+32.07
I	+27.25

All species were calculated as a isomers to avoid the influence of the Coulomb term.

Chloroform halide exchange

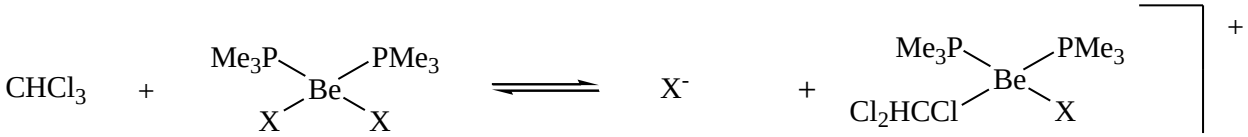

Fig. S138 Displacement of halide X by chloroform in $(PMe_3)_2BeX_2$ (**1**) (X = Cl, Br, I)-

Table S36: Calculated relative energies required for halide displacement by chloroform in $(PMe_3)_2BeX_2$ (**1**) (X = Cl, Br, I) in the **gas phase** at the wb97xd/def2tzvp level of theory.

X	E (kcal/mol)	*d* (Å) [a]
Cl	51.058	2.992
Br	47.361	2.606
I	43.777	2.440

[a] distance between the chloride from coordinated chloroform and the Be metal center
All species were calculated as a isomers to avoid the influence of the Coulomb term.

Chloroform halide exchange in the presence of three additional chloroform molecules

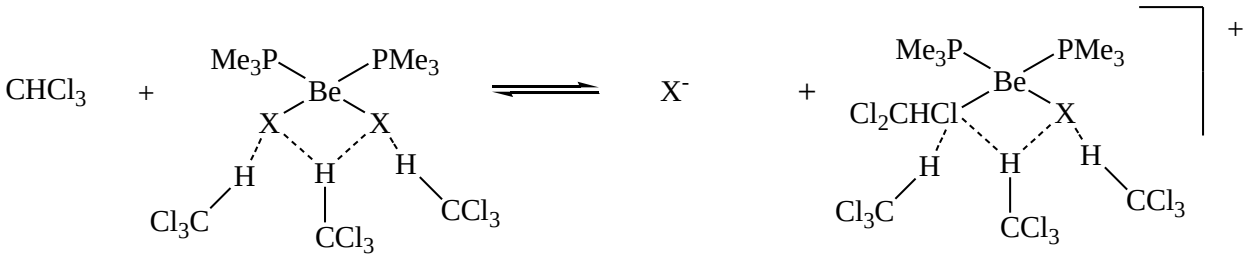

Fig. S139 Displacement of halide X by chloroform in $(PMe_3)_2BeX_2$ (**1**) (X = Cl, Br, I) with three additional chloroform molecules to model solvent interactions

Table S37: Calculated relative energies required for halide displacement by chloroform in $(PMe_3)_2BeX_2$ (**1**) (X = Cl, Br, I) in the **gas phase** at the wb97xd/def2tzvp level of theory with three additional chloroform molecules to model solvent interactions.

X	E (kcal/mol)	*d* (Å) [a]
Cl	52.647	2.907
Br	49.395	2.540
I	44.763	2.435

[a] distance between the chloride from coordinated chloroform and the Be metal center
All species were calculated as a isomers to avoid the influence of the Coulomb term.

Energy profile of PMe_3 exchange

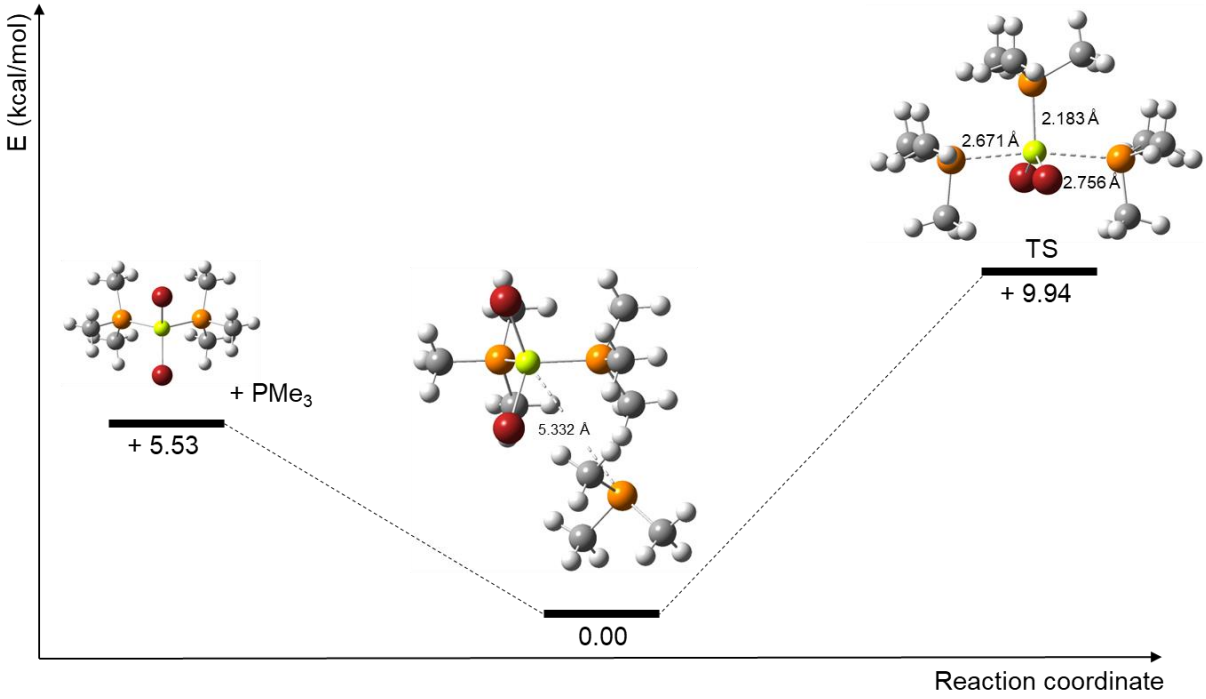

Fig. S140 Energy profile of PMe_3 exchange at $(PMe_3)_2BeBr_2$ (**1b**) calculated in the gas phase at the wb97xd/def2tzvp level of theory.

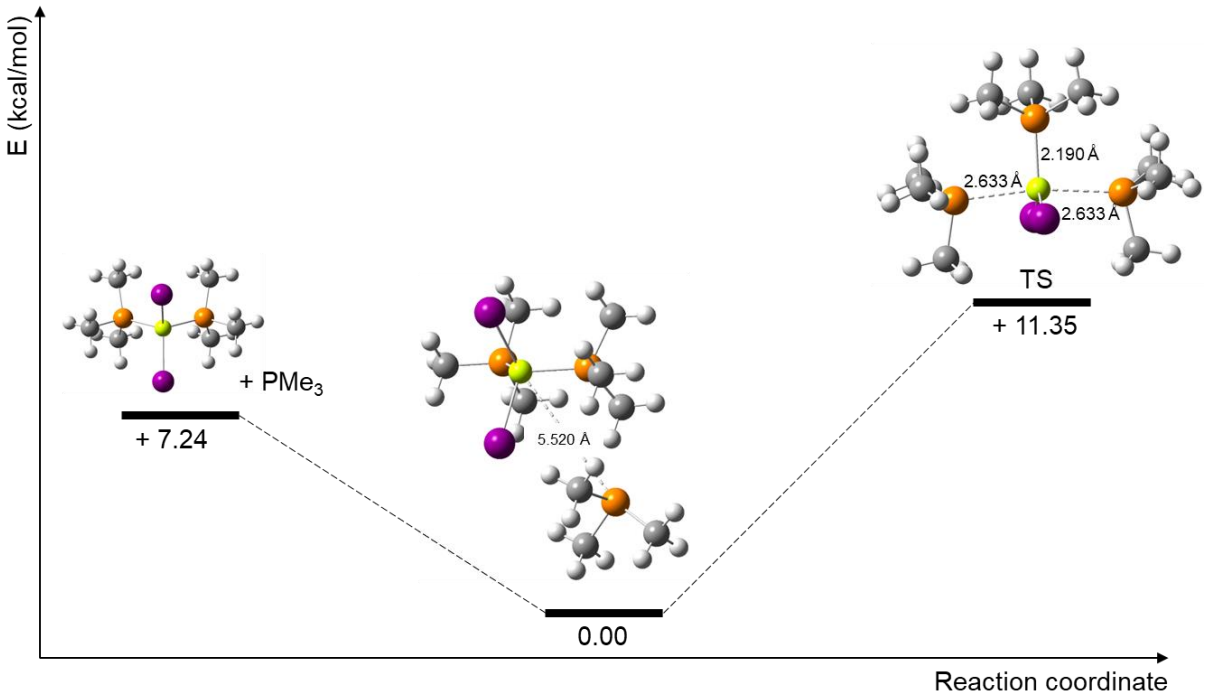

Fig. S141 Energy profile of PMe_3 exchange at $(PMe_3)_2BeI_2$ (**1c**) calculated in the gas phase at the wb97xd/def2tzvp level of theory.

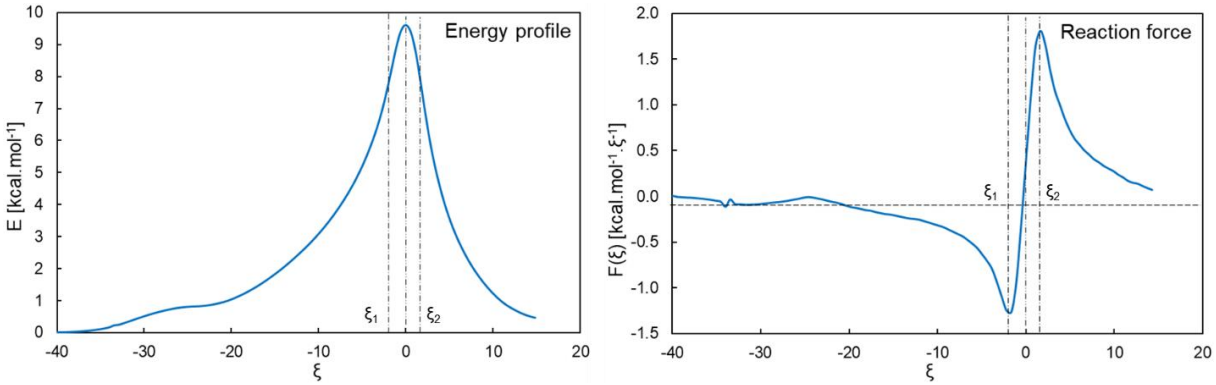

Fig. S142 Energetic properties through the intrinsic reaction coordinate of the PMe3 exchange reaction at **1b**.

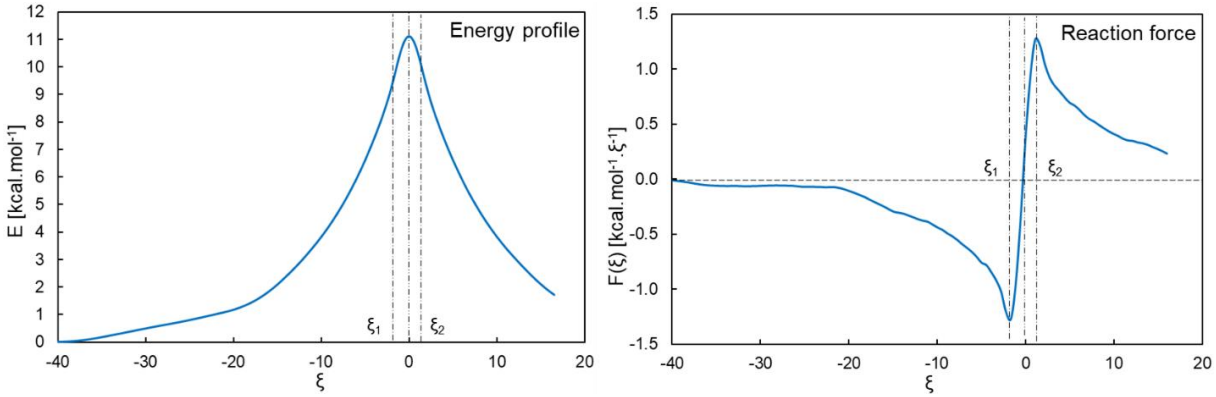

Fig. S143 Energetic properties through the intrinsic reaction coordinate of the PMe3 exchange reaction at **1c**.

Halide exchange by phosphine

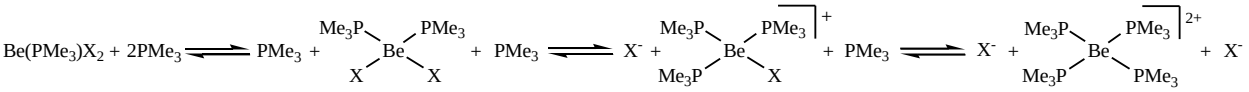

Fig. S144 Consecutive halide displacement by PMe_3 in $(PMe_3)_2BeX_2$ (**1**) (X = Cl, Br, I).

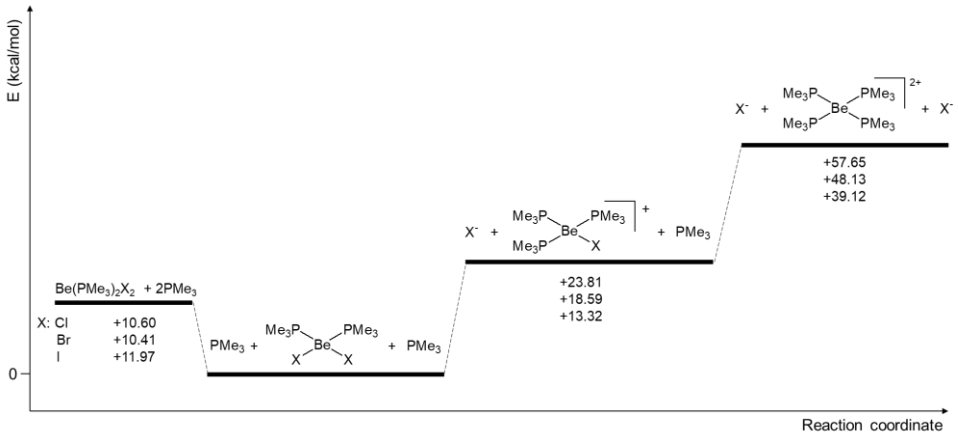

Fig. S145 Energy profile of the consecutive halide displacement by PMe_3 in $(PMe_3)_2BeX_2$ (**1**) (X = Cl, Br, I) in the gas phase at the wb97xd/def2tzvp level of theory.

Table S38: Relative stabilities [kcal/mol] of $(PMe_3)_2BeX_2$ (**1**) (X = Cl, Br, I) with two molecules of PMe_3, the corresponding reaction complex, $[(PMe_3)_3BeX]X$ with one molecule of PMe_3 and $[(PMe_3)_4Be]X_2$ in the gas phase at the wb97xd/def2tzvp level of theory.

X	$(PMe_3)_2BeX_2$ + 2 PMe_3	Reaction complex	$[(PMe_3)_3BeX]X$ + PMe_3	$[(PMe_3)_4Be]X_2$
Cl	+10.60	0	+23.81	+57.65
Br	+10.41	0	+18.59	+48.13
I	+11.97	0	+13.32	+39.12

Dimer dissociation on three different theory levels

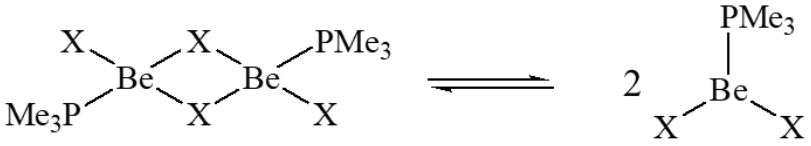

Fig. S146 Dissociation of $[(PMe_3)BeX_2]_2$ (**2**) (X = Cl, Br, I).

Table S39: Calculated dissociation energies [kcal/mol] for $[(PMe_3)BeX_2]_2$ (**2**) (X = Cl, Br, I) in the **gas phase** using full optimization on the wb97xd/def2tzvp level of theory and single point calculations on b3lyp/def2tzvp, b3lyp-GD3/def2tzvp and MP2(fc)/def2tzvp levels of theory using previously optimized (wb97xd/def2tzvp) structures.

	Full optimization (gas phase)	Single point calculations (gas phase)		
X	wb97xd/def2tzvp	b3lyp/def2tzvp	b3lyp-GD3/def2tzvp	MP2(fc)/def2tzvp
Cl	+23.41	+14.40	+23.70	+29.74
Br	+23.91	+13.24	+24.31	+32.50
I	+23.40	+10.49	+23.23	+33.99

Table S40: Calculated dissociation energies [kcal/mol] for $[(PMe_3)BeX_2]_2$ (**2**) (X = Cl, Br, I) employing a CPCM model of chloroform using full optimization on the wb97xd/def2tzvp level of theory and single point calculations on b3lyp/def2tzvp, b3lyp-GD3/def2tzvp and MP2(fc)/def2tzvp levels of theory using previously optimized (wb97xd/def2tzvp) structures.

	Single point calculations (CPCM chloroform)			
X	wb97xd/def2tzvp	b3lyp/def2tzvp	b3lyp-GD3/def2tzvp	MP2(full)/def2tzvp
Cl	+14.52	+5.96	+15.26	+22.14
Br	+14.89	+4.55	+15.62	+25.44
I	+14.64	+2.03	+14.77	+27.33

Table S41: Calculated dissociation energies [kcal/mol] for $[(PMe_3)BeX_2]_2$ (**2**) (X = Cl, Br, I) employing a CPCM model of toluene using full optimization on the wb97xd/def2tzvp level of theory and single point calculations on b3lyp/def2tzvp, b3lyp-GD3/def2tzvp and MP2(fc)/def2tzvp levels of theory using previously optimized (wb97xd/def2tzvp) structures.

	Single point calculations (CPCM toluene)			
X	wb97xd/def2tzvp	b3lyp/def2tzvp	b3lyp-GD3/def2tzvp	MP2(full)/def2tzvp
Cl	+17.09	+8.45	+17.75	+24.78
Br	+17.59	+7.17	+18.24	+28.21
I	+17.33	+4.64	+17.38	+30.11

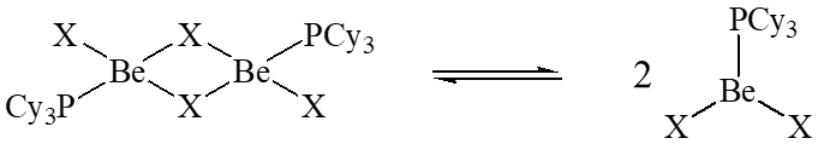

Fig. S147 Dissociation of $[(PCy_3)BeX_2]_2$ (**3**) (X = Cl, Br, I).

Table S42: Calculated dissociation energies [kcal/mol] for $[(PCy_3)BeX_2]_2$ (**3**) (X = Cl, Br, I) in the **gas phase** using full optimization on the wb97xd/def2tzvp level of theory and single point calculations on b3lyp/def2tzvp, b3lyp-GD3/def2tzvp and MP2(fc)/def2tzvp levels of theory using previously optimized (wb97xd/def2tzvp) structures.

	Full optimization (gas phase)	Single point calculations (gas phase)		
X	wb97xd/def2tzvp	b3lyp/def2tzvp	b3lyp-GD3/def2tzvp	MP2(fc)/def2tzvp
Cl	+39.98	+26.74	+42.54	+53.65
Br	+37.91	+23.00	+40.89	+55.04
I	+35.18	+17.18	+36.98	+55.21

Table S43: Calculated dissociation energies [kcal/mol] for $[(PCy_3)BeX_2]_2$ (**3**) (X = Cl, Br, I) employing a CPCM model of chloroform using full optimization on the wb97xd/def2tzvp level of theory and single point calculations on b3lyp/def2tzvp, b3lyp-GD3/def2tzvp and MP2(fc)/def2tzvp levels of theory using previously optimized (wb97xd/def2tzvp) structures.

	Single point calculations (chloroform)			
X	wb97xd/def2tzvp	b3lyp/def2tzvp	b3lyp-GD3/def2tzvp	MP2(full)/def2tzvp
Cl	+30.85	+17.62	+33.42	+46.48
Br	+29.21	+14.37	+32.26	+50.53
I	+26.96	+9.02	+28.83	+50.77

Table S44: Calculated dissociation energies [kcal/mol] for $[(PCy_3)BeX_2]_2$ (**3**) (X = Cl, Br, I) employing a CPCM model of toluene using full optimization on the wb97xd/def2tzvp level of theory and single point calculations on b3lyp/def2tzvp, b3lyp-GD3/def2tzvp and MP2(fc)/def2tzvp levels of theory using previously optimized (wb97xd/def2tzvp) structures.

	Single point calculations (toluene)			
X	wb97xd/def2tzvp	b3lyp/def2tzvp	b3lyp-GD3/def2tzvp	MP2(full)/def2tzvp
Cl	+33.47	+20.26	+36.06	+49.15
Br	+31.75	+16.91	+34.80	+53.10
I	+29.41	+11.47	+31.28	+53.24

Chloroform coordination to $[(PR_3)BeX_2]_2$

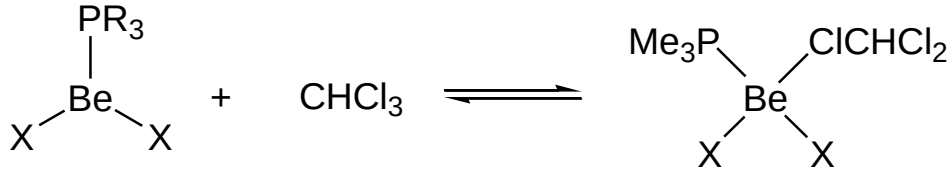

Fig. S148 Coordination of one $CHCl_3$ molecule to of $[(PR_3)BeX_2]$ (R = Me (**4**)) R = Cy (**10**)) (X = Cl, Br, I).

Table S45: Calculated association energies [kcal/mol] for the coordination of one $CHCl_3$ molecule to $[(PR_3)BeX_2]$ (R = Me (**4**)) R = Cy (**10**)) (X = Cl, Br, I) in the **gas phase** using full optimization on the wb97xd/def2tzvp level of theory.

R	X	E (kcal/mol)	R[Å]
Me	Cl	-6.51	3.31
	Br	-5.15	3.32
	I	-6.64	3.36
Cy	Cl	-5.82	3.42
	Br	-5.03	3.43
	I	-5.28	3.46

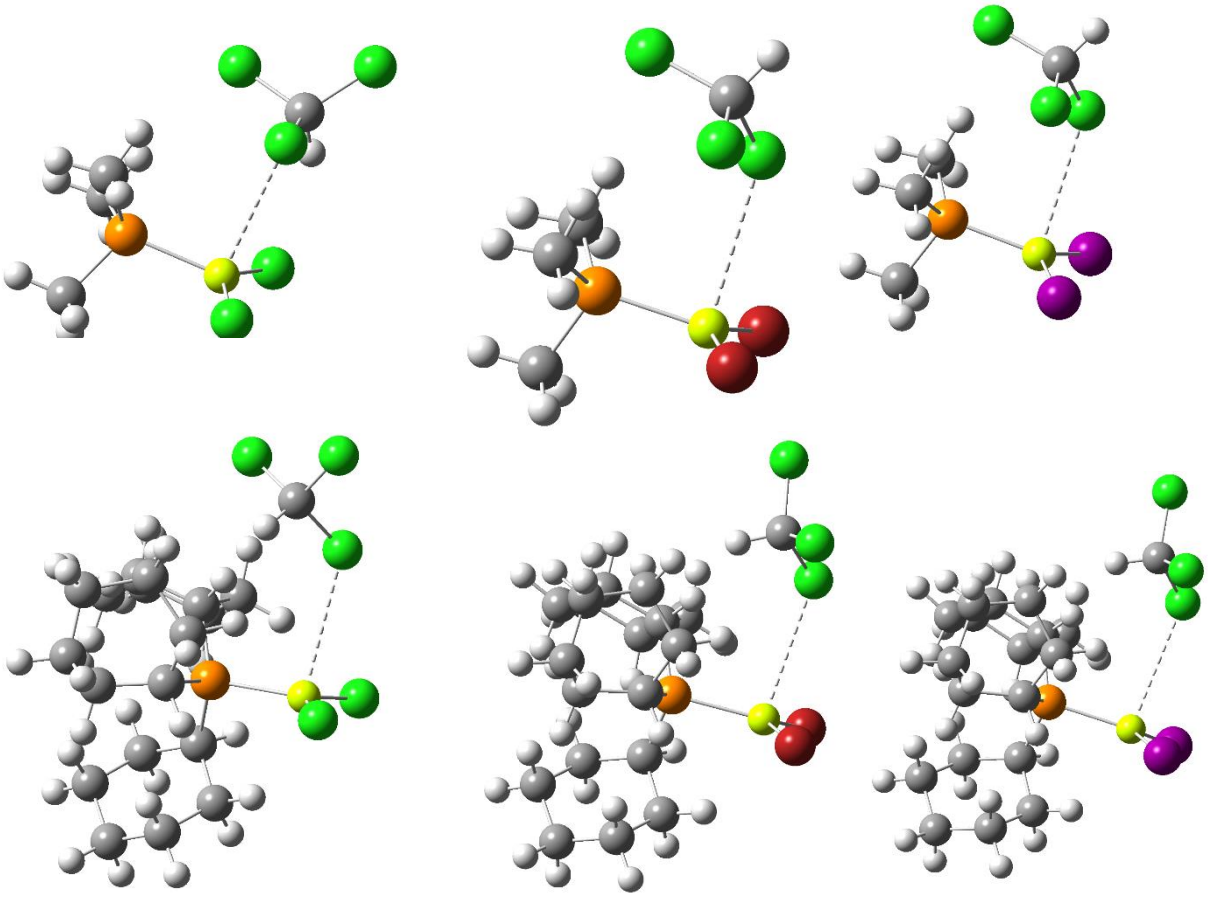

Fig. S149 Optimised gas phase structure of $(Me_3P)(CHCl_3)BeX_2$ (**5**) and $(Cy_3P)(CHCl_3)BeX_2$ (**11**) and at the wb97xd/def2tzvp level of theory including three additional chloroform molecules to model solvent interactions.

Phosphine dissociation from dinuclear complexes

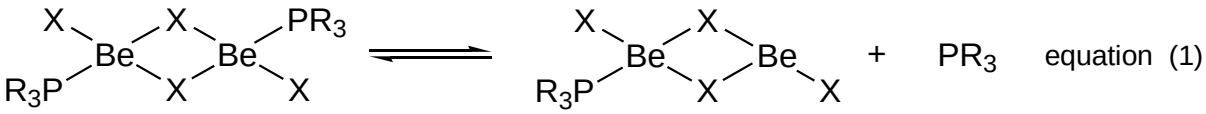

equation (1)

Fig. S150 Phosphine dissociation from $[(PMe_3)BeX_2]_2$ (**2**) (X = Cl, Br, I).

Table S46: Calculated dissociation energies [kcal/mol] for the dissociation of phosphine from $[(PR_3)BeX_2]_2$ (R = Me (**2**)) R = Cy (**3**)) (X = Cl, Br, I) in the **gas phase** using full optimization on the wb97xd/def2tzvp level of theory.

Equation (1)

R	X	E (kcal/mol)
Me	Cl	24.96
	Br	28.18
	I	28.07
Cy	Cl	27.62
	Br	29.09
	I	29.90

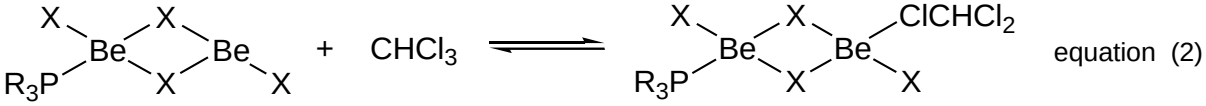

equation (2)

Fig. S151 Phosphine dissociation from $[(PCy_3)BeX_2]_2$ (**3**) (X = Cl, Br, I).

Table S47: Calculated association energies [kcal/mol] for the coordination of one $CHCl_3$ molecule to $[(PR_3)(BeX_2)_2]$ (R = Me (**12**)) R = Cy (1**3**)) (X = Cl, Br, I) in the **gas phase** using full optimization on the wb97xd/def2tzvp level of theory.

Equation(2)

R	X	E (kcal/mol)	R[Å]
Me	Cl	-2.71	3.29
	Br	-2.94	3.31
	I	-3.23	3.39
Cy	Cl	-5.16	2.77
	Br	-4.85	2.88
	I	-5.01	3.17

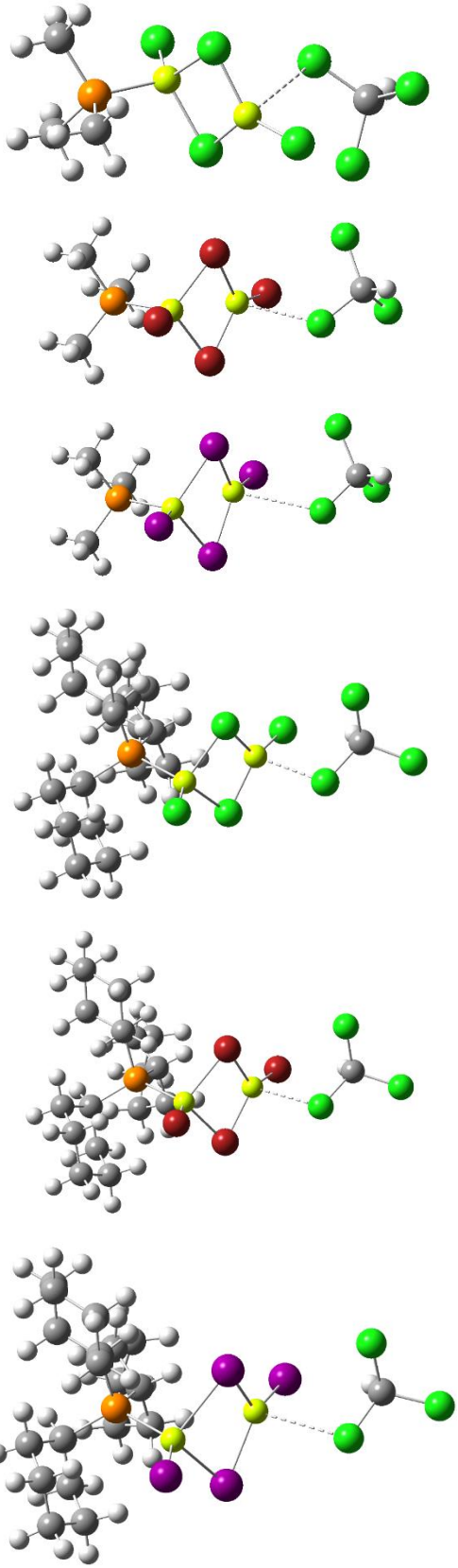

Fig. S152 Optimised gas phase structure of $(Me_3P)(CHCl_3)(BeX_2)_2$ (**5**) and $(Cy_3P)(CHCl_3)(BeX_2)_2$ (**11**) and at the wb97xd/def2tzvp level of theory including three additional chloroform molecules to model solvent interactions.

Dimer dissociation in the presence of six additional chloroform

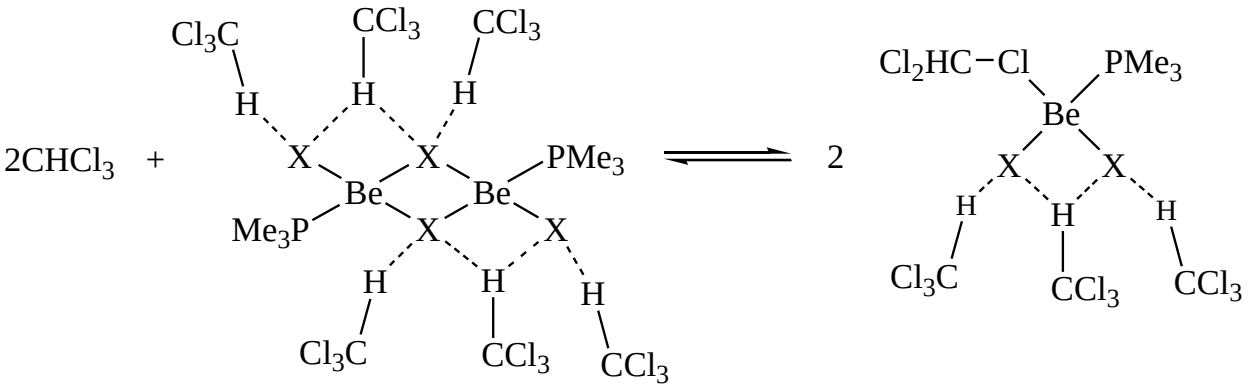

Fig. S153 Dissociation of $[(PMe_3)BeX_2]_2$ (**2**) (X = Cl, Br, I) with three additional chloroform molecules to model solvent interactions

Table S48: Dissociation energies of $[(PMe_3)BeX_2]_2$ (**2**) (X = Cl, Br, I) in the **gas phase** at the wb97xd/def2tzvp level of theory with three additional chloroform molecules to model solvent interactions.

X	E (kcal/mol)
Cl	17.033
Br	16.640
I	17.655

References

[1] M. R. Buchner, *Chem. Commun.*, **2020**, *56*, 8895–8907.

[2] M. R. Buchner, *Z. Naturforsch., B: J. Chem. Sci.*, **2020**, *75*, 405–412.

[3] D. Naglav, M. R. Buchner, G. Bendt, F. Kraus, S. Schulz, *Angew. Chem. Int. Ed.*, **2016**, *55*, 10562–10576.

[4] M. R. Buchner, F. Dankert, N. Spang, F. Pielnhofer, C. von Hänisch, *Inorg. Chem.*, **2020**, *59*, 16783–16788.

[5] M. Müller, F. Pielnhofer, M. R. Buchner, *Dalton Trans.*, **2018**, *47*, 12506–12510.

[6] M. L. Luetkens, A. P. Sattelberger, H. H. Murray, J. D. Basil, J. P. Fackler, *Inorg. Synth.*, **1990**, *28*, 305–310.

[7] X-AREA, Stoe & Cie GmbH, Darmstadt, Germany **2017**.

[8] C. B. Hübschle, G. M. Sheldrick, B. Dittrich, *J. Appl. Crystallogr.*, **2011**, *44*, 1281–1284.

[9] G. Sheldrick, *Acta Crystallogr.*, **2015**, *C71*, 3–8.

[10] G. Sheldrick, *Acta Crystallogr.*, **2015**, *A71*, 3–8.

[11] MESTRENOVA 14.2.1, Mestrelab Research S.L., Santiago de Compostela, Spain, **2021**.

[12] OPUS, Bruker Optik GmbH, Ettlingen, Germany, **2009**.

[13] J.-D. Chai, M. Head-Gordon, *Phys. Chem. Chem. Phys.*, **2008**, *10*, 6615–6620.

[14] R. Ahlrichs, F. Weigend, M. Häser, H. Patzelt, *Chem. Phys. Lett.*, **1998**, *294*, 143–152.

[15] F. Weigend, R. Ahlrichs, *Phys. Chem. Chem. Phys.*, **2005**, *7*, 3297–3305.

[16] K. Fukui, S. Kato, H. Fujimoto, *J. Am. Chem. Soc.*, **1975**, *97*, 1–7.

[17] D. Ćoćić, B. Petrović, R. Puchta, M. Chrzanowska, A. Katafias, R. van Eldik, *J. Comput. Chem.*, **2022**, *43*, 1161–1175.

[18] V. Barone, M. Cossi, *J. Phys. Chem. A*, **1998**, *102*, 1995–2001.

[19] M. Cossi, M. Rega, G. Scalmani, V. Barone, *J. Comput. Chem.*, **2003**, *24*, 669–681.

[20] A. D. Becke, *J. Phys. Chem.*, **1993**, *97*, 5648–5652.

[21] C. Lee, W. Yang, R. G. Parr, *Phys. Rev. B: Condens. Matter*, **1988**, *37*, 785–789.

[22] P. J. Stephens, F. J. Devlin, C. F. Chabalowski, M. J. Frisch, *J. Phys. Chem.*, **1994**, *98*, 11623–11627.

[23] S. Grimme, J. Antony, S. Ehrlich, H. Krieg, *J. Chem. Phys.*, **2010**, *132*, 154104.

[24] M. J. Frisch, M. Head-Gordon, J. A. Pople, *Chem. Phys. Lett.*, **1990**, *166*, 275–280.

[25] M. J. Frisch, M. Head-Gordon, J. A. Pople, *Chem. Phys. Lett.*, **1990**, *166*, 281–289.

[26] M. Head-Gordon, J. A. Pople, M. J. Frisch, *Chem. Phys. Lett.*, **1988**, *153*, 503–506.

[27] S. Saebø, J. Almlöf, *Chem. Phys. Lett.*, **1989**, *154*, 83–89.

[28] M. Head-Gordon, T. Head-Gordon, *Chem. Phys. Lett.*, **1994**, *220*, 122–128.

[29] M. J. Frisch, *et al.*, *Gaussian 09, Revision B.01. Gaussian Inc.*, **2009**, Wallingford.

[30] E. Espinosa, E. Molins, C. Lecomte, *Chem. Phys. Lett.*, **1998**, *285*, 170–173.

[31] L. Tian, F. Chen, *J. Comput. Chem.*, **2012**, *33*, 580–592.